Università degli Studi dell'Insubria

Department of Science and High Technology
Ph.D. Course in Computer Science and Computational Mathematics

Single- and multi-population kinetic models for vehicular traffic reproducing fundamental diagrams and with low computational complexity

Supervisors:

Prof. Gabriella Puppo
Prof. Matteo Semplice
Prof. Andrea Tosin

Student:

Giuseppe Visconti

Ph.D. Thesis – XXIX Cycle

Thanks to:

my supervisors *Gabriella, Matteo*
and *Andrea*, for their precious teachings
my family, always present in my life
my love *Sarah*, for her tireless support

Contents

List of Figures

List of Tables

Introduction

Prediction and control of traffic have become important aspects of the modern world. In fact, the necessity of forecasting the depletion time of a queue or optimizing traffic flows, thereby reducing congestion and the number of accidents, has arisen following the increase of circulating vehicles. In traffic flow theory a basic tool to analyze vehicular traffic problems is given by the so-called fundamental relations among the macroscopic quantities of the flow, as the density (number of vehicles per kilometer), the mean speed of the flow (kilometer per unit time) and the flux (number of vehicles per unit time). Mainly two fundamental relations are used: the flux-density diagram (or *fundamental diagram*) and the speed-density diagram. They allow one to study the macroscopic trends of vehicle dynamics as a result of the interactions taking place at the microscopic scale. Therefore, macroscopic relations can be used for instance to predict the maximum capacity of a road when certain traffic rules are imposed, such as, e.g., number of lanes, safety distance, inflow block of heavy vehicles or speed limits.

The qualitative structure of such diagrams is defined by the characteristics of different regimes, or phases, of traffic as discussed in detail in Section 2.2 and as widely studied, e.g., in [1, 46, 55]. In particular, the experimental diagrams usually show the presence of two regimes of traffic. The *free-flow phase* occurs at low densities and is characterized by a nearly linear increase of the flux with respect to the density of vehicles. In the *congested phase*, in which the road becomes progressively jammed, we observe the decrease of the speed of the flow due to the high congestion. As a consequence, in this regime, also the flux decreases as the density of the vehicles increases because of the drastic reduction of the mean speed. The transition between the two phases is characterized by the *capacity drop*, i.e. the sharp decrease of the average quantities across a density value called *critical density*. Moreover, since the macroscopic dynamics depends on different properties of the flow, such as the types of vehicles traveling on the road or the external conditions (e.g. weather or environmental conditions), experimental diagrams show a multivalued structure: several values of the flux of vehicles or of the mean speed may correspond to a given value of the vehicle density, see for instance Figure 2.1 in Chapter 2, with experimental data published in [70, 79]. The dispersion of the data is small in the free-flow phase, while is more evident in the congested regime.

Mathematical models for traffic flow capable of providing diagrams of traffic which reproduce the structure of experimental data play thus an important role. In this work, we focus on *kinetic theory* of vehicular traffic. Kinetic models are characterized by a statistical

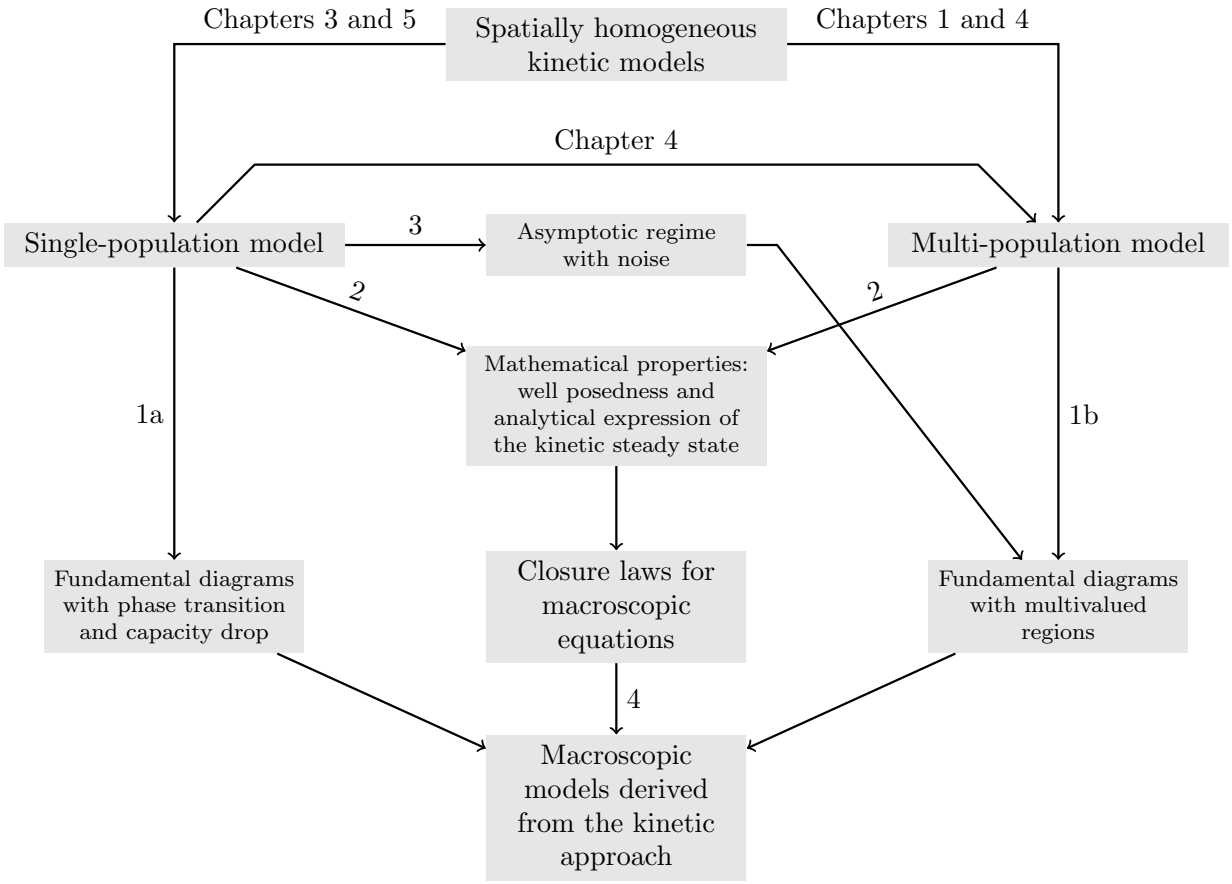

Figure 1: Diagram reproducing the conceptual structure of this thesis.

description of the microscopic states of vehicles (space positions and microscopic speeds), whose evolution is described by means of a statistical distribution function. The peculiarity of these models is to provide, thanks to a detailed characterization of the microscopic interactions among vehicles, information on the macroscopic trend of the flow, without assuming previous knowledge on the dependence of the flux and of the mean velocity on the local density of traffic, as it is done in standard macroscopic models based on fluid dynamics equations [5, 59, 77, 87].

The main goal of this thesis is the study of (Boltzmann-type and Fokker-Planck-type) kinetic models for traffic flow having properties which improve the already existing models in the mathematical literature, following the scheme of the diagram in Figure 1. In particular, we wish to propose kinetic models being amenable for computations and analytical investigations, but at the same time being able to characterize and to explain the features of experimental diagrams.

To this end, first we will aim at deriving models that reproduce and explain the characteristics of experimental diagrams of traffic, such as the multiphase structure, the capacity drop and the scattering of the measured data. See arrows 1a and 1b in Figure 1. In particular, we will try to reproduce the multivaluedness of diagrams by introducing a

multi-population kinetic model. In this way, we will propose a new interpretation of the dispersion of experimental data since it can be attributed to the heterogeneous composition of the flow along a road. In fact, the scattering is naturally obtained by treating traffic as a mixture of vehicles with different physical and kinematic characteristics (e.g. typical length, maximum speed, et cetera). Thus, the multi-population model will allow us to explain the possible microscopic causes which induce the dispersion of data. The multivalued nature of real diagrams is an aspect widely studied in the literature: for instance, it can be explained as a result of the variability of the microscopic speeds at equilibrium in a kinetic model, see [26], or as a consequence of the presence of nonlinear traveling wave solutions (called *jamitons*) in second order macroscopic models, see [79].

We recall that experimental diagrams are built assuming that traffic is uniform in space. From a mathematical point of view, this means that theoretical diagrams have to be recovered by linking the macroscopic variables at equilibrium. Since, in the kinetic approach, density, flux and mean speed are computed as moments of the kinetic distribution, the knowledge of the steady state is crucial in order to reproduce fundamental diagrams. Noticing that, usually, the complexity of the collision operator of a Boltzmann-type equation makes the computation of the steady state very demanding, here we aim at introducing kinetic models for which the analytical expression of the steady state can be computed explicitly (arrows 2 in Figure 1). We will see that this is possible thanks to the particular choice of the microscopic interactions which makes the continuous-velocity model consistent with a lattice-velocity model at equilibrium. Further, we will show that this simple and prototype steady state (because quantized on a reduced number of speeds) actually is sufficient to catch the macroscopic properties of the flow at equilibrium, as the phase transition, the capacity drop and the scattering of data.

We also wish to propose models being endowed with a robust mathematical structure. Thus, we will study the mathematical properties which induce the structure of diagrams, the well posedness with the existence and uniqueness proof of the solution of the kinetic spatially homogeneous equation. See arrows 2 in Figure 1.

Since the macroscopic trend of traffic and the corresponding fundamental diagrams depend on the behaviors of drivers at the microscopic level, a further goal of this thesis will be the analysis of the effects of the microscopic interaction rules on the macroscopic dynamics (arrow 3 in Figure 1). The kinetic framework seems to be the natural approach to investigate this purely multiscale issue which is tackled by an asymptotic study of the model in the Fokker-Planck kinetic limit (*grazing collision limit*). This approach will lead to the general expression of the equilibrium kinetic distribution, as function of microscopic parameters. Therefore, we will able to characterize the diagrams of traffic according to the microscopic hypotheses and to explain the realistic interaction rules taking place among vehicles.

We notice that kinetic models satisfying the above properties pave the way to formulate new macroscopic equations in which the closures are not derived from heuristic considerations or by fitting data, but using the equilibrium distributions of the kinetic model. See arrow 4 in Figure 1. These macroscopic equations, which simulate the traffic phenomena at equilibrium, may be also obtained as hydrodynamic limits of the spatially inhomogeneous

version of the kinetic model. These aspects will be discussed in the final chapter.

The thesis will be organized as follows and each chapter will be introduced by a short motivational section.

Chapter 1. We begin with a short introduction on mathematical models for traffic flow at each scale. In particular, we deal with the kinetic approach to traffic flow and we review several models introduced in the literature;

Chapter 2. We summarize the results published in the paper [76] in which, resting on the methods of kinetic theory, we introduce a new traffic model which takes into account the heterogeneous nature of the flow of vehicles along a road. In more detail, the model considers traffic as a mixture of two populations of vehicles (e.g., cars and trucks) with different microscopic characteristics, in particular different lengths and/or maximum speeds. With this approach we gain insight into the scattering of the data in the regime of congested traffic clearly shown by experimental measurements;

Chapter 3. We summarize the results proposed in the paper [75] in which the purpose is to study the properties of kinetic models for traffic flow described by a Boltzmann-type approach and based on a continuous space of microscopic velocities. In our models, the particular structure of the collision kernel allows one to find the analytical expression of a class of steady-state distributions, which are characterized by being supported on a quantized space of microscopic speeds. The number of these velocities is determined by a physical parameter describing the typical acceleration of a vehicle and the uniqueness of this class of solutions is supported by numerical investigations. This shows that it is possible to have the full richness of a kinetic approach with the simplicity of a space of microscopic velocities characterized by a small number of modes;

Chapter 4. We summarize, with a few minor changes, the results published in the paper [74]. In fact, in contrast to [74], here we modify the interaction rules in order to extend the continuous-velocity kinetic traffic model studied in [75] and in Chapter 3 to the case of more than one class of vehicles, each of which is characterized by few different microscopic features. We again consider a Boltzmann-type framework with binary interactions (as in the previous chapters), which take place among vehicles belonging to the various classes. This approach differs from the multi-population kinetic model proposed in [76] and in Chapter 2 because here we assume continuous velocity spaces and as in [75] the model is characterized by the presence of a finite parameter describing the physical velocity jump performed by a vehicle that increases its speed after an interaction. The model is discretized in order to investigate numerically the structure of the resulting fundamental diagrams and the system of equations is analyzed by studying well posedness. Moreover, we compute the equilibria of the discretized model and we show that the exact asymptotic kinetic distributions can

be obtained with a small number of velocities in the grid. Finally, we introduce a new probability law in order to attenuate the sharp capacity drop occurring in the diagrams of traffic;

Chapter 5. We summarize the results proposed in the paper [85] in which, starting from mean-field interaction rules based on two levels of stochasticity in drivers' subjective decisions, we study the influence of the microscopic dynamics on the macroscopic properties of vehicular flow. In particular, we study the qualitative structure of the resulting flux-density and speed-density diagrams for different choices of the desired speeds. We are able to recover multivalued diagrams as a result of the existence of a one-parameter family of stationary distributions, whose expression is analytically found by means of a Fokker-Planck approximation (grazing collision limit) of the initial Boltzmann-type model;

Chapter 6. We finally end with a conclusive chapter in which we summarize the mathematical and the modeling aspects discussed in this thesis. In particular, we focus on the improvements that, in our opinion, the thesis would introduce in the literature of traffic theory and on open perspectives in this research field. A further section will be devoted to a brief study of a single-population macroscopic model endowed with the closure law provided by the kinetic model proposed in Chapter 3.

Chapter 1

Background material on mathematical models for traffic flow

The aim of this introductory chapter is to briefly review several mathematical models already present in the literature and regarding vehicular traffic. In the current mathematical literature, there are three different approaches to model traffic flow phenomena, which differ from each other in the scale of representation.

1.1 Microscopic scale

Microscopic models look at vehicles as single entities of traffic and predict, using a system of ordinary differential equations, the evolution of their positions and speeds (namely, the microscopic states characterizing their dynamics) regarded as time dependent variables. See, e.g., [11, 47, 71].

In these models, vehicles are assimilated to point masses and no overtaking is allowed. The acceleration is prescribed for each entity as a function of time, position, and speed of the various particles of the system, also taking into account mutual interactions among vehicles. For example, the general form of a microscopic model can be expressed as

$$\frac{\mathrm{d}^2}{\mathrm{d}t^2}\mathbf{x}(t) = \mathbf{a}\left(t, \mathbf{x}(t), \frac{\mathrm{d}}{\mathrm{d}t}\mathbf{x}(t)\right),$$

where t is time, $\mathbf{x}(t) \in \mathbb{R}^N$ and $\frac{\mathrm{d}}{\mathrm{d}t}\mathbf{x}(t) \in \mathbb{R}^N$ are vectors of N components whose generic element $x_i(t) \geq 0$ and $\frac{\mathrm{d}}{\mathrm{d}t}x_i(t) \geq 0$ is the position and the speed of the i-th vehicle along the road, $N \in \mathbb{N}$ is the total number of vehicles and finally $\mathbf{a} : \mathbb{R} \times \mathbb{R}^N \times \mathbb{R}^N \to \mathbb{R}^N$ is the vector-valued function such that a_i describes the acceleration of the i-th vehicle. Clearly, the above system of differential equations requires the knowledge of the initial conditions $x_i(0)$ and $\frac{\mathrm{d}}{\mathrm{d}t}x_i(0)$, $\forall\ i = 1, \ldots, N$. Moreover, in microscopic models one usually assumes that $x_{i-1}(t) < x_i(t) < x_{i+1}(t)$, $\forall\ i = 2, \ldots, N-1$ and $\forall\ t \geq 0$.

As a matter of fact, in the well known *follow-the-leader* theory each vehicle is assumed to adapt its speed to that of the leading vehicle based on their instantaneous relative speed

and mutual distance, see e.g. [4, 30, 71], namely **a** depends at most on x_i, x_{i+1} and on $\frac{\mathrm{d}}{\mathrm{d}t}x_i(t)$, $\frac{\mathrm{d}}{\mathrm{d}t}x_{i+1}(t)$. Thus, we can write

$$\frac{\mathrm{d}^2}{\mathrm{d}t^2}x_i(t) = a_i\left(t, x_i(t), \frac{\mathrm{d}}{\mathrm{d}t}x_i(t), \delta x_i(t), \delta v_i(t)\right), \quad i = 1, \dots, N \tag{1.1}$$

where $\delta x_i(t) = x_{i+1}(t) - x_i(t)$ and $\delta v_i(t) = \frac{\mathrm{d}}{\mathrm{d}t}x_{i+1}(t) - \frac{\mathrm{d}}{\mathrm{d}t}x_i(t)$ are, respectively, the relative position and the relative speed of the i-th and $(i+1)$-th vehicle at time t.

Follow-the-leader models differ in the modeling of the interaction part of the acceleration function **a**, namely the part which takes into account the relative quantities $\delta x_i(t)$ and $\delta v_i(t)$.We describe two class of follow-the-leader models:

- models in which the interaction part depends on the relative position and speed, see, e.g., [30]. In this case the function a_i in (1.1) writes as

$$a_i = \underbrace{\frac{\delta v_i(t)}{\delta x_i(t)^{1+\gamma}}}_{\text{interaction term}} + \underbrace{\frac{v_d - \frac{\mathrm{d}}{\mathrm{d}t}x_i(t)}{\tau}}_{\text{relaxation term}}, \quad \gamma \geq 0,\ \tau > 0.$$

  Notice that, thanks to the denominator in the interaction term, the acceleration results to be inversely proportional to the distance between the interacting vehicles. Further, the numerator in the interaction term makes the acceleration positive if the leading car is faster, while negative otherwise. The relaxation term, instead, models the tendency of a driver to travel to a fixed desired speed $v_d > 0$ when no interactions take place. The parameter τ is the response time of a driver;

- models in which the interaction part depends only on the relative position, see, e.g., [6]. In this case the function a_i in (1.1) writes as

$$a_i = \frac{1}{\tau}\left(\underbrace{V(\delta x_i(t))}_{\text{interaction term}} - \underbrace{\frac{\mathrm{d}}{\mathrm{d}t}x_i(t)}_{\text{relaxation term}}\right), \quad \tau > 0,$$

  where $V : \mathbb{R}^+ \to [0, V_{\max}]$ is a sort of desired speed, with $V_{\max}$ maximum allowed speed. Clearly, V should be an increasing function of the distance $\delta x_i(t)$ of the two vehicles at time t. In [6] a possible choice of V is proposed.

In the context of the car-following theory we recall also the model introduced by Zhang and Kim [88] since the authors are able to reproduce both the so-called capacity drop and traffic hysteresis, two basic features characterizing the multiphase structure of fundamental traffic diagrams. The result is reached by means of an acceleration function **a** which, in contrast to classical follow-the-leader models, includes a non-constant driver response time τ, that can be also a function of the traffic regime. Thus, τ can be modeled differently according to the phase of traffic.

Although this class of models allows the description of the trajectory of each vehicle, the crucial problem of the microscopic scale is the large number of equations required for the modeling of traffic dynamics. Thus, the larger the number of vehicles, the more computationally expensive the model. Moreover, microscopic models do not provide a robust criterion to prescribe v_d or $V(\delta x_i(t))$, which are therefore given by heuristic considerations. Finally, we notice that these models are scarcely predictive because are too much detailed. In other words, there are many way to recover information on the overall trend of traffic.

For further discussions on microscopic models, we refer to the review [70] and references therein.

1.2 Macroscopic scale

Macroscopic models provide a large scale aggregate point of view, neglecting the microscopic dynamics. Thus, the focus is not on each single particle of the system. In fact, macroscopic models study only the evolution of the macroscopic quantities related to traffic flow by means of partial differential equations inspired by conservation and balance laws from fluid dynamics, following the seminal works of Lighthill and Whitham [59] and Richards [77].

First order macroscopic models describe the evolution (in space and time) of the density of vehicles on a road using a scalar conservation law of the form

$$\partial_t \rho(t,x) + \partial_x(\rho(t,x)u(\rho(t,x))) = 0, \tag{1.2}$$

where, at time $t \geq 0$ and at position x, $\rho(t,x) \geq 0$ is the *macroscopic density* (expressed for instance as number of vehicles per kilometer), while $u(\rho(t,x)) \geq 0$ is the *mean speed* of vehicles (expressed as kilometer per unit time) and thus the product $\rho(t,x)u(\rho(t,x)) \geq 0$ is the *flux function* (expressed as number of vehicles per unit time). Observe that equation (1.2) requires that, in order to be closed, u be a given function of the density ρ.

Let

$$N_{\mathsf{v}}(t) = \int_a^b \rho(t,x)\mathrm{d}x$$

be the number of vehicles in a stretch $[a,b] \subseteq \mathbb{R}^+$ of a road at time $t \geq 0$. Then, the continuity equation (1.2) is obtained by imposing that the time variation of the number of vehicles $N_{\mathsf{v}}(t)$ in the stretch $[a,b]$ is only due to the balance of vehicles which cross the positions $x = a$ and $x = b$:

$$\frac{\mathrm{d}}{\mathrm{d}t}\int_a^b \rho(t,x)\mathrm{d}x = (\rho u)(t,a) - (\rho u)(t,b).$$

In fact, from the above expression, since $(\rho u)(t,a) - (\rho u)(t,b) = -\int_a^b \partial_x(\rho u)(t,x)\mathrm{d}x$ and thanks to the arbitrariness of $[a,b]$, we finally get equation (1.2).

Improvements and further evolution of such a basic macroscopic description of traffic have been proposed over the years by several authors, as the classical mechanically consistent restatement of second order models proposed by Aw and Rascle [5] and Zhang [87].

In second order models the equation (1.2) is coupled with an additional equation for the evolution of the macroscopic speed u. The Aw-Rascle and Zhang model in conservation form writes as

$$\begin{cases} \partial_t \rho(t,x) + \partial_x(\rho u)(t,x) = 0 \\ \partial_t(\rho(u+p)) + \partial_x(\rho u(u+p)) = 0 \end{cases} \tag{1.3}$$

where $p = p(\rho)$ is the so-called *traffic pressure* and is a known function of the density ρ. Observe that, in contrast to first order models, here u is not an already given function of the density. Equation (1.3) overcomes the two drawbacks of the prototype second order model introduced by Payne [69] and Whitham [86]. In fact, as pointed out by Daganzo [19] the Payne-Whitham model leads to the following two non-physical effects: the presence of negative velocities (which is realistic in gas dynamics, not in traffic flow) and of characteristic speeds traveling faster than the velocity of vehicles. Second order macroscopic models for traffic flow of the type (1.3) are also studied to reproduce the scattering of data in traffic diagrams. In fact, in [79], Seibold et al. link such multivalued diagrams to the presence of nonlinear traveling wave solutions (*jamitons*) in second order models showing that the scattering is due to jamiton-dominated solutions. In fact, since a jamiton solution is non-constant in the density ρ and in the speed u, it would identify more than a single point in the diagrams of traffic.

Generalizations of the model [5, 87] have been proposed in the literature, see e.g. the Generalized Aw-Rascle-Zhang (GARZ) model studied in [23, 24] or the Generalized Second Order Model (GSOM) introduced in [54]. In these works, a relaxation term in the equation for the macroscopic speed is taken into account for different purposes. In particular, in the thesis [23] and in the paper [24], Seibold et al. present an approach to determine the parameters of the GARZ model using a fit of experimental data.

Although, in contrast to microscopic models, macroscopic ones are computationally very fast, it is necessary to complete the equations with a closure law. This relation defines a dependence between the macroscopic quantities. The closure law must provide the speed u as a function of the density ρ in first order models, or the pressure p as a function of the density ρ (and additionally of the speed u) in second order models. For example, in (1.2) one assumes that the macroscopic speed u is actually a given decreasing function of the local density ρ, i.e. $u = u(\rho)$, and several laws have been considered in the literature:

- the Greenshields' closure [32]: starting from the empirical fact that the fluid travels at the maximum speed $u = V_{\max}$ when the road is empty ($\rho = 0$) and at the minimum $u = 0$ when the road is congested ($\rho = \rho_{\max}$, i.e. in bumper-to-bumper condition), one assumes a linear speed-density relation interpolating the previous data. Thus, we have $u(\rho) = V_{\max}(1-\rho)$ and $\rho u(\rho) = V_{\max}\rho(1-\rho)$ is the fundamental diagram. See Figure 1.1a;

- Greenberg's closure [31]: the speed-density diagram is prescribed by the following logarithmic law $u(\rho) = \lambda \ln(\frac{\rho_{\max}}{\rho})$, $\lambda > 0$, and thus the fundamental diagram is given

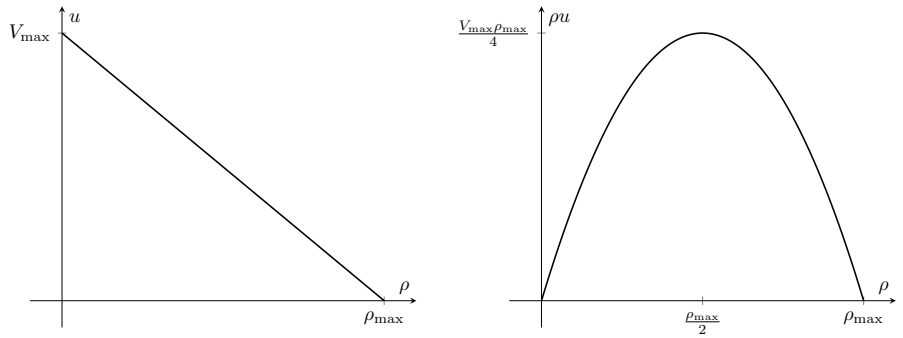

(A) Greenshields' closure.

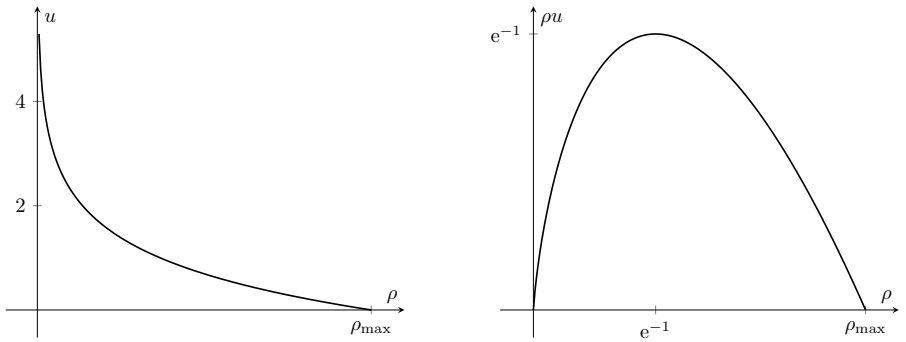

(B) Greenberg's closure.

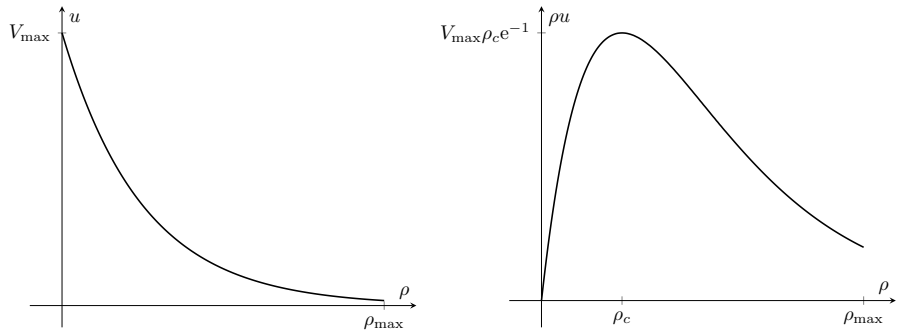

(C) Underwood's closure.

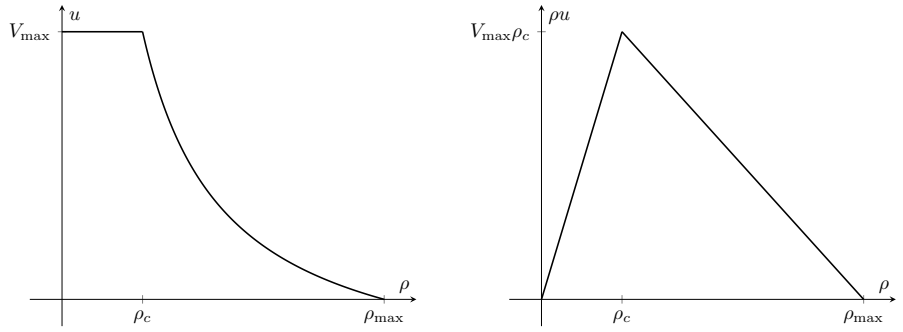

(D) Daganzo's closure.

Figure 1.1: Classical closures for first order macroscopic models.

by $\rho u(\rho) = \lambda\rho \ln(\frac{\rho_{\max}}{\rho})$. See Figure 1.1b obtained with $\lambda = 1$. Observe that the free-flow velocity is not bounded, in fact $u \xrightarrow{\rho\to 0^+} \infty$. Consequently, this closure appears reasonable only for large values of the density;

- Underwood's closure [83]: this model is proposed as a result of traffic studies on Merrit Parkway in Connecticut (USA). It tries to overcome the limitation of Greenberg's model, in which the speed is unbounded in free-flow conditions, using the exponential law $u(\rho) = V_{\max} \exp(-\rho/\rho_c)$, with $\rho_c \in [0, \rho_{\max}]$, which defines the fundamental diagram $\rho u(\rho) = V_{\max}\rho \exp(-\rho/\rho_c)$. See Figure 1.1c.

We notice that the closures provided in Figure 1.1 do not reproduce neither the phase transition or the capacity drop. For further closure laws we refer, e.g., to the book [78].

In second order macroscopic models, see (1.3), instead, the closure is given between the density ρ and the pressure p. In [5], the authors assume that $p(\rho) = \rho^\gamma$, $\gamma > 0$, namely a smooth increasing function of the density. In [87] the author takes $p(\rho) = V_{\max} - v_d(\rho)$, where $v_d > 0$ is a desired speed depending on the congestion of the road and such that $v_d(0) = V_{\max}$, so that $p(0) = 0$, consistently with [5].

The fact that macroscopic models require to close the equations means that the fundamental diagram of traffic is given as an a priori relation derived from heuristic or physical arguments, which therefore usually do not result from microscopic dynamics. We cannot thus expect that these models are able to provide neither realistic simulations of traffic dynamics nor the possibility of explaining the influence of the microscopic behaviors on the macroscopic effects. See however [4] in which the derivation of macroscopic models from microscopic follow-the-leader ones is proposed.

The closure laws just described above are single-regime closures because they are based on the assumption that the same relation is used for each regime of traffic. However, drivers' behaviors are naturally different at different regimes. This fact is indeed observed also in the experimental diagrams. Based on this concept, a variety of more refined macroscopic models (multiphase models) which provide flux-density relations by prescribing different flow conditions at certain stages, building the multiphase structure within the flow, are proposed, e.g., in [15, 53, 61]. The most simple multiphase model is a two-regime model which separates the closure used in the free and in the congested traffic. See, e.g., the bilinear law proposed by Daganzo in [18] which results in a flux-density diagram having a triangular shape, see Figure 1.1d. Although the closure in Figure 1.1d reproduces the phase transition, we stress the fact that the properties of fundamental diagrams are built-in artificially in the model. For a review of multiphase models at each scale see [10] and references therein.

Macroscopic models are also applied to road networks. In this context, see, e.g., the book of Garavello and Piccoli [29]. Finally, a generalization of the Lighthill and Whitham [59] and Richards [77] traffic flow model to the case of multiple populations of vehicles was proposed by Benzoni-Gavage and Colombo [7]. The aim was to describe the natural heterogeneity of traffic by considering distinct drivers' behaviors or types of vehicles. This model will be discussed in Section 2.4.

1.3 Mesoscopic scale

In the middle between microscopic and macroscopic scales, we have the *mesoscopic* (or *kinetic*) scale. This class of models is based on a statistical mechanics approach, which still provides an aggregate representation of traffic flow while linking collective dynamics to pairwise interactions among vehicles at a smaller microscopic scale. These models will be the main reference background of the present thesis.

Kinetic models are characterized by a statistical description of the microscopic states of vehicles. Therefore the evolution of their position x and speed v is described by means of a distribution function

$$f = f(t,\, x,\, v) : \mathbb{R}^+ \times \mathbb{R} \times \mathcal{V} \to \mathbb{R}^+ \tag{1.4}$$

where $\mathcal{V}$ is the continuous and bounded velocity space. The kinetic distribution (1.4) is such that $f(t,\, x,\, v)\,\mathrm{d}x\,\mathrm{d}v$ is the number of vehicles which at time t are located between x and $x + \mathrm{d}x$ with a speed between v and $v + \mathrm{d}v$.

Compared to microscopic models, the kinetic approach requires a smaller number of equations and parameters. On the other hand, unlike macroscopic models, at the mesoscopic scale the evolution equations do not require an a priori knowledge of the dependence of the mean velocity on the local density. In fact, the macroscopic quantities are provided by the statistical moments of the kinetic distribution function over the microscopic states:

$$\rho(t,x) = \int_{\mathcal{V}} f(t,x,v)\mathrm{d}v, \quad (\rho u)(t,x) = \int_{\mathcal{V}} v f(t,x,v)\mathrm{d}v, \quad u(t,x) = \frac{1}{\rho(t,x)} \int_{\mathcal{V}} v f(t,x,v)\mathrm{d}v.$$

In particular, the flux (ρu) and the average velocity u are obtained from the first momentum of f with respect to v. Consequently, speed-density and flux-density diagrams are recovered by means of the asymptotic (in time) kinetic distribution which provides the macroscopic variables at equilibrium. Therefore, kinetic models are a quite natural way to bridge microscopic causes and macroscopic effects.

The first kinetic models for vehicular traffic, introduced by Prigogine and coworkers [72, 73] and later by Paveri-Fontana in [68], were based on the Boltzmann equation that describes the statistical behavior of a system of particles in a gas. From the kinetic point of view, the system is seen as the resultant of the evolution of microscopic particles, with given microscopic positions and speeds, but its representation is provided in aggregate terms by the statistical distribution function (1.4), whose evolution is described by integro-differential equations. Noticing that, in traffic flow, and in contrast to gas theory, the space x and the velocity v are one-dimensional microscopic states, in traffic flow the Boltzmann-type equation, describing the evolution of the kinetic distribution (1.4), simplifies as

$$\partial_t f(t,x,v) + v\partial_x f(t,x,v) = Q[f,f](t,x,v). \tag{1.5}$$

The term $Q[f,f](t,x,v)$ is the so-called *collision operator*, which, in the classical assumption of binary interactions, depends quadratically on the kinetic distribution f and explicitly on the velocity v, but on t and x only via $f(t,x,v)$.

Thus, in Boltzmann-type kinetic models for traffic flow we still have a collision term which involves integrals and describes the relaxation in time of the kinetic distribution due to interactions among vehicles. Nevertheless, in traffic flow models, the classical cross section of the Boltzmann equation, giving the probability of an interaction between two gas particles, is replaced with a probability distribution depending on the local traffic conditions and which models the speed transitions. This framework permits to take the stochasticity of the drivers' behavior into account, thanks to the probability distribution which assigns a weight to the possible driver's decisions, while maintaining the general kinetic setting, based on the deterministic evolution of the distribution function.

However, the interaction integrals, appearing in kinetic Boltzmann-type models for traffic flow based on a continuous-velocity space, typically do not provide the analytical expression of the equilibrium distribution and they are very demanding from a computational point of view, see e.g. [48]. For this reason, two main approaches have been taken into account in order to compute the time-asymptotic distribution or to reduce the computational cost: on the one hand, one may consider Vlasov-Fokker-Planck type models in which the interaction integrals are replaced by differential operators, obtained also by means of suitable time scalings, see [36, 41, 44]; on the other hand, one may consider simplified kinetic models with a small number of velocities, namely the discrete-velocity models, see [16, 20, 25, 26, 42, 82].

Recently, kinetic models have been widely used, e.g. to model multilane traffic flow [9, 35, 50, 51, 60], flows on networks [27], control problems [39], homogeneous space problems [40], inhomogeneous space phenomena with non-local interactions [49], heterogeneous compositions of the flow [60, 74, 76] and safety aspects in vehicular traffic [28]. Also, kinetic models have been proposed to derive macroscopic equations, see [36, 37, 38].

For an overview of vehicular traffic models at the kinetic scale, the interested reader is referred e.g., to the review papers [52, 70] and references therein.

In the following we will review some kinetic models for vehicular traffic available in the mathematical literature.

1.3.1 Boltzmann-type models: first approaches

Prigogine's model

In this section we present the first version of the kinetic theory for modeling traffic phenomena, which was introduced by Prigogine and coworkers [72, 73] by modifying the kinetic theory of gases.

The core of a kinetic model is the modeling of microscopic interactions in order to specialize the expression of the collision operator $Q[f,f](t,x,v)$ appearing in the general form of the kinetic equation (1.5). Prigogine assumed that $Q[f,f](t,x,v)$ is split in two additional terms:

- $Q_{\text{int}}[f,f](t,x,v)$ which describes the speed transitions due to the microscopic slowing down interactions among vehicles. Under the hypothesis of *vehicular chaos* (similar to the *molecular chaos* in gas kinetic theory, see however [62] or [49]), which states

that vehicles are actually uncorrelated before interacting due to the mixing caused by overtaking, the interaction term proposed by Prigogine is

$$Q_{\text{int}}[f,f](t,x,v) = (1-P)f(t,x,v)\int_{\mathcal{V}}(v_*-v)f(t,x,v_*)\mathrm{d}v_*.$$

We notice that the collision term is indeed quadratic with respect to f. For $v_* > v$, the interaction term Q_{int} is positive and models the case in which a vehicle with velocity v_* brakes to the velocity v of the leading vehicle. Conversely, for $v_* < v$, the interaction term Q_{int} is negative and thus models the loss of the velocity v of a vehicle interacting with its leading car having velocity v_*. The quantity P is the so-called *probability of acceleration* and it was assumed to depend on the density ρ in a linear way:

$$P(\rho) = 1 - \frac{\rho}{\rho_{\max}}.$$

In the above formula $\rho_{\max}$ denotes the maximum density according to the road capacity. Thus, slowing down takes place with probability $1-P$ which increases as the road becomes congested, i.e. when $\rho \to \rho_{\max}$. For further discussions on the probability P see Section 2.3.2, or Section 4.4 for more complex choices;

- $Q_{\text{rel}}[f,f](t,x,v)$ which describes the *collective* relaxation of the kinetic distribution f towards a desired distribution $f_0(t,x,v)$, which is a mathematical idealization of the drivers' will to adjust the speed with respect to a target. The relaxation term proposed by Prigogine is

$$Q_{\text{rel}}[f,f](t,x,v) = -\frac{f(t,x,v)-f_0(t,x,v)}{T},$$

where T is the relaxation time which was also assumed to depend on the density:

$$T = \frac{\rho}{\rho_{\max}-\rho},$$

while $f_0(t,x,v)$ was taken as

$$f_0(t,x,v) = \rho(t,x)F_0(v),$$

being $F_0(v)$ a given function of the velocity not depending on the time and space variables. Recently, in [43] a novel distribution of desired velocities that is more suitable for describing real traffic conditions was analyzed.

Thus, in Prigogine's model two type of interactions are taken into account, which result in accelerating and braking. The first one is modeled by the relaxation term, the second one by the interaction part.

However, the choice of treating the acceleration by means of a collective relaxation of f towards f_0 has come under severe criticism. In fact, Paveri-Fontana [68] showed that this scenario results in physically unsatisfactory phenomena, discussed in the next paragraph.

Paveri-Fontana's model

According to Paveri-Fontana [68], the model by Prigogine is affected by a conceptual drawback consisting in the assumption of a collective relaxation of the distribution of the microscopic velocities. Paveri-Fontana argued that each single vehicle, in contrast to the molecules in a gas, has a desired velocity towards which it aims in the absence of interactions with other vehicles.

From a mathematical point of view, in [68] an additional microscopic state was considered: the desired velocity v_d, belonging to the same space $\mathcal{V}$ of the actual speeds. Therefore, a generalized distribution function $g = g(t, x, v, v_d)$ is introduced such that $g = g(t, x, v, v_d)\mathrm{d}x\mathrm{d}v\mathrm{d}v_d$ denotes the number of vehicles at time t, traveling in the stretch $[x, x + \mathrm{d}x]$ of the road with actual velocity between $[v, v + \mathrm{d}v]$ and desired velocity between $[v_d, v_d + \mathrm{d}v_d]$. Observe that the classical kinetic distribution function (1.4) and the desired distribution f_0 are recovered as moments of g with respect to v_d and v, respectively:

$$f(t, x, v) = \int_{\mathcal{V}} g(t, x, v, v_d)\mathrm{d}v_d, \quad f_0(t, x, v) = \int_{\mathcal{V}} g(t, x, v, v_d)\mathrm{d}v,$$

while the macroscopic quantities at time t at position x are

$$\rho(t, x) = \int_{\mathcal{V}} \mathrm{d}v \int_{\mathcal{V}} g(t, x, v, v_d)\mathrm{d}v_d, \quad (\rho u)(t, x) = \int_{\mathcal{V}} v\mathrm{d}v \int_{\mathcal{V}} g(t, x, v, v_d)\mathrm{d}v_d,$$
$$u(t, x) = \frac{1}{\rho(t, x)} \int_{\mathcal{V}} v\mathrm{d}v \int_{\mathcal{V}} g(t, x, v, v_d)\mathrm{d}v_d.$$

The kinetic equation (1.5) is then used for evolving the generalized distribution g as follows:

$$\partial_t g(t, x, v, v_d) + v\partial_x g(t, x, v, v_d) = Q[g, g](t, x, v, v_d). \tag{1.6}$$

Again, in [68] the collision term depends quadratically on g (possibly, also via f) and $Q[g, g](t, v)$ is split in two additional terms, a relaxation one having the form

$$Q_{\mathrm{rel}}[g](t, v) = -\frac{\partial}{\partial v}\left(\frac{v_d - v}{T} g\right),$$

and an interaction one inspired by the modeling of Prigogine [72]. In fact, the interaction term is built in such a way that, integrating (1.6) over the microscopic states v_d, the resulting evolution equation for the kinetic distribution f differs from Prigogine's model only in the relaxation term. Thus, also in this case, only braking are admissible when two vehicles interact, instead only later, models with a kinetic description also for the acceleration were developed [62]. However, a different probability of acceleration is taken into account by Paveri-Fontana:

$$P(\rho) = \left(1 - \frac{\rho}{\rho_{\max}}\right) H\left(1 - \frac{\rho}{\rho_c}\right)$$

where $H(\cdot)$ denotes the Heaviside step function and $\rho_c \in (0, \rho_{\max})$ is a critical density value above which acceleration is prohibited.

Finally, we observe that integrating (1.6) with respect to the microscopic state v we get an evolution equation for the desired distribution function f_0 which indeed confirms that f_0 depends now on the overall evolution of the system.

1.3.2 Enskog-like models

We notice that the classical kinetic equation of traffic (1.5) is characterized by localized interactions since the collision operator depends on the product of the kinetic distribution f evaluated at the same space position x. This introduces a serious shortcoming which produces non-physical phenomena, mathematically due to the positivity of the velocity v, because it prevents backward propagation of the perturbations in the negative x direction.

The above consideration can be analyzed by integrating (1.5) along the characteristic lines

$$\frac{\mathrm{d}x}{\mathrm{d}t} = v \quad \Longleftrightarrow \quad x - vt = \text{constant}$$

and we get

$$f(t,x,v) = f(0,x-vt,v) + \int_0^t Q[f,f](s,x+v(s-t),v)\mathrm{d}s. \tag{1.7}$$

Observe that since $v \geq 0$ and $s \leq t$, then $x - vt \leq x$ and $x + v(s-t) \leq x$. It is then clear that the kinetic distribution $f(t,x,v)$ depends, at position x and at time t, only on its value at positions $x' < x$. From the point of view of traffic, this means that perturbations of the flow in a point x' cannot propagates backward, on the contrary they follow the stream of traffic influencing the flow in points $x > x'$. This fact is certainly in contrast to realistic observations in congested traffic flow situations. However, we remark that the previous analysis does not apply to gas kinetic theory, since the velocity of gas particles can assume positive and negative values.

This aspect was not studied in the pioneering works of Prigogine [72, 73] and Paveri-Fontana [68] since they were aimed mainly to model the collision operator Q and to simulate spatially homogeneous problems, as stationary steady states or fundamental diagrams. However, if the kinetic equation (1.5) is used for the modeling of spatially inhomogeneous situations, the study of the propagation of the waves due to the convective term becomes crucial. In this context we refer to a series of papers by Klar and Wegener [49, 50, 51] or the review [52], which suggested a way, inspired by the Enskog theory of a dense gas [14], to overcome the aforementioned drawback.

In the simplest situation, the idea proposed in [49] is based on the following microscopic assumptions:

- the binary interactions involve a vehicle 1 at place x_1 with velocity v_1 and its leading vehicle 2 at $x_2 > x_1$ with velocity v_2. Vehicle 1 is assumed to change its velocity only in response to the leading vehicle;

- if the vehicle 1 is faster than the leading one and the distance $h = x_2 - x_1$ between them is smaller than a certain threshold, then vehicle 1 brakes (with probability

$1 - P(\rho)$) or overtakes the ahead vehicle (with probability $P(\rho)$). The probability $P(\rho)$ is assumed to have the same dependence on the local density ρ as in Prigogine's model, see Section 1.3.1;

- if vehicle 1 is slower than the leading one and the distance $h = x_2 - x_1$ between them is larger than another threshold, then vehicle 1 accelerates;

- two constant thresholds H_A, H_B are considered to model, respectively, the acceleration scenario when h becomes larger than H_A (and $0 < v_1 < v_2 < V_{\max}$), and the braking/overtaking scenario when the distance h becomes smaller than H_B (and $0 < v_2 < v_1 < V_{\max}$);

- for each threshold $i = A, B$, the velocity v acquired by vehicle 1 after an interaction is taken on instantaneously and is given by a distribution function

$$\sigma(v, v_1, v_2; \rho) = \begin{cases} \sigma_A(v, v_1, v_2; \rho), & \text{if } v_1 < v_2, \\ \sigma_B(v, v_1, v_2; \rho), & \text{if } v_1 > v_2, \end{cases}.$$

  Since σ is a density function, for each threshold $i = A, B$, it has to fulfill

$$\int_0^{V_{\max}} \sigma_i(v, v_1, v_2; \rho) \mathrm{d}v = 1.$$

  The dependence of σ on the local density ρ allows to prescribe the post-interaction speed v as a function of the congestion level of the road;

The kinetic equation is derived by (1.5) describing the collision operator in terms of the two-particles distribution function f_2, that is the joint distribution function such that $f_2(t, x_1, v_1, x_2, v_2)$ gives a measure of the joint probability to find vehicle 1 in the state (x_1, v_1) and simultaneously vehicle 2 in the state (x_2, v_2). The collision term writes as

$$Q[f_2] = \sum_{i=A,B} G_i[f_2] - \sum_{i=A,B} L_i[f_2]$$

where $G_i[f_2]$ and $L_i[f_2]$ are respectively the gain and loss terms due to the i-th threshold. Assuming, for simplicity, two equal interaction thresholds so that $H := H_A = H_B$, the form of the gain and the loss term proposed by Klar and Wegener [49] is the following:

$$\begin{aligned} G[f_2] &= \int_0^{V_{\max}} \int_0^{V_{\max}} |v_1 - v_2| \, \sigma(v, v_1, v_2; \rho) f_2(t, x_1, v_1, x_1 + H, v_2) \mathrm{d}v_1 \mathrm{d}v_2 \\ L[f_2] &= \int_0^{V_{\max}} |v - v_2| \, \sigma(v, v_1, v_2; \rho) f_2(t, x_1, v, x_1 + H, v_2) \mathrm{d}v_2. \end{aligned} \tag{1.8}$$

Notice that the interacting vehicles are not supposed to occupy the same position in space, because of the presence of the pair distribution f_2 denoting the distribution function of vehicles at position x_1 with velocity v_1 and leading vehicles at position $x_1 + H$ with velocity v_2. In fact, recalling the above listed microscopic assumptions, interactions, and

consequently speed transitions, take place among vehicles having distance $h = H$. Therefore, the introduction of the thresholds allows to delocalize the interactions, similarly to the Enskog-like kinetic theory of dense gases.

To obtain from equations (1.8) a closed equation for the sole kinetic distribution f, see equation (1.4), we need to express the pair distribution f_2 in terms of f. To this end, a modified version of the vehicular chaos assumption introduced in [62] is used, so that

$$f_2(t, x_1, v_1, x_1 + H, v_2) = f(t, x_1, v_1) f(t, x_1 + H, v_2) k(H, \rho(t, x)) \tag{1.9}$$

where the function k weights the interactions according to the threshold H and the local congestion of the road ρ. Its presence in the expression of f_2 makes the form of the collision operator similar to Enskog's kinetic theory of a dense gas. We refer to the book of Cercignani and Lampis [14] for further information on this theory.

Thus, the modeling of the collisional operator proposed by Klar and Wegener in [49] differs from Prigogine's and Paveri Fontana's models since now they consider interacting vehicles being at different positions. In fact, the two kinetic distributions at the right hand side of (1.9) are evaluated at different points in space. Therefore, the interactions occur in a range according to the threshold H and this fact allows to anticipate traffic conditions so that the behavior of a driver is influenced by the disturbances ahead in the flow. Mathematically, in this case one observes, due to the definition of the collision operator (1.8), that in equation (1.7) the kinetic distribution function f at position x and at time t depends not only on the kinetic distribution function at position $x' \leq x$ but also on the kinetic distribution function at $x' > x$. This allows backward propagating disturbances.

Finally, the collision operator defined by (1.8) is made explicit once the expressions of the probability distributions σ_A and σ_B are given. Taking into account the above assumptions on the microscopic interactions, they write as

$$\sigma_A(v, v_1, v_2; \rho) = \frac{1}{\alpha P(\rho)(V_{\max} - v)} \chi_{[v_1, v_1 + \alpha P(\rho)(V_{\max} - v)]}(v), \quad \alpha \in [0, 1]$$

$$\sigma_B(v, v_1, v_2; \rho) = P(\rho)\delta_{v_1}(v) + (1 - P(\rho)) \frac{1}{(1 - \beta)v_2} \chi_{[\beta v_2, v_2]}(v), \quad \beta \in [0, 1]$$

where χ_I is the indicator function of the set I. The expression of σ_A means that in the case of acceleration the new speed v is assumed to be uniformly distributed in the interval $[v_1, v_1 + \alpha P(\rho)(V_{\max} - v)]$. Instead, in the case of σ_B, the new speed v can either remain unchanged with respect to the initial velocity v_1 (the delta term), or stochastically can reduce to a fraction of the velocity v_2 of the leading vehicle.

The form of the probability distributions σ_A and σ_B proposed in [49] and the comparison with our microscopic choices will be also discussed in the next chapters.

1.3.3 Reduced complexity models

As anticipated at the beginning of this section, Boltzmann-type models can be very demanding since the integro-differential equation makes it difficult to compute the time

asymptotic solution of the kinetic equation. For this reason, reduced complexity models, as lattice-Boltzmann-type models or Fokker-Planck-type models, have been proposed in the literature. These models are interesting, both from the analytical and the computational point of view, since they keep the kinetic information on traffic without requiring the evaluation of the expensive velocity integrals appearing in Boltzmann-type models.

The aim of the class of lattice-Boltzmann-type kinetic models is to take into account the granular nature of the flow of vehicles, both in space and velocity. Indeed, these models arise from the assumption that cars along a road tend to cluster, which gives granularity in space, with a nearly constant speed within each cluster, which makes also the velocity a discretely distributed variable. For a brief review on the framework that characterizes these models, we refer to Section 2.3 in which, in particular, we recall the model recently introduced by Fermo and Tosin in [25, 26] which will be taken as starting point for the derivation of our models.

In particular, we wish to recall that the spatially inhomogeneous version of Fermo and Tosin's model [25] is endowed with the backward propagating waves studied by Klar and Wegener in [49], see Section 1.3.2. However, in [25] this property is obtained by including a *flux limiter* in the expression of the transport term in the kinetic equation, thus without resort to modeling non-local interactions.

Fokker-Planck-type models

In Chapter 5 we will discuss the effects of the microscopic behaviors on the macroscopic dynamics. To this end, we need the knowledge of the time asymptotic solution of the kinetic equation as functions of the microscopic parameters which define the interaction rules among vehicles. As already anticipated, for this purpose a Boltzmann-type kinetic model is demanding. For this reason, a different approach is to derive a Fokker-Planck-type model as a result of a time scaling (the *grazing collision limit*) of the classical spatially homogeneous kinetic equation with the aim of replacing the interaction integrals appearing in the collision operator with differential operators.

Several Fokker-Planck-type models for traffic flow have been proposed in the literature, in particular to analyze the stationary solutions provided by the kinetic approach. In this case, the prototype form of a Fokker-Planck-type model is given by the following drift-diffusion equation:

$$\partial_t f(t,v) + \partial_v \left(B[f] f(t,v) - D[f] \partial_v f(t,v) \right) = 0, \tag{1.10}$$

in which the dependence of the kinetic distribution f on the space variable x is neglected, since we are dealing with spatially homogeneous problems. The operators $B[f](t,v)$ and $D[f](t,v)$ are, respectively, the so-called *braking/acceleration* and *diffusive* terms.

In [44], Illner, Klar and Materne introduced a Fokker-Planck-type model for modeling traffic flow on multilane roads. However, here we focus on the simplest version, namely we consider a single lane road, which includes the case of equation (1.10). In [44], the braking/acceleration operator B and the diffusive operator D are heuristically given and they are assumed to depend on moments of the kinetic distribution f, i.e. on macroscopic

quantities as the density ρ or the mean speed u. The underlying assumption on both operators is that drivers interact with respect to average quantities and thus no binary interaction are taken into account. The diffusive term is introduced to model the possibility of an inexact observation of the average conditions. The following example for the operators $B[f]$ and $D[f]$ is taken from [44]:

$$B[f] = \begin{cases} -c_B(v-u)^2\rho, & \text{if } v > u, \\ c_A(u-v)^2(\rho_{\max}-\rho), & \text{if } v < u \end{cases}$$

$$D[f] = \sigma(\rho, u)\,|v-u|^{\gamma}\,.$$

In the above expressions c_A and c_B are positive constants corresponding to braking and acceleration, while $\sigma(\rho, u)$ is a smooth function chosen in such a way that it vanishes rapidly for large and small values of the density ρ and of the mean speed u. Finally, γ is a positive constant such that $\gamma < 3$ in order to obtain well-defined steady states.

Compared to the formulation given in [44], the above modeling of the operators $B[f]$ and $D[f]$ assumes a zero-probability of passing. In [44], the presence of this probability allows to recover multiple equilibrium solutions and thus the multivalued structure observed in experimental data. However, the scattering of diagrams is apparent only in a small range of density values in which, moreover, at most three multiple solutions are obtained.

In [41], Herty and Pareschi, instead, derive a Fokker-Planck-type model as an asymptotic limit of a Boltzmann-type model featuring microscopic interactions in which the drivers react to the mean speed. The authors are mainly interested in establishing links between Fokker-Planck-type models based on a heuristic modeling of braking/acceleration and diffusive operators, as the model proposed in [44], and Fokker-Planck type models obtained as limits of Boltzmann-type equations, thus based on microscopic motivations for the given form of the operators. For further details, see Chapter 5 in which we will compare our Fokker-Planck-type model with the work [41]. In fact, the investigations proposed in Chapter 5 and in [85] can be considered as a natural sequel to [41] since we will focus mainly on the study of macroscopic trends of traffic by means of the fundamental diagrams

Chapter 2

Fundamental diagrams in traffic flow: the case of heterogeneous kinetic models

2.1 Motivation

Experimental studies on vehicular traffic provide data on quantities like density, flux, and mean speed of the vehicles. However, the diagrams relating these variables (the *fundamental* and *speed* diagrams) show some peculiarities not yet fully reproduced nor explained by mathematical models.

Here, we describe a multi-population kinetic model for traffic flow which draws inspiration from the ideas presented in [7] for macroscopic models, recast in the frame of discrete-velocity kinetic models [16, 20, 25, 26, 82]. These results have been published in [76]. The main goal is to study fundamental diagrams computed from moments of equilibrium solutions of the kinetic equations. In particular, considering traffic flow as a mixture of populations with different microscopic characteristics helps to explain the experimentally observed scattering of fundamental diagrams in the phase of congested traffic. With this approach, scattered data in the congested phase are naturally *predicted* by the model by taking into account the macroscopic variability of the flux and mean speed at equilibrium due to the heterogeneous composition of the "mixture". This conclusion is reached without invoking further elements of microscopic randomness of the system: for example in [26], which inspired the present model, the explanation for the scattering of data appeals to the stochasticity of the drivers' behavior and to the consequent variability of the *microscopic* speeds at equilibrium. Moreover, the models proposed here and in [25, 26] predict a phase transition between the free and the congested phases of traffic, with a sharp, but meaningful, *capacity drop* across the phase transition. For a definition of capacity drop see [88] and references therein.

We wish to stress that we do not propose a model that interpolates experimental data. Rather, we use experimental data to validate the model we propose.

In the literature, a variety of multiphase models have been already introduced in order to reflect the features of traffic, for a review see [10] and references therein. However, typically these models reproduce a too sharp capacity drop, as in [20, 44], or the information for the phase transition is prescribed a priori, as in [15] for macroscopic models. The heterogeneity of traffic flow composition is often described by considering two or more classes of drivers with different behavioral attributes, see [54, 61]; here the heterogeneity will be described by introducing two or more classes of vehicles with different physical features, as in [7] for macroscopic models. In [60] a first attempt to describe the heterogeneity of traffic in the kinetic framework is proposed. However, the model introduced in [60] takes into account a large number of microscopic differences characterizing the flow of traffic. This fact increases the model complexity making difficult the analysis, both from the theoretical and the numerical point of view. Here, we will show that considering populations which differ in only two microscopic features is sufficient to explain on the whole the structure of the experimental data.

In detail, the structure of this chapter is as follows: in Section 2.2 we briefly review the role of fundamental diagrams in vehicular traffic practice. Next, in Section 2.3, we describe the discrete-velocity kinetic model developed in [25] by focusing on its spatially homogeneous version, see [26], which represents the mathematical counterpart of the experimental setting in which traffic equilibria and fundamental diagrams are measured. In Section 2.4 we first review the multi-population macroscopic model [7] and then introduce our new two-population kinetic model, proving in particular its consistency with the original single-population model and describing how to compute equilibrium solutions. Then, in Section 2.5, we present and analyze the resulting fundamental diagrams.

2.2 Fundamental diagrams

Before discussing on the mathematical modeling of traffic flow, we present a brief description of some basic tools for the analysis of traffic problems, namely the diagrams which relate the macroscopic flux and mean speed to the vehicle density in homogeneous steady conditions. The qualitative structure of such diagrams is defined by the properties of different regimes, or *phases*, of traffic as outlined in the following.

Flux-density diagrams Also called *fundamental diagrams*, they report the flow rate of vehicles as a function of the traffic density ρ, which can be defined as the number of vehicles per kilometer (Fig. 2.1, right), or as a function of the normalized density (Fig. 2.1, left). At low traffic densities, the so-called *free phase* in which interactions among vehicles are rare, the flux grows nearly linearly with the density until a *critical density* value is reached, at which the flux takes its maximum value (*road capacity*). Beyond such a critical value traffic switches to the *congested phase*, which in [46] is defined as complementary to the free phase. The two phases may be separated by a capacity drop, across which the flux drops suddenly from its maximum value at free flow to a lower maximum in the congested phase. In this regime the flux decreases as

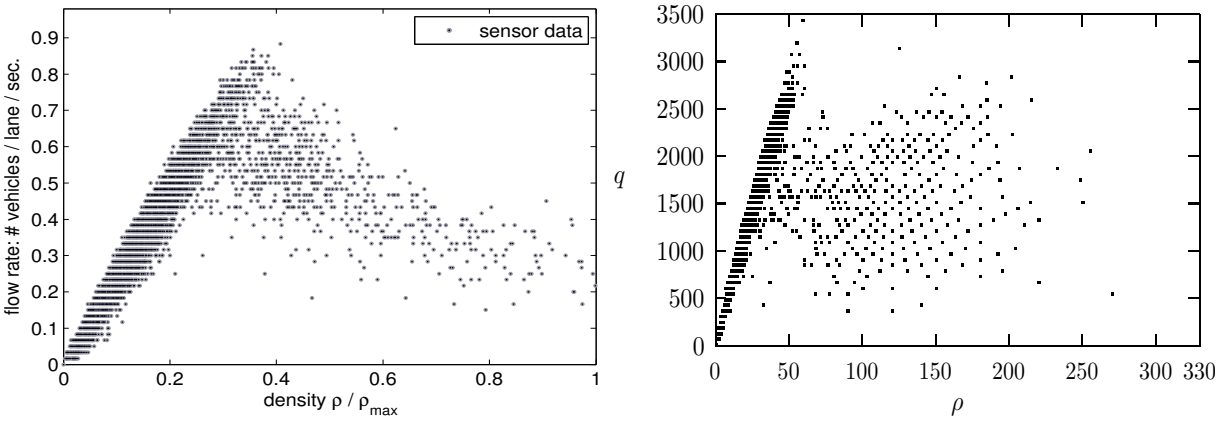

Figure 2.1: Fundamental diagrams obtained from experimental data. Left: measurements provided by the Minnesota Department of Transportation in 2003, reproduced by kind permission from Seibold et al. [79]. Right: experimental data collected in one week in Viale del Muro Torto, Roma, Italy, from [70].

the density increases. In fact interactions among vehicles are more and more frequent due to the higher packing, which causes faster vehicles to be hampered by slower ones. The formation of local slowdowns (*phantom traffic jams*) is first observed. Additional increments of the density cause a steep reduction of the flux until the so-called *traffic jam* is reached, in which the density reaches its maximum value $\rho_{\max}$, called *jam density*, and the flux is zero.

Speed-density diagrams They give the mean speed of the vehicles as a function of the local macroscopic density of traffic. In free flow conditions, vehicles travel at the maximum allowed speed (or almost the maximum), which depends on the environmental conditions (such as e.g., quality of the road, weather conditions, infrastructure), on the mechanical characteristics of the vehicles, and on the imposed speed limits. This speed, called the *free flow speed*, can be reached when there is a large distance among vehicles on the road. Conversely, in congested flow conditions vehicles travel closer to one another at a reduced speed, until the density reaches the jam density, at which vehicles stop and have zero speed.

These diagrams play an important role in the prediction of the capacity of a road and in the control of the flow of vehicles, see the studies in [1, 46].

Examples of fundamental diagrams provided by experimental measurements are shown in Fig. 2.1. They clearly exhibit the phase transition between free and congested flow: below the critical density the flux values distribute approximately on a line with positive slope, and so the flux can be regarded as a single-valued increasing function of the density with low, though nonzero, dispersion; conversely, above the critical density the flux decreases and experimental data exhibit a large scattering in the flux-density plane. In the congested phase, therefore, the flux can hardly be approximated by a single-valued function of the density. Moreover, in the plot on the right a capacity drop can also be seen.

Kinetic models of traffic flow give fundamental diagrams as stationary asymptotic solutions starting from a statistical description of microscopic interactions among vehicles. In addition, some kinetic models have proved to be able to catch a meaningful transition from the free to the congested phase of traffic without building the phase transition into the model, see [25, 26].

However, standard kinetic models do not account for the scattered data typical of the congested regime. For instance, in [38] multivalued fundamental diagrams are obtained supposing that the flow aims to stabilize around a multivalued heuristic equilibrium velocity which is not computed by the model itself. Otherwise, this characteristic of the flow is explained considering the statistical variability of driver behaviors, who may individually decide to drive at a different speed than the one resulting from the local density, see e.g., [26]. Instead, in [44] the multivaluedness of the diagrams is *naturally* obtained with a Fokker-Planck-type kinetic model but the scattered data are restricted only in a small region.

In this thesis, see [76], we propose instead a different interpretation of the scattering of the flux in congested traffic, based on the consideration that the flow along a road is naturally *heterogeneous*. That is, it is composed by different classes of vehicles with different physical and kinematic characteristics (e.g. size, maximum speed, et cetera). For this we will extend the aforementioned kinetic models [26] in order to deal with a mixture of two populations of vehicles, say cars and trucks, each described by its own statistical distribution function. The core of the model will be the statistical description of the microscopic interactions among the vehicles of the same population and of different populations, which will take into account the microscopic differences of the various types of vehicles. For the sake of simplicity, the model will be described for the case of a mixture of two populations, but it can be easily generalized to the case of several populations, see [7] for a macroscopic model and [74] or Chapter 4 for a continuous-velocity kinetic model.

2.3 A discrete kinetic model

In this section we briefly review the kinetic traffic model recently introduced in [25] for the spatially inhomogeneous case and we focus on its spatially homogeneous version [26]. This model will be the basis for our multi-population extension.

The model proposed in [25] is discrete both in space and in speed. Since in this chapter we focus on the space homogeneous case [26], we describe only the domain of the microscopic speeds, say $\mathcal{V} \subseteq [0, +\infty)$, that is

$$\mathcal{V} = \{v_1, v_2, \ldots, v_j, \ldots, v_n\},$$

where the v_j's are *speed classes* such that $0 \leq v_j < v_{j+1} \quad \forall\, j = 1, \ldots, n-1$, and $v_1 = 0$, $v_n = V_{\max}$, $V_{\max}$ being the maximum speed of a vehicle. For instance, $V_{\max}$ can be chosen as a speed limit imposed by safety regulations, or by the state of the road, or by the mechanical characteristics of the vehicles.

Recalling that in the kinetic approach we focus on a statistical description of the microscopic states of the vehicles, in the spatially homogeneous model, the microscopic state of a generic vehicle is given by $v_j \in \mathcal{V}$. Thus, in the discrete-velocity framework, the statistical distribution of vehicles is given by the time-dependent functions:

$$f_j = f_j(t) : [0,\, T_{\max}] \to [0,\, +\infty), \quad j = 1,\, \ldots,\, n,$$

i.e. $f_j(t)$ is the number of vehicles which, at time t, travel with speed v_j.

The macroscopic variables useful in the study of traffic, namely the vehicle density ρ, flux q, and mean speed u are obtained from the f_j's as statistical moments with respect to the speed. Thus, in the context of a lattice velocity framework we have

$$\rho(t) = \sum_{j=1}^{n} f_j(t), \qquad q(t) = \sum_{j=1}^{n} v_j f_j(t), \qquad u(t) = \frac{q(t)}{\rho(t)}. \tag{2.1}$$

As already mentioned in Section 2.2, the experimental diagrams are measured under flow conditions which are as much as possible homogeneous in space and stationary. Thus we study the evolution in time of $f_j(t)$ due to vehicle interactions towards equilibrium. The corresponding system of (spatially homogeneous) Boltzmann-type kinetic equations is

$$\frac{\mathrm{d}f_j}{\mathrm{d}t} = Q_j[\mathbf{f},\, \mathbf{f}], \quad j = 1,\, \ldots,\, n, \tag{2.2}$$

where Q_j is the j-th collisional operator, which describes the microscopic interactions among vehicles causing the change of v_j in time. We use the vector notation $\mathbf{f} := \{f_j\}_{j=1}^n$. Conservation of mass requires that

$$\sum_{j=1}^{n} Q_j[\mathbf{f},\, \mathbf{f}] = 0 \quad \forall\, \mathbf{f},$$

which ensures $\frac{\mathrm{d}\rho}{\mathrm{d}t} = 0$.

Stationary flow conditions mean that we are actually interested in equilibrium solutions (if any) to system (2.2), that is constant-in-time solutions $\mathbf{f}^\infty = \{f_j^\infty\}_{j=1}^n$ such that $Q_j[\mathbf{f}^\infty,\, \mathbf{f}^\infty] = 0$ for all $j = 1,\, \ldots,\, n$. In [26], the asymptotic analysis of the kinetic equation (2.2) is studied. In particular, using a result stated in [20], it is proven that $\forall \rho > 0,\ \exists !\, \mathbf{f}^\infty$. Hence equilibrium solutions are parameterized by specific values of the vehicle density ρ, which is given by the initial condition $\rho = \sum_{j=1}^n f_j(0)$. This fact allows one to define analytically the fundamental and speed diagrams of traffic by means of the following mappings:

$$\rho \mapsto \mathbf{f}^\infty \quad \Rightarrow \quad \rho \mapsto q(\rho) = \sum_{j=1}^{n} v_j f_j^\infty, \qquad \rho \mapsto u(\rho) = \frac{q(\rho)}{\rho}.$$

In particular, if for any given ρ, system (2.2) admits a unique stable equilibrium then these mappings are indeed functions of ρ; otherwise, they define multivalued diagrams. We stress that, contrary to macroscopic models, the mapping $\rho \mapsto q(\rho)$ is not based on a priori closure relations but is obtained from the large time evolution of the kinetic distribution function, as a result of microscopic vehicle interactions.

2.3.1 Modeling vehicle interactions

The operators Q_j model the microscopic interactions among vehicles. Following [25], the formalization of Q_j is based on assigning post-interaction speeds in a non-deterministic way, consistently with the intrinsic stochasticity of driver behaviors. We report here the construction of the operator Q_j, which will be extended later to the two-population case. We consider only binary interactions among vehicles, thus the collisional operator can be written as

$$Q_j[\mathbf{f},\, \mathbf{f}] = G_j[\mathbf{f},\, \mathbf{f}] - L_j[\mathbf{f}, \mathbf{f}].$$

Take

$$G_j[\mathbf{f},\, \mathbf{f}] := \sum_{h,k=1}^{n} \eta_{hk} A^j_{hk} f_h f_k \qquad \text{and} \qquad L_j[\mathbf{f}, \mathbf{f}] := f_j \sum_{k=1}^{n} \eta_{jk} f_k$$

which are the *gain* and *loss* terms, respectively. The coefficients η_{hk}, $\eta_{jk} > 0$ are the *interaction rates*, which depend on the relative speed of the interacting pairs: $\eta_{hk} = \eta(|v_k - v_h|)$ as in [16]. For simplicity, here we will assume the interaction rates independent of the pre-interaction speeds, so $\eta_{hk} \equiv \eta$ constant. The term G_j counts statistically the number of interactions which lead, in the unit time, a so-called *candidate* vehicle with speed v_h to switch to the *test* speed v_j after an interaction with a *field* vehicle with speed v_k. Conversely, the term L_j describes the loss of vehicles with test speed v_j after interactions with any field vehicle. Thus the single-population model writes as

$$\frac{\mathrm{d}f_j}{\mathrm{d}t} = \sum_{h,k=1}^{n} \eta A^j_{hk} f_h f_k - f_j \sum_{k=1}^{n} \eta f_k. \tag{2.3}$$

For each $j = 1, \ldots, n$, the matrix $\mathbf{A}^j = \{A^j_{hk}\}_{h,k=1}^n$ is called the *table of games*. It encodes the discrete probability distribution of gaining the test speed v_j:

$$A^j_{hk} = \mathrm{Prob}(v_h \to v_j | v_k,\, \rho), \qquad h,\, k,\, j = 1,\, \ldots,\, n,$$

which in the present model is further parameterized by the macroscopic density ρ so as to account for the influence of the macroscopic traffic conditions (local road congestion) on the microscopic interactions among vehicles. We stress that this is a further source of nonlinearity on the right-hand side of (2.2), besides the quadratic one typical of Boltzmann-like kinetic equations. Since for each fixed j the coefficients A^j_{hk} constitute a discrete probability distribution, they must satisfy the following conditions:

$$\left.\begin{array}{l} 0 \le A^j_{hk} \le 1 \\ \displaystyle\sum_{j=1}^{n} A^j_{hk} = 1 \end{array}\right\} \quad \forall\, h,\, k,\, j = 1,\, \ldots,\, n, \quad \forall\, \rho \in [0,\, \rho_{\max}], \tag{2.4}$$

$\rho_{\max} > 0$ being the maximum density of vehicles that can be locally accommodated on the road in bumper-to-bumper conditions. These conditions ensure mass conservation.

The table of games of model (2.3) is built appealing to the following assumptions:

Ansatz 2.1. A candidate vehicle with speed v_h can accelerate by at most one speed class at a time. However, it can decelerate by an arbitrary number of speed classes when it interacts with a field vehicle with lower speed $v_k < v_h$.

Ansatz 2.2. Let P be the probability that a candidate vehicle gets the maximum possible test speed resulting from an interaction. We assume that P is a decreasing function of the density ρ.

In more detail, we distinguish three types of interactions which determine completely the table of games.

- *Interaction with a faster field vehicle:* in this case we have $v_h < v_k$, or $h < k$. Following the interaction, we assume that the candidate vehicle can either accelerate or maintain its speed, thus:

$$A^j_{hk} = \begin{cases} 1-P & \text{if } j = h \\ P & \text{if } j = h+1 \\ 0 & \text{otherwise} \end{cases} \qquad h < k = 2, \dots, n. \tag{2.5}$$

- *Interaction with a slower field vehicle:* in this case we have $v_h > v_k$, or $h > k$. Following the interaction, we assume that the candidate vehicle can either maintain its speed, if for instance there is enough room to overtake the leading field vehicle, or decelerate to v_k and queue up, thus:

$$A^j_{hk} = \begin{cases} 1-P & \text{if } j = k \\ P & \text{if } j = h \\ 0 & \text{otherwise} \end{cases} \qquad h > k = 1, \dots, n-1. \tag{2.6}$$

  Notice that in this case P plays the role of a *probability of overtaking* as defined in [72, 73].

- *Interaction with a field vehicle with the same speed:* in this case we have $v_h = v_k$, or $h = k$. Following the interaction, we assume that the candidate vehicle can either maintain its pre-interaction speed, or accelerate to overtake the leading vehicle, or decelerate. Hence the test speed resulting from this interaction is either $v_j = v_{h+1}$ with probability P, or $v_j = v_{h-1}$ with probability P_B, or finally $v_j = v_h$ with probability $1-(P+P_B)$. Thus P_B is the *probability of braking* and it is chosen as an increasing function of ρ.

  We further distinguish three cases, in fact if the candidate vehicle is either in $v_1 = 0$ or in $v_n = V_{\max}$ then it cannot decelerate or accelerate, respectively. Thus:

$$A^j_{11} = \begin{cases} 1-P & \text{if } j = 1 \\ P & \text{if } j = 2 \\ 0 & \text{otherwise} \end{cases} \tag{2.7a}$$

$$A_{hh}^{j} = \begin{cases} P_B & \text{if } j = h-1 \\ 1-(P+P_B) & \text{if } j = h \\ P & \text{if } j = h+1 \\ 0 & \text{otherwise} \end{cases} \qquad h = 2, \ldots, n-1 \tag{2.7b}$$

$$A_{nn}^{j} = \begin{cases} P_B & \text{if } j = n-1 \\ 1-P_B & \text{if } j = n \\ 0 & \text{otherwise} \end{cases} \tag{2.7c}$$

Note that with these choices the candidate vehicle can accelerate at most by one speed class, which amounts to bounding the maximum acceleration, see [53]. In contrast, the deceleration is not bounded and this reflects the hypothesis that drivers behave differently in acceleration and deceleration, see the definition of *traffic hysteresis* in [88] and references therein. Moreover, in the third case we use two different probabilities for the acceleration and deceleration interactions, as proposed also in [36].

Once the interaction rules are assigned, by computing the evolution towards equilibrium of a given initial condition corresponding to a fixed value of ρ we obtain the fundamental and speed diagrams depicted in Fig. 2.2 for three different values of the number n of speed classes. For $\rho < \frac{1}{2}\rho_{\max}$ we recognize the free phase of traffic, in which the flux is an increasing linear function of the density. Conversely, for $\rho > \frac{1}{2}\rho_{\max}$ we find the congested phase, in which the specific form of the diagrams predicted by the model depends on the number n of speed classes. Note that for $n = 3$ and $n = 4$ the phenomenon of capacity drop becomes apparent.

These results confirm that the kinetic approach is able to catch successfully the phase transition in traffic flow as a consequence of more elementary microscopic interaction rules. In particular, such a phase transition need not be postulated a priori through heuristic closures of the flux as a given function of the density. Nevertheless, model (2.3) still provides a single-valued density-flux relationship. In fact, as shown in [26], for all $\rho \in [0,\, \rho_{\max}]$ there exists a unique stable and attractive equilibrium $\mathbf{f}^{\infty} = \{f_j^{\infty}\}_{j=1}^{n}$. Consequently, the flux q at equilibrium is uniquely determined by the initial density ρ, which does not explain the scattered data of the experimental diagrams.

2.3.2 Probability of acceleration

The choice of P is crucial in our model and it influences the qualitative structure of the fundamental diagrams. As in most traffic models, we will assume that accelerating is less likely in high density traffic, so P is chosen as a decreasing function of ρ. Conversely, the probability of braking, which is either P_B or $1 - P$, will be an increasing function of ρ. Following [26] we will choose, unless otherwise stated,

$$P = \alpha\left(1 - \frac{\rho}{\rho_{\max}}\right), \quad P_B = (1-\alpha)\,\frac{\rho}{\rho_{\max}}, \quad 0 \le \alpha \le 1, \tag{2.8}$$

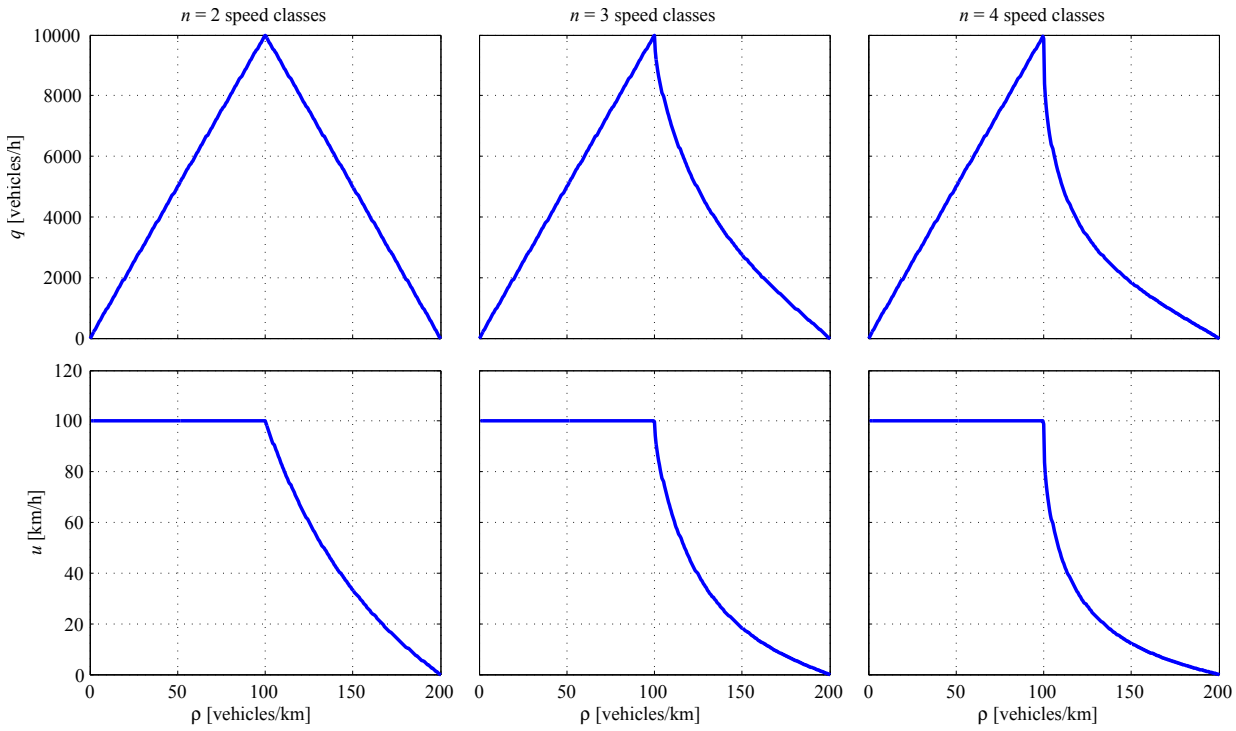

Figure 2.2: Top row: fundamental diagrams, bottom row: speed diagrams obtained from model (2.3) with $n = 2, 3, 4$ speed classes, maximum density $\rho_{\max} = 200$ vehicles/km, and uniformly distributed microscopic speeds in the interval [0, 100 km/h].

where the coefficient $\alpha \in [0, 1]$ can be thought of as a parameter describing the environmental conditions, for instance road or weather conditions, with $\alpha = 0$ and $\alpha = 1$ standing for prohibitive and optimal conditions, respectively.

The ansatz (2.8), which is the simplest choice, is chosen by several other authors, see [36, 48] and in particular the modeling of P is inspired by the standard Prigogine's assumption [72, 73]. Clearly, other choices are possible, see below and in particular Section 4.4 in which we analyze in detail more sophisticated alternatives. Further, P and P_B can also depend on the local states, i.e. $P = P(\rho, v_h, v_k)$ making thus P function also of the relative speeds of interacting vehicles. This would made the model richer, but our results show that the simple choice $P = P(\rho)$ already accounts for the complexity of macroscopic data. Thus, unless otherwise stated, in the following we will take P defined by (2.8) and $\alpha = 1$. We observe that in this case $P_B = 0$, i.e. the probability of braking is zero when the two interacting vehicles travel at the same velocity, cf. (2.7b)-(2.7c).

In Figure 2.2 the diagrams of traffic are computed by taking P and P_B as in (2.8). The value of $\rho_c = \frac{1}{2}\rho_{\max}$, in which the transition between the two phases of traffic occurs, is due to the particular choice of P. If we take instead

$$P = \alpha \left(1 - \left(\frac{\rho}{\rho_{\max}}\right)^{\gamma}\right), \quad \gamma > 0 \tag{2.9}$$

then the critical density ρ_c decreases when $\gamma < 1$, see Figure 2.8 in Section 2.5, and the

discussion in Section 2.4.3. As proved in [26], ρ_c is the value of the density at which a bifurcation of equilibria occurs, representing thus the mathematical counterpart of the physical phase transition mentioned in Section 2.2.

2.4 Two-population models

Starting from the kinetic approach discussed in the previous section, we now introduce a model which treats traffic as a mixture of different types of vehicles with different physical and kinematic characteristics. As far as we know, this is the first attempt to account for the heterogeneity of traffic in a kinetic model and, at the same time, to propose a deep analysis of the model itself which allows us to study in details the properties of the traffic flow by means of fundamental diagrams.

We will see that the proposed structure allows one to account for the nature of scattered data in experimental diagrams. For the sake of simplicity we will consider a two-population model, which can be easily extended to more complex mixtures, see [74] or Chapter 4.

Multi-population models of vehicular traffic are already available in the literature, e.g. see [7, 54, 61]. Here we start from [7], in which the authors describe an M-population generalization of the Lighthill-Whitham-Richards macroscopic traffic models [59, 77], that we briefly illustrate in the case of $M = 2$ species as an introduction to the forthcoming kinetic approach.

Let $N_{\mathsf{p}}(t, x)$ be the number of vehicles of the p-th population, $\mathsf{p} = 1, 2$, contained in a stretch of road of length L (typically L will be 1 kilometer). The model consists of two coupled one-dimensional conservation laws:

$$\begin{cases} \partial_t \rho_1 + \partial_x F_1(\rho_1,\, \rho_2) = 0 \\ \partial_t \rho_2 + \partial_x F_2(\rho_1,\, \rho_2) = 0 \end{cases} \tag{2.10}$$

where $\rho_{\mathsf{p}} = \rho_{\mathsf{p}}(t,\, x) = N_{\mathsf{p}}(t, x)/L$ is the macroscopic density of the p-th species, $F_{\mathsf{p}}(\rho_1,\, \rho_2) = \rho_{\mathsf{p}} v_{\mathsf{p}}(\rho_1,\, \rho_2)$ its flux function, and $v_{\mathsf{p}}(\rho_1,\, \rho_2)$ is the speed-density relation, which describes the attitude of drivers of the p-th population to change speed on the basis of the local values of $\rho_1,\, \rho_2$. The model is based on the idea that the p-th population is characterized by vehicles with length $l_{\mathsf{p}} > 0$ and maximum velocity $V_{\mathsf{p}} > 0$. Then, one can define the *fraction of road occupancy* as the dimensionless quantity

$$s := \rho_1 l_1 + \rho_2 l_2, \qquad 0 \le s \le 1,$$

and consider the following extension of the Greenshields' speed-density relation [32]:

$$v_{\mathsf{p}}(\rho_1,\, \rho_2) = (1 - s)\, V_{\mathsf{p}}, \quad \mathsf{p} = 1,\, 2.$$

With these choices, system (2.10) becomes

$$\begin{cases} \partial_t \rho_1 + \partial_x(\rho_1(1 - s)V_1) = 0 \\ \partial_t \rho_2 + \partial_x(\rho_2(1 - s)V_2) = 0 \end{cases} \tag{2.11}$$

with fluxes $F_{\mathsf{p}}(\rho_1, \rho_2) = \rho_{\mathsf{p}}(1-s)V_p$. We notice that the total flux $F_1 + F_2 = (1-s)(\rho_1 V_1 + \rho_2 V_2)$ is not a one-to-one function of the fraction of road occupancy s, as there might exist different pairs (ρ_1, ρ_2) giving rise to the same value of s and nevertheless to different total fluxes. This is possible provided $l_1 \neq l_2$ or $V_1 \neq V_2$.

2.4.1 A two-population kinetic model

In constructing our two-population kinetic model we confine ourselves to the spatially homogeneous case, in order to focus on the study of fundamental diagrams. To fix ideas, we identify the two classes of vehicles with "cars" (C) and "trucks" (T), respectively. Roughly speaking, the physical and kinematic differences between them consist in that cars are shorter and faster than trucks, therefore $l^C \leq l^T$ and $V^C_{\max} \geq V^T_{\max}$. Clearly, other choices are possible, see Section 2.5 and Chapter 4.

Notation. We adopt a compact notation, which makes use of two indices

$$\mathsf{p} \in \{C, T\}, \qquad \mathsf{q} = \neg\, \mathsf{p}$$

to label various quantities referred to either population of vehicles.

We assume that the discrete spaces of microscopic speeds for cars and trucks, $\mathcal{V}^C$, $\mathcal{V}^T$, respectively, are such that $\mathcal{V}^T \subseteq \mathcal{V}^C$, i.e. the speeds accessible to trucks are a subset of those accessible to cars. For simplicity, we take $\mathcal{V}^C$ as an equispaced lattice of speeds, i.e.

$$\mathcal{V}^C = \left\{ v_j = \frac{j-1}{n^C - 1} V_{\max}, \quad 1 \leq j \leq n^C \right\},$$

where n^C is the number of speed classes for cars, then we choose $\mathcal{V}^T = \{v_j\}_{j=1}^{n^T}$ with $n^T \leq n^C$. In this way the maximum speed of cars is $V^C_{\max} = V_{\max}$, whereas the maximum speed of trucks is $V^T_{\max} = \frac{n^T-1}{n^C-1} V_{\max} \leq V_{\max}$.

On the discrete space $\mathcal{V}^{\mathsf{p}}$ we introduce the kinetic distribution function

$$f^{\mathsf{p}}_j = f^{\mathsf{p}}_j(t) : [0, T_{\max}] \to [0, +\infty), \quad \mathsf{p} \in \{C, T\}, \quad j = 1, \ldots, n^{\mathsf{p}},$$

which gives the statistical distribution of p-vehicles traveling with speed v_j at time t. The macroscopic observable quantities referred to such a class of vehicles are recovered as (cf. (2.1))

$$\rho^{\mathsf{p}}(t) = \sum_{j=1}^{n^{\mathsf{p}}} f^{\mathsf{p}}_j(t), \qquad q^{\mathsf{p}}(t) = \sum_{j=1}^{n^{\mathsf{p}}} v_j f^{\mathsf{p}}_j(t), \qquad u^{\mathsf{p}}(t) = \frac{q^{\mathsf{p}}(t)}{\rho^{\mathsf{p}}(t)}. \tag{2.12}$$

We model the evolution of the f^{p}_j's by means of the following equation

$$\frac{\mathrm{d} f^{\mathsf{p}}_j}{\mathrm{d}t} = Q^{\mathsf{p}}_j \left[\mathbf{f}^{\mathsf{p}}, (\mathbf{f}^{\mathsf{p}}, \mathbf{f}^{\mathsf{q}}) \right], \quad j = 1, \ldots, n^{\mathsf{p}} \tag{2.13}$$

where the term $Q^{\mathsf{p}}_j [\mathbf{f}^{\mathsf{p}}, (\mathbf{f}^{\mathsf{p}}, \mathbf{f}^{\mathsf{q}})]$ describes the interactions of p-vehicles with all other vehicles, in which, as a result, the p vehicle assumes the velocity v_j. Since we consider only

binary interactions, we can follow an approach frequently used for mixtures of two gases in kinetic theory, see e.g., [13, 33, 34], which consists in writing the collisional operator as the sum of two terms:

$$Q_j^{\mathsf{p}}\left[\mathbf{f}^{\mathsf{p}},\,(\mathbf{f}^{\mathsf{p}},\,\mathbf{f}^{\mathsf{q}})\right] = Q_j^{\mathsf{pp}}[\mathbf{f}^{\mathsf{p}},\,\mathbf{f}^{\mathsf{p}}] + Q_j^{\mathsf{pq}}[\mathbf{f}^{\mathsf{p}},\,\mathbf{f}^{\mathsf{q}}],\quad j=1,\,\dots,\,n^{\mathsf{p}}. \tag{2.14}$$

In particular, the term $Q_j^{\mathsf{pp}}[\mathbf{f}^{\mathsf{p}},\,\mathbf{f}^{\mathsf{p}}]$ accounts for *self-interactions* within the population p, i.e., interactions in which p-vehicles play also the role of field vehicles. Conversely, the term $Q_j^{\mathsf{pq}}[\mathbf{f}^{\mathsf{p}},\,\mathbf{f}^{\mathsf{q}}]$ accounts for *cross-interactions* between the two populations. Following the same logic underlying the single-population model, cf. Section 2.3.1, each term is written as a balance of gain and loss contributions:

$$\begin{aligned} Q_j^{\mathsf{pp}}[\mathbf{f}^{\mathsf{p}},\,\mathbf{f}^{\mathsf{p}}] &= \sum_{h,k=1}^{n^{\mathsf{p}}} \eta_{hk}^{\mathsf{p}} A_{hk}^{\mathsf{p},j} f_h^{\mathsf{p}} f_k^{\mathsf{p}} - f_j^{\mathsf{p}} \sum_{k=1}^{n^{\mathsf{p}}} \eta_{jk}^{\mathsf{p}} f_k^{\mathsf{p}} \\ Q_j^{\mathsf{pq}}[\mathbf{f}^{\mathsf{p}},\,\mathbf{f}^{\mathsf{q}}] &= \sum_{h=1}^{n^{\mathsf{p}}}\sum_{k=1}^{n^{\mathsf{q}}} \eta_{hk}^{\mathsf{pq}} B_{hk}^{\mathsf{pq},j} f_h^{\mathsf{p}} f_k^{\mathsf{q}} - f_j^{\mathsf{p}} \sum_{k=1}^{n^{\mathsf{q}}} \eta_{jk}^{\mathsf{pq}} f_k^{\mathsf{q}} \end{aligned} \qquad j=1,\,\dots,\,n^{\mathsf{p}}, \tag{2.15}$$

where $\mathbf{A}^{\mathsf{p},j}$, $\mathbf{B}^{\mathsf{pq},j}$, $j=1,\,\dots,\,n^{\mathsf{p}}$, are the self-interaction and cross-interaction tables of games, respectively. Since the coefficients of the two tables of games model the transition probabilities, we require that

$$\begin{aligned} &0 \le A_{hk}^{\mathsf{p},j},\, B_{hk}^{\mathsf{pq},j} \le 1, \quad \forall\, h,\, k,\, j,\, \mathsf{p},\, \mathsf{q} \\ &\sum_{j=1}^{n^{\mathsf{p}}} A_{hk}^{\mathsf{p},j} = \sum_{j=1}^{n^{\mathsf{p}}} B_{hk}^{\mathsf{pq},j} = 1, \quad \forall\, h,\, k,\, \mathsf{p},\, \mathsf{q} \end{aligned}$$

so that for each h, k fixed, the coefficients $A_{hk}^{\mathsf{p},j}$ and $B_{hk}^{\mathsf{pq},j}$ with $j=1,\dots,\mathsf{p}$ form indeed discrete probability densities. This ensures that

$$\sum_{j=1}^{n^{\mathsf{p}}} Q_j^{\mathsf{p}}[\mathbf{f}^{\mathsf{p}},\,\mathbf{f}^{\mathsf{q}}] = \sum_{j=1}^{n^{\mathsf{p}}} Q_j^{\mathsf{pp}}[\mathbf{f}^{\mathsf{p}},\,\mathbf{f}^{\mathsf{p}}] + \sum_{j=1}^{n^{\mathsf{p}}} Q_j^{\mathsf{pq}}[\mathbf{f}^{\mathsf{p}},\,\mathbf{f}^{\mathsf{q}}] = 0,$$

whence from (2.13) mass conservation for each species is obtained:

$$\frac{\mathrm{d}}{\mathrm{d}t}\sum_{j=1}^{n^{\mathsf{p}}} f_j^{\mathsf{p}} = \frac{\mathrm{d}\rho^{\mathsf{p}}}{\mathrm{d}t} = 0.$$

Finally, the two-population model resulting from (2.13)–(2.15) can be written as

$$\frac{\mathrm{d}f_j^{\mathsf{p}}}{\mathrm{d}t} = \sum_{h,k=1}^{n^{\mathsf{p}}} \eta_{hk}^{\mathsf{p}} A_{hk}^{\mathsf{p},j} f_h^{\mathsf{p}} f_k^{\mathsf{p}} + \sum_{h=1}^{n^{\mathsf{p}}}\sum_{k=1}^{n^{\mathsf{q}}} \eta_{hk}^{\mathsf{pq}} B_{hk}^{\mathsf{pq},j} f_h^{\mathsf{p}} f_k^{\mathsf{q}} - f_j^{\mathsf{p}} \left(\sum_{k=1}^{n^{\mathsf{p}}} \eta_{jk}^{\mathsf{p}} f_k^{\mathsf{p}} + \sum_{k=1}^{n^{\mathsf{q}}} \eta_{jk}^{\mathsf{pq}} f_k^{\mathsf{q}} \right), \tag{2.16}$$

for each $j=1,\,\dots,\,n^{\mathsf{p}}$.

Here, the *interaction rates* η_{hk}^{p}, η_{hk}^{pq} may depend on the type of interacting vehicles and on the relative speeds between the vehicles, but, for the sake of simplicity, in the following we will assume that they are constant, let $\eta = \eta_{hk}^{\mathsf{p}} = \eta_{hk}^{\mathsf{pq}}$. In particular, in all numerical tests, since we are interested in equilibrium solutions, η will be taken equal to 1 without loss of generality.

Remark 2.3. In [20], it is proven that for a single-population, if $f_j(0) \geq 0 \ \forall j$, then $f_j(t) \geq 0$ for all times, and the equilibrium distribution $\mathbf{f}^\infty$ is uniquely determined by the initial condition. Here, our numerical evidence suggests that the same properties are inherited also by the multi-population model when the well balanced scheme of Section 2.4.2 is used. This fact can also be proven, see [74] or Section 4.3.2.

Modeling self- and cross-interactions

The total number of p-vehicles present in a stretch of road of length $L > 0$ is $N^\mathsf{p} = L \sum_{j=1}^{n^\mathsf{p}} f_j^\mathsf{p}$. Recall that $l^\mathsf{p} > 0$ is the characteristic length of p-vehicles, therefore the total space occupied by population p along the road is $N^\mathsf{p} l^\mathsf{p}$, while the total space occupied by all vehicles is $S = \sum_{\mathsf{p}\in\{C,T\}} N^\mathsf{p} l^\mathsf{p}$. Ultimately, the *fraction of road occupancy* over the length L is

$$s := \frac{S}{L} = \sum_{\mathsf{p}\in\{C,T\}} \frac{N^\mathsf{p}}{L} l^\mathsf{p} = \sum_{\mathsf{p}\in\{C,T\}} \left(\sum_{j=1}^{n^\mathsf{p}} f_j^\mathsf{p} \right) l^\mathsf{p} = \sum_{\mathsf{p}\in\{C,T\}} \rho^\mathsf{p} l^\mathsf{p}. \tag{2.17}$$

Let $\rho^\mathsf{p}_{\max}$ be the maximum density of vehicles of the p-th population, which is obtained when the road is completely filled and $\rho^\mathsf{q} = 0$. Obviously, given l^C, l^T, the admissible pairs of densities $(\rho^C, \rho^T) \in [0, \rho^C_{\max}] \times [0, \rho^T_{\max}]$ are those such that $0 \leq s \leq 1$.

Notice that $\rho^\mathsf{p}_{\max} = \frac{1}{l^\mathsf{p}}$, therefore s can be rewritten as

$$s = \sum_{\mathsf{p}\in\{C,T\}} \frac{\rho^\mathsf{p}}{\rho^\mathsf{p}_{\max}}.$$

From this expression it is clear that s is the natural generalization of the term $\frac{\rho}{\rho_{\max}}$ appearing in the probabilities P, P_B of the single-population model, cf. Section 2.3.1. Therefore we will assume that in the two-population model the transition probabilities depend on s. In other words, following the same logic of the single-population case, the elements of the table of games depend on the local state of occupancy of the road, which, when more than one population is present, is given by s. More precisely, P is a decreasing function of s, while P_B is an increasing function of s. Following (2.8), the simplest choice is

$$P = \alpha(1 - s), \qquad P_B = (1 - \alpha)s. \tag{2.18}$$

Other choices are possible, as in the case of the γ-law (2.9), see Section 2.4.3 and Fig. 2.8, or Section 4.4. It would also be possible to consider different reactive behaviors in the two populations. But the simplest choice, which, as we will see, results in a realistic macroscopic behavior, is to suppose that both types of vehicles react in the same way to the single parameter which accounts for the state of occupation of the road, which is s. The result of this ansatz is that the tables of games differ only in their dimensions.

For the matrices $\mathbf{A}^{\mathsf{p},j}$ we use the same construction as in (2.5)–(2.7c), because they express self-interactions within either population of vehicles regardless of the presence of the other population. The only difference is that they are $n^\mathsf{p} \times n^\mathsf{p}$ matrices, hence their dimensions change depending on the specific population.

The tables of games $\mathbf{B}^{\mathsf{pq},j}$ are instead $n^{\mathsf{p}} \times n^{\mathsf{q}}$ rectangular matrices, therefore we need to slightly revise the basic interaction rules of the single-population model in order to take into account the different maximum speeds of the two populations in the description of the speed transitions.

The table $\mathbf{B}^{CT,j}$ gives the probability distribution that candidate cars switch to the test speed v_j upon interacting with field trucks. The coefficients $B^{CT,j}_{hk}$ are constructed as in (2.5)–(2.7c), considering however that the case (2.7b) applies only for $h = 2, \ldots, n^T \leq n^C$ and that the case (2.7c) applies only if $n^T = n^C$. Thus the matrices $\mathbf{B}^{CT,j}$ are $n^T \times n^C$.

Conversely, the table $\mathbf{B}^{TC,j}$ gives the probability distribution that candidate trucks switch to the test speed v_j upon interacting with field cars. If the candidate truck is faster than the field car then the coefficient $B^{TC,j}_{hk}$ is constructed as in (2.6). Instead, when interactions involve also accelerations it is necessary to consider that the candidate truck might not be able to increase its speed if it is already traveling at its maximum possible velocity v_{n^T}, which, unless $n^T = n^C$, is in general smaller than $V_{\max}$. In other words, in the case (2.5) the option of accelerating may not apply. Hence for candidate trucks traveling at speed v_{n^T} which encounter faster field cars, i.e., cars traveling at speed v_k with $k = n^T + 1, \ldots, n^C$, we modify the transition probabilities (2.5) as

$$B^{TC,j}_{n^T k} = \begin{cases} 1 & \text{if } j = n^T \\ 0 & \text{otherwise,} \end{cases} \qquad k > n^T.$$

Notice instead that the other cases which include an acceleration, namely (2.7a) and (2.7b), can be borrowed from the single-population model without modifications.

Interestingly, model (2.16) along with the tables of games discussed above satisfies an *indifferentiability principle* similar to the one valid for kinetic models of gas mixtures, see e.g., [3]: when all the species composing the gas are identical one recovers the equations of a single-component gas. In the present case, the indifferentiability principle can be stated as follows:

Theorem 2.4 (Indifferentiability principle). – *Assume that the two types of vehicles are identical, i.e., they have the same physical and kinematic characteristics, and f^{p}_j exists $\forall\, \mathsf{p} \in \{C, T\}$, $\forall\, j$. Then the total distribution function*

$$f_j := \sum_{\mathsf{p} \in \{C,T\}} f^{\mathsf{p}}_j \tag{2.19}$$

obeys the evolution equations of the single-population model (2.3).

Proof. If the two types of vehicles are the same we have $l^C = l^T =: l$, $\rho^C_{\max} = \rho^T_{\max} = \frac{1}{l} =: \rho_{\max}$. It follows

$$s = \frac{\rho^C + \rho^T}{\rho_{\max}} = \frac{\rho}{\rho_{\max}}.$$

Since $\mathcal{V}^T \subseteq \mathcal{V}^C$, if the maximum speed is the same then $n^C = n^T := n$ and $\mathcal{V}^T = \mathcal{V}^C$. This implies $\mathbf{A}^{\mathsf{p},j} = \mathbf{B}^{\mathsf{pq},j} = \mathbf{A}^j$, the latter being the table of games of the single-population

model, cf. Section 2.3.1. Further, since the two populations are identical, the interaction rates are the same. So taking these facts into account and summing (2.16) over p yields

$$\frac{\mathrm{d}}{\mathrm{d}t}\sum_{\mathsf{p}\in\{C,T\}} f_j^{\mathsf{p}} = \sum_{h,k=1}^{n} \eta_{hk} A_{hk}^j \left(\sum_{\mathsf{p}\in\{C,T\}} f_h^{\mathsf{p}}\right)\left(f_k^{\mathsf{p}} + f_k^{\mathsf{q}}\right) - \left(\sum_{\mathsf{p}\in\{C,T\}} f_j^{\mathsf{p}}\right)\sum_{k=1}^{n}\eta_{jk}\left(f_k^{\mathsf{p}} + f_k^{\mathsf{q}}\right),$$

whence, using the definition (2.19), we have

$$\frac{\mathrm{d}f_j}{\mathrm{d}t} = \sum_{h,k=1}^{n} \eta_{hk} A_{hk}^j f_h f_k - f_j \sum_{k=1}^{n} \eta_{jk} f_k,$$

which concludes the proof. ■

Remark 2.5. In [3] the indifferentiability principle is proved for a model featuring a single collision operator, which hinders the description of cross-interactions among particles of different species in the mixture. In more standard models for gas mixtures the collision terms are separate, as in our case, but the indifferentiability principle holds only at equilibrium. Here, instead, Theorem 2.4 holds at all times, moreover without having to merge the two collision terms into one.

2.4.2 A well-balanced formulation for computing equilibria

Our numerical evidence suggests that, for any pair of densities $(\rho^C, \rho^T) \in [0, \rho_{\max}^C] \times [0, \rho_{\max}^T]$, with $0 \le s \le 1$, all initial distributions $(\mathbf{f}^C(0) \ge 0, \mathbf{f}^T(0) \ge 0)$ such that $\sum_{j=1}^{n^{\mathsf{p}}} f_j^{\mathsf{p}}(0) = \rho^{\mathsf{p}}$, $\mathsf{p} \in \{C, T\}$, converge in time to the same pair of equilibrium distributions $(\mathbf{f}^{\infty,C}, \mathbf{f}^{\infty,T})$, which is therefore uniquely determined by ρ^C and ρ^T. The proof of this and other analytical properties can be found in [74] and in Section 4.3.2. To get the correct equilibrium, however, it is important to devise a well balanced numerical scheme. As we will see, round-off error can drive the solution to spurious equilibrium states, if the model is not integrated properly.

Under the simplifying assumption $\alpha = 1$, in [26] the analytic expressions of stable equilibria for the single-population model (2.3) are computed. In the general case, it is necessary to integrate numerically in time the system of ODEs (2.16) until steady state is reached.

It is worth pointing out that in [26] equilibria are studied by rewriting the loss term $-f_j \sum_{k=1}^{n} f_k$ of (2.3) in the analytically equivalent form $-\rho f_j$. This allows one to take advantage of the fact that ρ is indeed a parameter of system (2.3) fixed by the initial condition, since it is constant in time. However, such a simplification cannot be carried out when the system is integrated numerically, because of instabilities triggered by round-off errors.

For the sake of simplicity, we illustrate this phenomenon for the single-population model (2.3) but our considerations apply to the two-population model (2.16) as well. For

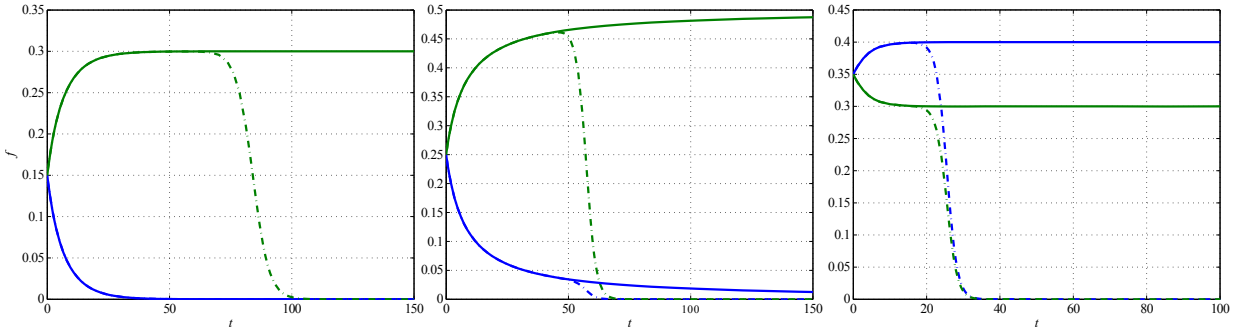

Figure 2.3: Solution to the spatially homogeneous problem for the single-population model obtained with (continuous line) and without (dashed line) the well-balanced formulation (2.20a). Left $\rho = 0.3$, center $\rho = 0.5$, right $\rho = 0.7$.

this purpose, we consider the numerical approximation of the following two analytically equivalent formulations of the single-population model:

$$\frac{\mathrm{d}f_j}{\mathrm{d}t} = \sum_{h,k=1}^{n} A^j_{hk} f_h f_k - f_j \sum_{k=1}^{n} f_k \tag{2.20a}$$

$$\frac{\mathrm{d}f_j}{\mathrm{d}t} = \sum_{h,k=1}^{n} A^j_{hk} f_h f_k - \rho f_j, \tag{2.20b}$$

where the first, which we will call *well-balanced*, leads to the computation of the correct equilibria while the second does not preserve stationary solutions and possibly leads to a violation of mass conservation. The context is similar to the construction of well-balanced numerical schemes for balance laws, where particular care is needed in order to preserve stationary solutions at the discrete level, see e.g., [57, 63, 64] and references therein.

Let $y(t) = \sum_{j=1}^{n} f_j(t)$. Summing over j both sides of (2.20a) yields $\frac{\mathrm{d}y}{\mathrm{d}t} = 0$ as expected, while the same operation performed on (2.20b) gives

$$\frac{\mathrm{d}y}{\mathrm{d}t} = (y - \rho)y.$$

In this case y is in general not constant in time and moreover two equilibria exist, $y_1^\infty = 0$ and $y_2^\infty = \rho$, where the first is stable and attractive, whereas the second is unstable. This means that mass conservation $y(t) = \rho$ holds for all t if and only if $y(0) = \rho$ and y is computed without round-off. Otherwise, any small perturbation will drive y away from the unstable equilibrium $y_2^\infty = \rho$ towards the stable equilibrium $y_1^\infty = 0$ and mass conservation fails.

Figure 2.3 shows the results of the numerical integration of the two equations (2.20a), (2.20b) in the simple case with $n = 2$ speed classes and $\alpha = 1$, starting from initial conditions for which the density is $\rho = 0.3$, $\rho = 0.5$, or $\rho = 0.7$ respectively. As proved in [26], the correct equilibrium distribution is $\mathbf{f}^\infty = (0,\, \rho)$ for $\rho \leq 0.5$, but from the first two panels of Fig. 2.3 it can be seen that only the solution of (2.20a) converges to such an equilibrium, while (2.20b) is attracted toward the state $(0,\, 0)$ which violates mass conservation. For

$0.5 < \rho < 1$ the correct equilibrium distribution $\mathbf{f}^\infty$ consists instead of two strictly positive values, which once again are reached only by the numerical solution of the well-balanced formulation (2.20a) as it is evident from the third panel of Fig. 2.3.

2.4.3 Transition from free to congested phase

In this section, we compute the value of s which determines the transition from the free to the congested phase. For this purpose, we will compute the equilibria of the system (2.16) in the free flow phase and we show that the phase transition corresponds to a bifurcation of equilibrium solutions. Our goal is to investigate analytically the main characteristics of the fundamental diagrams resulting from our model. In particular, using the equilibria of the sum of the two distribution functions, we compute the value of occupied space, the *critical space* s_c, at which the transition from the free to the congested phase occurs, and we will see how s_c depends on the choice of the probability P.

In order to compute the equilibria, we need the explicit expression of the interaction matrices. We will write the table of games explicitly for the γ-law (2.9), with $\alpha = 1$. Thus we have

$$P = 1 - s^\gamma, \qquad P_B = 0.$$

As a result, the structure of the tables of games is considerably simplified, nevertheless the wealth of information which can be extracted from the model is still surprising. Note also the sparsity pattern of the matrices $\mathbf{A}^{\mathsf{p},j}$, $\mathbf{B}^{\mathsf{pq},j}$, which permits a fast evaluation of the collision terms in (2.13).

Let $R := 1 - P$. We report only the non zero elements, drawing a circle around the elements which belong to the j-th row and column of each of the interaction matrices, $\mathbf{A}^{\mathsf{p},j}$ and $\mathbf{B}^{\mathsf{pq},j}$ respectively. Inside the circle we indicate the value of the corresponding element.

Concerning the self-interaction table of games we have

$$\mathbf{A}^{\mathsf{p},1} = \begin{bmatrix} \textcircled{R} & \textcircled{R} & \textcircled{R} & \cdots & \textcircled{R} \\ \textcircled{R} & & & & \\ \textcircled{R} & & & & \\ \vdots & & & & \\ \textcircled{R} & & & & \end{bmatrix}, \qquad \mathbf{A}^{\mathsf{p},n^\mathsf{p}} = \begin{bmatrix} & & & & \textcircled{0} \\ & & & & \textcircled{0} \\ & & & & \vdots \\ & & & P & \textcircled{P} \\ \textcircled{P} & \cdots & \textcircled{P} & \textcircled{P} & \textcircled{1} \end{bmatrix},$$

while the general expression for $1 < j < n^\mathsf{p}$ is

$$\mathbf{A}^{\mathsf{p},j} = \begin{bmatrix} & & & \textcircled{0} & \\ & & & \vdots & \\ & & P & \textcircled{P} \cdots & P \\ \textcircled{P} & \cdots & \textcircled{P} & \textcircled{R} \cdots & \textcircled{R} \\ & & & \textcircled{R} & \\ & & & \vdots & \\ & & & \textcircled{R} & \end{bmatrix}.$$

These matrices are all $n^{\mathsf{p}} \times n^{\mathsf{p}}$. The cross-interaction matrices $\mathbf{B}^{CT,j}$ between cars (candidates) and trucks (fields) have the same structure as the $\mathbf{A}^{\mathsf{p},j}$'s, apart from being rectangular of dimensions $n^C \times n^T$. Differences however arise for $j \geq n^T$, for example:

$$\mathbf{B}^{CT,n^T} = \begin{bmatrix} & & & \textcircled{0} \\ & & & \vdots \\ & & P & \textcircled{P} \\ \textcircled{P} & \cdots & \textcircled{P} & \textcircled{R} \\ & & & \textcircled{R} \\ & & & \vdots \\ & & & \textcircled{R} \end{bmatrix}, \qquad \mathbf{B}^{CT,n^T+1} = \begin{bmatrix} & & & P \\ \textcircled{P} & \cdots & \cdots & \textcircled{P} \\ & & & \end{bmatrix}$$

and in general

$$\mathbf{B}^{CT,j} = \begin{bmatrix} & & & \\ & & & \\ \textcircled{P} & \cdots & \cdots & \textcircled{P} \\ & & & \end{bmatrix}, \quad j > n^T + 1.$$

Finally, the cross-interaction matrices $\mathbf{B}^{TC,j}$ between trucks (candidates) and cars (fields) are $n^T \times n^C$. They can in turn be easily derived from the $\mathbf{A}^{\mathsf{p},j}$'s, the only different case being the one for $j = n^T$:

$$\mathbf{B}^{TC,n^T} = \begin{bmatrix} & & & \textcircled{0} & & \\ & & & \vdots & & \\ & & P & \textcircled{P} & \cdots & P \\ \textcircled{P} & \cdots & \textcircled{P} & \textcircled{1} & \textcircled{1} & \textcircled{1} \end{bmatrix}.$$

We will assume that the distribution functions are non negative in time provided $f_j^{\mathsf{p}}(0) \geq 0, \forall j$. Our numerical evidence supports this assumption, but see also [74] or Theorem 4.9 and 4.10 in Section 4.3.2 for the analytical proof. Let $F_j = \sum_{\mathsf{p}} f_j^{\mathsf{p}}$ and $\rho = \sum_{\mathsf{p}} \rho^{\mathsf{p}}$.

Summing the equations $\frac{\mathrm{d}f_1^{\mathsf{p}}}{\mathrm{d}t} = 0$ and $\frac{\mathrm{d}f_1^{\mathsf{q}}}{\mathrm{d}t} = 0$, we have

$$-R\left(F_1\right)^2 + (2R-1)\rho F_1 = 0 \tag{2.21}$$

which is a quadratic equation whose non-negative roots can be written in terms of P as

$$F_1 = \begin{cases} 0 \\ \frac{(1-2P)\rho}{1-P}, & \text{if } P \leq \frac{1}{2}. \end{cases}$$

Since the leading coefficient of the equation (2.21) is negative, the stable and attractive equilibrium is always the largest root: thus, for $P \geq 1/2$, the equilibrium solution is $F_1 = 0$. Since the two distribution functions are non negative, the equilibrium for each population is $f_1^{\mathsf{p}} = 0$, i.e. no vehicle travels with velocity $v_1 = 0$.

Henceforth, we take $P \geq 1/2$ and we suppose $f_{j-1}^{\mathsf{p}} = 0, \mathsf{p} = C, T$, $\forall\, j < n^T$ (inductive hypothesis) and we prove that $f_j^{\mathsf{p}} = 0$. By summing again the equations $\frac{\mathrm{d}f_j^{\mathsf{p}}}{\mathrm{d}t} = 0$, we obtain

$$-R\left(F_j\right)^2 + F_j\left[(1-3R)\sum_{k=1}^{j-1} F_k + (2R-1)\rho\right] + (1-R)F_{j-1}\left[\rho - \sum_{k=1}^{j-2} F_k\right] = 0$$

and using the inductive step, this expression reduces to

$$-R\left(F_j\right)^2 + (2R-1)\rho F_j = 0$$

which is identical to (2.21) and thus again has a stable root at $F_j = 0$ for $P \geq 1/2$, closing the induction. Therefore, if $P \geq 1/2$, the stable and attractive equilibrium of each species is $f_j^{\mathsf{p}} = 0$, $\forall\, j = 1, \ldots, n^T - 1$. For $j = n^T$, using mass conservation for trucks we have

$$\rho^T = \sum_{j=1}^{n^T} f_j^T = f_{n^T}^T.$$

Thus, for $P \geq 1/2$, all trucks travel with the maximum velocity allowed in $\mathcal{V}^T$, at equilibrium. Using this result, the remaining equations for $f_j^C, j = n^T, \ldots, n^C$ can be written once $\mathbf{f}^T$ is known. The equilibrium related to the distribution function of cars traveling at the velocity v_{n^T} can be found by solving the quadratic equation of $f_{n^T}^C$ resulting from $\frac{\mathrm{d}}{\mathrm{d}t} f_{n^T}^C = 0$:

$$-R\left(f_{n^T}^C\right)^2 + f_{n^T}^C\left[(2R-1)\rho^C - \rho^T\right] + R\rho^C\rho^T = 0.$$

Since the discriminant (expressed in terms of P)

$$\mathcal{D}_{n^T} = \left[(1-2P)\rho^C - \rho^T\right]^2 + 4(1-P)^2\rho^C\rho^T$$

is non-negative $\forall\, P \in [0,1]$, all solutions are real. In particular, clearly they have opposite sign if ρ^C and ρ^T are non zero, and the positive root can be written in terms of P as

$$f_{n^T}^C = \frac{(1-2P)\rho^C - \rho^T + \sqrt{\mathcal{D}_{n^T}}}{2(1-P)}.$$

This root represents the stable and attractive equilibrium. This result depends implicitly on the assumption $P \geq 1/2$ because it exploits the fact that $\mathbf{f}^{\infty,T} = [0, \ldots, 0, \rho^T]$ which holds if $P \geq 1/2$. For $j = n^T + 1, \ldots, n^C - 1$, equilibrium distributions of cars result from the equations

$$-R\left(f_j^C\right)^2 + f_j^C\left[(1-3R)\sum_{k=n^T}^{j-1} f_k^C + (2R-1)\rho^C - R\rho^T\right] + (1-R)c_j = 0,$$
$$j = n^T + 1, \ldots, n^C - 1,$$

where the coefficient c_j is

$$c_j = \begin{cases} f^C_{n^T}\rho, & \text{if } j = n^T + 1 \\ f^C_{j-1}\left(\rho^C - \sum_{k=n^T}^{j-2} f^C_k\right), & \text{if } j = n^T + 2, \dots, n^C - 1. \end{cases}$$

Again, the roots of the quadratic equation are real and of opposite sign. The largest one is expressed in terms of P as

$$f^C_j = \frac{(3P-2)\sum_{k=n^T}^{j-1} f^C_k + (1-2P)\rho^C - (1-P)\rho^T + \sqrt{\mathcal{D}_j}}{2(1-P)}, \quad j = n^T + 1, \dots, n^C - 1$$

and it is the stable and attractive equilibrium, where

$$\mathcal{D}_j = \left[(3P-2)\sum_{k=n^T}^{j-1} f^C_k + (1-2P)\rho^C - (1-P)\rho^T\right]^2 + 4(1-P)Pc_j, \quad j = n^T+1, \dots, n^C-1$$

is the non-negative discriminant of the equation for f^C_j, $j = n^T + 1, \dots, n^C - 1$.

Finally, by mass conservation, the asymptotic distribution related to cars traveling at the maximum velocity v_{n^C} is

$$f^C_{n^C} = \rho^C - \sum_{k=n^T}^{n^C-1} f^C_k.$$

Note that if there are no trucks, $\rho^T = 0$, the equilibrium distribution for the cars is $\mathbf{f}^{\infty,C} = [0, \dots, 0, \rho^C]$. Since now the equilibrium distributions are known, we obtain the total flux of vehicles in the case $P \geq 1/2$,

$$q(\rho^C, \rho^T) = \rho^T v_{n^T} + \sum_{j=n^T}^{n^C} v_j f^C_j. \tag{2.22}$$

Therefore the flux depends not only on P, but also on the composition of the mixture. When the critical value $P = 1/2$ is crossed, f^C_j, f^T_j, $j = 1, \dots, n^T - 1$ are turned on, meaning that there are vehicles at lower velocities. This leads to a decrease in the flow values.

We conclude that the maximum flow is found for $P = 1/2$, which means that the critical space, across which the phase transition occurs, is given by $s_c = (1/2)^{1/\gamma}$. Thus the critical space depends on the particular γ-law chosen.

The maximum traffic flow is obtained at $P = 1/2$, for $\rho^T = 0$, and it corresponds to $V_{\max}\rho^C_{\max}/2^{1/\gamma}$, because then $P = 1/2$ implies that the flow is composed only of cars traveling at maximum speed, thus the slope of the fundamental diagram is strongly dependent on $V_{\max}$. A more detailed study of equilibria and of dependence of phase transition on the choice of $P(\rho)$ is shown in [74] and in Chapter 4 of this thesis.

Table 2.1: Parameters of model (2.16) common to all simulations.

Parameter	Description	Value
α	Environmental parameter	1
l^C	Typical length of a car	4 m
l^T	Typical length of a truck	12 m
$\rho^C_{\max}$	Maximum car density	250 vehicles/km
$\rho^T_{\max}$	Maximum truck density	83.3 vehicles/km
$V_{\max}$	Maximum speed	100 km/h

2.5 Fundamental diagrams of the two-population model

In this section we investigate numerically the fundamental diagrams resulting from the two-population kinetic model (2.16). As we will see, they do not only capture the main qualitative features of the experimental diagrams of Fig. 2.1, including especially the data dispersion in the congested flow regime, but they also provide tools to better understand the behavior of traffic at the macroscopic scale.

In all cases studied, system (2.16) is integrated numerically up to equilibrium, using the well balanced formulation (2.20a). Once the equilibrium distributions have been computed, the flux and the mean speed are obtained as moments of the kinetic distributions as indicated in (2.12). Since in the space homogeneous case the total density $\rho = \sum_{\mathsf{p}} \rho^{\mathsf{p}}$ is constant in time, it acts as a parameter, fixed by the initial condition, characterizing the macroscopic quantities.

As a matter of fact, each ρ^{p} is also constant in time, therefore the fraction of road occupancy s defined in (2.17) remains also stationary. It is then possible to study the flux and mean speed at equilibrium as functions of the density, and also as functions of s. Summarizing, we will study two types of equilibrium diagrams:

- *Flux-density diagrams*, that is diagrams relating the total flux at equilibrium $q = \sum_{\mathsf{p}} q^{\infty,\mathsf{p}} = \sum_{\mathsf{p}} \sum_{j=1}^{n^{\mathsf{p}}} v_j f_j^{\infty,\mathsf{p}}$ to the total density $\rho = \sum_{\mathsf{p}} \rho^{\mathsf{p}}$, which corresponds to the total number of vehicles per unit length, irrespective of the size of the different vehicles. Experimental diagrams are indeed expected to represent such a relationship.

- *Flux-space diagrams*, that is diagrams relating the total flux at equilibrium to the fraction of road occupancy s.

Except when otherwise stated, all simulations are performed with the parameters indicated in Table 2.1. Initially we consider $n^C = 3$ speed classes for cars and $n^T = 2$ speed classes for trucks, hence the corresponding spaces of microscopic speeds are

$$\mathcal{V}^C = \{0,\ 50\ \text{km/h},\ 100\ \text{km/h}\}, \qquad \mathcal{V}^T = \{0,\ 50\ \text{km/h}\},$$

cf. Section 2.4.1.

Table 2.2: Deterministic pairs (ρ^C, ρ^T) used in the fundamental diagrams of Figs. 2.4–2.6 for given values of the fraction of road occupancy s.

Combination type	Marker	Expression	ρ^C	ρ^T
Space occupied mostly by cars	Crosses	$\rho^T l^T = \frac{1}{2}\rho^C l^C$	$\frac{2s}{3l^C}$	$\frac{s}{3l^T}$
Space evenly occupied by cars and trucks	Circles	$\rho^T l^T = \rho^C l^C$	$\frac{s}{2l^C}$	$\frac{s}{2l^T}$
Space occupied mostly by trucks	Dots	$\rho^T l^T = 2\rho^C l^C$	$\frac{s}{3l^C}$	$\frac{2s}{3l^T}$

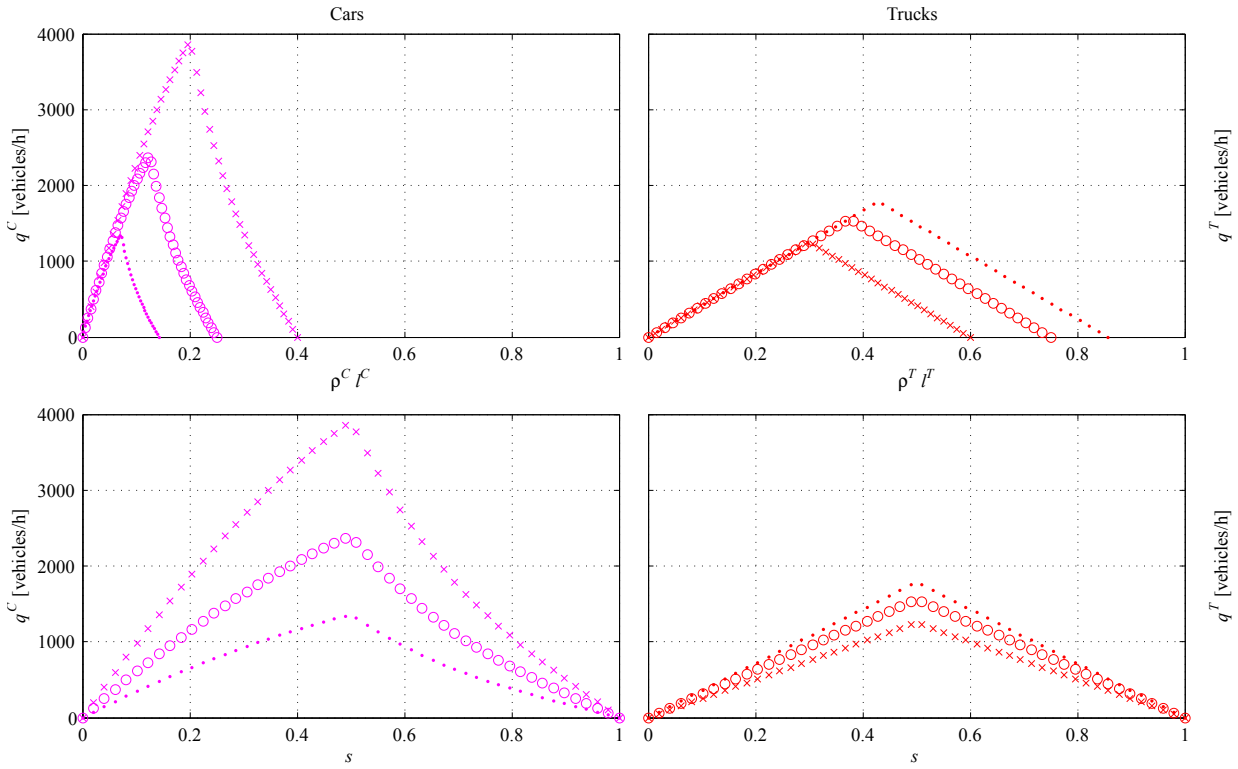

Figure 2.4: Flux-space diagrams for the three conditions of road occupancy listed in Table 2.2.

In Fig. 2.4 we show the flux-space diagrams of each class of vehicles obtained using deterministic initial conditions: for each $s \in [0, 1]$ we select three prototypical pairs $(\rho^C, \rho^T) \in [0, \rho^C_{\max}] \times [0, \rho^T_{\max}]$ such that $\rho^C l^C + \rho^T l^T = s$, corresponding to different conditions of road occupancy, cf. Table 2.2. The resulting fundamental diagrams are qualitatively similar to those obtained from the single-population model (2.2) with analogous numbers of speed classes. For instance, the fundamental diagram of the trucks alone compares well with the one shown in Fig. 2.2 with $n = 2$ speed classes.

All plots in Fig. 2.4 show clearly that there is a critical fraction of occupied space, beyond which the flow starts to decrease. On the top section of the figure, the two subplots show that the critical space for each species changes depending on the mixture we consider. In fact, the space occupied by a class of vehicles is only one contribution to the fraction of occupied space which determines the transition matrices. In other words,

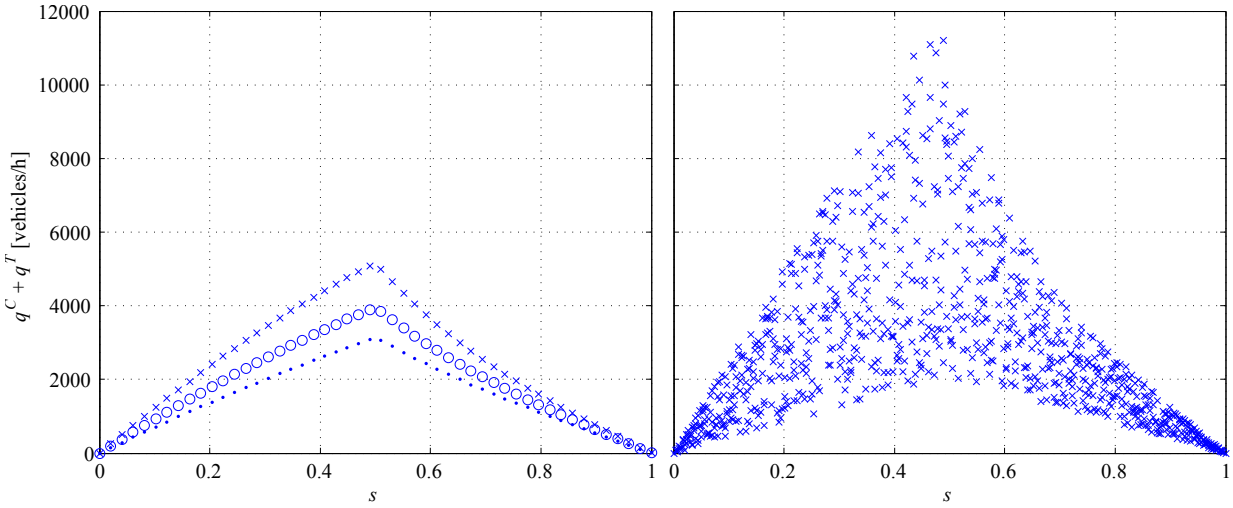

Figure 2.5: Flux-space diagrams. Left: deterministic choice of the pairs (ρ^C, ρ^T) according to Table 2.2. Right: random choice of the pairs (ρ^C, ρ^T) for each $s \in [0, 1]$.

even the dynamics of a single species depends on the dynamics of the complete mixture. Consequently, the flow depends on the composition of traffic.

In the bottom section of the figure, the flow of cars and trucks is shown as a function of the total fraction of occupied space s. One can immediately note that there is a single value for the critical space which corresponds to $s_c = \frac{1}{2}$ for all three combinations. This result seems to suggest that the transition from the free to the congested phase does not depend on how the road is occupied but on how much of it is occupied. This value of s_c depends on the particular choice $\gamma = 1$ in the expression of the probability P, see Section 2.4.3.

In Fig. 2.5 we compare the fundamental diagrams obtained by using either the three deterministic pairs (ρ^C, ρ^T) given in Table 2.2 or three pairs chosen randomly for each s. The left of Fig. 2.5 shows the total flux as a function of s, again, for the three combinations of Table 2.2, and on the right for three random combinations, for each fixed s. Here the role of the critical value $s = \frac{1}{2}$ is even more apparent. In spite of the apparent data dispersion, this diagram does not reproduce the experimental data, because the information brought by the fraction of road occupancy s is too synthetic to take into account the heterogeneity of traffic.

Motivated by this argument, now we turn to flux-density diagrams, which give the flux as a function of the number of vehicles per kilometer. Indeed experimental fundamental diagrams are expected to result out of this type of observations. In this case, the composition of traffic is taken into account, because the same fraction of occupied space $s \in [0, 1]$ can be obtained by different initial densities ρ^C, ρ^T.

Again, for each $s \in [0, 1]$ the graphs in Fig. 2.6 are obtained by taking three pairs (ρ^C, ρ^T) corresponding to the combinations reported in Table 2.2. The plots on the left correspond to the flux of each single species, as a function of its corresponding number density (top) and of the total number of vehicles (bottom). The plot on the right gives the total flux as a function of the total number of vehicles. This deterministic choice allows

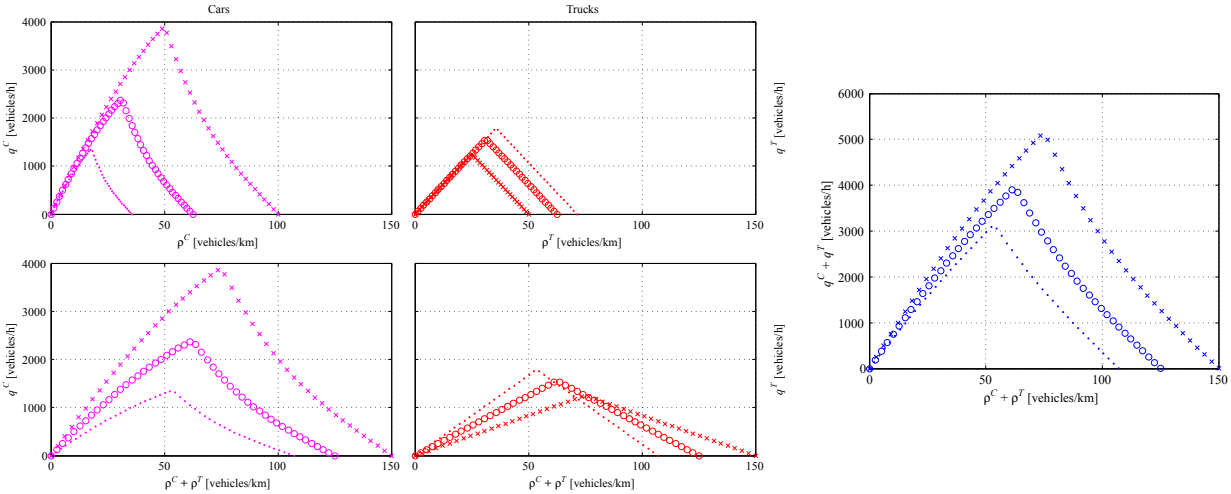

Figure 2.6: Flux-density diagrams for the three conditions of road occupancy listed in Table 2.2.

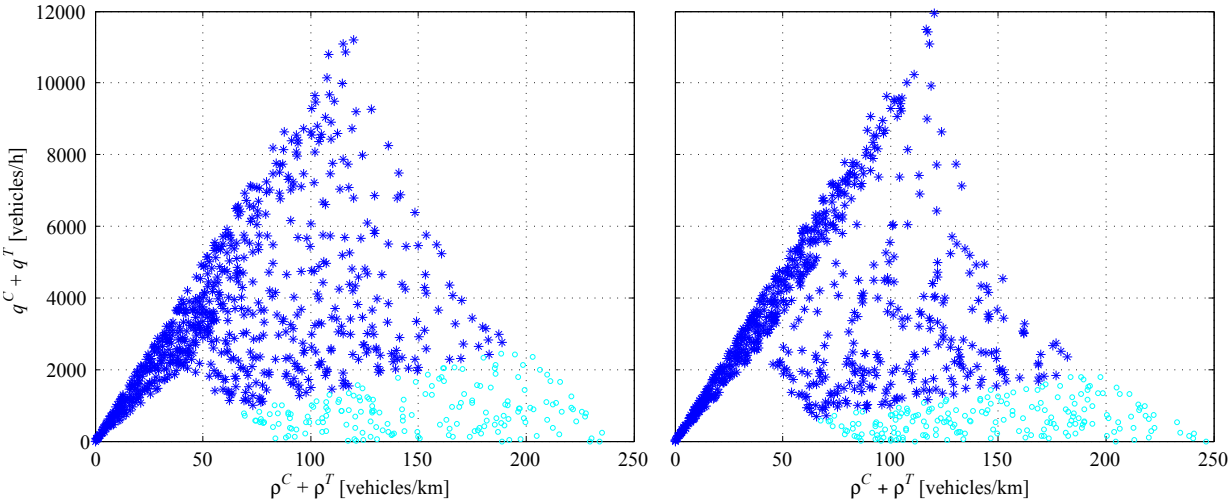

Figure 2.7: Flux-density diagram of the complete mixture obtained with three random pairs (ρ^C, ρ^T) for each $s \in [0, 1]$. Left: $n^C = 3$, $n^T = 2$; right: $n^C = 4$, $n^T = 3$. Blue star markers: data for $s \leq 0.8$; cyan circle markers: data for $s > 0.8$.

us to look at the transition from free to congested phase. Here, each combination has a different critical value of the density for the phase transition, which depends on the ratio of the different species within the mixture. But we know from Fig. 2.5 that each of these critical values of the density will correspond to the single value $s = \frac{1}{2}$. Note that the plot on the right begins to resemble the experimental fundamental diagrams of Fig. 2.1.

By sampling three random pairs (ρ^C, ρ^T) for any given $s \in [0, 1]$ we obtain the fundamental diagrams illustrated in Fig. 2.7, which clearly capture the main characteristics of the experimental diagrams discussed in Section 2.2. In particular, at low densities the total flux grows nearly linearly with small dispersion, while at higher densities it decreases with larger dispersion due to the frequent interactions between fast and slow vehicles. In

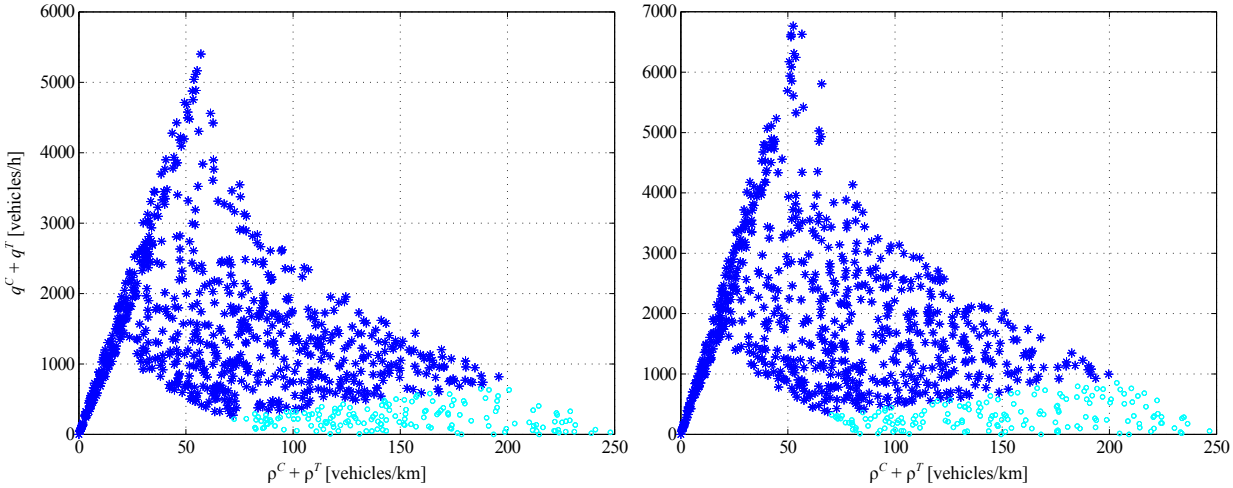

Figure 2.8: Fundamental diagrams with $n^C = 4$ and $n^T = 3$ velocity classes and probability transition $P = 1 - \sqrt{s}$. The maximum speeds $V_{\max} = 100$ km/h (on the left) and $V_{\max} = 130$ km/h (on the right) are considered. The diagrams are obtained with three random pairs (ρ^C, ρ^T) for each $s \in [0, 1]$. Blue star markers: data for $s \leq 0.8$; cyan circle markers: data for $s > 0.8$.

the graph, cyan circles indicate the total density-total flux pairs obtained for $s \in (0.8, 1]$, whereas blue stars indicate those obtained for $s \in [0, 0.8]$. As a matter of fact, the latter are the most likely to occur in practice, since even in traffic jams vehicles attain seldom a state of maximum density and complete stop (see e.g., Fig. 2.1, where a residual movement always appears). Note also that the plot on the right exhibits a capacity drop across the critical density. The behavior of the model with respect to the number of discrete velocities is analyzed in [75] or in Chapter 3.

In Figures 2.4-2.7 the transition probabilities were $P = 1 - s$ and $P_B = 0$, as given in (2.18). This choice determines flux-space diagrams in which the transition from free to congested phase occurs at the value $s = 1/2$ for any composition of the mixture, see Figures 2.4, 2.5 and Section 2.4.3. This leads to fundamental diagrams in which the maximum value of the flow is reached when $\rho^T = 0$ and $\rho = \rho^C_{\max}/2 = 125$ vehicles/km, see Figures 2.6 and 2.7, because in this case the flow is composed only of cars traveling at their maximum speed. Choosing instead $P = 1 - s^\gamma$, with $\gamma < 1$, the phase transition occurs at $s_c = \left(\frac{1}{2}\right)^{\frac{1}{\gamma}}$ and it decreases when γ is decreased. In particular, in the left plot of Figure 2.8 we consider $\gamma = 1/2$ and we observe that the fundamental diagram, obtained with $n^C = 4$ and $n^T = 3$, shows a better reproduction of experimental data, see Section 2.2, Figure 2.1. In the right plot, instead, we consider $\gamma = 1/2$ but $V_{\max} = 130$ km/h, showing that a greater maximum speed causes an increase in the slope of the diagram in the free flow phase.

The examples discussed so far suggest that the bulk characteristics of traffic at equilibrium could be predicted *deterministically* once the composition of traffic, i.e., the pair (ρ^C, ρ^T), is known. This induces to interpret the scattering of data in the congested phase as a consequence of the possible heterogeneity of vehicles in traffic, for a given level of road

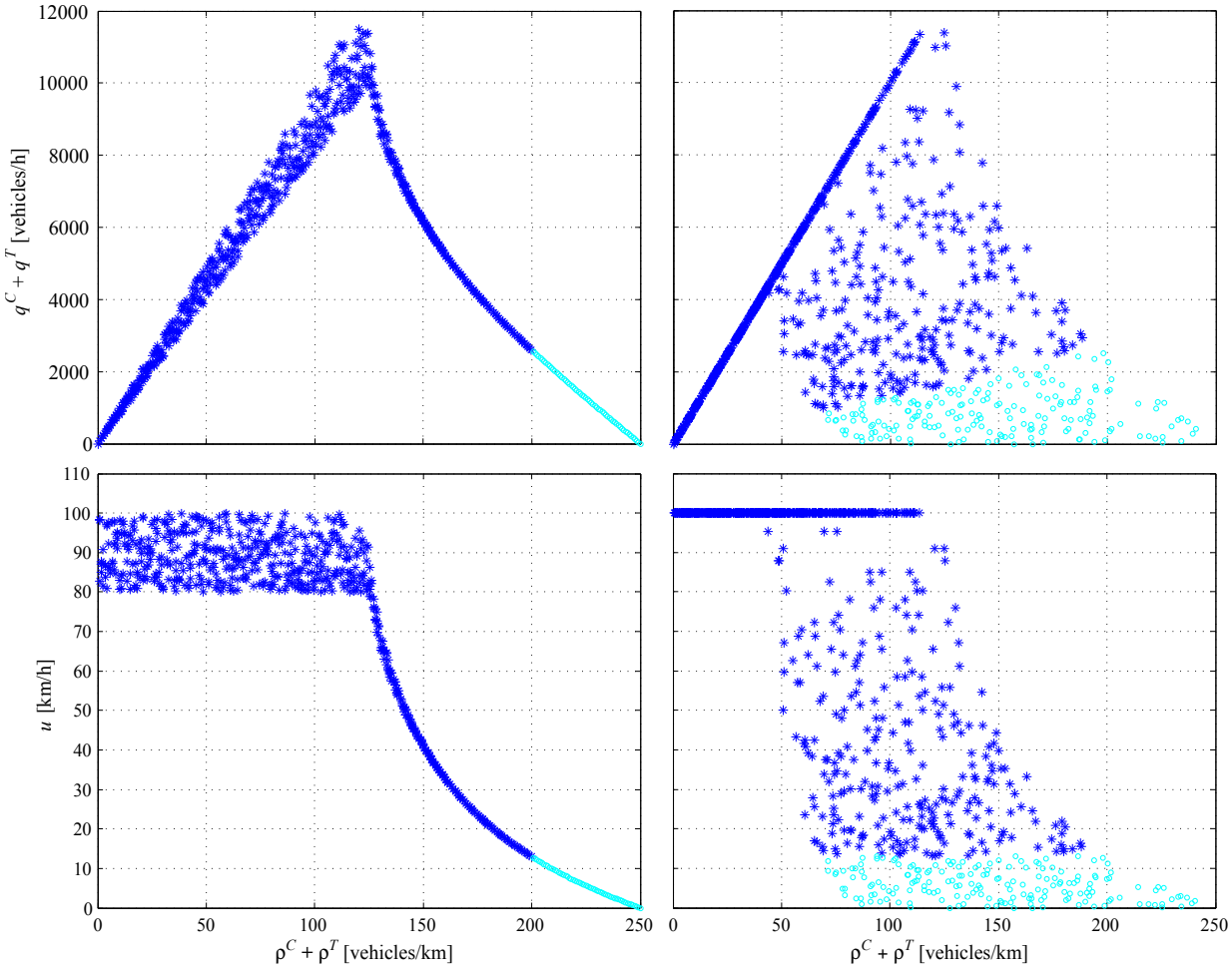

Figure 2.9: Top row: flux-density diagrams, bottom row: speed-density diagrams vs. the total density for two populations of vehicles having either the same length and different microscopic speeds (left) or different lengths and same microscopic speeds (right). Blue star markers: data for $s \leq 0.8$; cyan circle markers: data for $s > 0.8$.

occupancy, rather than as an effect of the unpredictability of driver behaviors.

This affirmation can be articulated more precisely, by considering the 2-population model in which vehicles differ by only one characteristic. The plot on the left of Figure 2.9 shows the flux-density diagram when the two classes of vehicles have the same length, but they differ in their maximum speed: $\mathcal{V}^C = \{0, 50, 80, 100\}$ and $\mathcal{V}^T = \{0, 50, 80\}$. We can interpret this case as thinking that vehicles are now identical, but we are considering two different types of driver, according to the maximum speed they are willing to settle on when the road is free (say, fast and slow drivers). The plot on the right of Figure 2.9 is obtained by considering vehicle classes which have different lengths, as given in Table 2.1, but the same microscopic speeds.

By inspecting them we infer that differences in the speeds (in particular, the maximum ones) of the vehicles composing the traffic mixture seem to be responsible for the small

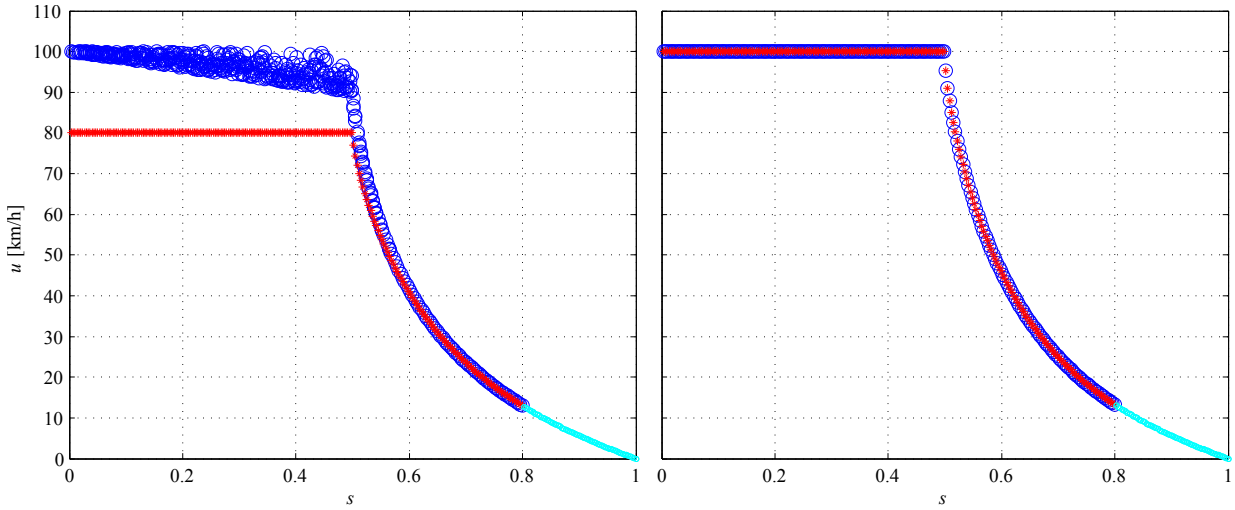

Figure 2.10: Mean speed versus fraction of road occupancy s for cars (blue) and trucks (red) having either the same length and different microscopic speeds (left) or different lengths and same microscopic speeds (right). Cyan circle markers refer to data for $s > 0.8$.

scattering of the data in the free flow phase, whereas differences in the length determine the larger scattering of the data in the congested flow phase.

The same two cases are further investigated in Fig. 2.10 by focusing on the speed diagram vs. the fraction of road occupancy s. In particular, when vehicles have different microscopic speeds but same length (diagram on the left) we deduce that, in free flow conditions, the slower population is not affected by the faster one, while fast drivers may have to slow down due to their interactions with slower cars. On the other hand, both types of drivers are forced to slow down, reaching finally the same mean speed, as the road becomes congested. Conversely, when vehicles have the same microscopic speeds but different lengths (diagram on the right) we discover that the mean speed is the same for both populations in both traffic regimes, i.e., in other words, it is a one-to-one function of the fraction of occupied space.

These remarks are indeed consistent with daily experience of driving on highways: in free flow drivers can choose their speed, and thus they keep different maximum speeds according to their driving style, while in congested flow they tend to travel all at the same speed, which steadily decreases as the traffic congestion increases.

Finally, Figure 2.11 shows the fundamental diagram for the traffic mixture modeled by the two-population macroscopic model [7] summarized in Section 2.4. It is immediate to notice that there is no trace of the sharp phase transition predicted by our kinetic model and that the scattering of the data is very high also at low densities.

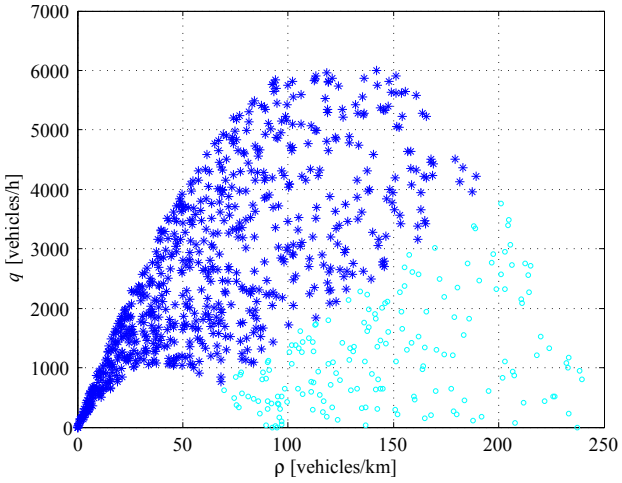

Figure 2.11: Flux-density diagram of the two-population macroscopic model [7], see also (2.11), obtained by sampling three random pairs (ρ_1, ρ_2) for every $s \in [0, 1]$. Blue star markers: data for $s \leq 0.8$; cyan circle markers: data for $s > 0.8$.

Chapter 3

Kinetic models for traffic flow resulting in a reduced space of microscopic velocities

3.1 Motivation

In Chapter 2 we have introduced a multi-population kinetic model which allows us to recover and to provide a possible explanation the origin of the scattering of the experimental measurements. The model is proposed in the framework of the discrete-velocity kinetic theory, following the approach in [25, 26]. However, we think that the hypothesis of a lattice of speeds does not reflect the dynamics of traffic. In fact, the experience suggests that the velocities of vehicles along a road span continuously the whole space of admissible speeds.

The assumption of a discrete space of velocities leads also to the following drawbacks. First of all, observe that the interaction rules, proposed in Section 2.3.1 for a single-population model and generalized to the multi-population model in Section 2.4.1, prescribe that the output speed after an acceleration is ruled by the number of speeds in the lattice. In fact, we have assumed that the candidate vehicle can accelerate from the actual speed v_h to the post-interaction speed v_{h+1}, see left panel of Figure 3.1. This means that the model is not able to account for the physical acceleration of vehicles which, in a realistic framework, should not depend on the size of the lattice. Moreover, the model does not give information on the choice of the size of the discrete space of speeds and, resting on the case of the single-population model (2.3), the limit of the fundamental diagram does not fit experimental data when the number of discrete speeds goes to infinity, see the right panel of Figure 3.1.

For these reasons, in [75] and in this chapter, we relax the hypothesis of a discrete-velocity space. Therefore, following the classical Boltzmann-like setting of binary interactions, we study a kinetic model based on a continuous-velocity space. However, usually the interaction integrals appearing in kinetic Boltzmann-type models for traffic flow based on

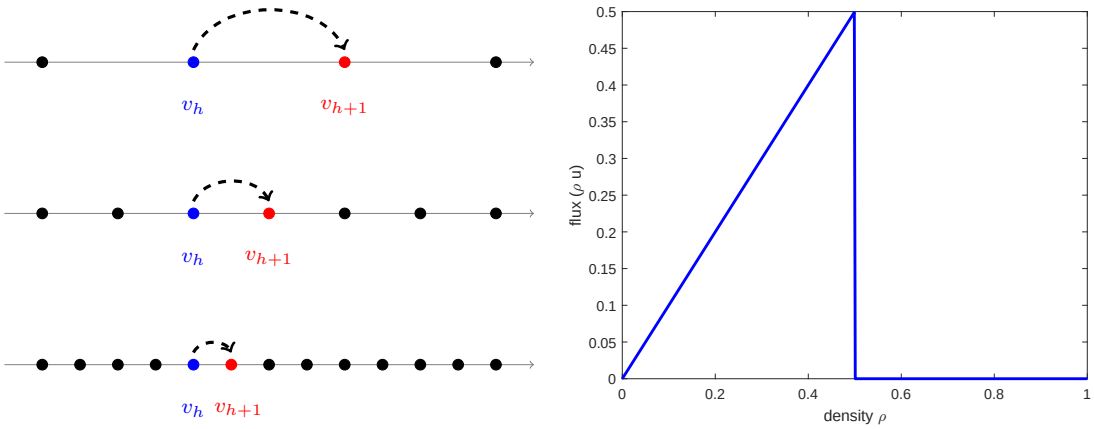

Figure 3.1: Left: post-interaction speed (red filled circles) prescribed by the discrete-velocity model (2.3) after an acceleration. Right: limit of the fundamental diagram provided by the discrete-velocity model (2.3) for $n \to \infty$.

a continuous-velocity space, see e.g. [48], typically do not provide the analytical expression of the equilibrium distribution and they are very demanding from a computational point of view. Instead, the model proposed here does not suffer from the aforementioned drawbacks. We focus only on spatially homogeneous problems and we propose two models which differ in the modeling of acceleration interactions: one is based on quantized velocity jumps, i.e., if acceleration occurs the new speed is obtained by increasing the pre-interaction velocity of a fixed quantity Δv (δ model); the other one is based on a continuous uniform distribution defined on a bounded interval parametrized by Δv (χ model), see also [48, 49].

The models are characterized by the presence of a finite parameter Δv. The introduction of Δv allows us to model the physical velocity jump performed by vehicles when they increase their speeds as a result of an interaction. Clearly, this parameter may depend on the mechanical characteristics of vehicles, see [74], but here we will assume that Δv is fixed. In the section on macroscopic properties, Section 3.5, we show that Δv is related to the maximum acceleration and we discuss how this parameter can be chosen through experimental data used by Lebacque [53].

We investigate the equilibria of the δ model, both from an analytical and a numerical point of view. Analytically we find that velocity distributions formed by a linear combination of Dirac delta may be equilibria only if the delta are centered at velocities spaced by multiples of Δv. Next, we compute equilibria using a numerical scheme capable of converging also to possible absolutely continuous equilibria. Here, actually, we find only the quantized equilibria described above, independently of the discretization parameters. This fact suggests that the class of discrete-velocity equilibria is the only one that the continuous-velocity Boltzmann-type δ model possesses. This situation is summarized graphically in Figure 3.2.

The chapter is organized as follows. In Section 3.2 we briefly recall the Boltzmann-type kinetic equation and we specialize it by giving two sets of interaction rules. The resulting

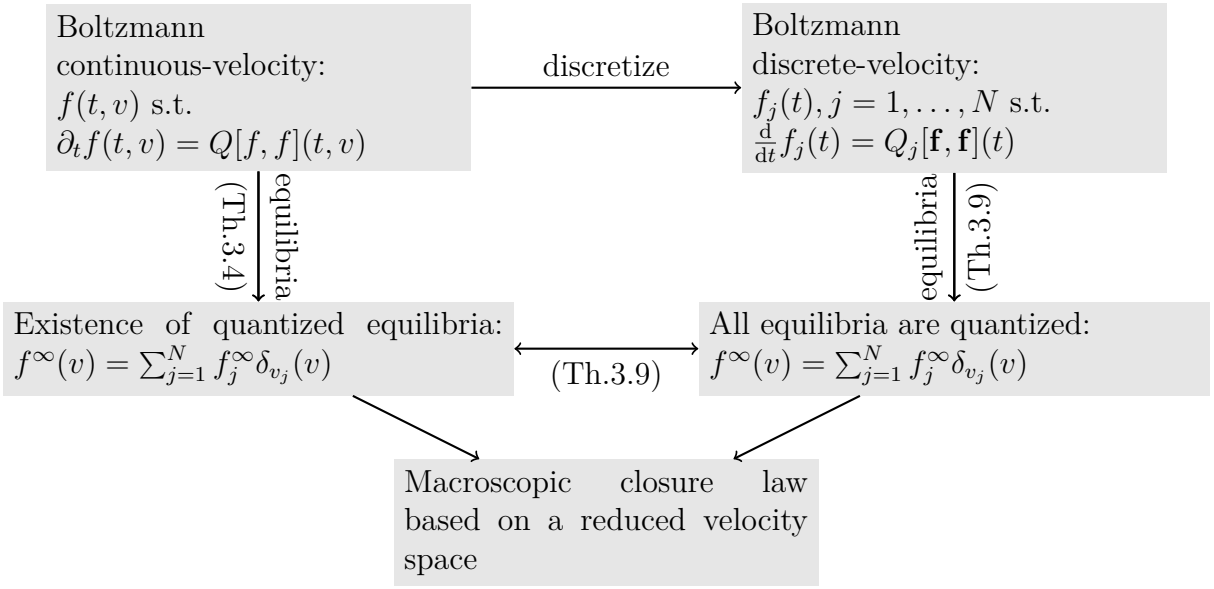

Figure 3.2: Connection between the δ model and a discrete-velocity model, having the same steady-state distribution.

δ and χ models are discussed in depth in Section 3.3 and in Section 3.4, respectively. In particular, in Section 3.3 we prove the existence of a class of quantized steady-state distributions. Since we are unable to prove their uniqueness, we discretize the model by approximating the kinetic distribution with a piecewise constant function and we then show by numerical evidence that the class of stationary solutions of the δ model is only the one we have already studied analytically. In Section 3.4, we show the somewhat surprising result that the equilibrium distributions of the perhaps more natural, but more complex and more computationally demanding, χ model yield a macroscopic flow that is extremely well approximated by the discrete-velocity-based closure law resulting from the δ model. This is illustrated in the final section Section 3.5, where we show that the fundamental diagrams, that is the flux-density relationships, obtained from the two models tend to coincide under grid refinement. Next we compare these diagrams with experimental data, finding that our models reproduce well experimental fundamental diagrams and thus they capture the characteristics of macroscopic traffic flow. Further, we compute the macroscopic acceleration induced by the model, proving in particular its link with Δv.

3.2 The general form of the kinetic model

In this section we briefly recall the general structure of a Boltzmann-type kinetic traffic model, which we will then specialize by prescribing a set of binary interaction rules in order to derive two models which differ only in the modeling of the acceleration interaction. Both models are defined on a continuous-velocity space and they are characterized by a parameter Δv related to the typical acceleration of a vehicle.

We will focus on the space homogeneous case, because we want to investigate the structure of the collision term and of the resulting equilibrium distributions. In particular, we show that the simplified model (δ model) permits to describe the complexity of the equilibrium solutions with a very small number of discrete velocities.

Let $f = f(t, v) : \mathbb{R}^+ \times \mathcal{V} \to \mathbb{R}^+$ be the *kinetic distribution function*, where $\mathcal{V} = [0, V_{\max}]$ is the continuous-domain of the microscopic speeds and $V_{\max}$ is the maximum speed, which, as discussed in Section 2.4.1, may depend on the mechanical characteristics of the vehicles, on imposed speed limits, environmental conditions (such as the quality of the road, the weather conditions, etc). The statistical distribution f is such that $f(t, v)\mathrm{d}v$ gives the number of vehicles with velocity in $[v, v + \mathrm{d}v]$ at time t.

As usual, macroscopic quantities are obtained as moments of the distribution function f with respect to the velocity v:

$$\rho(t) = \int_{\mathcal{V}} f(t, v)\mathrm{d}v, \quad q(t) = \int_{\mathcal{V}} v f(t, v)\mathrm{d}v, \quad u(t) = \frac{1}{\rho(t)} \int_{\mathcal{V}} v f(t, v)\mathrm{d}v$$

where ρ is the density, i.e. the number of vehicles per unit length (tipically, kilometers), u is the macroscopic speed and $q = \rho u$ is the flux of vehicles. Note that ρ can also be interpreted as the reciprocal of the average distance between cars, see [5].

In the homogeneous case, the Boltzmann-type equation can be written as

$$\partial_t f(t, v) = Q[f, f](t, v) \tag{3.1}$$

where $Q[f, f](t, v)$ is the collisional operator which describes the relaxation to equilibrium due to the microscopic binary interactions among vehicles. For mass conservation to hold, the collision term must satisfy

$$\int_{\mathcal{V}} Q[f, f](t, v)\mathrm{d}v = 0.$$

In fact, this ensures that, in the space homogeneous case, the density remains constant in time.

The collisional operator is usually split into a gain term $G[f, f]$ and a loss term $L[f, f]$, that model statistically the interactions which lead to gain or to loose the test speed v. Denoting with $A(v_* \to v|v^*)$ the probability that the velocity $v \in \mathcal{V}$ results from a microscopic interaction between candidate vehicles with velocity v_* and field vehicles with speed v^*, we write the model as an integro-differential equation

$$\partial_t f(t, v) = \underbrace{\int_{\mathcal{V}} \int_{\mathcal{V}} \eta(v_*, v^*) A(v_* \to v|v^*) f(t, v_*) f(t, v^*)\mathrm{d}v_*\mathrm{d}v^*}_{G[f,f](t,v)} - \underbrace{f(t, v) \int_{\mathcal{V}} \eta(v, v^*) f(t, v^*)\mathrm{d}v^*}_{L[f,f](t,v)} \tag{3.2}$$

in which $\eta(v_*, v^*)$ is the interaction rate possibly depending on the relative speed of the interacting vehicles, e.g. $\eta(v_*, v^*) = |v_* - v^*|$ as in [48]. Although such a choice would make the model richer, in [76] we found that a constant interaction rate is already sufficient to

account for many aspects of the complexity of traffic. Another possibility is to consider η as dependent on the local congestion of the road, that is $\eta = \eta(\rho)$. However this is not relevant in the homogeneous case, where ρ is constant, for then η would affect only the relaxation time towards equilibrium. Thus in this case we will set η =constant.

Notation. In the whole chapter, in order to shorten formulas, we adopt the following traditional shorthand $f(t, v_*) = f_*$, $f(t, v^*) = f^*$, etc. Note in particular that in the space homogeneous case f^* and f_* are not different distribution functions, but the evaluation of the same $f(t, v)$ at two different points v_* and v^*.

We will suppose that A depends also on the macroscopic density ρ in order to account for the influence of the macroscopic traffic conditions (local road congestion) on the microscopic interactions among vehicles, see [37, 48, 73, 76]. Thus, we suppose that A fulfills:

Ansatz 3.1.

$$A(v_* \to v | v^*; \rho) \geq 0, \quad \text{and} \int_{\mathcal{V}} A(v_* \to v | v^*; \rho) \mathrm{d}v = 1, \quad \text{for } v_*, v^*, v \in \mathcal{V},\ \rho \in [0, \rho_{\max}]$$

where $\rho_{\max}$ is the maximum density of vehicles, for instance the maximum number of vehicles per unit length in bumper-to-bumper conditions.

Remark 3.2. Any transition probability density A that satisfies Ansatz 3.1 guarantees mass conservation since

$$\partial_t \int_{\mathcal{V}} f(t, v) \mathrm{d}v = \int_{\mathcal{V}} Q[f, f](t, v) \mathrm{d}v = \int_{\mathcal{V}} \int_{\mathcal{V}} f(t, v_*) f(t, v^*) \mathrm{d}v_* \mathrm{d}v^* - \int_{\mathcal{V}} f(t, v) \mathrm{d}v \int_{\mathcal{V}} f(t, v^*) \mathrm{d}v^* = 0.$$

3.2.1 Choice of the probability density A

The probability density A has, at the continuous level, the same role of the table of games introduced in Section 2.3.1. Thus, it assignes a post-interaction speed in a non-deterministic way, consistently with the intrinsic stochasticity of the drivers' behavior. The construction of A is at the core of a kinetic model. Here, it is obtained with a very small set of rules.

- If $v_* \leq v^*$, i.e. the candidate vehicle is slower than the field vehicle, the post-interaction rules are:

  Do nothing: the candidate vehicle keeps its pre-interaction speed with probability $1 - P_1$, thus $v = v_*$;

  Accelerate: the candidate vehicle accelerates to a velocity $v > v_*$ with probability P_1.

- If $v_* > v^*$, i.e. the candidate vehicle is faster than the field vehicle, the post-interaction rules are:

Accelerate: in order to overtake the leading vehicle, the candidate vehicle accelerates to a velocity $v > v_*$ with probability P_2;

Brake: the candidate vehicle decelerates to the velocity $v = v^*$ with probability $1 - P_2$, thereby queuing up and following the leading vehicle.

From the previous rules, we observe that the probability density A has a term which will be proportional to a Dirac delta function at $v = v_*$, due to the interaction which preserves the pre-interaction microscopic speed (the "Do nothing" alternative). Note that this is a "false gain" for the distribution f, because the number of vehicles with speed v is not altered by this interaction.

In the following, we assign the speed after braking as proposed in [72] and used also in [25, 26] and in Chapter 2 in the context of a discrete-velocity model. Namely, we suppose that if a vehicle brakes, interacting with a slower vehicle, it slows down to the speed v^* of the leading vehicle. Thus, after the interaction it gets the speed $v = v^*$ without overtaking the leading field vehicle. Instead, for the post-interaction speed due to acceleration we propose two different models.

Quantized acceleration ($\boldsymbol{\delta}$ model): the output velocity v is obtained by accelerating instantaneously from v_* to the velocity $\min\{v_* + \Delta v, V_{\max}\}$. Considering all possible outcomes, the resulting probability distribution, in this case, is

$$A(v_* \to v | v^*; \rho) = \begin{cases} (1 - P_1)\delta_{v_*}(v) + P_1 \delta_{\min\{v_* + \Delta v, V_{\max}\}}(v), & \text{if } v_* \le v^* \\ (1 - P_2)\delta_{v^*}(v) + P_2 \delta_{\min\{v_* + \Delta v, V_{\max}\}}(v), & \text{if } v_* > v^*. \end{cases} \tag{3.3}$$

Uniformly distributed acceleration ($\boldsymbol{\chi}$ model): the new velocity v is uniformly distributed between v_* and $\min\{v_* + \Delta v, V_{\max}\}$. On the whole, the resulting probability distribution becomes

$$A(v_* \to v | v^*; \rho) = \begin{cases} (1 - P_1)\delta_{v_*}(v) + P_1 \frac{\chi_{[v_*, \min\{v_* + \Delta v, V_{\max}\}]}(v)}{\min\{v_* + \Delta v, V_{\max}\} - v_*}, & \text{if } v_* \le v^* \\ (1 - P_2)\delta_{v^*}(v) + P_2 \frac{\chi_{[v_*, \min\{v_* + \Delta v, V_{\max}\}]}(v)}{\min\{v_* + \Delta v, V_{\max}\} - v_*}, & \text{if } v_* > v^*. \end{cases} \tag{3.4}$$

Note that the acceleration of a vehicle in (3.3) is similar to the one assumed in [25, 26] and in Chapter 2, for the models based on a discrete-velocity space. However, there the *acceleration parameter* Δv is chosen as the distance between two adjacent discrete velocities, thus Δv depends on the number of elements in the speed lattice. In the present framework, instead, Δv is a physical parameter that represents the ability of a vehicle to change its pre-interaction speed v_*. With this choice, Δv does not depend on the discretization of the velocity space and, at the same time, the maximum acceleration is bounded, as in [53]. In contrast, deceleration can be larger than Δv, and this fact reflects the hypothesis that drivers tend to brake immediately if the flow becomes more congested, while they react more slowly when they can accelerate (see the concept of *traffic hysteresis* in [88] and references therein).

The acceleration performed in the χ model has some points of contact with the microscopic rules prescribed in [41, 48]. In [41], however, the post-interaction speed is selected through a random process in the interval $[v_*, V_{\max}]$. Here instead, the post-interaction speed is deterministic. In [48] instead, the velocity after acceleration is uniformly distributed over a range of speeds between v_* and $v_* + \alpha(V_{\max} - v_*)$, where α is supposed to depend on the local density; in a similar way, the output velocity from a braking interaction is assumed to be uniformly distributed in $[\beta v^*, v^*]$, with $\beta \in [0, 1]$.

In the following, the probabilities P_1 and P_2 are taken as $P_1 = P_2 =: P$ and P will be a decreasing function of the local density only, as already assumed in Ansatz 2.2 and in Section 2.3.2, following for instance the choices in [36, 72, 78]. In particular, from now on, we take P as in (2.9) with $\gamma \in (0, 1]$ and $\alpha = 1$.

The simplified choice $P_1 = P_2$ and the interaction rules described at the beginning of this section guarantee the continuity of the transition probability (3.3) and (3.4) along $v_* = v^*$.

Remark 3.3. Both choices (3.3) and (3.4) for A include terms of the form $\delta_{v_*}(v)$, which actually describe false gains mentioned above, because the velocity of the candidate vehicle does not change. They are automatically compensated by false losses, as it can be seen by rewriting the classical kinetic loss term of equation (3.2) in the following form:

$$L[f, f](t, v) = \int_{\mathcal{V}} \int_{\mathcal{V}} \eta \delta_{v_*}(v) f_* f^* \mathrm{d}v^* \mathrm{d}v_*.$$

3.3 The δ velocity model

Now, we focus on the steady states of model (3.3). We start with the existence of a particular set of equilibrium solutions of the continuous model, which are computed analytically. Next, we consider a finite volume discretization of the model, and we show that the discrete equilibria have precisely the structure found before analytically, thus suggesting that the particular set of equilibria found analytically are the only equilibria of the system.

It can be proven [28] that the Cauchy problem associated to (3.2) is well posed provided the probability density A is Lipschitz continuous with respect to v_* and v^* in a suitable Wasserstein metric. This is indeed the case of the A defined in (3.3), with $P_1 = P_2$.

Using the expression (3.3) for A, we rewrite the gain term in (3.2) as

$$G[f, f](t, v) = \eta \int_{\mathcal{V}} \int_{\mathcal{V}} \left[(1 - P)\delta_{\min\{v_*, v^*\}}(v) + P\delta_{\min\{v_* + \Delta v, V_{\max}\}}(v) \right] f_* f^* \mathrm{d}v_* \mathrm{d}v^*$$

and the following important result on the existence of a particular class of stationary solutions holds. More precisely, it characterizes the equilibrium distributions having the form of linear combinations of Dirac's masses. This theorem establishes the connection represented by the left vertical arrow in Figure 3.2.

Theorem 3.4. – *Let P be a given function of the density $\rho \in [0, \rho_{\max}]$ such that $P \in [0,1]$. Let $\{v_j\}_{j=1}^n$ be a set of velocities in $[0, V_{\max}]$. The distribution function*

$$f^\infty(v) = \sum_{j=1}^n f_j^\infty \delta_{v_j}(v), \quad f_j^\infty > 0 \quad \forall\, j = 1, \dots, n,$$

with $\sum_{j=1}^n f_j^\infty = \rho$, is a weak stationary solution of the δ model provided $v_j = v_1 + j\Delta v$, $j = 1, \dots, n$.

Proof. Without loss of generality suppose that $\{v_j\}_{j=1}^n$ is an ordered set of velocities such that $0 \le v_1 < \cdots < v_n \le V_{\max}$. Since the distribution function $f^\infty(v) = \sum_{j=1}^n f_j^\infty \delta_{v_j}(v)$ is a weak stationary solution of the δ model, it satisfies the following steady weak form of equation (3.2):

$$\int_{\mathcal{V}} \int_{\mathcal{V}} \left(\int_{\mathcal{V}} \phi(v) A(v_* \to v | v^*; \rho) \mathrm{d}v \right) f^\infty(v_*) f^\infty(v^*) \mathrm{d}v^* \mathrm{d}v_* - \rho \int_{\mathcal{V}} \phi(v) f^\infty(v) \mathrm{d}v = 0,$$

where $\phi \in C_c(\mathcal{V})$ is a test function, with $C_c(\mathcal{V})$ the space of continuous functions having compact support contained in $\mathcal{V}$, and the probability density A is given in (3.3). Substituting the expression of f^∞ in the above equation we obtain

$$\begin{aligned} &(1-P) \sum_{k=1}^n \sum_{h=1}^k \phi(v_h) f_h^\infty f_k^\infty + (1-P) \sum_{k=1}^n \sum_{h=k+1}^n \phi(v_k) f_h^\infty f_k^\infty \\ &+ P\rho \sum_{h=1}^n \phi(\min\{v_h + \Delta v, V_{\max}\}) f_h^\infty - \rho \sum_{j=1}^n \phi(v_j) f_j^\infty = 0. \end{aligned} \tag{3.5}$$

The proof will be organized as follows: in order to determine an equation for the f_j^∞'s, we consider a particular family of test functions ϕ_j defined as piecewise linear functions such that $\phi_j(v_j) = 1$ and $\phi_j(v_i) = 0$, $\forall\, i \neq j$; in this way, first we find an equation for f_1^∞, then we show that $f_2^\infty \neq 0$ if $v_2 = v_1 + \Delta v$ and finally by induction we prove that if $f_j^\infty \neq 0$, then $v_j = v_1 + j\Delta v$, for some $j \in \{1, \dots, n\}$.
Let $j = 1$, equation (3.5) with $\phi = \phi_1$ becomes

$$(1-P) \sum_{k=1}^n f_1^\infty f_k^\infty + (1-P) \sum_{h=2}^n f_h^\infty f_1^\infty + P\rho \sum_{h=1}^n \phi_1(v_1 + \Delta v) f_h^\infty - \rho f_1^\infty = 0.$$

Due to the particular construction of ϕ_1 and using $\sum_{j=1}^n f_j^\infty = \rho$, the above expression reduces to

$$-(1-P)(f_1^\infty)^2 + (1-2P)\rho f_1^\infty = 0$$

which admits the two roots $f_1^\infty = 0$ and $f_1^\infty = \rho \frac{1-2P}{1-P}$. If $P > 1/2$, only $f_1^\infty = 0$ is acceptable, because the other root is negative. If instead $P < 1/2$, both roots can be accepted, but only $f_1^\infty = \rho \frac{1-2P}{1-P} > 0$ is stable. This argument will be used for selecting a

single root throughout the proof.
Now, let $j = 2$ and $\phi = \phi_2$. Equation (3.5) writes as

$$-(1-P)(f_2^\infty)^2 + [(1-2P)\rho - 2(1-P)f_1^\infty]\, f_2^\infty + P\rho \sum_{h=1}^{n} \phi_2(\min\{v_h + \Delta v, V_{\max}\}) f_h^\infty = 0. \tag{3.6}$$

Note that $\phi_2(\min\{v_h + \Delta v, V_{\max}\}) = 1$ if $h = 1$ and $v_1 + \Delta v = v_2$. While $\phi_2(\min\{v_h + \Delta v, V_{\max}\}) = 0$ otherwise, due to the particular choice of ϕ_2 which is centered in v_2 and can be taken with support smaller than $2\,|v_2 - v_1 - \Delta v|$ around this point. Then, if $v_2 \neq v_1 + \Delta v$, the constant coefficient of (3.6) is zero for all $P \in [0,1]$ and the solutions of the equation are $f_2^\infty = 0$ or $f_2^\infty = \rho\frac{1-2P}{1-P} - 2f_1^\infty$. Exploiting the structure of f_1^∞ and the fact that $f_j^\infty \geq 0$, only $f_2^\infty = 0$ is the admissible solution for all values of $P \in [0,1]$.
Instead, if $v_2 = v_1 + \Delta v$, the third term in equation (3.6) is $P\rho f_1^\infty \geq 0$, for all $P \in [0,1]$. More precisely, if $P \geq 1/2$ then $f_1^\infty = 0$, thus the constant coefficient vanishes and again one concludes that $f_2^\infty = 0$. While if $P < 1/2$, $P\rho f_1^\infty$ is positive and since the discriminant $\mathcal{D} = ((1-2P)\rho - 2(1-P)f_1^\infty)^2 + 4P(1-P)\rho f_1^\infty$ of equation (3.6) is positive and the leading coefficient is negative, the equation has two real roots with opposite signs. Therefore

$$f_2^\infty = \frac{-(1-2P)\rho + 2(1-P)f_1^\infty - \sqrt{\mathcal{D}}}{-2(1-P)} > 0$$

and this is the only case in which f_2^∞ can be non-zero.
We now proceed by induction. Suppose that $v_k - v_1$ is an integer multiple of Δv and

$$f_k^\infty = \begin{cases} 0, & \text{if } P \geq 1/2 \\ \dfrac{-(1-2P)\rho + 2(1-P)\sum_{l=1}^{k-1} f_l^\infty - \sqrt{\mathcal{D}_k}}{-2(1-P)}, & \text{if } P < 1/2 \end{cases}$$

for all $k = 3, \ldots, j-1$, where $\mathcal{D}_k = \left((1-2P)\rho - 2(1-P)\sum_{l=1}^{k-1} f_l^\infty\right)^2 + 4P(1-P)\rho \sum_{l=1}^{k-1} f_l^\infty$.
We show that f_j^∞ can be non-zero only if $v_j = v_1 + j\Delta v$, for $j \in \{1, \ldots, n\}$.
Taking the test function $\phi = \phi_j$, the equation for f_j^∞ writes as

$$-(1-P)(f_j^\infty)^2 + \left[(1-2P)\rho - 2(1-P)\sum_{l=1}^{j-1} f_l^\infty\right] f_j^\infty + P\rho \sum_{h=1}^{n} \phi_j(\min\{v_h + \Delta v, V_{\max}\}) f_h^\infty = 0. \tag{3.7}$$

Note that $\phi_j(\min\{v_h + \Delta v, V_{\max}\}) = 1$ if $h = j-1$ and $v_{j-1} + \Delta v = v_j$. While $\phi_j(\min\{v_h + \Delta v, V_{\max}\}) = 0$ otherwise, due to the particular choice of ϕ_j which is centered in v_j and can be taken with support smaller than $2\,|v_j - v_{j-1} - \Delta v|$ around this point. If $v_j = v_1 + j\Delta v$, then $v_j = v_{j-1} + \Delta v$ and the above equation becomes

$$-(1-P)(f_j^\infty)^2 + \left[(1-2P)\rho - 2(1-P)\sum_{l=1}^{j-1} f_l^\infty\right] f_j^\infty + P\rho f_{j-1}^\infty = 0$$

which has two real roots. If $P \geq 1/2$, using the inductive hypothesis $f_k^\infty = 0$ for all $k \leq j-1$. Thus $f_j^\infty = \rho\frac{1-2P}{1-P}$ (which is again not acceptable since it is negative) or $f_j^\infty = 0$, confirming the induction. If $P < 1/2$, we have two real roots with opposite signs, so one proves that f_j^∞ can be chosen strictly positive.
If instead $v_j \neq v_1 + j\Delta v$ then the constant term of equation (3.7) is zero and the two roots are $f_j^\infty = 0$ and $f_j^\infty = S_j = \frac{(1-2P)\rho - 2(1-P)\sum_{l=1}^{j-1} f_l^\infty}{1-P}$ which is negative for all values of $P \in [0,1]$ using the Lemma 3.5 below. ■

In the previous proof we use the following technical fact.

Lemma 3.5. – *Let P be a given function of the density $\rho \in [0, \rho_{\max}]$ such that $P \in [0,1]$. Consider $\{f_j\}_{j=1}^K \in \mathbb{R}$ defined as*

$$f_j = \frac{2(1-P)\sum_{l=1}^{j-1} f_l - (1-2P)\rho - C_j}{-2(1-P)}$$

with $C_j > 0$. Assume that f_j is positive for all j. Then,

$$S_k = \frac{(1-2P)\rho - 2(1-P)\sum_{l=1}^{k-1} f_l}{1-P} < 0$$

for all $2 \leq k \leq K$.

Proof. We proceed by induction on k. Let $k = 2$:

$$S_2 = \frac{(1-2P)\rho - 2(1-P)f_1}{1-P} = -\frac{C_1}{1-P} < 0.$$

Suppose $S_j < 0$, $j = 3, \ldots, k-1$, then $S_k < 0$. In fact,

$$S_k = S_{k-1} - 2f_{k-1} < 0.$$ ■

3.3.1 Discretization of the model

Observe that Theorem 3.4 ensures the existence of a class of steady solutions for the δ model which are characterized by the fact that the total mass of vehicles on the road is distributed only on the velocities which are multiples of Δv. We cannot prove the uniqueness of such a class of steady solutions. However we can show by numerical evidence that the asymptotic distributions of the δ model are only of the type stated by Theorem 3.4. Thus, in this subsection we introduce a discretization of the model (3.3).

To this end, the explicit formulation of the gain term is now useful. Notice that the Dirac delta function at $v = \min\{v_* + \Delta v, V_{\max}\}$ can be split as

$$\delta_{\min\{v_*+\Delta v, V_{\max}\}}(v) = \begin{cases} \delta_{v_*+\Delta v}(v), & \text{if } v_* \in [0, V_{\max} - \Delta v] \\ \delta_{V_{\max}}(v), & \text{if } v_* \in (V_{\max} - \Delta v, V_{\max}] \end{cases}$$

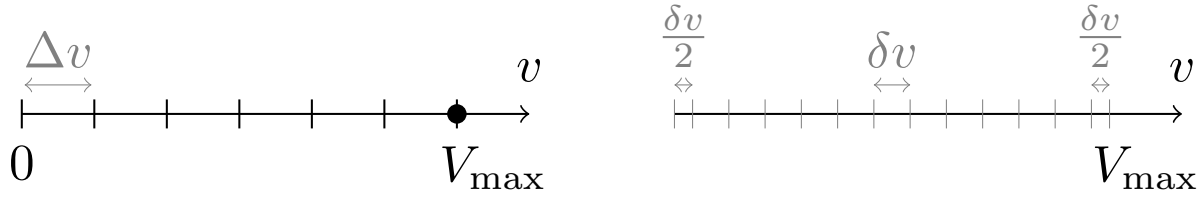

Figure 3.3: Left: ratio between Δv and $V_{\max}$. Right: discretization of the velocity space.

because the velocity jump of size Δv, leading to the output velocity $v = v_* + \Delta v$, can be performed only if $v_* \leq V_{\max} - \Delta v$. If instead $v_* \in (V_{\max} - \Delta v, V_{\max}]$, the post-interaction velocity will be $v = V_{\max}$. Thus the gain term of the δ model can be written as

$$\begin{aligned} G[f,f](t,v) =& \eta(1-P)f(t,v)\left[\int_v^{V_{\max}} f^* \mathrm{d}v^* + \int_v^{V_{\max}} f_* \mathrm{d}v_*\right] \\ &+ \eta P \rho \left[f(t, v-\Delta v) H_{\Delta v}(v) + \delta_{V_{\max}}(v) \int_{V_{\max}-\Delta v}^{V_{\max}} f_* \mathrm{d}v_*\right] \end{aligned} \tag{3.8}$$

where $H_\alpha(x)$ denotes the Heaviside step function with jump located in α, namely $H_\alpha(v) := \frac{\mathrm{d}}{\mathrm{d}v}\max\{0, v-\alpha\}$, $\alpha \in \mathbb{R}$. The last term in the expression of G means that, as a result of the microscopic interactions, the mass $P\rho\int_{V_{\max}-\Delta v}^{V_{\max}} f_* \mathrm{d}v_*$ is allocated entirely to the speed $V_{\max}$. Note that, in space-nonhomogeneous models, f_* and f^* may refer to distributions evaluated at different locations in space, see for instance [48] and [49]. For this reason we keep the integrals over field and candidate particles separate.

We suppose for simplicity that the fixed parameter Δv satisfies the following assumption:

Ansatz 3.6. The velocity jump Δv is an integer submultiple of the maximum speed $V_{\max}$ so that $\Delta v = V_{\max}/T$ with $T \in \mathbb{N}$, see the left panel of Figure 3.3.

We discretize the velocity space defining the *velocity cells* $I_j = [(j-\frac{3}{2})\delta v, (j-\frac{1}{2})\delta v] \cap [0, V_{\max}]$, for $j = 1, \ldots, n$. Note that all cells have amplitude $\delta v = V_{\max}/(n-1)$ except I_1 and I_n which have amplitude $\delta v/2$, see the right panel of Figure 3.3.

We consider a piecewise constant approximation of the kinetic distribution so that

$$f(t,v) \approx f_{\delta v}(t,v) = \sum_{j=1}^{n} f_j(t) \frac{\chi_{I_j}(v)}{|I_j|}, \tag{3.9}$$

where f_j represents the number of vehicles traveling with velocity $v \in I_j$.

By integrating the kinetic equation (3.1) over the cells I_j and using $f_{\delta v}(t,v)$ in place of $f(t,v)$ we obtain the following system of ordinary differential equations

$$f_j'(t) = Q_j[f_{\delta v}, f_{\delta v}](t) := \int_{I_j} Q[f_{\delta v}, f_{\delta v}](t,v)\mathrm{d}v, \tag{3.10}$$

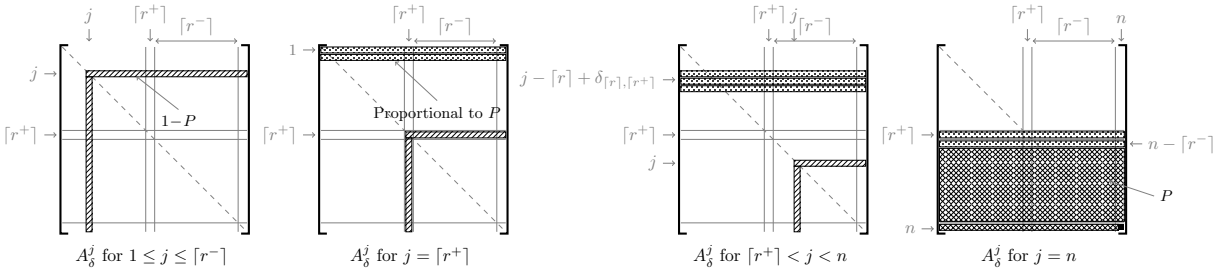

Figure 3.4: Structure of the probability matrices of the δ model, with $\Delta v = V_{\max}/2$.

whose initial conditions $f_1(0), \dots, f_n(0)$ are such that

$$\sum_{j=1}^{n} f_j(0) = \int_{\mathcal{V}} f(t=0, v)\mathrm{d}v = \rho$$

and ρ is the initial density, which remains constant during the time evolution in the spatially homogeneous case.

We set $r := \Delta v/\delta v \in \mathbb{R}^+$ and we define $r^+ := r + \frac{1}{2}$, $r^- := r - \frac{1}{2}$. Then $I_{\lceil r^+ \rceil}$ is the cell which contains $v = \Delta v$, where $\lceil r^+ \rceil$ denotes the integer part of r^+. By computing the right hand side of the ODE system (3.10), we obtain explicitly

$$\begin{aligned}\frac{1}{\eta}Q_j[f,f](t) =&(1-P)f^j f_j + (1-P)f_j \sum_{k=j+1}^{n} f^k + (1-P)f^j \sum_{h=j+1}^{n} f_h \\ &- f_j \sum_{k=1}^{n} f^k, \quad \text{for } j = 1, \dots, \left\lceil r^- \right\rceil\end{aligned} \tag{3.11a}$$

$$\begin{aligned}\frac{1}{\eta}Q_j[f,f](t) =&(1-P)f^j f_j + (1-P)f_j \sum_{k=j+1}^{n} f^k + (1-P)f^j \sum_{h=j+1}^{n} f_h \\ &+ P\rho\left[2f_1 \min\{\frac{1}{2}, \left\lceil r^+ \right\rceil - \frac{1}{2} - r\} + \delta_{\lceil r \rceil, \lceil r^- \rceil} f_2(\left\lceil r^- \right\rceil - r)\right] \\ &- f_j \sum_{k=1}^{n} f^k, \quad \text{for } j = \left\lceil r^+ \right\rceil\end{aligned} \tag{3.11b}$$

$$\begin{aligned}\frac{1}{\eta}Q_j[f,f](t) =&(1-P)f^j f_j + (1-P)f_j \sum_{k=j+1}^{n} f^k + (1-P)f^j \sum_{h=j+1}^{n} f_h \\ &+ P\rho\left[(1+\delta_{\lceil r \rceil, \lceil r^+ \rceil}\delta_{j, \lceil r^+ \rceil + 1}) f_{j-\lceil r \rceil}(1 + r - \lceil r \rceil) + f_{j-\lceil r \rceil + 1}(-r + \lceil r \rceil)\right] \\ &- f_j \sum_{k=1}^{n} f^k, \quad \text{for } j = \left\lceil r^+ \right\rceil + 1, \dots, n-1\end{aligned} \tag{3.11c}$$

$$\begin{aligned}\frac{1}{\eta}Q_n[f,f](t) =&(1-P)f^n f_n \\ &+ \underbrace{P\rho\delta_{\lceil r\rceil,\lceil r^+\rceil}\left[f_{n-\lceil r^+\rceil}(r-\left\lceil r^-\right\rceil)+f_{n-\lceil r^-\rceil}(\left\lceil r^+\right\rceil-\frac{1}{2}-r)\right]}\\ &\underbrace{P\rho f_{n-\lceil r^-\rceil}\left[\frac{1}{2}\delta_{\lceil r\rceil,\lceil r^-\rceil}+(r-\left\lceil r^-\right\rceil+\frac{1}{2})\right]+P\rho\sum_{h=n-\lceil r^+\rceil+2}^{n}f_h}\\ &- f_n\sum_{k=1}^{n}f^k,\end{aligned} \tag{3.11d}$$

where here $\delta_{i,j}$'s are Kronecker's delta's. The terms with a wavy underline are those deriving from the acceleration term. In the formulae above, the position of the index of the components of $\mathbf{f}=[f_1,\dots,f_n]^\mathsf{T}\in\mathbb{R}^n$ distinguishes the distribution of the field and of the candidate vehicles: bottom right for the candidate vehicles (as in f_h), top right for the field vehicles (as in f^k). In vector form:

$$\frac{\mathrm{d}}{\mathrm{d}t}f_j=\eta\left[\mathbf{f}^\mathsf{T}A_\delta^j\mathbf{f}-\mathbf{f}^\mathsf{T}\mathbf{e}_j\mathbf{1}_n^\mathsf{T}\mathbf{f}\right],\quad j=1,\dots,n \tag{3.12}$$

where $\mathbf{e}_j\in\mathbb{R}^n$ denotes the vector with a 1 in the j-th component and 0's elsewhere, $\mathbf{1}_n^\mathsf{T}=[1,\dots,1]\in\mathbb{R}^n$. The matrices A_δ^j have a sparse structure, shown in Fig. 3.4 in which the nonzero elements are shaded with different hatchings, corresponding to the different values of the elements, as indicated in the panels in which they appear for the first time.

As it can be checked using (3.11), these matrices are stochastic with respect to the index j, i.e. $\sum_{j=1}^n\left(A_\delta^j\right)_{hk}=1,\ \forall\, h,k\in\{1,\dots,n\}$. This property comes from Ansatz 3.1, and it guarantees mass conservation.

Recall that the elements of the matrix $\left(A_\delta^j\right)_{hk}$ are the probabilities that the candidate vehicle with velocity in I_h, interacting with a field vehicle with velocity in I_k, acquires a velocity in I_j. The fact that these matrices are sparse means that a velocity in I_j can be acquired only for special values of the velocity of candidate and field vehicles. In particular, the j-th row of the matrix A_δ^j contains the probability of what we called "false gains" in Remark 3.3, that is the probability that the candidate vehicle *does not* change its speed. The non zero elements of the j-th column are the probabilities that a candidate vehicle acquires a speed in I_j by braking down to the speed of the leading vehicle. The non zero rows, located at $h=j-\lceil r\rceil+\delta_{\lceil r\rceil,\lceil r^+\rceil}$, $h-1$ and $h+1$, contain the probabilities that the candidate vehicle accelerates by Δv, acquiring therefore a velocity in $v_*+\Delta v\in I_j$ starting from a velocity v_* in I_{h-1}, I_h or I_{h+1}. The band between the rows $j-\lceil r\rceil+\delta_{\lceil r\rceil,\lceil r^+\rceil}+2$ and $j-1$ is filled with zeros, because in the δ model the acceleration is quantized. As we will see in Section 3.4.1, this band will be filled by non zero elements in the χ model, where the acceleration is distributed uniformly between $[v_*,v_*+\Delta v]$, where v_* is the actual speed of the candidate vehicle.

In Table 3.1 we summarize the numerical parameters introduced in order to discretize the continuous-velocity model.

Table 3.1: Table of the numerical parameters.

Parameter	Description	Definition
n	Number of discrete speeds	–
δv	Cell amplitude	$\delta v = {}^{V_{\max}}/_{n-1}$
r	Ratio between the speed jump Δv and the cell amplitude δv	$r = {}^{\Delta v}/_{\delta v}$
T	Number of speed jumps Δv contained in $[0, V_{\max}]$	$T = {}^{V_{\max}}/_{\Delta v}$

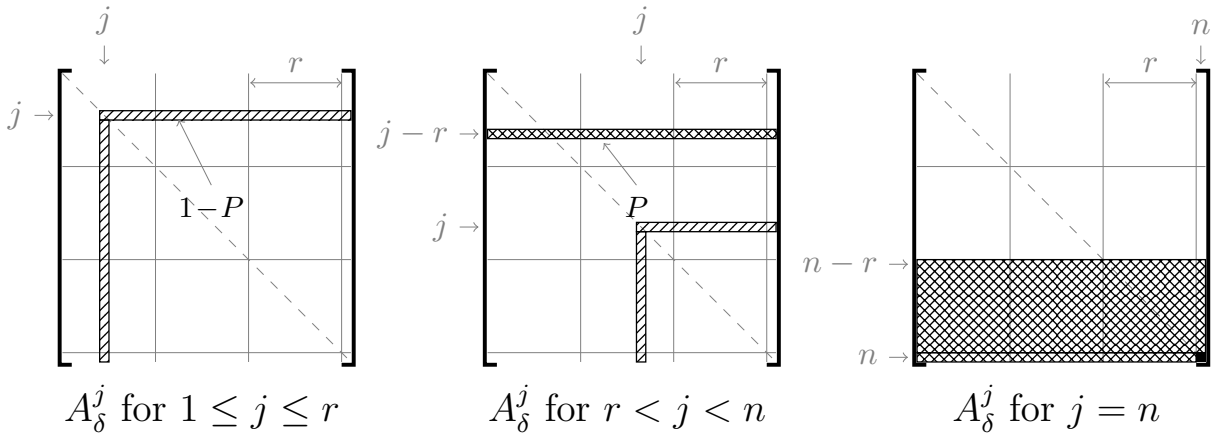

Figure 3.5: Structure of the probability matrices of the δ model with δv integer sub-multiple of Δv.

Remark 3.7. Model (3.12) has the same structure of the single-population model (2.2) introduced in [26]. However, (3.12) differs from (2.2) because now the interaction matrices (already called table of games in Chapter 2 in the context of discrete-velocity spaces) depend on the finite parameter Δv, which allows us to separate the physical and the discretization parameters.

***δv* as integer sub-multiple of *Δv*.** For the special choice of the velocity grid which ensures that $r = \Delta v/\delta v \in \mathbb{N}$, then the formulae (3.11) simplify as follows:

$$\begin{aligned}\frac{1}{\eta}Q_j[f,f](t) =&(1-P)f^j f_j + (1-P)f_j \sum_{k=j+1}^{n} f^k + (1-P)f^j \sum_{h=j+1}^{n} f_h \\ &- f_j \sum_{k=1}^{n} f^k, \quad \text{for } j = 1,\dots,r\end{aligned} \tag{3.13a}$$

$$\begin{aligned}\frac{1}{\eta}Q_j[f,f](t) =&(1-P)f^j f_j + (1-P)f_j \sum_{k=j+1}^{n} f^k + (1-P)f^j \sum_{h=j+1}^{n} f_h + \underbrace{P\rho f_{j-r}} \\ &- f_j \sum_{k=1}^{n} f^k, \quad \text{for } j = r+1,\dots,n-1\end{aligned} \tag{3.13b}$$

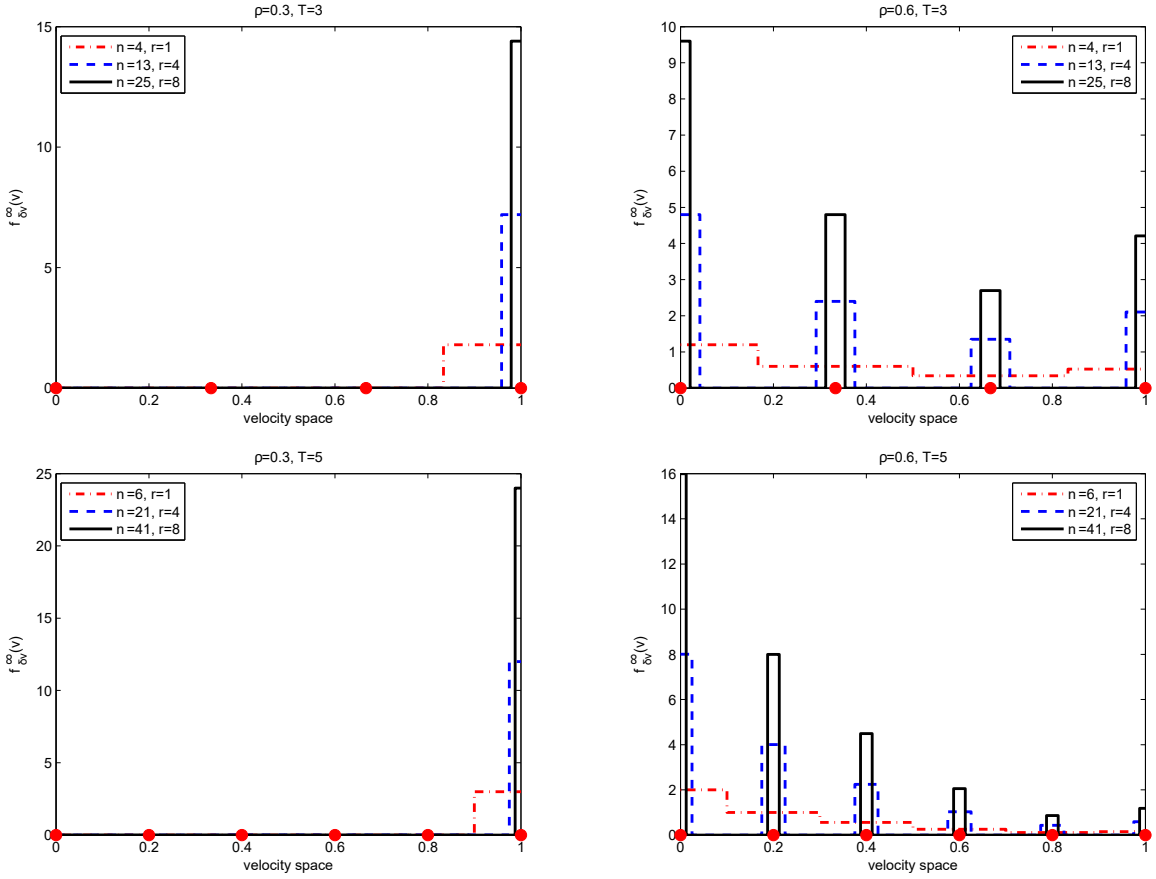

Figure 3.6: Approximation of the asymptotic kinetic distribution function obtained with two acceleration terms $\Delta v = 1/T$, $T = 3$ (top), $T = 5$ (bottom), and $n = rT + 1$ velocity cells, with $r \in \{1, 4, 8\}$; $\rho = 0.3$ (left) and $\rho = 0.6$ (right) are the initial densities. We mark with red circles on the x-axes the center of the $T + 1$ cells obtained with $r = 1$.

$$\frac{1}{\eta} Q_n[f, f](t) = (1 - P) f^n f_n + P\rho \underbrace{\sum_{h=n-r}^{n} f_h} - f_n \sum_{k=1}^{n} f^k \tag{3.13c}$$

The resulting interaction matrices are given in Figure 3.5. Notice that the rows $j - r \pm 1$ are filled with zeros. In fact, since δv is an integer sub-multiple of Δv, a velocity in I_j can be obtained as result of an acceleration only if the pre-interaction speed is a velocity in I_{j-r}.

The structure of the matrices A^j_δ determines the equilibrium of the discrete model (3.12). In Figure 3.6 we show the function

$$f^\infty_{\delta v}(v) := \lim_{t \to \infty} f_{\delta v}(t, v)$$

obtained by integrating numerically the system of equations up to steady state, for a few typical cases. In all numerical tests we take $P = 1 - \rho$ (that is as in (2.9) with $\alpha = \gamma = 1$), and with $V_{\max} = \rho_{\max} = 1$. As initial macroscopic densities, we choose $\rho = 0.3, 0.6$ (plots

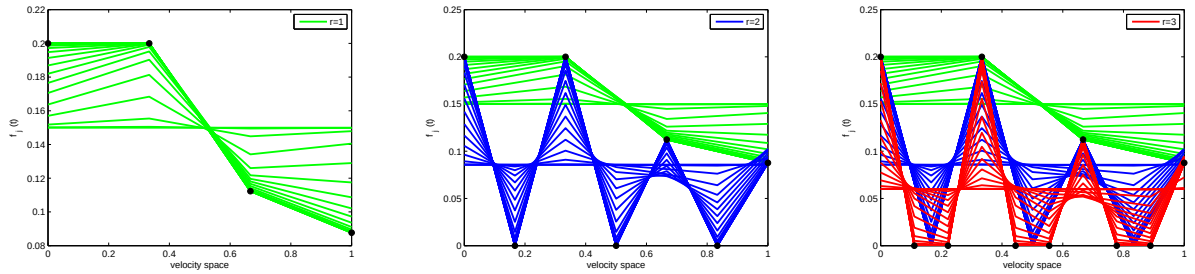

Figure 3.7: Evolution towards equilibrium of the discretized model (3.12) with $n = 4$ (green), $n = 7$ (blue) and $n = 10$ (red) grid points. The acceleration parameter Δv is taken as $V_{\max}/3$ and the density is $\rho = 0.6$. Black circles indicate the equilibrium values.

to the left and right of the figure). We consider two values for the acceleration parameter, $\Delta v = V_{\max}/T$, $T = 3, 5$ (top and bottom of the figure). The number of velocities in the grid is taken as $n = rT + 1$, with $r \in \{1, 4, 8\}$. The three curves in each plot contain the data for the cell averages of the equilibrium distribution for the different values of r. It is clear that in all cases, $f^{\infty}_{\delta v}(v)$ is a function of the density ρ and it approaches a series of delta functions, centered in the velocities which are multiples of Δv and indicated in the picture by red dots on the horizontal axis.

This means that, as $\delta v \to 0$, only a finite number, precisely $T + 1$, of velocities carry a non-zero mass of vehicles at equilibrium. More precisely, the discrete asymptotic function $f^{\infty}_{\delta v}(v)$ is different from zero only in the $T + 1$ cells $I_1, I_r, I_{2r}, \ldots, I_n$. Therefore, as time goes to infinity the number of nonzero values of the f_j's appearing in (3.9) is univocally determined by the acceleration term $\Delta v = V_{\max}/T$.

The previous considerations can be supported by the numerical results in Figure 3.7, in which we show the evolution towards equilibrium of the f_j's, $j = 1, \ldots, n$. In this figure, $\Delta v = V_{\max}/3$, and the different plots are obtained starting from a uniform initial distribution, namely in (3.9) we take $f_j(t = 0) = \rho/n, \forall j = 1, \ldots, n$, with $r = 1$ (green), $r = 2$ (blue) and $r = 3$ (red), which correspond to $n = 4, 7$ and 10 velocity cells respectively, and $\rho = 0.6$. It is clear that under grid refinement the number of nonzero steady values does not change. In fact, note that a different dynamics towards equilibrium is observed, for different values of the number n of cells, but as equilibrium is approached, the values of the f_j's go to zero except for the velocities corresponding to integer multiples of Δv. Moreover, the non zero values of the steady-state distribution $f^{\infty}_{\delta v}$ do not depend on the discretization parameter δv. This fact can be also deduced by looking at equations (3.11) of the discrete collision operator. These expressions are not functions of δv. Thus all exact values of the equilibria can be obtained using a coarse grid.

Theorem 3.9 below confirms, with an analytical proof, the structure of the equilibria that we have just observed in the numerical results and it states that the steady-state solution of the δ model, prescribed by Theorem 3.4, can be reconstructed numerically on the grid with $\delta v = \Delta v$. To this end, we first recall a result from [20], where the existence and well posedness of the solution of such systems is proved and then we show that the

discrete equilibria of additional equations resulting from the choice $r > 1$ give actually no contribution.

Theorem 3.8. – *(Delitala-Tosin) Let $f_j(t=0) \geq 0$, with $\sum_{j=1}^{n} f_j(t=0) = \rho$, be the initial condition for the system*

$$\frac{\mathrm{d}}{\mathrm{d}t} f_j = \mathbf{f}^{\mathsf{T}} A^j \mathbf{f} - \mathbf{f}^{\mathsf{T}} \mathbf{e}_j \mathbf{1}_n^{\mathsf{T}} \mathbf{f}, \quad j = 1, \dots, n,$$

where the matrices A^j are stochastic matrices with respect to the index j, i.e. $\sum_j A^j_{hk} = 1$ for all h, k. Then there exists $t_* = +\infty$ such that the system admits a unique non-negative local solution $f \geq 0$ satisfying the a priori estimate

$$||f(t)||_1 = ||f_0||_1 = \rho \qquad \forall t \in (0, t_* = +\infty].$$

The following result, together with Remark 3.10, shows that all equilibria of the discrete model are of the quantized form described by Theorem 3.4. Thus the next Theorem establishes the correspondences symbolized by the right vertical and the middle horizontal arrows in Figure 3.2.

Theorem 3.9. – *Let P be a given function of the density ρ. For any fixed $\Delta v = V_{\max}/T$, $T \in \mathbb{N}$, let $\mathbf{f}_r^\infty(\rho)$ denote the vector of the equilibrium solutions of the ODE system (3.12), obtained on the grid with spacing δv given by $\Delta v = r\delta v$ with $r = (n-1)/T \in \mathbb{N}$. Then*

$$(\mathbf{f}_r^\infty)_j = \begin{cases} (\mathbf{f}_1^\infty)_{\lceil \frac{j}{r} \rceil} & \text{if} \mod (j-1, r) = 0 \\ 0 & \text{otherwise} \end{cases}$$

is the unique stable equilibrium and the values of $\mathbf{f}_1^\infty$ depend uniquely on the initial density ρ, with $\sum_{k=1}^{T+1} (\mathbf{f}_1^\infty)_k = \rho$.

Proof. We already know from Theorem 3.8 that the solution of (3.12) exists, is non-negative and is uniquely determined by the initial condition.

To prove the statement, we compute explicitly the equilibrium solutions of (3.12), using the explicit expression of the collision kernel given in (3.11a), (3.11b), (3.11c) and (3.11d), with $r \in \mathbb{N}$ and $n = rT+1$. Since here we are interested in the solutions of the homogeneous problem, we will take identical distributions for the candidate and the field vehicles, i.e. $f_j = f^j$.

For $j = 1$, using the expression (3.11a) and the fact that $\sum_{k=1}^{n} f_k = \rho$ we obtain

$$\frac{\mathrm{d}}{\mathrm{d}t} f_1 = 0 \quad \Leftrightarrow \quad -(1-P) f_1^2 + (1-2P)\, \rho f_1 = 0.$$

This is a quadratic equation for f_1, which has the two roots $f_1 = 0$ and $f_1 = \rho(1-2P)/(1-P)$. It is easy to see that one solution is stable, and the other one unstable, depending on the value of P. Here we are interested only in the stable root, so we find

$$(\mathbf{f}_r^\infty)_1 = \begin{cases} 0 & P \geq \frac{1}{2} \\ \rho \frac{1-2P}{1-P} & \text{otherwise} \end{cases} \tag{3.14}$$

Thus, no vehicle is in the lowest speed cell I_1 if $P \geq \frac{1}{2}$, which, for the simple case $P = 1-\rho$ means that all cars are moving if $\rho \leq \frac{1}{2}$.

The case $j = 1$ we just computed is typical. Also for larger values of j, we find a quadratic equation for the unknown f_j, which involves only previously computed values of $f_k, k < j$. Thus, we can easily compute iteratively all components of $\mathbf{f}_r^\infty$.

For $2 \leq j \leq r$, the equilibrium equation is obtained by using again the expressions (3.11a) with $r \in \mathbb{N}$. Then

$$-(1-P)f_j^2 + \left[(1-2P)\rho - 2(1-P)\sum_{k=1}^{j-1} f_k\right] f_j = 0.$$

Start from $j = 2$. Clearly, for $P \geq \frac{1}{2}$, substituting equation (3.14), we again have $(\mathbf{f}_r^\infty)_2 = 0$. For $P < \frac{1}{2}$, the equation for f_2, with f_1 given by (3.14), becomes

$$-(1-P)f_2^2 - (1-2P)\,\rho f_2 = 0.$$

Comparing with the equation for f_1, we see that now the stable root is $f_2 = 0$. Thus, at equilibrium, we have $(\mathbf{f}_r^\infty)_2 = 0$, for all values of P. Analogously, it is easy to see that $(\mathbf{f}_r^\infty)_j = 0$, $\forall j = 3, \ldots, r$.

For $r+1 \leq j < n$, in place of (3.11a), we use (3.11b) and (3.11c) in order to obtain the equilibrium equation. Then

$$-(1-P)f_j^2 + \left[(1-2P)\rho - 2(1-P)\sum_{k=1}^{j-1} f_k\right] f_j + P\rho f_{j-r} = 0. \tag{3.15}$$

The equation has a positive discriminant

$$\mathcal{D}_j = \left[(1-2P)\rho - 2(1-P)\sum_{k=1}^{j-1} f_k\right]^2 + 4P(1-P)\rho f_{j-r}$$

thus it always admits two real roots. To fix ideas, let us consider $r+1 \leq j \leq 2r$. If $j = r+1$, since $(\mathbf{f}_r^\infty)_k = 0$, $\forall k = 2, \ldots, r$, equation (3.15) becomes

$$-(1-P)f_{r+1}^2 + \left[(1-2P)\rho - 2(1-P)f_1\right] f_{r+1} + P\rho f_1 = 0.$$

Thus, we find $(\mathbf{f}_r^\infty)_{r+1} = 0$ for $P \geq 1/2$, because the equation for f_{r+1} becomes identical to (3.3.1). If instead $P < 1/2$, substituting the expression for f_1, the equation for f_{r+1} becomes

$$-(1-P)f_{r+1}^2 - (1-2P)\rho f_{r+1} + \rho^2 \frac{P(1-2P)}{1-P} = 0.$$

This equation has a negative and a positive real root, which is stable. Thus

$$(\mathbf{f}_r^\infty)_{r+1} = \begin{cases} 0 & P \geq \frac{1}{2} \\ \dfrac{-(1-2P)\rho + \rho\sqrt{(1-4P^2)}}{2(1-P)} & \text{otherwise.} \end{cases}$$

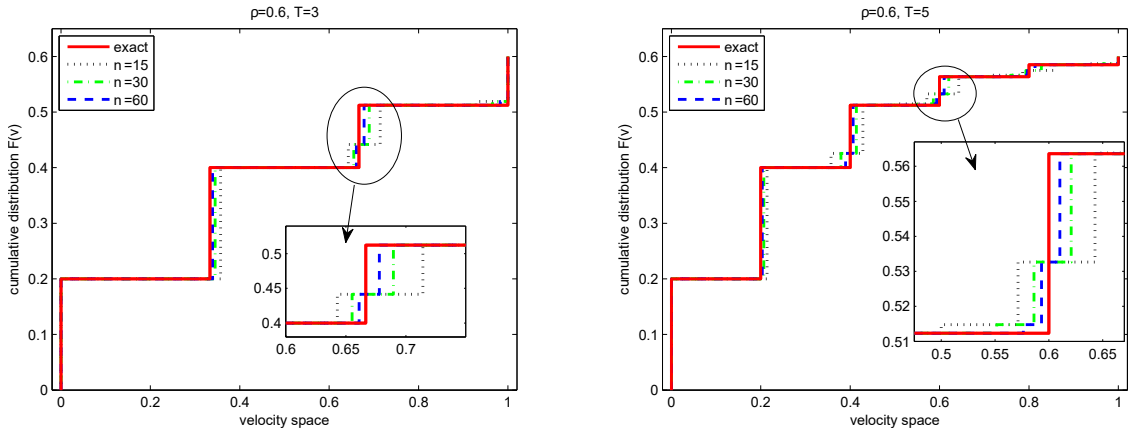

Figure 3.8: Cumulative density at equilibrium for several values of $\delta v \to 0$. The density is $\rho = 0.6$ and Δv is chosen as 1/3 (left), 1/5 (right).

Now, let $r+1 < j \leq 2r$. Since $f_{j-r} = 0$, the constant term of equation (3.15) is zero. Then, as seen for $j = 2, \dots, r$, it is easy to prove that, for each $j = r+2, \dots, 2r$ and for all values of P, one solution is negative and thus $(\mathbf{f}_r^\infty)_j = 0$.

Clearly, this procedure can be repeated and we find that

$$(\mathbf{f}_r^\infty)_j = \begin{cases} 0 & P \geq \frac{1}{2} \\ \dfrac{-2(1-P)\displaystyle\sum_{k=1}^{j-1} f_k + (1-2P)\rho + \sqrt{\mathcal{D}_j}}{2(1-P)} & \text{otherwise} \end{cases}$$

if $j = lr+1$, $l = 0, \dots, T-1$, while $(\mathbf{f}_r^\infty)_j = 0$ otherwise. From these considerations, the thesis easily follows. Finally, just note that for the last value, f_n, we can use mass conservation

$$(\mathbf{f}_r^\infty)_{rT+1} = (\mathbf{f}_r)_n = \rho - \sum_{l=0}^{T-1} (\mathbf{f}_r)_{lr+1}(\rho). \qquad \blacksquare$$

Notice that the result above proves that equilibria are determined by the initial density ρ, which is constant in time in the spatially homogeneous case, but they do not depend on the number of cells n used to approximate the kinetic distribution. In fact, the stable equilibria just computed correspond exactly to the values f_j^∞ given in Theorem 3.4 and they can all be recovered on the coarse grid $\delta v = \Delta v$, i.e. choosing $r = 1$.

Remark 3.10 (The case of a generic δv). In order to further investigate the existence of stable equilibria, we can seek more general ones numerically. In fact, the finite volume discretization (3.9) is capable of converging to absolutely continuous equilibria, but so far we proved that it converges to sums of Dirac masses if δv is an integer submultiple of Δv. Here we apply our discretization scheme with non-integer ratios $r = \Delta v/\delta v$ and show that the resulting equilibria converge, in the sense of distributions, to the equilibria already described in Theorems 3.4 and 3.9.

When $r = \Delta v/\delta v$ is not integer, Theorem 3.9 cannot be applied, but numerical integration of equation (3.12) shows that, for large time, the solution approaches equilibria that have masses concentrated at points spaced by Δv. More precisely, in this more general case, only a small finite number of components of $\mathbf{f}_r^\infty$ are nonzero and the cumulative distribution function induced by the discrete $f_{\delta v}^\infty(v)$, cf. (3.9),

$$F_{\delta v}(v) = \int_0^v f_{\delta v}^\infty(v)\mathrm{d}v, \quad v \in [0, V_{\max}],$$

approximates the cumulative distribution of a sum of Dirac masses centered at multiples of Δv. That is, $F_{\delta v}(v)$ converges to a piecewise constant function with jump discontinuities at multiples of Δv. See Figure 3.8.

Furthermore, Figure 3.8 shows that the jump discontinuities of the cumulative distribution in the limit $\delta v \to 0$ are located exactly in the points computed analytically by Theorem 3.9 in the case $r \in \mathbb{N}$. In particular, the figure shows the cumulative distribution at equilibrium computed by solving numerically (3.12) for several values of the discretization parameter δv with non-integer ratio $\Delta v/\delta v$. In both panels the density is $\rho = 0.6$, while $\Delta v = 1/3$ in the left plot and $\Delta v = 1/5$ in the right one. The continuous red curve represents the cumulative distribution of the stationary solution for $\delta v = \Delta v$, computed by Theorem 3.9. The black dotted curve is computed with $n = 15$ velocity cells, the green dot-dashed line with $n = 30$ and finally the blue dashed one with $n = 60$. We observe that as $\delta v \to 0$ the cumulative distribution tends to that of the analytic solution of Theorem 3.4, where only the velocities centered in multiples of Δv give rise to a jump discontinuity.

We conclude the section with a few remarks on the structure of the equilibria of (3.12).

Remark 3.11 (Reduced velocity space). The δ model is characterized by a small number of non-trivial values for the microscopic velocities, which allows one to compute analytically the equilibrium of the system. This fact provides an analytic closure of the macroscopic equations. This fact can also be exploited from a numerical point of view, justifying the use of a small number of discretization points in simulations aimed at capturing equilibrium effects. In this sense, the model seems to suggest that kinetic corrections can be accounted for with a computational cost which is not much higher than the one needed for a macroscopic model.

Remark 3.12 (Unstable equilibria). Theorem 3.9 gives the uniqueness of the stable equilibrium of the model with $\Delta v/\delta v = r \in \mathbb{N}$. Unstable ones may occur if the initial condition is such that $f_1(0) = 0$. In fact, the interaction rules related to the case $v_* > v^*$ do not generate a post-interaction velocity v which is less than v^*. Thus if $f_1(0) = 0$, i.e. if there are no vehicles with velocity $v_1 = 0$ at the initial time, there will not be interactions leading to an increase of f_1. This consideration can be generalized: if $f_j(0) = 0$ for $j = 1, \ldots, \bar{j} < r$, then the computed equilibria will be $f_j = (\mathbf{f}_r^\infty)_{j-\bar{j}}$, where $\mathbf{f}_r$ is the vector containing the stable equilibria. In this sense, the equilibrium solution of the δ model does not only depend on ρ but also on the initial condition $f(0, v)$. These solutions however are

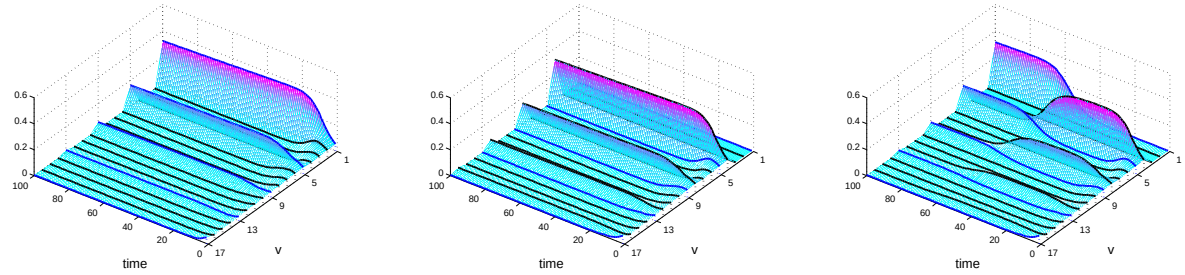

Figure 3.9: Evolution towards equilibrium, $\rho = 0.7$, $T = 4$, $n = 17$. Left: $f_j(t = 0) \equiv \rho/n$. Middle: $f_j(t = 0) = 0, j = 1, 2, 3$, $f_j(t = 0) \equiv (\rho/(n - 3)), j > 3$. Right: $f_1 = \epsilon = 10^{-6}, f_2 = f_3 = 0$ and $f_j(t = 0) \equiv ((\rho - \epsilon)/(n - 3))$. The thick lines highlight the components f_j and the blue ones are for those that appear in stable equilibria, i.e. with $j = kr + 1$ for $k = 0, \dots, T$.

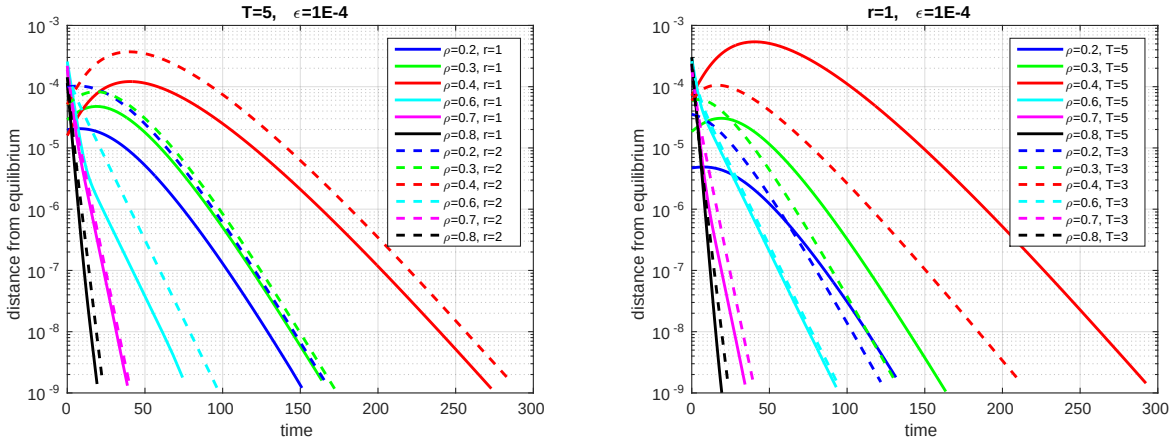

Figure 3.10: Speed of convergence towards the stable equilibria of the δ model. The initial condition is a small random perturbation of the steady-states.

unstable: a small perturbation on $f_1(t = 0)$ is enough to trigger the evolution towards the stable equilibrium, which depends only on ρ.

This is illustrated in Figure 3.9: in the left panel we show the evolution towards equilibrium when $f_j(t = 0) \neq 0$ for all classes (this is the stable equilibrium), while in the middle we show the case when $f_1 = f_2 = f_3 = 0$. In the rightmost panel we show a perturbation of the previous case, where f_1 takes a very small but nonzero value. It is clear that the evolution goes at first towards the unstable equilibrium of the middle panel, but then, in the long run, the stable equilibrium of Theorem 3.9 emerges.

Remark 3.13 (Convergence rate to equilibrium). In Figure 3.10 we study the rate of convergence towards the stable steady-states. For the set of densities $\rho \in \{0.2, 0.3, 0.4, 0.6, 0.7, 0.8\}$ we integrate numerically the system (3.12) for large times starting from a small random perturbation of the stable equilibrium. In both panels, we use a linear scale for the x-axis (time) and a logarithmic scale for the y-axis (error). The error is computed at each step as $e(t) := \|f(t) - f^\infty\|_2$. The figure suggests that the rate of

convergence towards the stable equilibrium depends on the density. In fact, in the left panel we consider different values of the ratio $\Delta v/\delta v = r$, in particular $r = 1$ (solid lines) and $r = 2$ (dashed lines), and we note that the slopes of the curves corresponding to the same value of ρ are the same. A similar behavior is observed in the right plot in which two different Δv are taken, $\Delta v = 1/5$ (solid lines) and $\Delta v = 1/3$ (dashed lines). We can conjecture that for large enough times the distance from equilibrium behaves as $e(t) \simeq Ce^{-M(\rho)t} \|f(t=0) - f^\infty\|_2$, where $C = C(r, \Delta v)$, $M(\rho) > 0$.

3.4 The χ velocity model

The structure of the steady-state distribution of the δ model clearly depends on the particular choice of the acceleration interaction made in (3.3), in which a vehicle accelerates by jumping from its pre-interaction velocity v_* to the new velocity $v_* + \Delta v$. Thus it could seem quite natural that only velocities 0, Δv, $2\Delta v, \ldots, V_{\max}$ give a non zero contribution at equilibrium.

Here we study the χ model, already introduced in Section 3.2.1 (see equation (3.4)), in which vehicles can assume a post-interaction velocity uniformly distributed over a range of speeds when the acceleration interaction occurs. We will show that, although this model is more refined than the δ model, at equilibrium the essential information is already caught by the simpler δ model.

Using the formulation (3.4) for the transition probability density A, we rewrite the gain term in (3.2) as

$$G[f,f](t,v) = \eta \int_{\mathcal{V}} \int_{\mathcal{V}} \left[(1-P)\delta_{\min\{v_*,v^*\}}(v) + P \frac{\chi_{[v_*,\min\{v_*+\Delta v, V_{\max}\}]}(v)}{\min\{v_* + \Delta v, V_{\max}\} - v_*} \right] f_* f^* \mathrm{d}v_* \mathrm{d}v^*.$$

Notice that the χ function can be split as

$$\frac{\chi_{[v_*,\min\{v_*+\Delta v, V_{\max}\}]}(v)}{\min\{v_* + \Delta v, V_{\max}\} - v_*} = \begin{cases} \frac{\chi_{[v_*,v_*+\Delta v]}(v)}{\Delta v}, & \text{if } v_* \in [0, V_{\max} - \Delta v] \\ \frac{\chi_{[v_*,V_{\max}]}(v)}{V_{\max} - v_*}, & \text{if } v_* \in (V_{\max} - \Delta v, V_{\max}] \end{cases}$$

hence substituting in the above equation and evaluating explicitly the integrals, we find

$$\begin{aligned} G[f,f](t,v) =& \eta(1-P) f(t,v) \left[\int_v^{V_{\max}} f^* \mathrm{d}v^* + \int_v^{V_{\max}} f_* \mathrm{d}v_* \right] \\ &+ \eta P \rho \left[\frac{1}{\Delta v} \int_0^{V_{\max}-\Delta v} \chi_{[v_*,v_*+\Delta v]}(v) f_* \mathrm{d}v_* + \int_{V_{\max}-\Delta v}^{V_{\max}} \frac{\chi_{[v_*,V_{\max}]}(v)}{V_{\max} - v_*} f_* \mathrm{d}v_* \right]. \end{aligned} \tag{3.16}$$

Observe that (3.16) differs from the gain operator of the δ model given in (3.8) only in the terms proportional to P.

3.4.1 Discretization of the model

To compute the steady-state solution of the χ model, we need to integrate the equations numerically. We use the same discretization of the velocity space $\mathcal{V}$ introduced to discretize the δ model and therefore the kinetic distribution is approximated as in (3.9).

Integrating the kinetic equation (3.1) over each cell, we find the system of ODEs (3.10), but now the gain term is given by (3.16). Although in this case the integrals are laborious, they can be computed recalling that $\Delta v = V_{\max}/T$ with $T \in \mathbb{N}$ (see Ansatz 3.6) and assuming that δv is an integer submultiple of Δv. Thus we will take $n - 1 \equiv 0 \mod T$ and $r = \frac{n-1}{T}$.

In order to compute explicitly the matrix elements resulting from the discretization of the χ model we just need to compute the terms resulting from

$$\frac{1}{\eta}\widetilde{G}[f,f](t,v) = \frac{P\rho}{\Delta v}\int_0^{V_{\max}-\Delta v} \chi_{[v_*,v_*+\Delta v]}(v) f_* \mathrm{d}v_* + P\rho \int_{V_{\max}-\Delta v}^{V_{\max}} \frac{\chi_{[v_*,V_{\max}]}(v)}{V_{\max}-v_*} f_* \mathrm{d}v_*.$$

When the terms above are integrated over the cells I_1, we get

$$\int_{I_1} \frac{1}{\eta}\widetilde{G}[f,f](t,v)\mathrm{d}v = \frac{P\rho}{4r} f_1. \tag{3.17a}$$

For $j = 2, \dots, r$,

$$\int_{I_j} \frac{1}{\eta}\widetilde{G}[f,f](t,v)\mathrm{d}v = \frac{P\rho}{r}\sum_{h=1}^{j-1} f_h + \frac{P\rho}{2r} f_j. \tag{3.17b}$$

For $j = r + 1$,

$$\int_{I_{r+1}} \frac{1}{\eta}\widetilde{G}[f,f](t,v)\mathrm{d}v = \frac{3P\rho}{4r} f_{j-r} + \frac{P\rho}{r}\sum_{h=j-r+1}^{j-1} f_h + \frac{P\rho}{2r} f_j. \tag{3.17c}$$

For $j = r + 2, \dots, n - r - 1$,

$$\int_{I_j} \frac{1}{\eta}\widetilde{G}[f,f](t,v)\mathrm{d}v = \frac{P\rho}{2r} f_{j-r} + \frac{P\rho}{r}\sum_{h=j-r+1}^{j-1} f_h + \frac{P\rho}{2r} f_j. \tag{3.17d}$$

For $j = n - r$,

$$\int_{I_{n-r}} \frac{1}{\eta}\widetilde{G}[f,f](t,v)\mathrm{d}v = \frac{P\rho}{2r} f_{j-r} + \frac{P\rho}{r}\sum_{h=j-r+1}^{j-1} f_h + P\rho\left[\frac{3}{8r} + \frac{1}{2} + \left(\frac{1}{2} - r\right)\log\left(\frac{2r}{2r-1}\right)\right] f_j. \tag{3.17e}$$

For $j = n-r+1, \dots, n-1$,

$$\begin{aligned}\int_{I_j} \frac{1}{\eta}\widetilde{G}[f,f](t,v)\mathrm{d}v =& \frac{P\rho}{2r} f_{j-r} + \frac{P\rho}{r}\sum_{h=j-r+1}^{n-r-1} f_h + P\rho\left[\frac{1}{2r} + \log\left(\frac{2r}{2r-1}\right)\right] f_{n-r} \qquad (3.17f)\\ &+ P\rho \sum_{h=n-r+1}^{j-1} \log\left(\frac{n-h+\frac{1}{2}}{n-h-\frac{1}{2}}\right) f_h\\ &+ P\rho\left[1 + \left(j+\frac{1}{2}-n\right)\log\left(\frac{n-j+\frac{1}{2}}{n-j-\frac{1}{2}}\right)\right] f_j.\end{aligned}$$

Finally, for $j = n$,

$$\begin{aligned}\int_{I_n} \frac{1}{\eta}\widetilde{G}[f,f](t,v)\mathrm{d}v =& P\rho\left[\frac{1}{8r} + \frac{1}{2}\log\left(\frac{2r}{2r-1}\right)\right] f_{j-r} \qquad (3.17g)\\ &+ \frac{P\rho}{2}\sum_{h=j-r+1}^{j-1} \log\left(\frac{n-h+\frac{1}{2}}{n-h-\frac{1}{2}}\right) f_h + P\rho f_n. \qquad (3.17h)\end{aligned}$$

We point out that, as in the case of the δ model, the ODE system can be conveniently rewritten in vector form as

$$\frac{\mathrm{d}}{\mathrm{d}t} f_j = \eta\left[\mathbf{f}^\mathsf{T} A_\chi^j \mathbf{f} - \mathbf{f}^\mathsf{T}\mathbf{e}_j \mathbf{1}_n^\mathsf{T}\mathbf{f}\right], \quad j = 1, \dots, n \qquad (3.18)$$

where $\mathbf{f} = [f_1, \dots, f_n]^\mathsf{T} \in \mathbb{R}^n$ is the vector of the unknown functions, $\mathbf{e}_j \in \mathbb{R}^n$ denotes the vector with a 1 in the j-th coordinate and 0's elsewhere, $\mathbf{1}_n^\mathsf{T} = [1, \dots, 1] \in \mathbb{R}^n$ and A_χ^j is the j-th interaction matrix such that $\left(A_\chi^j\right)_{hk}$ contains the probabilities that a candidate vehicle with velocity in I_h interacting with a field vehicle with velocity in I_k acquires a velocity in I_j. The matrices A_χ^j can be formed by removing the underlined terms in (3.13) with $r \in \mathbb{N}$ and adding the contributions given in (3.17).

Since model (3.18) is again of the form (2.2) and the matrices appearing in (3.18) are again stochastic, we can apply Theorem 3.8 to guarantee the well posedness of the associated Cauchy problem.

In Figure 3.11 we show the structure of the χ matrices: they are less sparse than the δ matrices because of the uniformly distributed acceleration in $[v_*, v_* + \Delta v]$, where v_* is the pre-interaction speed. In fact the matrix A_χ^j contains non-zero elements also in the rows from the $(j-r+1)$-th to the $(j-1)$-th, see the shaded areas in Figure 3.11, which represent non-zero probabilities of accelerating to a speed in I_j. Since $\Delta v = r\delta v$, exactly r rows fill up. Instead, the area drawn using hatching contains the same probabilities already shown in Figure 3.5 for the case of the δ model, with $r \in \mathbb{N}$. Note that the elements of the matrices depend on δv (see equations (3.17)). Thus, in contrast to the δ model, steady solutions of the ODE system (3.18) depend on the number of velocity cells n chosen to approximate the kinetic distribution (see (3.9)). In other words, although δv is an integer sub-multiple of Δv, this model does not converge, as time goes to infinity, to the asymptotic distribution

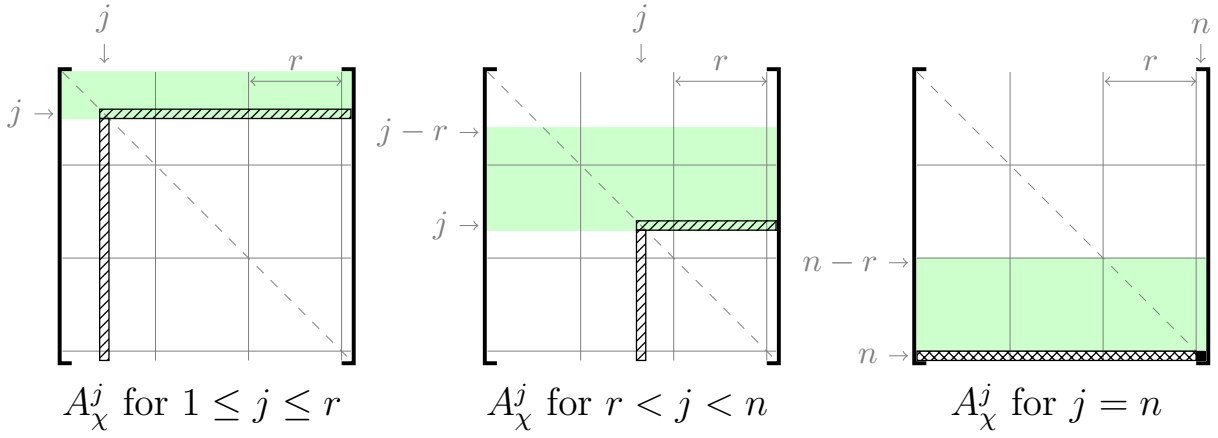

Figure 3.11: Structure of the probability matrices of the χ model with δv integer sub-multiple of Δv.

using a coarse grid as in the δ model. However, we do recover the asymptotic distribution in the limit $\delta v \to 0$.

Finally, notice from equations (3.17) that all the elements in the rows $j-r, \dots, j-1$ of the matrices A^j_χ, $j = 1, \dots, n$, tend to 0 as $1/r$ when the grid is refined. In particular, for $j = 1, \dots, r$, $A^j_\chi \to A^j_\delta$. This consideration is not true for the matrices A^j_χ, for $j = r+1, \dots, n$.

3.4.2 Expected speed of the δ and the χ model

Despite their differences the χ and the δ model are deeply related. This can be seen by computing the expected output speed in each model resulting from a fixed pre-interaction speed. We define the expected value $\langle v \rangle$ of the post-interaction velocity as

$$\langle v \rangle = \int_0^{V_{\max}} v A(v_* \to v | v^*; \rho)\, \mathrm{d}v, \quad (v_*, v^*) \in \mathcal{V} \times \mathcal{V}. \tag{3.19}$$

For brevity we indicate with $A_\delta(v)$ and $A_\chi(v)$ the probability densities given in (3.3) and (3.4) respectively. Again we assume that $P_1 = P_2 = P$ as decreasing function of the density ρ (cf. Ansatz 2.2). For the δ model we obtain

$$\begin{aligned} \langle v \rangle_\delta &= \int_0^{V_{\max}} v \left[(1-P)\, \delta_{\min\{v_*, v^*\}}(v) + P\, \delta_{\min\{v_* + \Delta v_\delta, V_{\max}\}}(v) \right] \mathrm{d}v \\ &= (1-P)\, \min\{v_*, v^*\} + P \begin{cases} v_* + \Delta v_\delta, & \text{if } v_* + \Delta v_\delta \le V_{\max} \\ v_* + (V_{\max} - v_*), & \text{if } v_* + \Delta v_\delta > V_{\max} \end{cases} \end{aligned} \tag{3.20}$$

In contrast, if we consider the χ model we have

$$\begin{aligned}\langle v\rangle_\chi &= \int_0^{V_{\max}} v\left[(1-P)\,\delta_{\min\{v_*,v^*\}}(v) + P\,\frac{\chi_{[v_*,\min\{v_*+\Delta v_\chi,V_{\max}\}]}(v)}{\min\{v_*+\Delta v_\chi, V_{\max}\}-v_*}\right]\mathrm{d}v\\ &= (1-P)\,\min\{v_*,v^*\} + P\begin{cases}\dfrac{1}{\Delta v_\chi}\displaystyle\int_{v_*}^{v_*+\Delta v_\chi} v\,\mathrm{d}v, & \text{if } v_*+\Delta v_\chi \le V_{\max}\\ \dfrac{1}{V_{\max}-v_*}\displaystyle\int_{v_*}^{V_{\max}} v\,\mathrm{d}v, & \text{if } v_*+\Delta v_\chi > V_{\max}\end{cases}\end{aligned}$$

and thus

$$\langle v\rangle_\chi = (1-P)\,\min\{v_*,v^*\} + P\begin{cases}v_* + \dfrac{\Delta v_\chi}{2}, & \text{if } v_*+\Delta v_\chi \le V_{\max}\\ v_* + \dfrac{1}{2}\,(V_{\max}-v_*), & \text{if } v_*+\Delta v_\chi > V_{\max}\end{cases} \tag{3.21}$$

By comparing the last lines of (3.20) and (3.21), it is clear that

$$\langle v\rangle_\chi = \langle v\rangle_\delta \qquad \forall\, v_* \le V_{\max}-\Delta v_\chi, \qquad \text{provided } \Delta v_\delta = \tfrac{1}{2}\Delta v_\chi. \tag{3.22}$$

Remark 3.14 (Uniformly distributed deceleration). The computation of the expected speed shows a link between the δ model and the χ model. In fact, under the constraint $\Delta v_\delta = \frac{1}{2}\Delta v_\chi$, the two models provide the same expected speed. Similarly, if we consider a braking scenario in which the candidate vehicle brakes to a speed uniformly distributed in an interval centered on v^*, then the expected speed results to be again $(1-P)v^*$.

Remark 3.15. Let us compare the A_χ^j matrices (Figure 3.11) for $r < j \le n-r$ with a given Δv and the corresponding A_δ^j matrices (Figure 3.5) with $\frac{\Delta v}{2}$. For the case $r \in \mathbb{N}$, the isolated nonzero row of A_δ^j is at $j-\frac{r}{2}$, which corresponds to the middle of the green shaded area in A_χ^j. Moreover, for any fixed Δv, it can be proved that, for $\delta v \to 0$, the sum of the quantities located in the shaded area of A_χ^j is equal to the total contribution provided by the $\left(j-\frac{r}{2}\right)$-th row of the δ matrices obtained with the acceleration parameter $\frac{\Delta v}{2}$. In other words, as $\delta v \to 0$, the total effect of the $\left(j-\frac{r}{2}\right)$-th row of A_δ^j with $\frac{\Delta v}{2}$ is spread over $r+1$ rows in the matrices A_χ^j with Δv, which are the rows shaded in green in Figure 3.11.

3.5 Macroscopic properties

Macroscopic acceleration In order to explain the relation of Δv with the acceleration of the vehicles in the model, we compute the rate of change of the macroscopic velocity:

$$\begin{aligned}\frac{\partial u}{\partial t} &= \frac{\partial}{\partial t}\left[\frac{1}{\rho}\int_V v f(t,v)\,\mathrm{d}v\right] = \frac{1}{\rho}\int_V v Q[f,f](t,v)\,\mathrm{d}v \\ &= \frac{\eta}{\rho}\left[\int_V v\,\mathrm{d}v\int_V\int_V A(v_*\to v|v^*;\rho) f_* f^*\,\mathrm{d}v_*\mathrm{d}v^* - \rho\int_V v f(t,v)\,\mathrm{d}v\right] \\ &= \frac{\eta}{\rho}\left[\int_V\int_V \langle v\rangle f_* f^*\,\mathrm{d}v_*\mathrm{d}v^* - \rho\int_V v f(t,v)\,\mathrm{d}v\right]\end{aligned}$$

where $\langle v\rangle$ is a function of v_* and v^* as defined in (3.19).

In the case of the δ model, $\langle v\rangle_\delta$ is given by (3.20) and thus

$$\begin{aligned}\frac{\partial u}{\partial t} = \frac{\eta}{\rho}\Bigg[&(1-P)\int_0^{V_{\max}}\int_0^{v_*} v^* f_* f^*\,\mathrm{d}v^*\mathrm{d}v_* + (1-P)\int_0^{V_{\max}}\int_{v_*}^{V_{\max}} v_* f_* f^*\,\mathrm{d}v^*\mathrm{d}v_* \\ &+ P\rho\int_0^{V_{\max}-\Delta v}(v_*+\Delta v_\delta) f_*\,\mathrm{d}v_* + P\rho\int_{V_{\max}-\Delta v}^{V_{\max}} V_{\max} f_*\,\mathrm{d}v_* - \rho\int_0^{V_{\max}} v f(t,v)\,\mathrm{d}v\Bigg].\end{aligned}$$

Given an initial distribution $f(t=0,v)$, the equation above yields the evolution of the macroscopic acceleration in time. It is easy to study analytically this quantity at the initial time. In particular, we compute the initial acceleration in the case in which all vehicles are still but the density is below the value for which $P = 1/2$ (that is $\rho/\rho_{\max} = 1/2$ when taking $P = 1 - \rho/\rho_{\max}$). By considering an initial distribution with all vehicles in the lowest velocity class, i.e. of the form $f(0,v) = \frac{2\rho}{\delta v}\chi_{I_1}(v)$, we have

$$\left.\frac{\partial u}{\partial t}\right|_{t=0} = \eta P\Delta v_\delta\int_0^{V_{\max}-\Delta v_\delta} f_*\,\mathrm{d}v_* + \mathcal{O}(\delta v) = \eta\rho P\Delta v_\delta + \mathcal{O}(\delta v).$$

The above equation shows that the acceleration of the vehicles in the δ model depends linearly on Δv. Analogously, for the χ model, using (3.21), one obtains

$$\left.\frac{\partial u}{\partial t}\right|_{t=0} = \frac{1}{2}\eta\rho P\Delta v_\chi + \mathcal{O}(\delta v)$$

which reinforces the remark made in (3.22) about the similarities of the χ and the δ model when $\Delta v_\chi = 2\Delta v_\delta$.

Remark 3.16 (Acceleration). Recall that $(\eta\rho)^{-1}$ is a time. Thus $\eta\rho\Delta v$ is the built-in acceleration of the model, which, not surprisingly, is linked to Δv. We can use dimensional arguments to estimate the order of magnitude of Δv. According to Lebacque [53], the maximum acceleration of cars is approximately $a_{LB} = 2.5$ m/s^2. The maximum speed is approximately $V_{\max} \simeq 28$m/s, and we expect the maximum acceleration when $P = 1$. Thus $\eta\rho\Delta v \simeq a_{LB}$.

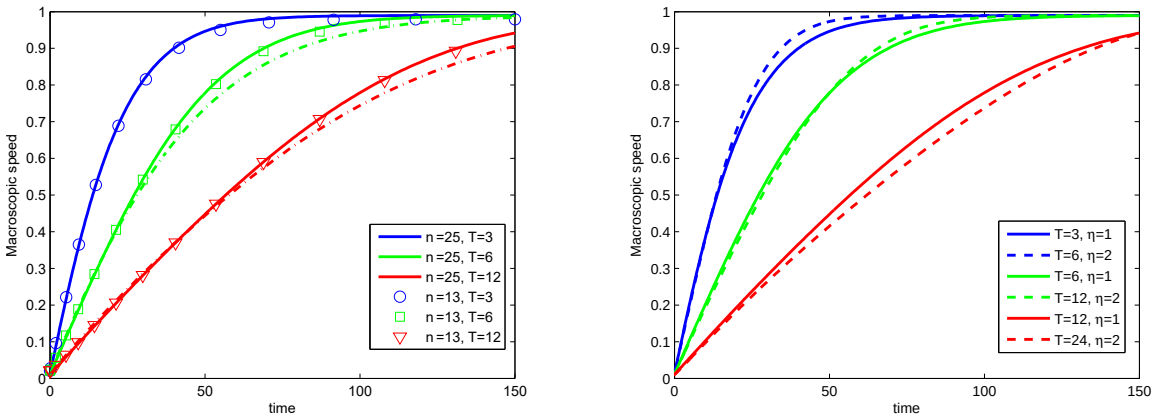

Figure 3.12: Evolution of the macroscopic velocity in time. Left: comparison of different values of T and δv. The dot-dashed lines without markers correspond to the χ model. Right: relaxation to steady state for different combinations of η and T.

Remark 3.17. The computation of the macroscopic acceleration for the δ and the χ model shows that they account for a bounded physical acceleration of vehicles through the finite parameter Δv. This fact overcomes the classical drawback of the discrete-velocity model (2.2) introduced in [26], see the corresponding discussion in Section 3.1. Moreover, the results of Section 3.3 show that at equilibrium the δ model is consistent with a discrete-velocity model. since the steady state is quantized on a finite number of speeds spaced by Δv. Thus, the number of velocities which really care important in the lattice, namely which allow to compute exactly the steady state using a reduced space of discrete speeds, is controlled by a physical concept: the acceleration of vehicles. Summarizing, the δ model is a continuous-velocity model converging to a lattice model at equilibrium for which we now have a recipe to choose n.

The estimates above provide the trend of the macroscopic acceleration starting from rest. For the general case, we now study the evolution of the macroscopic velocity u in time, up to steady state. These data are shown in Fig. 3.12 and Fig. 3.13, for various combinations of the model parameters. The results shown are obtained integrating the equations for the δ and the χ model found in (3.12) and (3.18), respectively, with $r \in \mathbb{N}$, and computing at each time $u(t) = \frac{1}{\rho} \int_V v f(t, v)\, \mathrm{d}v$.

Figure 3.12 shows a typical case in which we expect *acceleration*. We take $\rho_{\max} = V_{\max} = 1$. The density is $\rho = 0.15$, well below the value corresponding to $P = 1/2$ when $P = 1 - \rho$, and we start with an initial distribution in which $f_1(t = 0) = \rho$, while $f_j(t = 0) = 0$, for all $j \geq 2$. Thus initially all vehicles are still, and, since the density is low, they will accelerate to reach the maximum speed. The duration of the transient depends on the product $\eta \Delta v = \eta / T$, for a fixed density, as is apparent in the right panel of the figure, because the acceleration, i.e. the slope of the curves, is proportional to $\eta \Delta v$. The left panel shows the effect of the grid discretization, i.e. the role of $\delta v = 1/(n-1)$. It is clear that the discretization grid has no influence on the results, as expected from Theorem 3.9. The

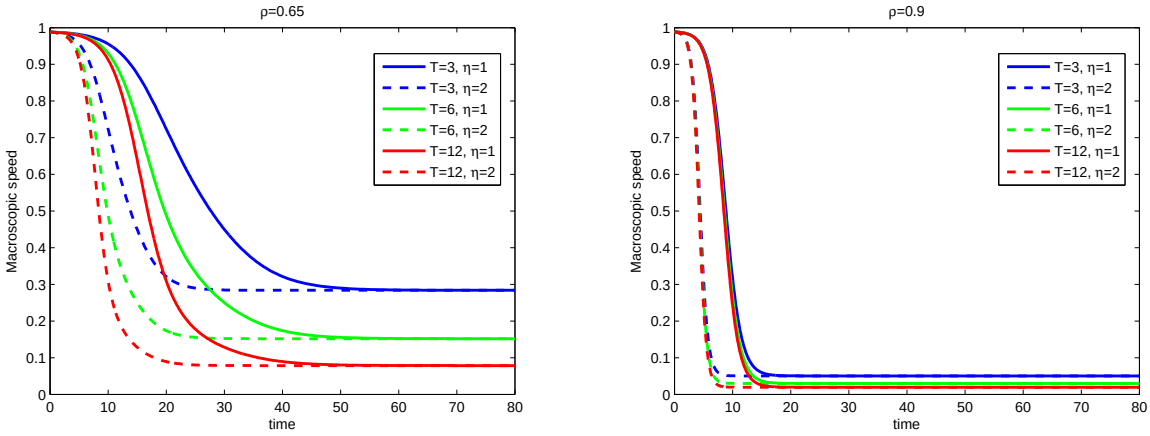

Figure 3.13: Evolution of the macroscopic velocity in time, for different values of T and η. Left: $\rho = 0.65$. Right: $\rho = 0.9$.

dot-dashed lines without markers show the evolution of the macroscopic velocity obtained with the χ model. The colour code is chosen to ensure that the curves with $\Delta v_\delta = \frac{1}{2}\Delta v_\chi$ are drawn in the same colour. As expected, the macroscopic velocity for the χ and the δ model behave very similarly, provided the parameter Δv is chosen correctly.

Next, in Figure 3.13, we show the evolution of the macroscopic velocity in two cases when we expect *deceleration* for the δ model. Namely, we consider $\rho = 0.65$ in the left panel and $\rho = 0.9$ in the right panel. The initial distribution is $f_n(t = 0) = \rho - \epsilon$, $f_1(t = 0) = \epsilon$, and $f_j(t = 0) = 0, j = 2, \dots, n-1$. The value ϵ is introduced to ensure convergence to the stable equilibrium, see Remark 3.12. Here $\epsilon = 0.01$. In other words, we start with a congested traffic, in which initially almost all vehicles are traveling at the fastest speed available. Clearly, this situation is somewhat artificial, but surely we expect the vehicles to brake. Since braking does not depend on Δv, we expect that the relaxation time towards equilibrium depends mainly on η and only weakly on T. This is clearly seen in both pictures. The macroscopic speed to which the model relaxes on the other hand will depend on Δv and on ρ, but not on η. Note that when $\rho = 0.9$, in all cases considered here, the equilibrium speed is nearly zero: in fact the traffic is extremely jammed. For $\rho = 0.65$ instead, we expect that the traffic will have a residual speed, because we are well below the value $P = 1/2$, but cars are not "bumper to bumper", and this residual speed does depend on Δv.

Fundamental diagrams As already discussed in the previous section, the nonzero elements of the matrix A^j_χ can be lumped in the matrix A^j_δ for n sufficiently large, with the only exception of the elements in the rectangle $r \times n$ (see Figure 3.11) of the matrices for $j = n - r + 1, \dots, n$. This is shown, for instance, in the evaluation of the expected value of the resulting speeds due to acceleration interactions in (3.20) and (3.21), which are comparable, except again for high speed values close to $V_{\max}$ (and different from it by at most Δv). Thus, although the χ model is apparently more refined then the δ model,

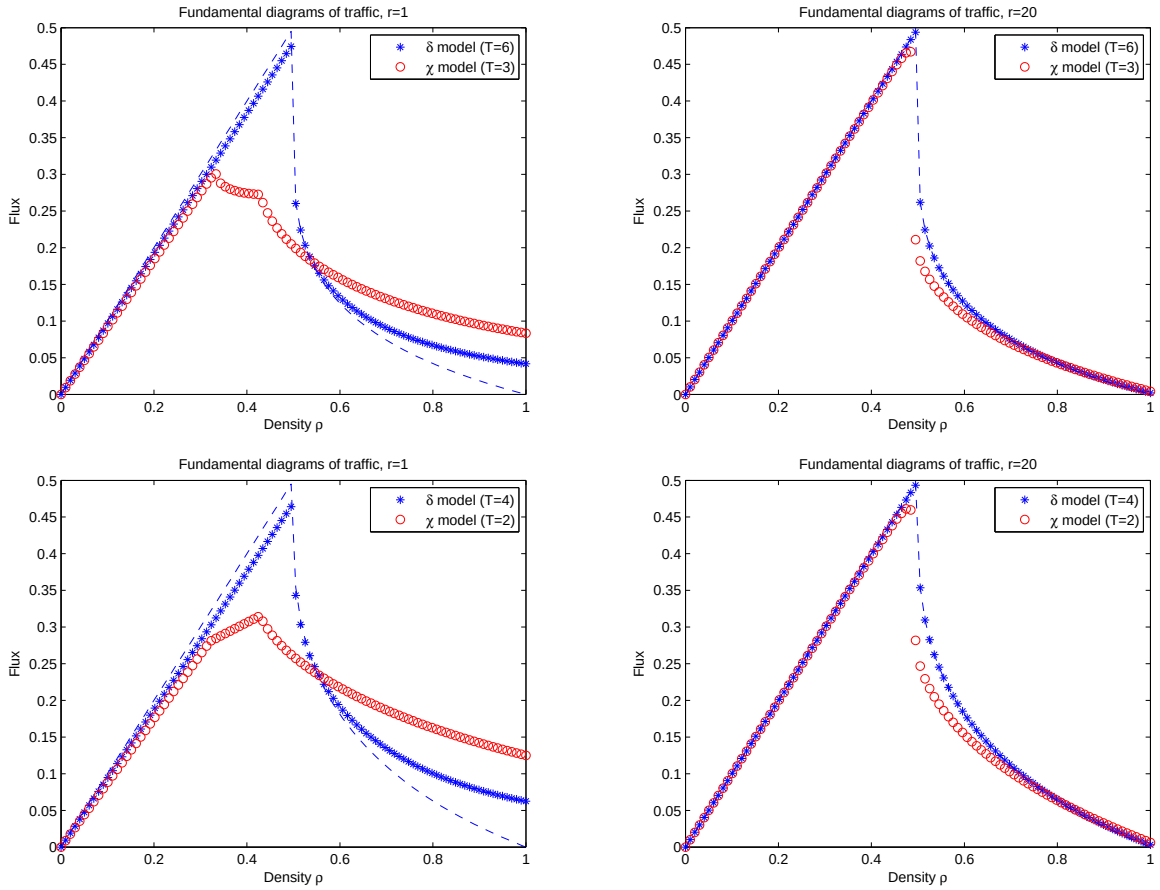

Figure 3.14: Fundamental diagrams resulting from the δ model (blue *-symbols) and from the χ model with acceleration parameter $\Delta v_\delta = \frac{1}{2}\Delta v_\chi$ (red circles). The dashed line is the flux of the δ model in the limit $r \to \infty$.

we expect both models to provide similar macroscopic information, for large n. This is usually analyzed by computing the density and the flux as moments of the asymptotic kinetic distribution $f^\infty(v)$:

$$\rho = \int_0^{V_{\max}} f^\infty(v)\,\mathrm{d}v, \quad (\rho u) = \int_0^{V_{\max}} v f^\infty(v)\,\mathrm{d}v$$

and by studying the characteristics of the related fundamental diagram which is obtained plotting the flux against the density.

Notice that, for the δ model, Theorem 3.9 ensures that only few velocities, obtained with $\delta v = \Delta v$, are necessary to describe completely the exact asymptotic kinetic distribution. We expect therefore that the macroscopic behavior of the δ model will be apparent even on the coarse velocity grids, i.e. for $r = 1$.

Figure 3.14 shows the fundamental diagrams provided by the δ model (blue curves) and the χ model (red curves), computed with $\Delta v_\chi = 2\Delta v_\delta$, for two different values of Δv_δ. In the left panel, $r = 1$, while $r = 20$ on the right. The figure shows that the

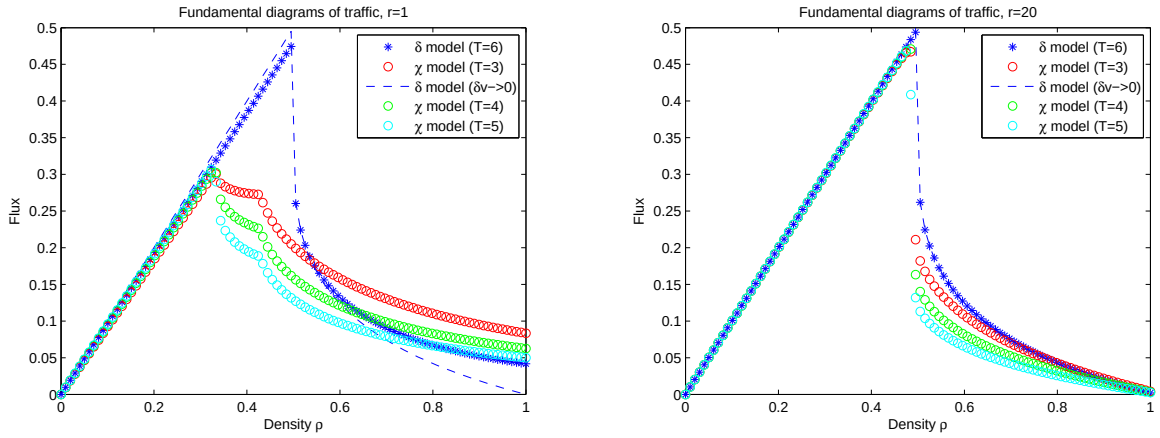

Figure 3.15: Fundamental diagrams resulting from the δ model (blue *-symbols) with $T = 6$ and from the χ model with acceleration parameter $\Delta v_\chi = k\Delta v_\delta$ for $k = 2, \frac{3}{2}, \frac{6}{5}$ (red, green and cyan circles respectively). The dashed line is the flux of the δ model in the limit $r \to \infty$.

diagram of the χ model is very similar to the diagram of the δ model when $n \to \infty$ and this result is in agreement with the fact that the expected output speed of the two models is mostly the same (i.e., the same in a large range of pre-interaction speeds) when choosing the acceleration parameter of the δ model as a half of the acceleration parameter of the χ model. The only difference is provided by the maximum speeds which, as already noted, are slightly different. Note that the similarity of the fundamental diagrams does not mean that the asymptotic equilibrium functions of the χ and of the δ model converge to the same function as n tends to ∞. In Figure 3.15 we reproduce the same diagrams computed in the top panels of Figure 3.14, adding two diagrams resulting from the χ model and corresponding to $\Delta v_\chi = \frac{3}{2}\Delta v_\delta$ (green data) and $\Delta v_\chi = \frac{6}{5}\Delta v_\delta$ (cyan data). As it can be observed, setting $\Delta v_\chi \neq 2\Delta v_\delta$ affects essentially the sharpness of the capacity drop of the χ model which, in the limit $n \to \infty$, becomes not comparable with the capacity drop of the δ model.

Observe that the fundamental diagrams given by the δ model in both plots in each line of Figure 3.14 use the same information. In fact, following the results of Theorem 3.9, the macroscopic flux is given by

$$\mathrm{Flux}_\delta(r) = \int_0^{V_{\max}} v f_{\delta v}^\infty(v)\mathrm{d}v = \sum_{j=1}^{n} (\mathbf{f}_r^\infty)_j \frac{1}{|I_j|}\int_{I_j} v\,\mathrm{d}v = \sum_{l=1}^{T+1} (\mathbf{f}_1^\infty)_l v_{(l-1)r+1}$$

where v_j denotes the center of the cell I_j and $\mathbf{f}_r^\infty$ is the vector containing the equilibria of the system (3.12) with $\Delta v/\delta v = r \in \mathbb{N}$. Recalling the definition of I_j, we have that $v_1 = \Delta v/4r$, $v_n = V_{\max} - \Delta v/4r$ and $v_{(l-1)r+1} = (l-1)\Delta v$. Thus, in order to compute the fundamental diagram of the δ model with any value of r, it is enough to compute the equilibria $\mathbf{f}_1^\infty$, i.e. using $r = 1$, and then compute the flux with the formula above. In particular, using only $\mathbf{f}_1^\infty$, one may also compute the fundamental diagram of the δ model

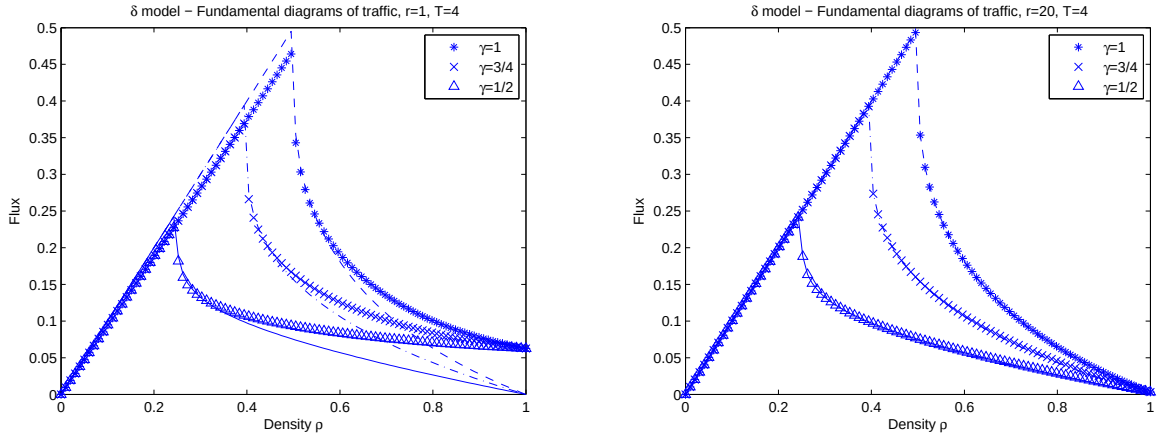

Figure 3.16: Fundamental diagrams resulting from the δ model with acceleration parameter $\Delta v_\delta = \frac{1}{4}$. The probability P is taken as in (2.9) with $\alpha = 1$ and $\gamma = 1$ (blue data), $\gamma = 3/4$ (green data) and $\gamma = 1/4$ (cyan data). The dashed lines are the fluxes in the limit $r \to \infty$.

also in the limit $r \to \infty$ with the formula

$$\mathrm{Flux}_\delta(\infty) = \sum_{l=1}^{T+1} (\mathbf{f}_1^\infty)_l (l-1)\Delta v.$$

The dashed blue line in all panels of Figure 3.14 shows the quantity $\mathrm{Flux}_\delta(\infty)$ just defined. Note that in the case of the χ model, for each value of r, one has instead to compute the full equilibrium distribution with $n = rT + 1$ velocities.

When increasing r, we observe that the flux at $\rho_{\max}$ approaches zero. This is because for $\rho = \rho_{\max}$, $(\mathbf{f}_1^\infty)_1$ is the only non zero component at equilibrium, all vehicles travel at a velocity in the lowest speed class I_1 and the flux is therefore $\frac{\Delta v}{4r}(\mathbf{f}_1^\infty)_1$. Similarly, in the free phase all vehicles travel at a velocity in the highest speed class I_n and the flux is therefore $(V_{\max} - \frac{\Delta v}{4r})(\mathbf{f}_1^\infty)_{T+1} = (V_{\max} - \frac{\Delta v}{4r})\rho$. The free-phase flux is therefore linear in ρ and its slope approaches $V_{\max}$ when $r \to \infty$.

In Figure 3.14, we observe that both models provide a sharp decrease in the flux, beyond the critical density, namely the value of the density marking the transition from free to congested flow. This phenomenon is well known in traffic modeling, and it is called capacity drop, see [88] and references therein. From Theorem 3.9 it is apparent that, for the δ model, the critical density corresponds to a bifurcation of the equilibrium solutions. In fact, one deduces that for $P \geq \frac{1}{2}$ the equilibrium distribution is $f^\infty(v) = \rho\delta_{V_{\max}}(v)$, which means that all vehicles travel at maximum speed. Only when $P < \frac{1}{2}$ the lower speed classes begin to fill up. Thus, the physical concept of phase transition in traffic flow theory has a rigorous mathematical counterpart in the present model. Using the law given in (2.9) the value of ρ for which $P = 1/2$ is $\rho_c := \left(\frac{1}{2}\right)^{\frac{1}{\gamma}}$ and then we may act on γ in order to change the critical density. For instance, see Figure 3.16 in which we plot three fundamental diagrams of the δ model with P as in (2.9) with $\alpha = 1$ and $\gamma = 1$ ($*$-markers), $\gamma = 3/4$ ($\times$), $\gamma = 1/4$ ($\triangle$). We notice that taking different γ in the P law means that we

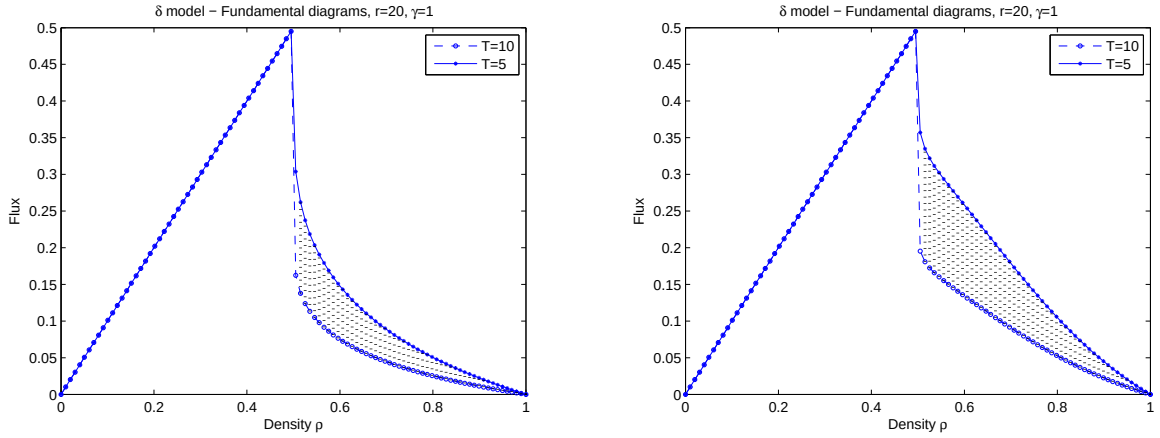

Figure 3.17: Fundamental diagrams resulting from the δ model with acceleration parameter $\Delta v_\delta = \frac{1}{5}$ (*-symbol) and $\Delta v_\delta = \frac{1}{10}$ (circles). The probability P is taken as in (2.9) with $\alpha = 1$ and $\gamma = 1$ (left plot) and as in (4.38) (right plot) (see Section 4.4).

assume different types of drivers on the road (less and less aggressive as $\gamma \to 0$), thus the scattering observed in Figure 3.16 can be linked to a multi-population framework.

Another way to reproduce the scattering of data in the congested regime is to consider different Δv and thus models related to different accelerations. For instance, focus on the δ model and see Figure 3.17, in which the upper branch and the lower one are referred to the maximum and the minimum typical acceleration of a vehicle. They define a region of fluxes in the congested phase. In fact, the hatched region is due to the variability of the acceleration and it represents the area in which the multivalued behavior appear. However, observe that the dispersion of the values is not comparable with the scattering usually reproduced by experimental diagrams. Again this scattering of data can be linked to a multi-population framework (different types of drivers on the road according to the typical velocity jump Δv).

Remark 3.18. Observe from Figure 3.14 that the critical density of the χ model approaches the critical density of the δ model when $n \to \infty$. In fact, since the matrix $A^1_\chi \xrightarrow{r\to\infty} A^1_\delta$, we also have that $\left(\mathbf{f}^\infty_{r,\chi}\right)_1 \xrightarrow{r\to\infty} \left(\mathbf{f}^\infty_{1,\delta}\right)_1$. More precisely, the analogous of (3.3.1) for the χ model is

$$-(1-P)\, f_1^2 + \left(1 - 2P + \frac{P}{2r}\right) \rho f_1 = 0$$

and the stable equilibrium is thus

$$\begin{cases} 0 & P \geq \frac{2r}{4r-1} \\ \rho \frac{1-2P}{1-P} + \mathcal{O}(\frac{1}{r}) & \text{otherwise} \end{cases}$$

In Figure 3.18 we show the fundamental diagrams of the χ model for $r = 1$ and $r = 20$, together with a few representative f_j's at equilibrium, as functions of ρ. In the left part, for $r = 1$, two phase transitions appear in the fundamental diagram (top left). Comparing

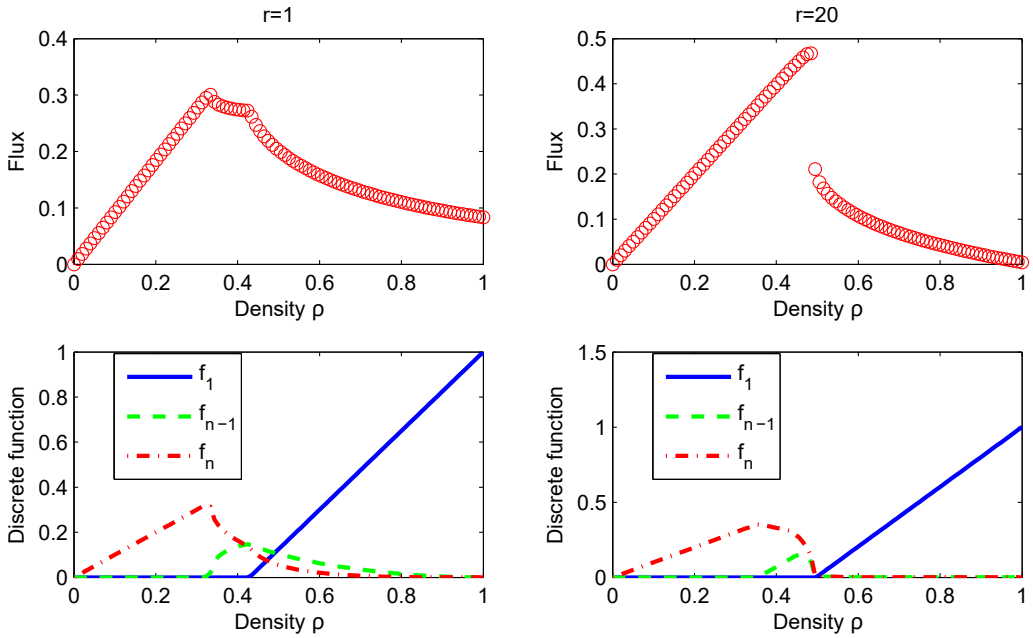

Figure 3.18: Top: fundamental diagrams provided by the χ model with $n = 4$ (left) and $n = 61$ (right) velocities. Bottom: equilibria of the function f_1 (blue solid line), f_{n-1} (green dashed) and f_n (red dot-dashed) for any density in $[0, 1]$.

with the bottom left plot, the origin of this phenomenon can be appreciated. A first transition occurs when the density becomes large enough to force a few drivers to brake: thus the second largest speed class I_{n-1} starts being populated (green dashed curve), while the fastest speed class begins to be depleted (red curve). A second transition occurs when some vehicles enter the lowest speed class (blue curve). This latter transition is the one that, when increasing r, moves towards the critical density $\rho = 1/2$, see Remark 3.18. The first phase transition is not observable for large r, because f_{n-1} is related to the velocity $v_{n-1} \to V_{\max}$, as $\delta v \to 0$, so that the transition of vehicles from I_n to I_{n-1} is not enough to determine an abrupt change in the flux.

Comparison with experimental data Figure 3.19 shows the comparisons of the results produced by the δ model with experimental data published in [79]. In the left figure we have tuned the critical density to reproduce the correct position of the phase transition. The experimental data are normalized and the fundamental diagram computed by the model is provided for all values of the density between 0 and $\rho_{\max}$, which corresponds to a situation in which all vehicles are bumper-to-bumper and still. The figure on the right stems from the observation that experimental data contain a residual movement even in the congested phase. Thus the bumper-to-bumper situation is never actually observed. Therefore in the figure on the right we also tune the maximum density $\tilde{\rho}_{\max}$ actually observed, with $\tilde{\rho}_{\max} < \rho_{\max}$. In this case we obtain a very good agreement with experimental data. With the present model we do not reproduce the scattering of the data, but this can be explained

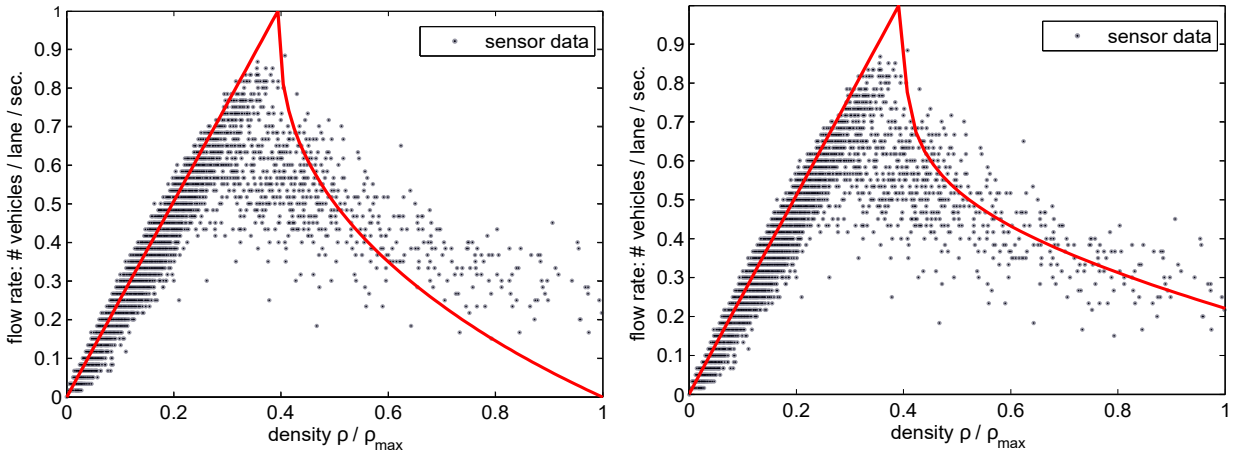

Figure 3.19: Comparison between experimental data and the diagram resulting from the δ model, with $\Delta v = 1/4$, $P = 1 - \rho^{1/4}$. The experimental diagram is reproduced by kind permission of Seibold et al. [79].

keeping into account a mixture of two different populations of drivers and/or vehicles, as we have proposed in [74, 76], see Chapter 2 and Chapter 4 of this thesis.

Chapter 4

Analysis of a multi-population kinetic model for traffic flow

4.1 Motivation

In [76] and in Chapter 2 we introduced a Boltzmann-like kinetic model for traffic flow, which draws inspiration from the ideas presented in [7] for macroscopic models, in order to take into account the heterogeneous composition of the flow of vehicles on the road. This aspect, which is rather neglected in the literature, is important to obtain a richer description of the macroscopic behavior of traffic flow. In fact, we showed that the model is able to recover the whole structure of the diagrams relating the macroscopic flux and speed to the vehicle density in homogeneous space conditions and which represents a basic tool to study traffic problems.

This chapter can be seen as a natural sequel of [76] and Chapter 2 because we revisit and refine the model by extending the construction introduced in [75] and in Chapter 3 to the case of traffic mixtures. We will consider more than one class of vehicles, characterized by a few parameters accounting for the microscopic differences which allow one to distinguish more types of vehicles. As in Chapter 2, these parameters will be the typical length and the maximum speed, and we will introduce a kinetic distribution function for each class of vehicles. We stress that the heterogeneity of traffic is not only described by introducing more classes with different physical features, but also by considering two or more types of drivers with different behavioral attributes according to the maximum velocity they intend to keep, as in [7, 54, 61] for macroscopic models.

However, this approach differs from the model proposed in [76] and in Chapter 2 because the latter is based on a lattice of admissible microscopic speeds and the output of an interaction depends on the number of velocities chosen in the lattice. Here, instead, using the framework discussed in [75] and in Chapter 3 for the δ model, we will consider continuous and bounded velocity spaces. The model will be characterized by the presence of a parameter proportional to the actual acceleration of a vehicle in order to describe the physical velocity jump performed by vehicles when they increase their speed as a result of

an interaction. Clearly, this parameter may depend on the mechanical characteristics of a vehicle, but, in order to simplify the study, we will suppose that it is fixed. This choice preserves the quantized structure of the asymptotic functions, already observed in [75] and in Chapter 3 for the single-population model. In fact, Theorem 4.12 in Section 4.3.2 shows that the asymptotic kinetic distribution approaches a combination of delta functions, centered in the velocities which are proportional to the fixed parameter. However, we also briefly analyze the case of the velocity jump depending on the class of vehicles showing that we are able to preserve the quantization of the equilibrium solutions.

The chapter is organized as follows. In Section 4.2 we introduce the general framework of the continuous-velocity multi-population model, then we discuss the modeling of the probability density and we prove an indifferentiability principle. In Section 4.3 we discretize the model in order to find the asymptotic behavior of the distribution functions. Then we analyze the resulting system of ordinary differential equations by studying well posedness and the asymptotic kinetic distribution for the case of two populations. In Section 4.4 we show the macroscopic diagrams of traffic provided by the model with three classes of vehicles. We also discuss the impact that different probabilities of achieving the maximum speed in an interaction have on the sharp capacity drop observed at the transition between free and congested traffic flow.

4.2 A multi-population kinetic model

In this section we present the general form of a kinetic model for vehicular traffic with a new structure accounting for the heterogeneous composition of the traffic flow on the road. Next, we derive a simplified model based on particular choices made on the microscopic interaction rules. This model is a generalization of the single-population model discussed in Chapter 3 and in [75] to the case of a multi-population framework. Therefore, unlike [76], see model (2.16), in this chapter we suppose that each class of vehicles (*population*) admits a continuous space of admissible velocities and we introduce a parameter describing the physical acceleration of each vehicle, as already done in Chapter 3. Our approach differs from standard kinetic models in that we consider more than one kinetic distribution function. Each one refers to a class of vehicles characterized by precise physical features, in this case the maximum speed and the typical length of a vehicle.

Again, we will focus only on the space homogeneous case, since we are interested in the investigation of the structure of the collision term, and of the resulting equilibrium distributions which allow one to obtain the fundamental diagrams of traffic. From now on, we adopt the compact notation already introduced in Section 2.4.1, which makes use of an index p, to label various quantities referred to the different classes of vehicles. Thus, let

$$f^{\mathsf{p}} = f^{\mathsf{p}}(t, v) : \mathbb{R}^+ \times \mathcal{V}^{\mathsf{p}} \to \mathbb{R}^+$$

be the kinetic distribution function of the p-th class of vehicles, then $f^{\mathsf{p}}(t, v)\mathrm{d}v$ gives the number of vehicles belonging to the p-class with velocity in $[v, v + \mathrm{d}v]$ at time t. The space $\mathcal{V}^{\mathsf{p}} = [0, V^{\mathsf{p}}_{\max}]$ is the domain of the microscopic speeds related to the p-class, where $V^{\mathsf{p}}_{\max}$

is the maximum speed which can be reached by the p-vehicles. In this framework $V^{\mathsf{p}}_{\max}$ will depend on the mechanical characteristics of the vehicles, or on the type of drivers, according to the maximum velocity they intend to keep in free road conditions. Thus, the different maximum speeds allow one to model a first microscopic feature which identifies a class of vehicles. Another difference is introduced by considering the typical length l^{p} of vehicles which will be used later to define the concept of the total space occupied on the road.

As usual, macroscopic quantities are obtained as moments of the distribution functions f^{p} with respect to the velocity v:

$$\rho^{\mathsf{p}}(t) = \int_{\mathcal{V}^{\mathsf{p}}} f^{\mathsf{p}}(t,v)\mathrm{d}v, \quad q^{\mathsf{p}}(t) = \int_{\mathcal{V}^{\mathsf{p}}} v f^{\mathsf{p}}(t,v)\mathrm{d}v, \quad u^{\mathsf{p}}(t) = \frac{q^{\mathsf{p}}(t)}{\rho^{\mathsf{p}}(t)} \tag{4.1}$$

where ρ^{p} is the density, i.e. the number of vehicles of the p-class per unit length (typically, kilometers), q^{p} and u^{p} are the macroscopic flux of vehicles and the mean speed of the p-th class, respectively.

Here we again consider a Boltzmann-type kinetic model for vehicular traffic, in which the relaxation to equilibrium is due to binary interactions. In the homogeneous case, we model the evolution of the f^{p}'s in time by means of the following system of equations:

$$\partial_t f^{\mathsf{p}}(t,v) = Q^{\mathsf{p}}\left[f^{\mathsf{p}}, (f^{\mathsf{p}}, f^{\mathsf{q}})\right](t,v), \quad \forall\, \mathsf{p} \tag{4.2}$$

where $Q^{\mathsf{p}}\left[f^{\mathsf{p}}, (f^{\mathsf{p}}, f^{\mathsf{q}})\right](t,v)$ is the collision operator which accounts for the change of f^{p} in time due to the microscopic interactions among vehicles. Clearly, a multi-population model has to consider also the interactions taking place between p- and q-vehicles, where q represents all classes of vehicles which are not p. For this reason, and following the approach already used in Section 2.4.1 and for gas mixtures in [3, 13, 33, 34], Q^{p} can be naturally thought of as a sum of two or more collision operators, one describing the interactions among vehicles belonging to the same class (self-interactions) and the other ones describing the interactions among vehicles belonging to different classes (cross-interactions), so that

$$Q^{\mathsf{p}}\left[f^{\mathsf{p}}, (f^{\mathsf{p}}, f^{\mathsf{q}})\right](t,v) = \underbrace{Q^{\mathsf{pp}}\left[f^{\mathsf{p}}, f^{\mathsf{p}}\right](t,v)}_{\text{self-interactions}} + \sum_{\mathsf{q}\in\neg\mathsf{p}} \underbrace{Q^{\mathsf{pq}}\left[f^{\mathsf{p}}, f^{\mathsf{q}}\right](t,v)}_{\text{cross-interactions}}$$

For mass conservation to hold the right-hand side of the above expression has to vanish when it is integrated over the space of admissible speeds of the p-th class, and this is verified e.g. if we assume that the collision terms satisfy

$$\int_{\mathcal{V}^{\mathsf{p}}} Q^{\mathsf{pp}}[f^{\mathsf{p}}, f^{\mathsf{p}}](t,v)\mathrm{d}v = \int_{\mathcal{V}^{\mathsf{p}}} Q^{\mathsf{pq}}[f^{\mathsf{p}}, f^{\mathsf{q}}](t,v)\mathrm{d}v = 0,$$

for all $\mathsf{q} \in \neg\mathsf{p}$. In fact, this ensures that, in the space homogeneous case, the density remains constant:

$$\frac{\mathrm{d}}{\mathrm{d}t}\rho^{\mathsf{p}}(t) = \partial_t \int_{\mathcal{V}^{\mathsf{p}}} f^{\mathsf{p}}(t,v)\mathrm{d}v = \int_{\mathcal{V}^{\mathsf{p}}} Q^{\mathsf{p}}\left[f^{\mathsf{p}}, (f^{\mathsf{p}}, f^{\mathsf{q}})\right](t,v)\mathrm{d}v = 0.$$

Following the same logic underlying the construction of a classical Boltzmann-like kinetic model, each collision operator is written as a balance of a gain (G^{pp} or G^{pq}) and a loss term that model statistically the interactions which lead to get or to loose the speed $v \in \mathcal{V}^{\mathsf{p}}$:

$$Q^{\mathsf{pp}}[f^{\mathsf{p}}, f^{\mathsf{p}}](t,v) = \underbrace{\int_{\mathcal{V}^{\mathsf{p}}} \int_{\mathcal{V}^{\mathsf{p}}} \eta^{\mathsf{p}}(v_*, v^*) A^{\mathsf{p}}(v_* \to v | v^*; s) f^{\mathsf{p}}(t, v_*) f^{\mathsf{p}}(t, v^*) \mathrm{d}v^* \mathrm{d}v_*}_{G^{\mathsf{pp}}[f^{\mathsf{p}}, f^{\mathsf{p}}](t,v)} \tag{4.3a}$$

$$- f^{\mathsf{p}}(t,v) \int_{\mathcal{V}^{\mathsf{p}}} \eta^{\mathsf{p}}(v_*, v^*) f^{\mathsf{p}}(t, v^*) \mathrm{d}v^*,$$

$$Q^{\mathsf{pq}}[f^{\mathsf{p}}, f^{\mathsf{q}}](t,v) = \underbrace{\int_{\mathcal{V}^{\mathsf{p}}} \int_{\mathcal{V}^{\mathsf{q}}} \eta^{\mathsf{pq}}(v_*, v^*) A^{\mathsf{pq}}(v_* \to v | v^*; s) f^{\mathsf{p}}(t, v_*) f^{\mathsf{q}}(t, v^*) \mathrm{d}v^* \mathrm{d}v_*}_{G^{\mathsf{pq}}[f^{\mathsf{p}}, f^{\mathsf{q}}](t,v)} \tag{4.3b}$$

$$- f^{\mathsf{p}}(t,v) \int_{\mathcal{V}^{\mathsf{q}}} \eta^{\mathsf{pq}}(v_*, v^*) f^{\mathsf{q}}(t, v^*) \mathrm{d}v^*.$$

Throughout the chapter, following the notation used in Chapter 3, we will denote by $v_* \in \mathcal{V}^{\mathsf{p}}$ the pre-interaction velocity of the p-vehicle which is likely to change speed after an interaction. Conversely, $v^* \in \mathcal{V}^{\mathsf{p}}$ or $v^* \in \mathcal{V}^{\mathsf{q}}$ identifies the velocity of other p- or q-vehicles which induce the gain or loss of the speed $v \in \mathcal{V}^{\mathsf{p}}$. In order to shorten formulas, we will use the notation introduced in Section 3.2, so that $f^{\mathsf{p}}(t, v_*) = f^{\mathsf{p}}_*$, $f^{\mathsf{p}}(t, v^*) = f^{\mathsf{p}*}$, $\forall\, \mathsf{p}$, and similarly for f^{q}_*, $f^{\mathsf{q}*}$, $\forall\, \mathsf{q} \in \neg\mathsf{p}$.

In (4.3), $\eta^{\mathsf{p}}(v_*, v^*)$ and $\eta^{\mathsf{pq}}(v_*, v^*)$ are the interaction rates which model the frequency of self- and cross-interactions respectively. Since in [76] and in Chapter 2 we found that a constant interaction rate is already sufficient to account for many aspects of the complexity of traffic, we will not consider more refined choices for the interaction rates, e.g. dependent on the relative speed of interacting vehicles. Moreover, observe that, in the space homogeneous case, a constant interaction rates affect only the relaxation time towards equilibrium. Thus, in this chapter we will set again $\eta^{\mathsf{p}}(v_*, v^*) = \eta^{\mathsf{p}}$ and $\eta^{\mathsf{pq}}(v_*, v^*) = \eta^{\mathsf{pq}}$.

Finally, $A^{\mathsf{p}}(v_* \to v | v^*; s)$ and $A^{\mathsf{pq}}(v_* \to v | v^*; s)$ are the probability densities of gaining the speed $v \in \mathcal{V}^{\mathsf{p}}$ in the case of self- and cross-interactions, respectively. More precisely, $A^{\mathsf{p}}(v_* \to v | v^*; s)$ ($A^{\mathsf{pq}}(v_* \to v | v^*; s)$, resp.) gives the probability that a p-vehicle modifies its pre-interaction speed $v_* \in \mathcal{V}^{\mathsf{p}}$ in the speed $v \in \mathcal{V}^{\mathsf{p}}$ when it interacts with a p-vehicle (q-vehicle, resp.) traveling at the speed $v^* \in \mathcal{V}^{\mathsf{p}}$ ($v^* \in \mathcal{V}^{\mathsf{q}}$, resp.).

We will suppose that these probabilities depend also on the macroscopic traffic conditions (local road congestion) through the fraction of occupied space on the road:

$$0 \leq s = \sum_{\mathsf{p}} l^{\mathsf{p}} \rho^{\mathsf{p}} \leq 1. \tag{4.4}$$

Notice that s was already introduced in [7] for a multi-population macroscopic model and it was also used in [76] and in Section 2.4.1 for a two-population kinetic model based on a discrete-velocity framework. The quantity ρ^{p} appearing in (4.4) is defined in (4.1). We will assume that $\rho^{\mathsf{p}} \in [0, \rho^{\mathsf{p}}_{\max}]$ where $\rho^{\mathsf{p}}_{\max}$ is the maximum density of p-vehicles chosen as $\frac{1}{l^{\mathsf{p}}}$,

i.e. as the maximum number of vehicles per unit length in bumper-to-bumper conditions when $\rho^{\mathsf{q}} = 0$, $\forall\ \mathsf{q} \in \neg\mathsf{p}$. Therefore, s can be rewritten as

$$0 \leq s = \sum_{\mathsf{p}} \frac{\rho^{\mathsf{p}}}{\rho^{\mathsf{p}}_{\max}} \leq 1.$$

From the last expression it is clear that the parameter s generalizes the term $\frac{\rho}{\rho_{\max}}$ appearing in the case of single-population models, see [37, 48, 73].

Following the Ansatz 3.1 and since $A^{\mathsf{p}}(v_* \to v|v^*; s)$ and $A^{\mathsf{pq}}(v_* \to v|v^*; s)$ are probability densities, they fulfill the properties:

$$\begin{aligned} A^{\mathsf{p}}(v_* \to v|v^*; s) \geq 0, \quad \int_{\mathcal{V}^{\mathsf{p}}} A^{\mathsf{p}}(v_* \to v|v^*; s)\mathrm{d}v = 1, \quad \text{for } v_*, v^*, v \in \mathcal{V}^{\mathsf{p}},\ s \in [0,1] \\ A^{\mathsf{pq}}(v_* \to v|v^*; s) \geq 0, \quad \int_{\mathcal{V}^{\mathsf{p}}} A^{\mathsf{pq}}(v_* \to v|v^*; s)\mathrm{d}v = 1, \quad \text{for } v_*, v \in \mathcal{V}^{\mathsf{p}},\ v^* \in \mathcal{V}^{\mathsf{q}},\ s \in [0,1]. \end{aligned} \tag{4.5}$$

Remark 4.1. All transition probability densities $A^{\mathsf{p}}(v_* \to v|v^*; s)$ and $A^{\mathsf{pq}}(v_* \to v|v^*; s)$ satisfying properties (4.5) guarantee mass conservation. In fact, by integrating over the velocity space $\mathcal{V}^{\mathsf{p}}$ we obtain

$$\int_{\mathcal{V}^{\mathsf{p}}} Q^{\mathsf{pp}}[f^{\mathsf{p}}, f^{\mathsf{p}}](t,v)\mathrm{d}v = \int_{\mathcal{V}^{\mathsf{p}}}\int_{\mathcal{V}^{\mathsf{p}}} f^{\mathsf{p}}_* f^{\mathsf{p}*}\left(\int_{\mathcal{V}^{\mathsf{p}}} A^{\mathsf{p}}(v_* \to v|v^*; s)\mathrm{d}v\right)\mathrm{d}v_*\mathrm{d}v^* - \int_{\mathcal{V}^{\mathsf{p}}} f^{\mathsf{p}}\mathrm{d}v \int_{\mathcal{V}^{\mathsf{p}}} f^{\mathsf{p}*}\mathrm{d}v^* = 0.$$

Analogously for the cross-interaction operators we have $\int_{\mathcal{V}^{\mathsf{p}}} Q^{\mathsf{pq}}[f^{\mathsf{p}}, f^{\mathsf{q}}](t,v)\mathrm{d}v = 0$, for all $\mathsf{q} \in \neg\mathsf{p}$.

Remark 4.2. Since the mass of each population is conserved, also s given in (4.4) is conserved. In particular, it satisfies the prescribed bounds if the f^{p}'s are properly chosen at the initial time.

4.2.1 Choice of the probability densities

As in any Boltzmann-like kinetic traffic model, the introduction of a probability density allows one to assign a post-interaction speed taking into account the stochasticity of the drivers' behavior. Therefore, the construction of $A^{\mathsf{p}}(v_* \to v|v^*; s)$ and $A^{\mathsf{pq}}(v_* \to v|v^*; s)$, $\forall\ \mathsf{p}, \mathsf{q} \in \neg\mathsf{p}$, is at the core of the model we propose.

We will suppose that all types of vehicles react in the same way to the parameter s, accounting for the state of congestion of the road, and to all field classes of vehicles. Clearly, it would also be possible to consider different reactive behaviors for different classes of vehicles. However, this choice is coherent with the experience and, as we will see later in Section 4.4, this simpler choice results in a realistic macroscopic behavior.

Precisely, we consider the same very small set of rules described in Section 3.2.1 and introduced in [75]. In particular, for the post-interaction speed due to acceleration we assume that the output velocity v is obtained by accelerating instantaneously from v_* to $v_* + \Delta v^{\mathsf{p}}$, unless the resulting speed is larger than $V^{\mathsf{p}}_{\max}$, namely the new speed is

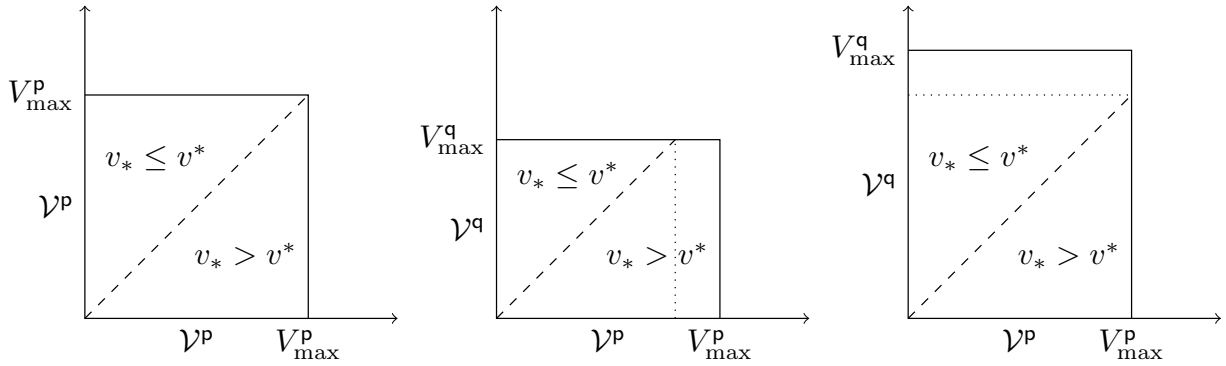

Figure 4.1: The domain of the probability density $A^{\mathsf{p}}(v_* \to v|v^*; s)$ (left), the domains of the probability densities $A^{\mathsf{pq}}(v_* \to v|v^*; s)$ in the case $\mathcal{V}^{\mathsf{p}} \supset \mathcal{V}^{\mathsf{q}}$ (center) and $\mathcal{V}^{\mathsf{p}} \subset \mathcal{V}^{\mathsf{q}}$ (right).

$\min\{v_* + \Delta v^{\mathsf{p}}, V^{\mathsf{p}}_{\max}\}$. This choice corresponds to the case of the quantized acceleration (or δ model) introduced in [75] and in equation (3.3) for a single-population model. Clearly, other choices are possible, in particular the case of a uniformly distributed acceleration. However, in Chapter 3 we proved that although a model with such an acceleration is more refined, at equilibrium the essential information is caught by the simpler δ model. For this reason, here we will not investigate other models.

Considering all possible outcomes, the resulting probability distribution accounting for self-interactions is

$$A^{\mathsf{p}}(v_* \to v|v^*; s) = \begin{cases} (1 - P_1(s))\,\delta_{v_*}(v) + P_1(s)\,\delta_{\min\{v_*+\Delta v^{\mathsf{p}}, V^{\mathsf{p}}_{\max}\}}(v), & \text{if } v_* \le v^* \\ (1 - P_2(s))\,\delta_{v^*}(v) + P_2(s)\,\delta_{\min\{v_*+\Delta v^{\mathsf{p}}, V^{\mathsf{p}}_{\max}\}}(v), & \text{if } v_* > v^*. \end{cases} \tag{4.6}$$

Since we have assumed that all classes of vehicles react in the same way to the parameter s and to different interacting populations, the probability densities describing the cross-interactions differ from $A^{\mathsf{p}}(v_* \to v|v^*; s)$ only in their domain. In fact, $A^{\mathsf{p}}(v_* \to v|v^*; s)$ is defined for $(v_*, v^*) \in \mathcal{V}^{\mathsf{p}} \times \mathcal{V}^{\mathsf{p}}$ and $v \in \mathcal{V}^{\mathsf{p}}$, while $A^{\mathsf{pq}}(v_* \to v|v^*; s)$ for $(v_*, v^*) \in \mathcal{V}^{\mathsf{p}} \times \mathcal{V}^{\mathsf{q}}$ and $v \in \mathcal{V}^{\mathsf{p}}$, see Figure 4.1.

Note that the modeling (4.6) of $A^{\mathsf{p}}(v_* \to v|v^*; s)$ and $A^{\mathsf{pq}}(v_* \to v|v^*; s)$, $\forall\ \mathsf{p}, \mathsf{q} \in \neg\mathsf{p}$, preserves all the good properties of the model introduced in Chapter 3. In particular, in contrast to [76] in which the velocity jump Δv^{p} is chosen as the distance between two adjacent discrete velocities, namely Δv^{p} depends on the number of elements in the speed lattice, in this chapter, instead, Δv^{p} is a *physical* parameter that represents the ability of a class of vehicles to change its pre-interaction speed v_*. With this choice, Δv^{p} does not depend on the discretization of the velocity space $\mathcal{V}^{\mathsf{p}}$ and the maximum acceleration is bounded, as in [53] and [75]. In contrast, deceleration can be larger than Δv^{p}, and this fact again reflects the concept of traffic hysteresis in [88] and references therein.

Following the choice made in Section 3.2.1, the probabilities P_1 and P_2 are taken as $P = P_1 = P_2$ and P is a function of the fraction of occupied space s only as in Section 2.3.2. In general P should be a decreasing function of s, see Section 2.3.2 and also [36] or [78]. Usually, P will be taken as in (2.9) but in Section 4.4 we will analyze a more complex

choice of P and its impact on the capacity drop. In more sophisticated models, one may also choose P as a function of the relative velocity of the interacting vehicles, but we will not explore this possibility in the present work.

Remark 4.3. As noticed in Section 3.2.1, in [48] Klar and Wegener assume that the velocity after an acceleration is uniformly distributed over a range of speeds between v_* and $v_* + \alpha(V_{\max} - v_*)$, where α is supposed to depend on the local density. Thus, they suppose that the output speed resulting from the acceleration rule depends on the free space on the road, in other words they consider the velocity jump as function of s. Instead, here Δv^{p} (or simply Δv in the single-population model introduced in Chapter 3) is fixed while P is function of s, so that when the road becomes congested the probability of accelerating decreases.

4.3 Analysis of the model

In this section, first we rewrite explicitly the model using the expression (4.6) for $A^{\mathsf{p}}(v_* \to v|v^*; s)$ and $A^{\mathsf{pq}}(v_* \to v|v^*; s)$. Next, we discretize it in order to analyze later numerically the asymptotic traffic behavior, see Section 4.4. Furthermore, we study the well-posedness (existence, uniqueness, and continuous dependence of the solution on initial data) of the discretized model and we characterize explicitly the asymptotic distributions $(f^{\mathsf{p}})^{\infty}$ of the discrete-velocity model.

The gain term of the collision operator (4.3a) describing self-interactions can be easily rewritten in the following way by exploiting the explicit expression of $A^{\mathsf{p}}(v_* \to v|v^*; s)$ given in (4.6) and without distinguishing the cases $v_* \le v^*$ and $v_* > v^*$:

$$G^{\mathsf{pp}}[f^{\mathsf{p}}, f^{\mathsf{p}}](t,v) = \eta^{\mathsf{p}} \int_0^{V_{\max}^{\mathsf{p}}} \int_0^{V_{\max}^{\mathsf{p}}} \left[(1-P)\delta_{\min\{v_*,v^*\}}(v) + P\delta_{\min\left\{v_*+\Delta v^{\mathsf{p}}, V_{\max}^{\mathsf{p}}\right\}}(v)\right] f_*^{\mathsf{p}} f^{\mathsf{p}*} \mathrm{d}v^* \mathrm{d}v_*.$$

Observe that the Dirac delta function at $v = \min\{v_* + \Delta v^{\mathsf{p}}, V_{\max}^{\mathsf{p}}\}$ can be split as

$$\delta_{\min\left\{v_*+\Delta v^{\mathsf{p}}, V_{\max}^{\mathsf{p}}\right\}}(v) = \begin{cases} \delta_{v_*+\Delta v^{\mathsf{p}}}(v), & \text{if } v_* \in [0, V_{\max}^{\mathsf{p}} - \Delta v^{\mathsf{p}}] \\ \delta_{V_{\max}^{\mathsf{p}}}(v), & \text{if } v_* \in (V_{\max} - \Delta v^{\mathsf{p}}, V_{\max}^{\mathsf{p}}] \end{cases},$$

and since Q^{p} is defined on $\mathcal{V}^{\mathsf{p}} \times \mathcal{V}^{\mathsf{p}}$, then $G^{\mathsf{pp}}[f^{\mathsf{p}}, f^{\mathsf{p}}](t,v)$ corresponds to the gain term of the single-population model. Thus, recalling the computations in [75] and in Section 3.3.1, $G^{\mathsf{pp}}[f^{\mathsf{p}}, f^{\mathsf{p}}](t,v)$ can be written as

$$\begin{aligned} G^{\mathsf{pp}}[f^{\mathsf{p}}, f^{\mathsf{p}}](t,v) =& \eta^{\mathsf{p}}(1-P) f^{\mathsf{p}} \left[\int_v^{V_{\max}^{\mathsf{p}}} f^{\mathsf{p}*} \mathrm{d}v^* + \int_v^{V_{\max}^{\mathsf{p}}} f_*^{\mathsf{p}} \mathrm{d}v_*\right] \\ &+ \eta^{\mathsf{p}} P \rho^{\mathsf{p}} \left[f^{\mathsf{p}}(t, v - \Delta v^{\mathsf{p}}) H_{\Delta v^{\mathsf{p}}}(v) + \delta_{V_{\max}^{\mathsf{p}}}(v) \int_{V_{\max}^{\mathsf{p}} - \Delta v^{\mathsf{p}}}^{V_{\max}^{\mathsf{p}}} f_*^{\mathsf{p}} \mathrm{d}v_*\right] \end{aligned} \tag{4.7}$$

where $H_\alpha(v)$ is the Heaviside step function defined as $H_\alpha(v) := \frac{\mathrm{d}}{\mathrm{d}v} \max\{0, v - \alpha\}$, $\alpha \in \mathbb{R}$. Notice that the first two integrals on the right-hand side actually coincide, in the space

homogeneous case. However, we kept them separate to stress the fact that they come from different contributions.

Conversely, the gain term resulting from the collision operators (4.3b) describing the cross-interactions has to be treated differently because Q^{pq} is defined on $\mathcal{V}^{\mathsf{p}} \times \mathcal{V}^{\mathsf{q}}$ and we have to distinguish $V^{\mathsf{p}}_{\max} > V^{\mathsf{q}}_{\max}$ (i.e. $\mathcal{V}^{\mathsf{p}} \supset \mathcal{V}^{\mathsf{q}}$) from $V^{\mathsf{p}}_{\max} < V^{\mathsf{q}}_{\max}$ (i.e. $\mathcal{V}^{\mathsf{p}} \subset \mathcal{V}^{\mathsf{q}}$), see Figure 4.1. First of all we rewrite the generic gain term $G^{\mathsf{pq}}[f^{\mathsf{p}}, f^{\mathsf{q}}](t,v)$ as

$$G^{\mathsf{pq}}[f^{\mathsf{p}}, f^{\mathsf{q}}](t,v) = \eta^{\mathsf{pq}} \int_0^{V^{\mathsf{p}}_{\max}} \int_0^{V^{\mathsf{q}}_{\max}} \left[(1-P)\delta_{\min\{v_*, v^*\}}(v) + P\delta_{\min\left\{v_* + \Delta v^{\mathsf{p}}, V^{\mathsf{p}}_{\max}\right\}}(v) \right] f^{\mathsf{p}}_* f^{\mathsf{q}*} \mathrm{d}v^* \mathrm{d}v_*. \tag{4.8}$$

Computing explicitly the terms appearing in $G^{\mathsf{pq}}[f^{\mathsf{p}}, f^{\mathsf{q}}](t,v)$, we obtain two different expressions. If $V^{\mathsf{p}}_{\max} > V^{\mathsf{q}}_{\max}$:

$$\begin{aligned} G^{\mathsf{pq}}[f^{\mathsf{p}}, f^{\mathsf{q}}](t,v) =& \eta^{\mathsf{pq}}(1-P) f^{\mathsf{p}} \chi_{\left[0, V^{\mathsf{q}}_{\max}\right]}(v) \int_v^{V^{\mathsf{q}}_{\max}} f^{\mathsf{q}*} \mathrm{d}v^* + \eta^{\mathsf{pq}}(1-P) f^{\mathsf{q}} \int_v^{V^{\mathsf{p}}_{\max}} f^{\mathsf{p}}_* \mathrm{d}v_* \\ &+ \eta^{\mathsf{pq}} P \rho^{\mathsf{q}} \left[f^{\mathsf{p}}(t, v - \Delta v^{\mathsf{p}}) \chi_{\Delta v^{\mathsf{p}}}(v) + \delta_{V^{\mathsf{p}}_{\max}}(v) \int_{V^{\mathsf{p}}_{\max} - \Delta v^{\mathsf{p}}}^{V^{\mathsf{p}}_{\max}} f^{\mathsf{p}}_* \mathrm{d}v_* \right], \end{aligned} \tag{4.9}$$

while if $V^{\mathsf{p}}_{\max} < V^{\mathsf{q}}_{\max}$:

$$\begin{aligned} G^{\mathsf{pq}}[f^{\mathsf{p}}, f^{\mathsf{q}}](t,v) =& \eta^{\mathsf{pq}}(1-P) f^{\mathsf{p}} \int_v^{V^{\mathsf{q}}_{\max}} f^{\mathsf{q}*} \mathrm{d}v^* + \eta^{\mathsf{pq}}(1-P) f^{\mathsf{q}} \chi_{[0, V^{\mathsf{p}}_{\max}]}(v) \int_v^{V^{\mathsf{p}}_{\max}} f^{\mathsf{p}}_* \mathrm{d}v_* \\ &+ \eta^{\mathsf{pq}} P \rho^{\mathsf{q}} \left[f^{\mathsf{p}}(t, v - \Delta v^{\mathsf{p}}) H_{\Delta v^{\mathsf{p}}}(v) + \delta_{V^{\mathsf{p}}_{\max}}(v) \int_{V^{\mathsf{p}}_{\max} - \Delta v^{\mathsf{p}}}^{V^{\mathsf{p}}_{\max}} f^{\mathsf{p}}_* \mathrm{d}v_* \right]. \end{aligned} \tag{4.10}$$

Using the expressions (4.7), (4.9) and (4.10) of the gain term, the model is then globally defined and it can be discretized as we do in the following subsection.

Finally, the following theorem states that when all the classes of vehicles composing the mixture of traffic have the same microscopic characteristics then the multi-population model is consistent with the equation defining the single-population model introduced in [75] and in Chapter 3. This property is known in the kinetic theory of gas mixtures as *indifferentiability principle*, see e.g. [3], and thus Theorem 2.4 proved in Section 2.4.1 for the lattice multi-population model holds also at the continuous level.

Theorem 4.4 (Indifferentiability principle). – *Assume that the types of vehicles have the same physical and kinematic characteristics, i.e.*

$$l^{\mathsf{p}} := l, \quad V^{\mathsf{p}}_{\max} := V_{\max}, \quad \Delta v^{\mathsf{p}} := \Delta v, \ \forall\, \mathsf{p}.$$

Let $\eta^{\mathsf{p}} = \eta^{\mathsf{pq}} =: \eta$ be the interaction rate. Then the total distribution function $f : \mathbb{R}^+ \times \mathcal{V} \to \mathbb{R}^+$, defined as

$$f(t,v) = \sum_{\mathsf{p}} f^{\mathsf{p}}(t,v) \tag{4.11}$$

obeys, at each time, the evolution equation of the single-population model introduced in [75] and in Chapter 3.

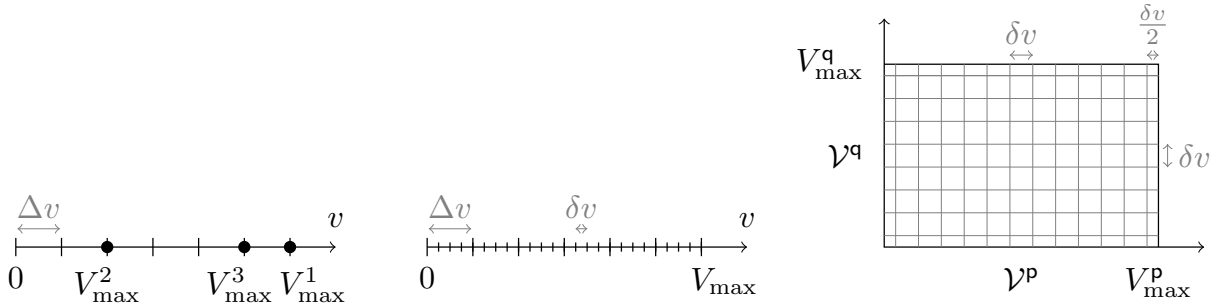

Figure 4.2: Discretization of velocity spaces.

Proof. If the populations have the same microscopic features then for any fixed p in the set of all classes of vehicles the velocity spaces are such that $\mathcal{V}^{\mathsf{p}} = \mathcal{V}^{\mathsf{q}} := \mathcal{V}$, $\forall\ \mathsf{q} \in \neg\mathsf{p}$, and the gain terms (4.7)-(4.8) are the same because now the probability densities $A^{\mathsf{p}}(v_* \to v|v^*; s)$ and $A^{\mathsf{pq}}(v_* \to v|v^*; s)$ are defined on the same velocity space $\mathcal{V}\times\mathcal{V}$. Then, we have $A^{\mathsf{p}}(v_* \to v|v^*; s) = A^{\mathsf{pq}}(v_* \to v|v^*; s) := A(v_* \to v|v^*; s)$ and moreover $s = \sum_{\mathsf{p}} \frac{\rho^{\mathsf{p}}}{\rho^{\mathsf{p}}_{\max}} = \frac{\sum_{\mathsf{p}} \rho^{\mathsf{p}}}{\rho_{\max}} = \frac{\rho}{\rho_{\max}}$. In addition to that, the interaction rates are the same because the populations are identical, hence finally the multi-population model writes as

$$\begin{aligned}\partial_t f^{\mathsf{p}} &= Q^{\mathsf{pp}}[f^{\mathsf{p}}, f^{\mathsf{p}}](t,v) + \sum_{\mathsf{q}\in\neg\mathsf{p}} Q^{\mathsf{pq}}[f^{\mathsf{p}}, f^{\mathsf{q}}](t,v)\\ &= \eta \int_{\mathcal{V}}\int_{\mathcal{V}} A(v_* \to v|v^*; s) f^{\mathsf{p}}_* \sum_{j=\mathsf{p},\mathsf{q}\in\neg\mathsf{p}} f^{j*}\mathrm{d}v^*\mathrm{d}v_* - \eta f^{\mathsf{p}} \int_{\mathcal{V}} \sum_{j=\mathsf{p},\mathsf{q}\in\neg\mathsf{p}} f^{j*}\mathrm{d}v^*.\end{aligned}$$

Summing this equation over p and using the definition (4.11), we obtain

$$\partial_t f(t,v) = \eta \int_{\mathcal{V}}\int_{\mathcal{V}} A(v_* \to v|v^*; s) f(t,v_*) f(t,v^*)\mathrm{d}v^*\mathrm{d}v_* - \eta f(t,v)\int_{\mathcal{V}} f(t,v^*)\mathrm{d}v^*$$

which represents the equation for the single-population model given in [75] and in Chapter 3, see equation (3.2). ∎

4.3.1 Discretization of the model

In order to address the qualitative properties of the model, we consider a discretization of the velocity spaces. The study becomes simpler with the following assumptions:

Ansatz 4.5. The velocity jump Δv^{p} is a fixed parameter and $\Delta v^{\mathsf{p}} = \Delta v$, $\forall\ \mathsf{p}$.

Ansatz 4.6. The fixed parameter Δv is such that $\Delta v = V^{\mathsf{p}}_{\max}/T^{\mathsf{p}}$, with $T^{\mathsf{p}} \in \mathbb{N}$, $\forall\ \mathsf{p}$.

Ansatz 4.7. Let δv be the numerical parameter of the velocity space discretization. Then, we take $\delta v = \frac{\Delta v}{r}$.

Notice that Ansatz 4.5 is not as restrictive as it appears. Since Δv^{p} represents the instantaneous velocity jump of a vehicle as a result of the acceleration interaction, it might be thought of as another microscopic feature characterizing the classes of vehicles. Then we may suppose that the populations do not differ in the jump of velocity but we can characterize them by assuming that the jump of velocity is performed with different microscopic accelerations a^{p}. As proved in [75] and in Chapter 3 in the case of a single-population model, the acceleration of the vehicles depends on the product of Δv and the interaction rate, thus in order to account for different accelerations in each class we could act on the interaction rates η^{p} and η^{pq}, without modifying Δv. However, this is relevant only in the spatially inhomogeneous model because in the framework analyzed in this work the interaction rates influence only the rate of convergence towards equilibrium solutions. The equilibrium solutions themselves do not depend on the interaction rates.

Ansatz 4.6 implies that

$$|V^{\mathsf{p}}_{\max} - V^{\mathsf{q}}_{\max}| = m^{\mathsf{pq}}\Delta v, \quad \forall\ \mathsf{p},\ \mathsf{q} \in \neg\mathsf{p},\ m^{\mathsf{pq}} \in \mathbb{N},$$

i.e. the distance between the maximum velocities of the populations is a multiple of Δv, see the left panel of Figure 4.2.

Finally, observe that Ansatz 4.7 means that Δv corresponds to an integer number of intervals in the velocity discretization, see the center panel of Figure 4.2. Thus $r = \frac{n^{\mathsf{p}}-1}{T^{\mathsf{p}}} \in \mathbb{N}$ depends on the number of grid points n^{p}. This assumption is justified by the investigations provided in Section 3.3.1 in which we show that the choice $r \in \mathbb{N}$ is sufficient, and thus not restrictive, in order to compute the exact equilibrium solutions numerically. In this chapter, we will show the computation of the equilibrium solutions for the case of two populations showing that they are quantized reproducing the structure of the single-population δ model (see Theorem 4.12 in Section 4.3.2). In the general case we can proceed numerically using the fact that the asymptotic state can be recovered exactly with a reduced number of discrete speeds.

We define the (p dependent) velocity cells $I^{\mathsf{p}}_j = [(j-\frac{3}{2})\delta v, (j-\frac{1}{2})\delta v] \cap [0, V^{\mathsf{p}}_{\max}]$, $\forall\ \mathsf{p}$ and for $j = 1, \dots, n^{\mathsf{p}} = \frac{V^{\mathsf{p}}_{\max}}{\delta v} + 1$. Note that all cells have amplitude δv except I^{p}_1 and $I^{\mathsf{p}}_{n^{\mathsf{p}}}$ which have amplitude $\delta v/2$. The velocity grid nodes, located at the center of each cell, are $v^{\mathsf{p}}_1 = \delta v/4, v^{\mathsf{p}}_{n^{\mathsf{p}}} = V^{\mathsf{p}}_{\max} - \delta v/4$, and $v^{\mathsf{p}}_j = (j-1)\delta v$ for $j = 2, \dots, n^{\mathsf{p}} - 1$. This choice was already used in [75], and in Sections 3.3.1 - 3.4.1, since it is convenient for computations because all grids with $r > 1$ contain all the points of the coarser mesh with $r = 1$ (except the first and the last point). See the right panel of Figure 4.2 for the discretization of $\mathcal{V}^{\mathsf{p}} \times \mathcal{V}^{\mathsf{q}}$.

In order to discretize the model, we approximate each velocity distribution with the piecewise constant function

$$f^{\mathsf{p}}(t,v) \approx f^{\mathsf{p}}_{\delta v}(t,v) = \sum_{j=1}^{n^{\mathsf{p}}} f^{\mathsf{p}}_j(t) \frac{\chi_{I^{\mathsf{p}}_j}(v)}{\left|I^{\mathsf{p}}_j\right|} \tag{4.12}$$

where $f^{\mathsf{p}}_j : \mathbb{R}^+ \to [0, \rho^{\mathsf{p}}]$ represents the number of p-vehicles traveling with velocity $v \in I^{\mathsf{p}}_j$.

By integrating the kinetic equation (4.2) over the cells I_j^{p} we obtain the following system of ordinary differential equations:

$$\begin{aligned}\frac{\mathrm{d}f_j^{\mathsf{p}}(t)}{\mathrm{d}t} =& Q_j^{\mathsf{p}}[f_{\delta v}^{\mathsf{p}}, (f_{\delta v}^{\mathsf{p}}, f_{\delta v}^{\mathsf{q}})](t) \\ =& \underbrace{\int_{I_j^{\mathsf{p}}} Q^{\mathsf{pp}}[f_{\delta v}^{\mathsf{p}}, f_{\delta v}^{\mathsf{p}}](t,v)\mathrm{d}v}_{Q_j^{\mathsf{pp}}[f_{\delta v}^{\mathsf{p}}, f_{\delta v}^{\mathsf{p}}](t)} + \underbrace{\int_{I_j^{\mathsf{p}}} Q^{\mathsf{pq}}[f_{\delta v}^{\mathsf{p}}, f_{\delta v}^{\mathsf{q}}](t,v)\mathrm{d}v}_{Q_j^{\mathsf{pq}}[f_{\delta v}^{\mathsf{p}}, f_{\delta v}^{\mathsf{q}}](t)}, \quad j = 1, \dots, n^{\mathsf{p}}, \forall\, \mathsf{p}\end{aligned} \tag{4.13}$$

whose initial condition $f_1^{\mathsf{p}}(0), \dots, f_{n^{\mathsf{p}}}^{\mathsf{p}}(0)$ are such that

$$\sum_{j=1}^{n^{\mathsf{p}}} f_j^{\mathsf{p}}(0) = \int_{\mathcal{V}^{\mathsf{p}}} f^{\mathsf{p}}(t=0, v)\mathrm{d}v = \rho^{\mathsf{p}}, \quad \forall\, \mathsf{p},\ \rho^{\mathsf{p}} \in [0, \rho_{\max}^{\mathsf{p}}]$$

and ρ^{p} is the initial density, which remains constant in the spatially homogeneous case, see Remark 4.1.

The terms $Q_j^{\mathsf{pp}}[f_{\delta v}^{\mathsf{p}}, f_{\delta v}^{\mathsf{p}}](t)$ and $Q_j^{\mathsf{pq}}[f_{\delta v}^{\mathsf{p}}, f_{\delta v}^{\mathsf{q}}](t)$ can be explicitly written out. Starting from the self-collision term Q_j^{pp} and recalling the computations in [75] and in Section 3.3.1 for the single-population model, we obtain

$$\begin{aligned}\frac{1}{\eta^{\mathsf{p}}} Q_j^{\mathsf{pp}}[f_{\delta v}^{\mathsf{p}}, f_{\delta v}^{\mathsf{p}}](t) =& (1-P) f^{\mathsf{p}j} f_j^{\mathsf{p}} + (1-P) f_j^{\mathsf{p}} \sum_{k=j+1}^{n^{\mathsf{p}}} f^{\mathsf{p}k} + (1-P) f^{\mathsf{p}j} \sum_{h=j+1}^{n^{\mathsf{p}}} f_h^{\mathsf{p}} \\ & - f_j^{\mathsf{p}} \sum_{k=1}^{n^{\mathsf{p}}} f^{\mathsf{p}k}, \quad \text{for } j = 1, \dots, r\end{aligned} \tag{4.14a}$$

$$\begin{aligned}\frac{1}{\eta^{\mathsf{p}}} Q_j^{\mathsf{pp}}[f_{\delta v}^{\mathsf{p}}, f_{\delta v}^{\mathsf{p}}](t) =& (1-P) f^{\mathsf{p}j} f_j^{\mathsf{p}} + (1-P) f_j^{\mathsf{p}} \sum_{k=j+1}^{n^{\mathsf{p}}} f^{\mathsf{p}k} + (1-P) f^{\mathsf{p}j} \sum_{h=j+1}^{n^{\mathsf{p}}} f_h^{\mathsf{p}} \\ & + P f_{j-r}^{\mathsf{p}} \sum_{k=1}^{n^{\mathsf{p}}} f^{\mathsf{p}k} - f_j^{\mathsf{p}} \sum_{k=1}^{n^{\mathsf{p}}} f^{\mathsf{p}k}, \quad \text{for } j = r+1, \dots, n^{\mathsf{p}} - 1\end{aligned} \tag{4.14b}$$

$$\frac{1}{\eta^{\mathsf{p}}} Q_{n^{\mathsf{p}}}^{\mathsf{pp}}[f_{\delta v}^{\mathsf{p}}, f_{\delta v}^{\mathsf{p}}](t) = (1-P) f^{\mathsf{p}n^{\mathsf{p}}} f_{n^{\mathsf{p}}}^{\mathsf{p}} + P \sum_{h=n^{\mathsf{p}}-r}^{n^{\mathsf{p}}} f_h^{\mathsf{p}} \sum_{k=1}^{n^{\mathsf{p}}} f^{\mathsf{p}k} - f_{n^{\mathsf{p}}}^{\mathsf{p}} \sum_{k=1}^{n^{\mathsf{p}}} f^{\mathsf{p}k}. \tag{4.14c}$$

For the cross-collision terms, we distinguish the two cases described in (4.9) and (4.10).

Therefore, let $\mathcal{V}^{\mathsf{p}} \subset \mathcal{V}^{\mathsf{q}}$, we obtain

$$\frac{1}{\eta^{\mathsf{pq}}} Q_j^{\mathsf{pq}}[f_{\delta v}^{\mathsf{p}}, f_{\delta v}^{\mathsf{q}}](t) = (1-P) f^{\mathsf{q}j} f_j^{\mathsf{p}} + (1-P) f_j^{\mathsf{p}} \sum_{k=j+1}^{n^{\mathsf{q}}} f^{\mathsf{q}k} + (1-P) f^{\mathsf{q}j} \sum_{h=j+1}^{n^{\mathsf{p}}} f_h^{\mathsf{p}} \tag{4.15a}$$

$$- f_j^{\mathsf{p}} \sum_{k=1}^{n^{\mathsf{q}}} f^{\mathsf{q}k}, \quad \text{for } j = 1, \dots, r$$

$$\frac{1}{\eta^{\mathsf{pq}}} Q_j^{\mathsf{pq}}[f_{\delta v}^{\mathsf{p}}, f_{\delta v}^{\mathsf{q}}](t) = (1-P) f^{\mathsf{q}j} f_j^{\mathsf{p}} + (1-P) f_j^{\mathsf{p}} \sum_{k=j+1}^{n^{\mathsf{q}}} f^{\mathsf{q}k} + (1-P) f^{\mathsf{q}j} \sum_{h=j+1}^{n^{\mathsf{p}}} f_h^{\mathsf{p}} \tag{4.15b}$$

$$+ P f_{j-r}^{\mathsf{p}} \sum_{k=1}^{n^{\mathsf{q}}} f^{\mathsf{q}k} - f_j^{\mathsf{p}} \sum_{k=1}^{n^{\mathsf{q}}} f^{\mathsf{q}k}, \quad \text{for } j = r+1, \dots, n^{\mathsf{p}} - 1$$

$$\frac{1}{\eta^{\mathsf{pq}}} Q_{n^{\mathsf{p}}}^{\mathsf{pq}}[f_{\delta v}^{\mathsf{p}}, f_{\delta v}^{\mathsf{q}}](t) = (1-P) f_{n^{\mathsf{p}}}^{\mathsf{p}} \sum_{k=n^{\mathsf{p}}}^{n^{\mathsf{q}}} f^{\mathsf{q}k} + P \sum_{h=n^{\mathsf{p}}-r}^{n^{\mathsf{p}}} f_h^{\mathsf{p}} \sum_{k=1}^{n^{\mathsf{q}}} f^{\mathsf{q}k} - f_{n^{\mathsf{p}}}^{\mathsf{p}} \sum_{k=1}^{n^{\mathsf{q}}} f^{\mathsf{q}k}. \tag{4.15c}$$

Finally, let $\mathcal{V}^{\mathsf{p}} \supset \mathcal{V}^{\mathsf{q}}$, we obtain

$$\frac{1}{\eta^{\mathsf{pq}}} Q_j^{\mathsf{pq}}[f_{\delta v}^{\mathsf{p}}, f_{\delta v}^{\mathsf{q}}](t) = (1-P) f^{\mathsf{q}j} f_j^{\mathsf{p}} + (1-P) f_j^{\mathsf{p}} \sum_{k=j+1}^{n^{\mathsf{q}}} f^{\mathsf{q}k} + (1-P) f^{\mathsf{q}j} \sum_{h=j+1}^{n^{\mathsf{p}}} f_h^{\mathsf{p}} \tag{4.16a}$$

$$- f_j^{\mathsf{p}} \sum_{k=1}^{n^{\mathsf{q}}} f^{\mathsf{q}k}, \quad \text{for } j = 1, \dots, r$$

$$\frac{1}{\eta^{\mathsf{pq}}} Q_j^{\mathsf{pq}}[f_{\delta v}^{\mathsf{p}}, f_{\delta v}^{\mathsf{q}}](t) = (1-P) f^{\mathsf{q}j} f_j^{\mathsf{p}} + (1-P) f_j^{\mathsf{p}} \sum_{k=j+1}^{n^{\mathsf{q}}} f^{\mathsf{q}k} + (1-P) f^{\mathsf{q}j} \sum_{h=j+1}^{n^{\mathsf{p}}} f_h^{\mathsf{p}} \tag{4.16b}$$

$$+ P f_{j-r}^{\mathsf{p}} \sum_{k=1}^{n^{\mathsf{q}}} f^{\mathsf{q}k} - f_j^{\mathsf{p}} \sum_{k=1}^{n^{\mathsf{q}}} f^{\mathsf{q}k}, \quad \text{for } j = r+1, \dots, n^{\mathsf{q}} - 1$$

$$\frac{1}{\eta^{\mathsf{pq}}} Q_{n^{\mathsf{q}}}^{\mathsf{pq}}[f_{\delta v}^{\mathsf{p}}, f_{\delta v}^{\mathsf{q}}](t) = (1-P) f^{\mathsf{q}n^{\mathsf{q}}} f_{n^{\mathsf{q}}}^{\mathsf{p}} + (1-P) f^{\mathsf{q}n^{\mathsf{q}}} \sum_{h=n^{\mathsf{q}}+1}^{n^{\mathsf{p}}} f_h^{\mathsf{p}} + P f_{n^{\mathsf{q}}-r}^{\mathsf{p}} \sum_{k=1}^{n^{\mathsf{q}}} f^{\mathsf{q}k} \tag{4.16c}$$

$$- f_{n^{\mathsf{q}}}^{\mathsf{p}} \sum_{k=1}^{n^{\mathsf{q}}} f^{\mathsf{q}k}, \tag{4.16d}$$

$$\frac{1}{\eta^{\mathsf{pq}}} Q_j^{\mathsf{pq}}[f_{\delta v}^{\mathsf{p}}, f_{\delta v}^{\mathsf{q}}](t) = P f_{j-r}^{\mathsf{p}} \sum_{k=1}^{n^{\mathsf{q}}} f^{\mathsf{q}k} - f_j^{\mathsf{p}} \sum_{k=1}^{n^{\mathsf{q}}} f^{\mathsf{q}k}, \quad \text{for } j = n^{\mathsf{q}}+1, \dots, n^{\mathsf{p}} - 1 \tag{4.16e}$$

$$\frac{1}{\eta^{\mathsf{pq}}} Q_{n^{\mathsf{p}}}^{\mathsf{pq}}[f_{\delta v}^{\mathsf{p}}, f_{\delta v}^{\mathsf{q}}](t) = P \sum_{h=n^{\mathsf{p}}-r}^{n^{\mathsf{p}}} f_h^{\mathsf{p}} \sum_{k=1}^{n^{\mathsf{q}}} f^{\mathsf{q}k} - f_{n^{\mathsf{p}}}^{\mathsf{p}} \sum_{k=1}^{n^{\mathsf{q}}} f^{\mathsf{q}k}. \tag{4.16f}$$

In the above formulas, the kinetic distribution functions of candidate and field vehicles are distinguished by the position of the index of the components: bottom-right for candidate vehicles (such as e.g. f_h^{p}), top-right for field vehicles (such as e.g. $f^{\mathsf{p}k}$ or $f^{\mathsf{q}k}$).

Once the right-hand side of (4.13) is computed, then the ODE system can be easily rewritten by means of the matrices $\mathbf{A}^{\mathsf{p},j}$ and $\mathbf{B}^{\mathsf{pq},j}$, for $j = 1, \dots, n^{\mathsf{p}}$, which are the so-called

self- and cross-interaction matrices, respectively. Then, the multi-population model writes finally as

$$\begin{aligned}\frac{\mathrm{d}f_j^{\mathsf{p}}(t)}{\mathrm{d}t} =&\eta^{\mathsf{p}} \sum_{h,k=1}^{n^{\mathsf{p}}} A_{hk}^{\mathsf{p},j} f_h^{\mathsf{p}} f^{\mathsf{p}k} + \sum_{\mathsf{q}\in\neg\mathsf{p}} \eta^{\mathsf{pq}} \sum_{h=1}^{n^{\mathsf{p}}}\sum_{k=1}^{n^{\mathsf{q}}} B_{hk}^{\mathsf{pq},j} f_h^{\mathsf{p}} f^{\mathsf{q}k} \\ &- f_j^{\mathsf{p}} \left(\eta^{\mathsf{p}} \sum_{k=1}^{n^{\mathsf{p}}} f^{\mathsf{p}k} + \sum_{\mathsf{q}\in\neg\mathsf{p}} \eta^{\mathsf{pq}} \sum_{k=1}^{n^{\mathsf{q}}} f^{\mathsf{q}k} \right), \quad j = 1,\dots,n^{\mathsf{p}}, \forall\ \mathsf{p}.\end{aligned} \tag{4.17}$$

The matrices $\mathbf{A}^{\mathsf{p},j}$ and $\mathbf{B}^{\mathsf{pq},j}$ are defined as

$$A_{hk}^{\mathsf{p},j} = \mathrm{Prob}\left(v_* \in I_h^{\mathsf{p}} \to v \in I_j^{\mathsf{p}} | v^* \in I_k^{\mathsf{p}}\right),\ B_{hk}^{\mathsf{pq},j} = \mathrm{Prob}\left(v_* \in I_h^{\mathsf{p}} \to v \in I_j^{\mathsf{p}} | v^* \in I_k^{\mathsf{q}}\right),$$

namely they contain in the position (h,k) the probability that the candidate vehicle belonging to the p-th class and with velocity in I_h^{p} will acquire a velocity in I_j^{p} when it interacts with a field vehicle traveling at a velocity in I_k^{p}, if the p-vehicles play also the role of field class, or in I_k^{q} otherwise.

In Figure 4.3a we show the sparse structure of the self-interaction matrices $\mathbf{A}^{\mathsf{p},j} \in \mathbb{R}^{n^{\mathsf{p}}\times n^{\mathsf{p}}}$, for $j = 1,\dots,n^{\mathsf{p}}$. The cross-interaction matrices $\mathbf{B}^{\mathsf{pq},j}$ for the case $\mathcal{V}^{\mathsf{p}} \supset \mathcal{V}^{\mathsf{q}}$ have the same structure as the $\mathbf{A}^{\mathsf{p},j}$'s, apart from being rectangular of dimensions $n^{\mathsf{p}} \times n^{\mathsf{q}}$, with $n^{\mathsf{p}} > n^{\mathsf{q}}$. Differences however arise for $j \geq n^{\mathsf{q}}$, see Figure 4.3b in which for simplicity we have assumed that $n^{\mathsf{q}} + r = n^{\mathsf{p}}$ (i.e. $V_{\max}^{\mathsf{p}} - V_{\max}^{\mathsf{q}} = \Delta v$). Finally, the cross-interaction matrices $\mathbf{B}^{\mathsf{pq},j}$ for the case $\mathcal{V}^{\mathsf{p}} \subset \mathcal{V}^{\mathsf{q}}$ are $n^{\mathsf{p}} \times n^{\mathsf{q}}$, with $n^{\mathsf{p}} < n^{\mathsf{q}}$. They can in turn be easily derived from the $\mathbf{A}^{\mathsf{p},j}$'s, the only different case being the one for $j = n^{\mathsf{p}}$, see Figure 4.3c in which for simplicity we have assumed that $n^{\mathsf{q}} = n^{\mathsf{p}} + r$ (i.e. $V_{\max}^{\mathsf{q}} - V_{\max}^{\mathsf{p}} = \Delta v$).

In all these figures, the nonzero elements are shaded with different hatchings, corresponding to the different values of the elements, as indicated in the panels in which they appear for the first time.

As it can be checked, both the self- and the cross-interaction matrices are stochastic with respect to the index j, i.e. all their elements are positive and bounded above by 1 and

$$\sum_{j=1}^{n^{\mathsf{p}}} \mathbf{A}^{\mathsf{p},j} = \mathfrak{O}_{n^{\mathsf{p}}\times n^{\mathsf{p}}}, \quad \sum_{j=1}^{n^{\mathsf{p}}} \mathbf{B}^{\mathsf{pq},j} = \mathfrak{O}_{n^{\mathsf{p}}\times n^{\mathsf{q}}}, \quad \forall\ \mathsf{p},\ \mathsf{q} \in \neg\mathsf{p}.$$

where $\mathfrak{O}_{N\times M}$ is the matrix of size $N \times M$ with the value 1 in each entry. These properties come from (4.5), and they guarantee mass conservation.

4.3.2 Qualitative analysis

Now we study the well-posedness of the discrete-velocity model (4.17) and for the sake of simplicity we work with two populations only, but the analysis can be generalized to multiple populations. We show that the model has a unique solution, which remains positive and bounded in time, and finally we compute the analytical equilibria.

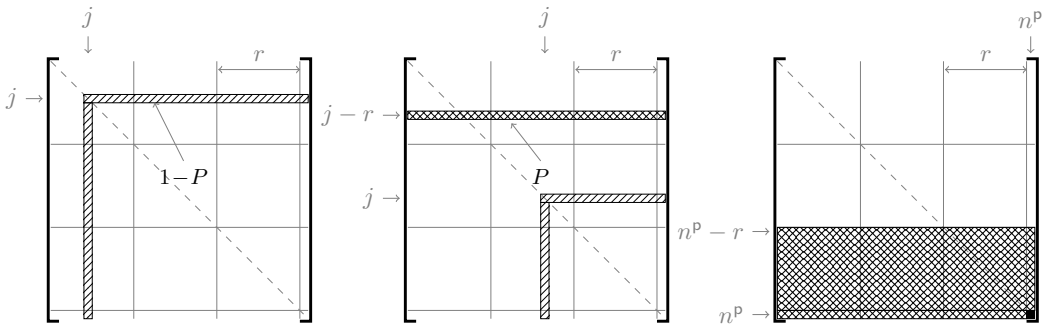

$\mathbf{A}^{\mathsf{p},j}$ for $1 \le j \le r$ $\mathbf{A}^{\mathsf{p},j}$ for $r < j < n^{\mathsf{p}}$ $\mathbf{A}^{\mathsf{p},j}$ for $j = n^{\mathsf{p}}$

(A) Self-interaction matrices $\mathbf{A}^{\mathsf{p},j}$, $j = 1, \dots, n^{\mathsf{p}}$.

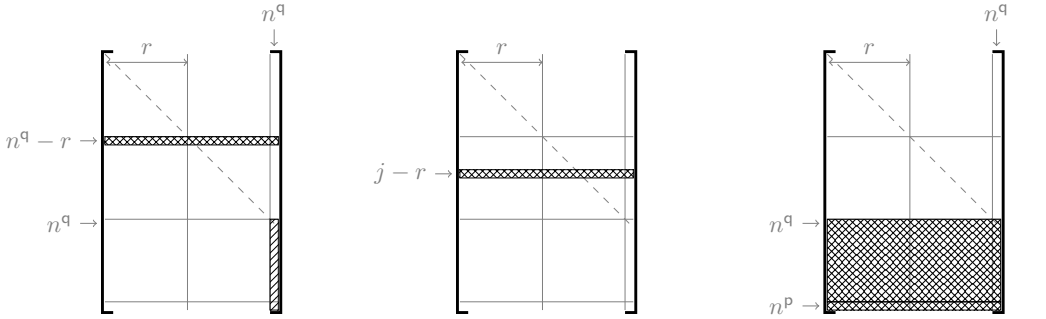

$\mathbf{B}^{\mathsf{pq},j}$ for $j = n^{\mathsf{q}}$ $\mathbf{B}^{\mathsf{pq},j}$ for $n^{\mathsf{q}} < j < n^{\mathsf{q}} + r$ $\mathbf{B}^{\mathsf{pq},j}$ for $j = n^{\mathsf{q}} + r = n^{\mathsf{p}}$

(B) Cross-interaction matrices $\mathbf{B}^{\mathsf{pq},j}$, $j \ge n^{\mathsf{q}}$, for the case $\mathcal{V}^{\mathsf{p}} \supset \mathcal{V}^{\mathsf{q}}$.

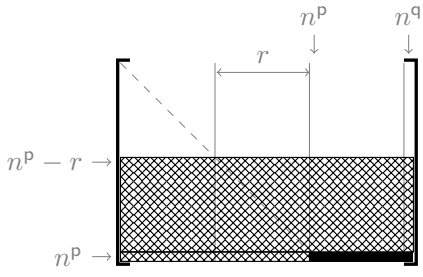

$\mathbf{B}^{\mathsf{pq},j}$ for $j = n^{\mathsf{p}}$

(C) Cross-interaction matrices $\mathbf{B}^{\mathsf{pq},j}$, $j = n^{\mathsf{p}}$, for the case $\mathcal{V}^{\mathsf{p}} \subset \mathcal{V}^{\mathsf{q}}$.

Figure 4.3: General structure of the interaction matrices.

To this end, we consider the Cauchy problem associated to the ODE system (4.17) with initial data $f_j^{\mathsf{p}}(0)$, $j = 1, \dots, n^{\mathsf{p}}$, $\forall\ \mathsf{p}$. Since in spatially homogeneous conditions the density is constant in time, the generic equation of the Cauchy problem can be written as

$$\frac{\mathrm{d}f_j^{\mathsf{p}}(t)}{\mathrm{d}t} = \eta^{\mathsf{p}} \sum_{h,k=1}^{n^{\mathsf{p}}} A_{hk}^{\mathsf{p},j} f_h^{\mathsf{p}} f_k^{\mathsf{p}} + \sum_{\mathsf{q}\in\neg\mathsf{p}} \eta^{\mathsf{pq}} \sum_{h=1}^{n^{\mathsf{p}}} \sum_{k=1}^{n^{\mathsf{q}}} B_{hk}^{\mathsf{pq},j} f_h^{\mathsf{p}} f_k^{\mathsf{q}} - R^{\mathsf{p}} f_j^{\mathsf{p}}, \quad j = 1, \dots, n^{\mathsf{p}}, \forall\ \mathsf{p} \tag{4.18}$$

where $R^{\mathsf{p}} := \eta^{\mathsf{p}}\rho^{\mathsf{p}} + \sum_{\mathsf{q}\in\neg\mathsf{p}} \eta^{\mathsf{pq}}\rho^{\mathsf{q}}$. Notice that in (4.18) we do not use the upper index to distinguish the distributions, but the index h is referred to the candidate vehicle distribution, while the index k to the field vehicle distributions. We assume that each density ρ^{p} is normalized with respect to $\rho_{\max}^{\mathsf{p}}$ so that

$$\begin{aligned} &0 \le f_j^{\mathsf{p}}(0) \le \rho^{\mathsf{p}} \le 1, \quad j = 1, \dots, n^{\mathsf{p}}, \forall\ \mathsf{p} \\ &0 \le \sum_{j=1}^{n^{\mathsf{p}}} f_j^{\mathsf{p}}(0) = \rho^{\mathsf{p}} \le 1, \quad \forall\ \mathsf{p}. \end{aligned} \tag{4.19}$$

In the following, we propose two different proofs of the well posedness of the Cauchy problem (4.18) associated to the model (4.17). The first one (Theorem 4.9) uses the Fixed Point Theorem. Instead, the second one (Theorem 4.10) uses the theorem on global existence and uniqueness of solutions to first order ODE systems with sublinear growth.

Starting from the first approach it is suitable to rewrite the Cauchy problem (4.18) in its integral formulation. To this end, we define $F(t) := tR^{\mathsf{p}}$ and multiplying the equation (4.18) by $e^{F(t)}$ and integrating in time we obtain its integral formulation:

$$f_j^{\mathsf{p}}(t) = e^{-tR^{\mathsf{p}}} f_j^{\mathsf{p}}(0) + \int_0^t e^{(\tau-t)R^{\mathsf{p}}} \left[\eta^{\mathsf{p}} \sum_{h,k=1}^{n^{\mathsf{p}}} A_{hk}^{\mathsf{p},j} f_h^{\mathsf{p}} f_k^{\mathsf{p}} + \sum_{\mathsf{q}\in\neg\mathsf{p}} \eta^{\mathsf{pq}} \sum_{h=1}^{n^{\mathsf{p}}} \sum_{k=1}^{n^{\mathsf{q}}} B_{hk}^{\mathsf{pq},j} f_h^{\mathsf{p}} f_k^{\mathsf{q}} \right] d\tau,\ j = 1, \dots, n^{\mathsf{p}}, \forall\ \mathsf{p}.$$

In order to prove the existence and uniqueness of the solution of the Cauchy problem, we rewrite it in explicit formulation assuming that the two populations are labeled one with p and the other one with q:

$$\begin{cases} f_j^{\mathsf{p}}(t) = e^{-tR^{\mathsf{p}}} f_j^{\mathsf{p}}(0) + \displaystyle\int_0^t e^{(\tau-t)R^{\mathsf{p}}} \left[\sum_{h,k=1}^{n^{\mathsf{p}}} \eta^{\mathsf{p}} A_{hk}^{\mathsf{p},j} f_h^{\mathsf{p}} f_k^{\mathsf{p}} + \sum_{h=1}^{n^{\mathsf{p}}} \sum_{k=1}^{n^{\mathsf{q}}} \eta^{\mathsf{pq}} B_{hk}^{\mathsf{pq},j} f_h^{\mathsf{p}} f_k^{\mathsf{q}} \right] d\tau, \quad j = 1, \dots, n^{\mathsf{p}} \\ f_j^{\mathsf{q}}(t) = e^{-tR^{\mathsf{q}}} f_j^{\mathsf{q}}(0) + \displaystyle\int_0^t e^{(\tau-t)R^{\mathsf{q}}} \left[\sum_{h,k=1}^{n^{\mathsf{q}}} \eta^{\mathsf{q}} A_{hk}^{\mathsf{q},j} f_h^{\mathsf{q}} f_k^{\mathsf{q}} + \sum_{h=1}^{n^{\mathsf{q}}} \sum_{k=1}^{n^{\mathsf{p}}} \eta^{\mathsf{qp}} B_{hk}^{\mathsf{qp},j} f_h^{\mathsf{q}} f_k^{\mathsf{p}} \right] d\tau, \quad j = 1, \dots, n^{\mathsf{q}} \end{cases} \tag{4.20}$$

Let

$$X = C\left([0, T_{\max}];\, \mathbb{R}^{n^{\mathsf{p}}}\right) \times C\left([0, T_{\max}];\, \mathbb{R}^{n^{\mathsf{q}}}\right)$$

be the space of vector-valued continuous functions on the interval $[0, T_{\max}]$ and let $(\mathbf{u}, \mathbf{v})$ be a generic element of X. Let $\mathbf{f}^{\mathsf{p}} = (f_1^{\mathsf{p}}, \dots, f_{n^{\mathsf{p}}}^{\mathsf{p}})$ and $\mathbf{f}^{\mathsf{q}} = (f_1^{\mathsf{q}}, \dots, f_{n^{\mathsf{q}}}^{\mathsf{q}})$ be the solution of

the Cauchy problem. We define

$$\mathcal{B} = \left\{ (\mathbf{u}, \mathbf{v}) \in X : 0 \leq u_j(t) \leq \rho^{\mathsf{p}}, 0 \leq v_j(t) \leq \rho^{\mathsf{q}}, \sum_{j=1}^{n^{\mathsf{p}}} u_j(t) = \rho^{\mathsf{p}}, \sum_{j=1}^{n^{\mathsf{q}}} v_j(t) = \rho^{\mathsf{q}} \right\}$$

the subset of X such that ρ^{p} and ρ^{q} are fixed constants, the same as in (4.18), then the elements of $\mathcal{B}$ have the properties we require for the solution $(\mathbf{f}^{\mathsf{p}}, \mathbf{f}^{\mathsf{q}})$ of (4.20).

From now on, we will endow $\mathbb{R}^{n^{\mathsf{p}}}$ and $\mathbb{R}^{n^{\mathsf{q}}}$ with the 1-norm. While on the spaces $C\left([0, T_{\max}]; \mathbb{R}^d\right)$, for $d \in \mathbb{N}$, and on the space X we use the norms defined as follows.

Definition 4.8. Let $\mathbf{u}(t) \in \mathbb{R}^d$ be a time dependent vector with $d \in \mathbb{N}$ real components. Then on $C\left([0, T_{\max}]; \mathbb{R}^d\right)$ the uniform norm of the vector $\mathbf{u}(t)$ is

$$\|\mathbf{u}\|_\infty = \sup_{t \in [0, T_{\max}]} \|\mathbf{u}(t)\|_1 = \sup_{t \in [0, T_{\max}]} \sum_{j=1}^{d} |u_j(t)| .$$

Instead, on the space X the following norm is defined:

$$\|(\mathbf{u}, \mathbf{v})\|_X = \|\mathbf{u}\|_\infty + \|\mathbf{v}\|_\infty .$$

Let $\mathscr{T} : \mathcal{B} \to X$ be the operator such that $(\mathbf{u}, \mathbf{v}) \mapsto \mathscr{T}(\mathbf{u}, \mathbf{v}) := (\mathscr{T}^{\mathsf{p}}(\mathbf{u}, \mathbf{v}), \mathscr{T}^{\mathsf{q}}(\mathbf{u}, \mathbf{v}))$, where the operators $\mathscr{T}^{\mathsf{p}} : \mathcal{B} \to C\left([0, T_{\max}]; \mathbb{R}^{n^{\mathsf{p}}}\right)$ and $\mathscr{T}^{\mathsf{q}} : \mathcal{B} \to C\left([0, T_{\max}]; \mathbb{R}^{n^{\mathsf{q}}}\right)$ are defined by

$$\begin{cases} \mathscr{T}^{\mathsf{p}}(\mathbf{u}, \mathbf{v})_j = e^{-tR^{\mathsf{p}}} f_j^{\mathsf{p}}(0) + \displaystyle\int_0^t e^{(\tau - t)R^{\mathsf{p}}} \left[\sum_{h,k=1}^{n^{\mathsf{p}}} \eta^{\mathsf{p}} A_{hk}^{\mathsf{p},j} u_h u_k + \sum_{h=1}^{n^{\mathsf{p}}} \sum_{k=1}^{n^{\mathsf{q}}} \eta^{\mathsf{pq}} B_{hk}^{\mathsf{pq},j} u_h v_k \right] d\tau \\ \mathscr{T}^{\mathsf{q}}(\mathbf{u}, \mathbf{v})_j = e^{-tR^{\mathsf{q}}} f_j^{\mathsf{q}}(0) + \displaystyle\int_0^t e^{(\tau - t)R^{\mathsf{q}}} \left[\sum_{h,k=1}^{n^{\mathsf{q}}} \eta^{\mathsf{q}} A_{hk}^{\mathsf{q},j} v_h v_k + \sum_{h=1}^{n^{\mathsf{q}}} \sum_{k=1}^{n^{\mathsf{p}}} \eta^{\mathsf{qp}} B_{hk}^{\mathsf{qp},j} v_h u_k \right] d\tau \end{cases} . \tag{4.21}$$

The solution of problem (4.20) can be restated as

$$\text{Find } (\mathbf{f}^{\mathsf{p}}, \mathbf{f}^{\mathsf{q}}) \in \mathcal{B} \text{ such that } (\mathbf{f}^{\mathsf{p}}, \mathbf{f}^{\mathsf{q}}) = \mathscr{T}(\mathbf{f}^{\mathsf{p}}, \mathbf{f}^{\mathsf{q}})$$

that is the solution is a fixed point of the operator $\mathscr{T}$ in $\mathcal{B}$.

Theorem 4.9 (Well posedness - 1). – *For any given initial condition* $(\mathbf{f}^{\mathsf{p}}(0), \mathbf{f}^{\mathsf{q}}(0)) \in \mathcal{B}$*, thus satisfying the assumptions* (4.19)*, there exists a unique fixed point* $(\mathbf{f}^{\mathsf{p}}, \mathbf{f}^{\mathsf{q}}) \in \mathcal{B}$ *of the operator* $\mathscr{T}$ *defined by* (4.21)*.*

Proof. The proof of the statement will be organized by steps and will be achieved by applying the Banach-Caccioppoli Fixed Point Theorem (or Contraction Mapping Theorem).

Step 1 First of all we prove that $\mathscr{T}$ maps $\mathcal{B}$ into itself, i.e.

$$\forall\ (\mathbf{u},\mathbf{v}) \in \mathcal{B} \Rightarrow \mathscr{T}(\mathbf{u},\mathbf{v}) \in \mathcal{B}.$$

It is obvious from (4.21) that $\mathscr{T}^{\mathsf{p}}(\mathbf{u},\mathbf{v})_j \geq 0$, $\forall\ j = 1,\dots,n^{\mathsf{p}}$ and $\mathscr{T}^{\mathsf{q}}(\mathbf{u},\mathbf{v})_j \geq 0$, $\forall\ j = 1,\dots,n^{\mathsf{q}}$. Moreover

$$\sum_{j=1}^{n^{\mathsf{p}}} \mathscr{T}^{\mathsf{p}}(\mathbf{u},\mathbf{v})_j = e^{-tR^{\mathsf{p}}} \sum_{j=1}^{n^{\mathsf{p}}} f_j^{\mathsf{p}}(0) + \int_0^t e^{(\tau-t)R^{\mathsf{p}}} \rho^{\mathsf{p}} R^{\mathsf{p}} d\tau = e^{-R^{\mathsf{p}}t}\rho^{\mathsf{p}} \left[1 + R^{\mathsf{p}} \int_0^t e^{\tau R^{\mathsf{p}}} d\tau\right] = \rho^{\mathsf{p}}.$$

Similarly, we have $\sum_{j=1}^{n^{\mathsf{q}}} \mathscr{T}^{\mathsf{q}}(\mathbf{u},\mathbf{v})_j = \rho^{\mathsf{q}}$. Therefore $\mathscr{T}(\mathcal{B}) \subseteq \mathcal{B}$.

Step 2 Now we show that $\mathcal{B}$ is closed in X. To this end we consider a sequence $\{(\mathbf{u}_k,\mathbf{v}_k)\}_{k\geq 1} \subseteq \mathcal{B}$ such that $(\mathbf{u}_k,\mathbf{v}_k) \xrightarrow{k\to\infty} (\mathbf{u}_\infty,\mathbf{v}_\infty) \in X$ and we prove that $(\mathbf{u}_\infty,\mathbf{v}_\infty) \in \mathcal{B}$. Since pointwise convergence $\mathbf{u}_k(t) \xrightarrow{k\to\infty} \mathbf{u}_\infty(t)$ holds then $(\mathbf{u}_k)_j(t) \geq 0$, $\forall\ k,j,t$, implies $(\mathbf{u}_\infty)_j(t) \geq 0$, $\forall\ j,t$. Moreover, for any fixed k and t, $\sum_{j=1}^{n^{\mathsf{p}}} (\mathbf{u}_k)_j(t) = \rho^{\mathsf{p}}$ and we obtain

$$\begin{aligned}
\left|\sum_{j=1}^{n^{\mathsf{p}}} (\mathbf{u}_\infty)_j(t) - \rho^{\mathsf{p}}\right| &= \left|\sum_{j=1}^{n^{\mathsf{p}}} (\mathbf{u}_\infty)_j(t) - \sum_{j=1}^{n^{\mathsf{p}}} (\mathbf{u}_k)_j(t)\right| \\
&\leq \sum_{j=1}^{n^{\mathsf{p}}} |(\mathbf{u}_\infty)_j(t) - (\mathbf{u}_k)_j(t)| = \|\mathbf{u}_\infty(t) - \mathbf{u}_k(t)\|_1 \\
&\leq \|\mathbf{u}_\infty - \mathbf{u}_k\|_\infty \to 0, \quad k \to \infty,
\end{aligned}$$

thus $\sum_{j=1}^{n^{\mathsf{p}}} (\mathbf{u}_\infty)_j(t) = \rho^{\mathsf{p}}$, $\forall\ t$. Similar considerations hold for $\mathbf{v}_\infty$, thus $(\mathbf{u}_\infty,\mathbf{v}_\infty) \in \mathcal{B}$ and then $\mathcal{B}$ is closed in X.

Step 3 We prove that $\mathscr{T}$ is a contraction mapping on $\mathcal{B}$. We define the following operators:

$$\mathscr{A}^{\mathsf{p}} : \mathcal{B} \to C\left([0,T_{\max}];\, \mathbb{R}^{n^{\mathsf{p}}}\right), \quad \mathscr{A}^{\mathsf{q}} : \mathcal{B} \to C\left([0,T_{\max}];\, \mathbb{R}^{n^{\mathsf{q}}}\right)$$

such that

$$\begin{cases}
\mathscr{A}^{\mathsf{p}}(\mathbf{u},\mathbf{v})_j(t) = e^{tR^{\mathsf{p}}} \left[\displaystyle\sum_{h,k=1}^{n^{\mathsf{p}}} \eta^{\mathsf{p}} A_{hk}^{\mathsf{p},j} u_h(t) u_k(t) + \sum_{h=1}^{n^{\mathsf{p}}} \sum_{k=1}^{n^{\mathsf{q}}} \eta^{\mathsf{pq}} B_{hk}^{\mathsf{pq},j} u_h(t) v_k(t)\right] \\
\mathscr{A}^{\mathsf{q}}(\mathbf{u},\mathbf{v})_j(t) = e^{tR^{\mathsf{q}}} \left[\displaystyle\sum_{h,k=1}^{n^{\mathsf{q}}} \eta^{\mathsf{q}} A_{hk}^{\mathsf{q},j} v_h(t) v_k(t) + \sum_{h=1}^{n^{\mathsf{q}}} \sum_{k=1}^{n^{\mathsf{p}}} \eta^{\mathsf{qp}} B_{hk}^{\mathsf{qp},j} v_h(t) u_k(t)\right]
\end{cases}$$

thus the operators $\mathscr{T}^{\mathsf{p}}$ and $\mathscr{T}^{\mathsf{q}}$ write as

$$\begin{cases}
\mathscr{T}^{\mathsf{p}}(\mathbf{u},\mathbf{v})(t) = e^{-tR^{\mathsf{p}}} \left(\mathbf{f}^{\mathsf{p}}(0) + \displaystyle\int_0^t \mathscr{A}^{\mathsf{p}}(\mathbf{u},\mathbf{v})(\tau) d\tau\right) \\
\mathscr{T}^{\mathsf{q}}(\mathbf{u},\mathbf{v})(t) = e^{-tR^{\mathsf{q}}} \left(\mathbf{f}^{\mathsf{q}}(0) + \displaystyle\int_0^t \mathscr{A}^{\mathsf{q}}(\mathbf{u},\mathbf{v})(\tau) d\tau\right)
\end{cases}.$$

We consider $(\mathbf{u}', \mathbf{v}'), (\mathbf{u}'', \mathbf{v}'') \in \mathcal{B}$ and we study the Lipschitz condition for $\mathscr{T}$:

$$\begin{aligned}
\|\mathscr{T}(\mathbf{u}'', \mathbf{v}'') - \mathscr{T}(\mathbf{u}', \mathbf{v}')\|_X &= \|\mathscr{T}^{\mathsf{p}}(\mathbf{u}'', \mathbf{v}'') - \mathscr{T}^{\mathsf{p}}(\mathbf{u}', \mathbf{v}')\|_\infty + \|\mathscr{T}^{\mathsf{q}}(\mathbf{u}'', \mathbf{v}'') - \mathscr{T}^{\mathsf{q}}(\mathbf{u}', \mathbf{v}')\|_\infty \\
&\leq \sup_{t\in[0,T_{\max}]} e^{-tR^{\mathsf{p}}} \sum_{j=1}^{n^{\mathsf{p}}} \int_0^t |\mathscr{A}^{\mathsf{p}}(\mathbf{u}'', \mathbf{v}'')_j(\tau) - \mathscr{A}^{\mathsf{p}}(\mathbf{u}', \mathbf{v}')_j(\tau)|\, d\tau \\
&\quad + \sup_{t\in[0,T_{\max}]} e^{-tR^{\mathsf{q}}} \sum_{j=1}^{n^{\mathsf{q}}} \int_0^t |\mathscr{A}^{\mathsf{q}}(\mathbf{u}'', \mathbf{v}'')_j(\tau) - \mathscr{A}^{\mathsf{q}}(\mathbf{u}', \mathbf{v}')_j(\tau)|\, d\tau \\
&\leq \sum_{j=1}^{n^{\mathsf{p}}} \int_0^{T_{\max}} |\mathscr{A}^{\mathsf{p}}(\mathbf{u}'', \mathbf{v}'')_j(\tau) - \mathscr{A}^{\mathsf{p}}(\mathbf{u}', \mathbf{v}')_j(\tau)|\, d\tau \\
&\quad + \sum_{j=1}^{n^{\mathsf{q}}} \int_0^{T_{\max}} |\mathscr{A}^{\mathsf{q}}(\mathbf{u}'', \mathbf{v}'')_j(\tau) - \mathscr{A}^{\mathsf{q}}(\mathbf{u}', \mathbf{v}')_j(\tau)|\, d\tau
\end{aligned}$$

because $\sup_{t\in[0,T_{\max}]} e^{-tR} = 1$ and the integral is positive. Now we focus our attention on the operator $\mathscr{A}^{\mathsf{p}}$, then similar considerations will apply also to the operator $\mathscr{A}^{\mathsf{q}}$:

$$\begin{aligned}
|\mathscr{A}^{\mathsf{p}}(\mathbf{u}'', \mathbf{v}'')_j(\tau) - \mathscr{A}^{\mathsf{p}}(\mathbf{u}', \mathbf{v}')_j(\tau)| \leq& \\
&\leq \eta^{\mathsf{p}} e^{tR^{\mathsf{p}}} \sum_{h,k=1}^{n^{\mathsf{p}}} A_{hk}^{\mathsf{p},j} \left|u_h''(\tau)u_k''(\tau) - u_h'(\tau)u_k'(\tau)\right| \\
&\quad + \eta^{\mathsf{pq}} e^{tR^{\mathsf{q}}} \sum_{h=1}^{n^{\mathsf{p}}} \sum_{k=1}^{n^{\mathsf{q}}} B_{hk}^{\mathsf{pq},j} \left|u_h''(\tau)v_k''(\tau) - u_h'(\tau)v_k'(\tau)\right| \\
&\leq e^{tR^{\mathsf{p}}} \left(2\eta^{\mathsf{p}}\rho^{\mathsf{p}} + \eta^{\mathsf{pq}}\rho^{\mathsf{q}}\right) \|\mathbf{u}''(\tau) - \mathbf{u}'(\tau)\|_1 \\
&\quad + e^{tR^{\mathsf{q}}} \eta^{\mathsf{pq}}\rho^{\mathsf{p}} \|\mathbf{v}''(\tau) - \mathbf{v}'(\tau)\|_1 \\
&\leq e^{T_{\max}R} \left(C_1 \|\mathbf{u}'' - \mathbf{u}'\|_\infty + C_2 \|\mathbf{v}'' - \mathbf{v}'\|_\infty\right) \\
&\leq e^{T_{\max}R} C \|(\mathbf{u}'', \mathbf{v}'') - (\mathbf{u}', \mathbf{v}')\|_X
\end{aligned}$$

where $R = \max(R^{\mathsf{p}}, R^{\mathsf{q}})$ and $C = \max(C_1, C_2) > 0$. On the whole we thus have

$$\|\mathscr{T}(\mathbf{u}'', \mathbf{u}'') - \mathscr{T}(\mathbf{u}', \mathbf{v}')\|_X \leq C\, T_{\max}\, e^{T_{\max}R} \|(\mathbf{u}'', \mathbf{v}'') - (\mathbf{u}', \mathbf{v}')\|_X$$

The function $C\, T_{\max}\, e^{T_{\max}R}$ vanishes for $T_{\max} = 0$ and it is non negative and continuous, thus there exists $T_{\max} > 0$ such that $C\, T_{\max}\, e^{T_{\max}R} < 1$ and $\mathscr{T}$ is a contraction. Finally, given an interval $[0, T_{\max}]$, $T_{\max} > 0$, and using the Banach Fixed Point Theorem, there exists a unique fixed point of $\mathscr{T}$ in $\mathcal{B}$. This proves the existence and uniqueness of a local solution of (4.20) and it guarantees also that the solution is non negative.

Step 4 In order to show the global existence and uniqueness of the solution, we observe that $(\mathbf{f}^{\mathsf{p}}(T_{\max}), \mathbf{f}^{\mathsf{q}}(T_{\max})) \in \mathcal{B}$. Thus $(\mathbf{f}^{\mathsf{p}}(T_{\max}), \mathbf{f}^{\mathsf{q}}(T_{\max}))$ can be considered as an initial condition and the previous Step 3 can be repeated on the interval $[T_{\max}, 2T_{\max}]$. In this way we extend the solution $\forall\, T_{\max} > 0$.

Step 5 Since $(\mathbf{f}^{\mathsf{p}}, \mathbf{f}^{\mathsf{q}}) \in \mathcal{B}$ and the matrices $\mathbf{A}^{\mathsf{p},j}$ and $\mathbf{B}^{\mathsf{pq},j}$ do not depend on the time variable t we conclude that the right-hand side of the differential system is continuous in t. Thus, $\frac{\mathrm{d}}{\mathrm{d}t} f_j^{\mathsf{p}}$ and $\frac{\mathrm{d}}{\mathrm{d}t} f_j^{\mathsf{q}}$ are continuous in time $\forall\ j$. Therefore, $(\mathbf{f}^{\mathsf{p}}, \mathbf{f}^{\mathsf{q}}) \in C^1\left([0, T_{\max}]; \mathbb{R}^{n^{\mathsf{p}}}\right) \times C^1\left([0, T_{\max}]; \mathbb{R}^{n^{\mathsf{q}}}\right)$ and a classical solution of the problem exists. Iterating this consideration, $(\mathbf{f}^{\mathsf{p}}, \mathbf{f}^{\mathsf{q}})$ are infinitely differentiable in time. ■

Finally, we prove the well posedness of the Cauchy Problem (4.18) using the second approach, namely exploiting a classical result on global existence and uniqueness to solutions of first order ODE systems.

Theorem 4.10 (Well posedness - 2). – *For any given initial condition* $(\mathbf{f}^{\mathsf{p}}(0), \mathbf{f}^{\mathsf{q}}(0))$ *satisfying the assumptions* (4.19)*, there exists a unique global solution* $(\mathbf{f}^{\mathsf{p}}, \mathbf{f}^{\mathsf{q}}) \in \mathcal{B}$ *of the Cauchy problem* (4.18)*.*

Proof. The proof of the theorem is organized by steps and is achieved by applying the basic general theorem on global existence and uniqueness of solutions to first order ODE systems with sublinear growth.

Step 1 First of all we prove that the solution $(\mathbf{f}^{\mathsf{p}}(t), \mathbf{f}^{\mathsf{q}}(t))$ (if any) of the Cauchy problem (4.18) remains positive in time if the initial conditions satisfy (4.19). For this, consider the population p and assume that there exists an index $j = 1, \dots, n^{\mathsf{p}}$ such that $f_j^{\mathsf{p}}(0) = 0$. Then, since the elements of the transition matrices are non-negative, $\frac{\mathrm{d} f_j^{\mathsf{p}}(t)}{\mathrm{d}t} \geq 0$ (see equation (4.18)). Therefore the solution $(\mathbf{f}^{\mathsf{p}}(t), \mathbf{f}^{\mathsf{q}}(t))$ of the first order ODE system (4.18) cannot cross the hyperplane $f_j^{\mathsf{p}} = 0$ of the phase space during the time evolution and this guarantees that the solution is non-negative.

Step 2 Now we show that the hypotheses of the general theorem on global existence and uniqueness of solutions to first order ODE systems with sublinear growth are satisfied. In particular, observe that the right hand side of equation (4.18) is continuous and locally Lipschitz continuous, since it is at most a quadratic function in the unknowns $\mathbf{f} = (\mathbf{f}^{\mathsf{p}}, \mathbf{f}^{\mathsf{q}})$. Moreover, focusing on the population p, since $A_{hk}^{\mathsf{p},j} \in [0,1]$ and $B_{hk}^{\mathsf{pq},j} \in [0,1]$, the non-negativeness of the solution (Step 1) and the conservation of mass yield the following bounds:

$$0 \leq \sum_{h=1}^{n^{\mathsf{p}}} A_{hk}^{\mathsf{p},j} f_h^{\mathsf{p}} \leq \sum_{h=1}^{n^{\mathsf{p}}} f_h^{\mathsf{p}} = \rho^{\mathsf{p}}, \quad 0 \leq \sum_{h=1}^{n^{\mathsf{p}}} B_{hk}^{\mathsf{pq},j} f_h^{\mathsf{p}} \leq \sum_{h=1}^{n^{\mathsf{p}}} f_h^{\mathsf{p}} = \rho^{\mathsf{p}}$$

which render each differential equation sublinear. In fact, we obtain

$$\begin{aligned}\left\| \frac{\mathrm{d}\mathbf{f}^{\mathsf{p}}}{\mathrm{d}t} \right\|_1 &= \sum_{j=1}^{n^{\mathsf{p}}} \left| \eta^{\mathsf{p}} \sum_{k=1}^{n^{\mathsf{p}}} \left(\sum_{h=1}^{n^{\mathsf{p}}} A_{hk}^{\mathsf{p},j} f_h^{\mathsf{p}} \right) f_k^{\mathsf{p}} + \eta^{\mathsf{pq}} \sum_{k=1}^{n^{\mathsf{q}}} \left(\sum_{h=1}^{n^{\mathsf{p}}} B_{hk}^{\mathsf{pq},j} f_h^{\mathsf{p}} \right) f_k^{\mathsf{q}} - R^{\mathsf{p}} f_j^{\mathsf{p}} \right| \\ &\leq \sum_{j=1}^{n^{\mathsf{p}}} \left| \eta^{\mathsf{p}} \left(\rho^{\mathsf{p}}\right)^2 + \eta^{\mathsf{pq}} \rho^{\mathsf{p}} \rho^{\mathsf{q}} - R^{\mathsf{p}} f_j^{\mathsf{p}} \right| = \sum_{j=1}^{n^{\mathsf{p}}} R^{\mathsf{p}} \left| \rho^{p} - f_j^{\mathsf{p}} \right| \leq R^{\mathsf{p}} (n^{\mathsf{p}} - 1) \left\| \mathbf{f}^{\mathsf{p}} \right\|_1 .\end{aligned}$$

Notice that a similar inequality holds for the population q:

$$\left\| \frac{\mathrm{d}\mathbf{f}^{\mathsf{q}}}{\mathrm{d}t} \right\|_1 \leq R^{\mathsf{q}}(n^{\mathsf{q}} - 1) \left\| \mathbf{f}^{\mathsf{q}} \right\|_1 .$$

This implies the existence and uniqueness of a global and infinitely differentiable in time solution of the Cauchy problem associated to the ODE system (4.18) with initial conditions (4.19).

Step 3 Finally, we show that the solution $\mathbf{f} = (\mathbf{f}^{\mathsf{p}}, \mathbf{f}^{\mathsf{q}})$ is an element of the subset $\mathcal{B}$. We have already proved that $\mathbf{f}$ remains non-negative in time (Step 1). Again, let us focus the attention on the population p. By Step 2 the following inequality holds:

$$\frac{\mathrm{d}f_j^{\mathsf{p}}}{\mathrm{d}t} + R^{\mathsf{p}} f_j^{\mathsf{p}} \leq R^{\mathsf{p}} \rho^{\mathsf{p}}.$$

Multiplying it by $e^{tR^{\mathsf{p}}}$ and integrating in time we obtain

$$f_j^{\mathsf{p}} e^{tR^{\mathsf{p}}} \leq f_j^{\mathsf{p}}(0) + \int_0^t R^{\mathsf{p}} \rho^{\mathsf{p}} e^{sR^{\mathsf{p}}} ds.$$

Evaluating explicitly the integral and multiplying both sides by $e^{-tR^{\mathsf{p}}}$ we finally get

$$f_j^{\mathsf{p}} \leq f_j^{\mathsf{p}}(0) e^{-tR^{\mathsf{p}}} + \rho^{\mathsf{p}}(1 - e^{-tR^{\mathsf{p}}})$$

which proves that $f_j^{\mathsf{p}} : \mathbb{R}^+ \to [0, \rho^{\mathsf{p}}] \subseteq [0, 1]$. Moreover, using the integral formulation of equation (4.18) we prove that the sum of the f_j^{p}'s is constant for all $t \geq 0$ and equal to the density ρ^{p}. In fact

$$\sum_{j=1}^{n^{\mathsf{p}}} f_j^{\mathsf{p}} = e^{-tR^{\mathsf{p}}} \sum_{j=1}^{n^{\mathsf{p}}} f_j^{\mathsf{p}}(0) + \int_0^t e^{(\tau - t)R^{\mathsf{p}}} \rho^{\mathsf{p}} R^{\mathsf{p}} d\tau = e^{-R^{\mathsf{p}} t} \rho^{\mathsf{p}} \left[1 + R^{\mathsf{p}} \int_0^t e^{\tau R^{\mathsf{p}}} d\tau \right] = \rho^{\mathsf{p}}.$$

Similarly, we have that $f_j^{\mathsf{q}} : \mathbb{R}^+ \to [0, \rho^{\mathsf{q}}] \subseteq [0, 1]$ and $\sum_{j=1}^{n^{\mathsf{q}}} f_j^{\mathsf{q}} = \rho^{\mathsf{q}}$, for all $t \geq 0$. This proves that the solution $\mathbf{f} = (\mathbf{f}^{\mathsf{p}}, \mathbf{f}^{\mathsf{q}}) \in \mathcal{B}$. ■

Remark 4.11. We notice that the ODE system associated to the lattice two-population model introduced in [76] and in Section 2.4.1, see equation (2.13), has the same structure of the Cauchy problem associated to system of equations (4.17) and obtained as discretization of the continuous-velocity multi-population model (4.2). Thus, the above analysis on the well posedness of the discretized model (4.17) can be actually applied also to prove the well posedness of the lattice model (2.13).

Next we investigate the structure of the equilibria resulting from the ODE system (4.17). In particular, we prove prove that equilibria of each p-class are uniquely determined by the initial densities ρ^{p}, ρ^{q}, $\forall\, \mathsf{q} \in \neg\mathsf{p}$, and that they do not depend on the number of grid points n^{p}. Observe that a fixed value of $s \in [0, 1]$ can be obtained with different values of

the initial densities ρ^{p}, ρ^{q}, $\forall\ \mathsf{q} \in \neg\mathsf{p}$, thus the equilibria will not be uniquely determined once s is chosen.

Moreover, the theorem shows that for any $s \in [0,1]$ the number of nonzero asymptotic distribution functions is determined by $T^{\mathsf{p}} = \frac{V^{\mathsf{p}}_{\max}}{\Delta v}$. More precisely, each p-class of vehicles has exactly $T^{\mathsf{p}} + 1$ non-vanishing equilibria, which are related to the cells I^{p}_1, I^{p}_{r+1}, $I^{\mathsf{p}}_{2r+1}, \dots, I^{\mathsf{p}}_{n^{\mathsf{p}}}$.

Theorem 4.12 (Stable equilibria). – *For any fixed Δv, let $(\mathbf{f}^{\infty}_r)^{\mathsf{p}}$ denote the vector of the equilibrium solutions of the ODE system* (4.17) *related to the p-class and obtained on the grid with spacing δv given by $\Delta v = r\delta v$ with $r = \frac{n^{\mathsf{p}}-1}{T^{\mathsf{p}}} \in \mathbb{N}$, $\forall\ \mathsf{p}$. Then*

$$(\mathbf{f}^{\infty}_r)^{\mathsf{p}}_j = \begin{cases} (\mathbf{f}^{\infty}_1)^{\mathsf{p}}_{\lceil \frac{j}{r} \rceil} & \text{if} \mod (j-1, r) = 0 \\ 0 & \text{otherwise} \end{cases}$$

is the unique stable equilibrium for all classes of vehicles p and the values of $(\mathbf{f}^{i}_1 nfty)^{\mathsf{p}}$ depend uniquely on the initial densities.

Proof. To prove the statement, we compute explicitly the equilibrium solutions of the discretized model, using the explicit expression of the collision kernel given in (4.14), (4.15) and (4.16). For the sake of simplicity we again consider only two populations and we assume that $\mathcal{V}^1 \supset \mathcal{V}^2$.

The equilibrium equations resulting from $\frac{\mathrm{d}}{\mathrm{d}t} f^{\mathsf{p}}_j = 0$, $\forall\ j = 1, \dots, n^{\mathsf{p}}$, $\forall\ \mathsf{p} \in \{1,2\}$, are quadratic functions of f^{p}_j and we prove that for any j they depend only on the previous $j-1$ equilibrium values. In order to find the stable equilibrium, we recall that it is the larger root of the quadratic equation if its leading coefficient is negative, while it is the smaller root otherwise. This consideration will be applied several times during the proof.

For $j = 1$, the equation $\frac{\mathrm{d}}{\mathrm{d}t} f^{\mathsf{p}}_1 = 0$ is computed by means of the expressions (4.14a)-(4.16a) if $\mathsf{p} = 1$ and (4.14a)-(4.15a) if $\mathsf{p} = 2$. Using the fact that $\sum_k f^{\mathsf{p}}_k = \rho^{\mathsf{p}}$, $\forall\ \mathsf{p} \in \{1,2\}$, we obtain

$$\frac{\mathrm{d}}{\mathrm{d}t} f^{\mathsf{p}}_1 = 0 \ \Leftrightarrow\ -(1-P)\,(f^{\mathsf{p}}_1)^2 + \left[-(1-P)\,f^{\mathsf{q}}_1 + (1-2P)\rho^{\mathsf{p}} - P\rho^{\mathsf{q}}\right] f^{\mathsf{p}}_1 + (1-P) f^{\mathsf{q}}_1 \rho^{\mathsf{p}} = 0,\ \forall\ \mathsf{p} \tag{4.22}$$

which is a quadratic equation for f^{p}_1, $\forall\ \mathsf{p}$. In order to define the asymptotic expression of f^{p}_1, we consider the sum of the equation (4.22) for $\mathsf{p} = 1$ and $\mathsf{p} = 2$:

$$-(1-P)\left(f^1_1 + f^2_1\right)^2 + (1-2P)\left(\rho^1 + \rho^2\right)\left(f^1_1 + f^2_1\right) = 0 \tag{4.23}$$

which has two real roots, $f^1_1 + f^2_1 = 0$ and $f^1_1 + f^2_1 = \frac{1-2P}{1-P}\,(\rho^1 + \rho^2)$. It is easy to see that one solution is stable and the other one unstable, depending on the value of P. More precisely, we find that the stable one is

$$f^1_1 + f^2_1 = \begin{cases} 0 & P \geq \frac{1}{2} \\ \frac{1-2P}{1-P}\,(\rho^1 + \rho^2) & P < \frac{1}{2} \end{cases}. \tag{4.24}$$

Since solutions of (4.17) are non-negative (see Theorem 4.9 and 4.10) the equilibrium distributions of each population are

$$f_1^1 = f_1^2 = 0, \quad \text{if } P \geq \frac{1}{2}.$$

On the other hand, if $P < \frac{1}{2}$, since ρ^1 and ρ^2 are arbitrary, the equilibrium of the sum is equal to the sum of the steady states of each vehicle class, so that

$$f_1^1 = \frac{1-2P}{1-P}\rho^1, \quad f_1^2 = \frac{1-2P}{1-P}\rho^2$$

and by substituting these quantities into the equation (4.22) we find indeed that the equation is satisfied. Moreover, since they are positive provided $P < \frac{1}{2}$ and the roots of (4.22) have opposite sign if $P < \frac{1}{2}$, the stable equilibrium solutions are

$$(\mathbf{f}_r^\infty)_1^{\mathsf{p}} = \begin{cases} 0 & P \geq \frac{1}{2} \\ \frac{1-2P}{1-P}\rho^{\mathsf{p}} & P < \frac{1}{2} \end{cases}, \quad \forall\, \mathsf{p} \in \{1,2\}. \tag{4.25}$$

Thus, no vehicle is in the lowest speed class I_1^{p} if $P \geq \frac{1}{2}$.

For $2 \leq j \leq r$, the equilibrium equation of each population is

$$-(1-P)\left(f_j^{\mathsf{p}}\right)^2 + \left[-2(1-P)\sum_{k=1}^{j-1} f_k^{\mathsf{p}} - (1-P)\sum_{k=1}^{j-1} f_k^{\mathsf{q}} - (1-P)\, f_j^{\mathsf{q}} + (1-2P)\rho^{\mathsf{p}} - P\rho^{\mathsf{q}}\right] f_j^{\mathsf{p}}$$
$$+(1-P) f_j^{\mathsf{q}} \left(\rho^{\mathsf{p}} - \sum_{k=1}^{j-1} f_k^{\mathsf{p}}\right) = 0, \quad \forall\, \mathsf{p}$$

and summing this for $\mathsf{p} = 1$ and $\mathsf{p} = 2$ we obtain

$$-(1-P)\left(f_j^1 + f_j^2\right)^2 + \left[-2(1-P)\sum_{k=1}^{j-1}\left(f_k^1 + f_k^2\right) + (1-2P)\left(\rho^1 + \rho^2\right)\right]\left(f_j^1 + f_j^2\right) = 0.$$

Start from $j = 2$. Clearly, for $P \geq \frac{1}{2}$, substituting the related equilibrium given in equation (4.24), the stable root is again $f_2^1 + f_2^2 = 0$. For $P < \frac{1}{2}$, the equation for $f_2^1 + f_2^2$, with $f_1^1 + f_1^2$ given by (4.24), becomes

$$-(1-P)\left(f_2^1 + f_2^2\right)^2 - (1-2P)\left(\rho^1 + \rho^2\right)\left(f_2^1 + f_2^2\right) = 0.$$

Comparing with the equation (4.23), we see that now the stable root is $f_2^1 + f_2^2 = 0$. Thus, recalling that the solutions of (4.17) are positive in time, the equilibrium values of each class of vehicles are $(\mathbf{f}_r)_2^{\mathsf{p}} \equiv 0$, $\forall\, P \in [0,1]$. Analogously, it is easy to prove that $(\mathbf{f}_r^\infty)_j^{\mathsf{p}} \equiv 0$, $\forall\, j = 3, \ldots, r$.

Consider now $r+1 \leq j \leq 2r$, the equilibrium equations $\frac{\mathrm{d}}{\mathrm{d}t} f_j^{\mathsf{p}} = 0$ is computed by using the self- and cross-collision terms given in (4.14b)-(4.16b) if $\mathsf{p} = 1$ and in (4.14b)-(4.15b) if $\mathsf{p} = 2$. Therefore, the equations will contain two extra terms:

$$P\rho^{\mathsf{p}} f_{j-r}^{\mathsf{p}} + P\rho^{\mathsf{q}} f_{j-r}^{\mathsf{p}}$$

and they write as

$$\begin{aligned} -(1-P)\left(f_j^{\mathsf{p}}\right)^2 + \left[-2(1-P)\sum_{k=1}^{j-1} f_k^{\mathsf{p}} - (1-P)\sum_{k=1}^{j-1} f_k^{\mathsf{q}} - (1-P)f_j^{\mathsf{q}} + (1-2P)\rho^{\mathsf{p}} - P\rho^{\mathsf{q}}\right] f_j^{\mathsf{p}} \\ +(1-P)f_j^{\mathsf{q}}\left(\rho^{\mathsf{p}} - \sum_{k=1}^{j-1} f_k^{\mathsf{p}}\right) + P f_{j-r}^{\mathsf{p}}\left(\rho^{\mathsf{p}} + \rho^{\mathsf{q}}\right) = 0, \ \forall\ \mathsf{p}. \end{aligned} \tag{4.26}$$

If $j = r+1$ and $P \geq \frac{1}{2}$, then from the previous step $f_k^{\mathsf{p}} = 0$, $\forall\ k = 1, \ldots, r$ and $\forall\ \mathsf{p}$. Therefore, the new terms are certainly zero and the equation is identical to (4.22), so $(\mathbf{f}_r^{\infty})_{r+1}^{\mathsf{p}} \equiv 0\ \forall\ \mathsf{p}$. Instead, if $P < \frac{1}{2}$, then $f_k^{\mathsf{p}} = 0$, $\forall\ k = 2, \ldots, r$ and $\forall\ \mathsf{p}$, thus the equation (4.26) reduces to

$$\begin{aligned} -(1-P)\left(f_{r+1}^{\mathsf{p}}\right)^2 + \left[-2(1-P)f_1^{\mathsf{p}} - (1-P)f_1^{\mathsf{q}} - (1-P)\, f_{r+1}^{\mathsf{q}} + (1-2P)\rho^{\mathsf{p}} - P\rho^{\mathsf{q}}\right] f_{r+1}^{\mathsf{p}} \\ +(1-P)f_{r+1}^{\mathsf{q}}\left(\rho^{\mathsf{p}} - f_1^{\mathsf{p}}\right) + P f_1^{\mathsf{p}}\left(\rho^{\mathsf{p}} + \rho^{\mathsf{q}}\right) = 0, \ \forall\ \mathsf{p}. \end{aligned} \tag{4.27}$$

Summing this equation for $\mathsf{p} = 1$ and $\mathsf{p} = 2$ and substituting the expression for $f_1^1 + f_1^2$ we obtain

$$-(1-P)\left(f_{r+1}^1 + f_{r+1}^2\right)^2 - (1-2P)\left(\rho^1 + \rho^2\right)\left(f_{r+1}^1 + f_{r+1}^2\right) + P\frac{1-2P}{1-P}\left(\rho^1 + \rho^2\right)^2 = 0.$$

The resulting stable equilibrium solution is $f_{r+1}^1 + f_{r+1}^2 = (\rho^1 + \rho^2)\,\frac{-(1-2P)+\sqrt{\mathcal{D}_{r+1}}}{2(1-P)}$ where $\mathcal{D}_{r+1} = 1 - 4P^2$ is positive provided $P < \frac{1}{2}$. The equilibria of population p can be found recalling that they depend only on the quantity ρ^{p}, so that

$$f_{r+1}^1 = \rho^1 \frac{-(1-2P)+\sqrt{\mathcal{D}_{r+1}}}{2(1-P)}, \quad f_{r+1}^2 = \rho^2 \frac{-(1-2P)+\sqrt{\mathcal{D}_{r+1}}}{2(1-P)}$$

and it can be checked that these are the positive solutions of (4.27). Thus, if $j = r+1$ the stable equilibrium values are

$$(\mathbf{f}_r)_{r+1}^{\mathsf{p}} = \begin{cases} 0 & P \geq \frac{1}{2} \\ \rho^{\mathsf{p}} \frac{-(1-2P)+\sqrt{\mathcal{D}_{r+1}}}{2(1-P)} & P < \frac{1}{2} \end{cases}, \quad \forall\ \mathsf{p}.$$

If, instead, $r+1 < j \leq 2r$, then $f^{\mathsf{p}}_{j-r} \equiv 0$, $\forall\, P \in [0,1]$ and $\forall\, \mathsf{p}$, so the equilibrium equation resulting from $\frac{\mathrm{d}}{\mathrm{d}t}\left(f^1_j + f^2_j\right) = 0$ is identical to (4.23) if $P \geq \frac{1}{2}$, while it is

$$-(1-P)\left(f^1_j + f^2_j\right)^2 - \sqrt{\mathcal{D}_{r+1}}\left(\rho^1 + \rho^2\right)\left(f^2_j + f^1_j\right) = 0$$

if $P < \frac{1}{2}$. Then, we obtain $(\mathbf{f}^\infty_r)^{\mathsf{p}}_j \equiv 0$, for $j = r+2, \ldots, 2r$ and $\forall\, P \in [0,1]$.

Clearly, this procedure can be repeated, in fact, the cases $j = 1, \ldots, 2r$ that we just computed are typical. Also for larger values of j we find a quadratic equation for the unknown f^{p}_j, which involves only previously equilibrium values, hence we can easily find successively all components of $(\mathbf{f}^\infty_r)^{\mathsf{p}}$, $\forall\, \mathsf{p}$.

For $j = lr+1$, $l = 2, \ldots, T^2-1$, the equation for f^{p}_j is again computed by using (4.14b)-(4.16b) if $\mathsf{p} = 1$ and (4.14b)-(4.15b) if $\mathsf{p} = 2$. Let $F_j = f^1_j + f^2_j$, then summing the evolution equation of both populations we obtain

$$-(1-P)\,F^2_{lr+1} + \left[-2(1-P)\sum_{k=0}^{l-1} F_{kr+1} + (1-2P)\left(\rho^1+\rho^2\right)\right] F_{lr+1} + P F_{(l-1)r+1}\left(\rho^{\mathsf{p}} + \rho^{\mathsf{q}}\right) = 0.$$

If $P \geq \frac{1}{2}$, then the above equation becomes identical to (4.22) and the stable root is $F_{lr+1} = 0$. If instead $P < \frac{1}{2}$, then the stable solution is

$$F_{lr+1} = \frac{-2(1-P)\sum_{k=0}^{l-1} F_{kr+1} + (1-2P)\left(\rho^1+\rho^2\right) + \sqrt{\mathcal{D}_{lr+1}}}{2(1-P)}$$

where

$$\mathcal{D}_{lr+1} = \left[-2(1-P)\sum_{k=0}^{l-1} F_{kr+1} + (1-2P)\left(\rho^1+\rho^2\right)\right]^2 + 4(1-P)P F_{(l-1)r+1}\left(\rho^1+\rho^2\right),$$

which is positive $\forall\, P \in [0,1]$ because it is a sum of two positive terms. The equilibrium solutions of population p can be again deduced by assuming that they are functions only of the quantities depending on p, so that

$$(\mathbf{f}^\infty_r)^{\mathsf{p}}_{lr+1} = \begin{cases} 0 & P \geq \frac{1}{2} \\ \dfrac{-2(1-P)\displaystyle\sum_{k=0}^{l-1} f^{\mathsf{p}}_{kr+1} + (1-2P)\rho^{\mathsf{p}} + \sqrt{\mathcal{D}^{\mathsf{p}}_{lr+1}}}{2(1-P)} & P < \frac{1}{2} \end{cases}, \quad l = 0, \ldots, T^2-1, \forall\, \mathsf{p}$$

where

$$\mathcal{D}^{\mathsf{p}}_{lr+1} = \left[-2(1-P)\sum_{k=0}^{l-1} f^{\mathsf{p}}_{kr+1} + (1-2P)\rho^{\mathsf{p}}\right]^2 + 4(1-P)P f^{\mathsf{p}}_{(l-1)r+1}\rho^{\mathsf{p}}.$$

Finally, if $lr+2 \leq j \leq (l+1)r$, $l = 2, \ldots, T^2-1$, then the equilibria are $(\mathbf{f}^\infty_r)^{\mathsf{p}}_j \equiv 0$, $\forall\, P \in [0,1]$ and $\forall\, \mathsf{p}$.

Note that for $j = n^2$, i.e. for the maximum speed of population $\mathsf{p} = 2$, the equilibrium value related to the population $\mathsf{p} = 2$ can be found by using mass conservation, so that

$$(\mathbf{f}_r^\infty)_{n^2}^2 = \rho^2 - \sum_{k=1}^{n^2-1} f_k^2. \tag{4.28}$$

Instead, for the population $\mathsf{p} = 1$, the equilibrium equation is obtained by means of (4.14b)-(4.16c). If $P < \frac{1}{2}$, then $f_j^{\mathsf{p}} \neq 0$, if $j = kr + 1$, $k = 0, \dots, T^2 - 1$ and $\forall\ \mathsf{p}$. Thus, we find

$$\begin{aligned} &-(1-P)\left(f_{n^2}^1\right)^2 + \left[-2(1-P)\sum_{k=0}^{T^2-1} f_{kr+1}^1 + (1-2P)\rho^1 - \rho^2\right] f_{n^2}^1 \\ &+(1-P) f_{n^2}^2 \left(\rho^1 - \sum_{k=0}^{T^2-1} f_{kr+1}^1\right) + P f_{n^2-r}^1 \left(\rho^1 + \rho^2\right) \end{aligned}$$

whose stable root is

$$(\mathbf{f}_r^\infty)_{n^2}^1 = \frac{-2(1-P)\sum_{k=0}^{T^2-1} f_{kr+1}^1 + (1-2P)\rho^1 - \rho^2 + \sqrt{\mathcal{D}_{n^2}}}{2(1-P)} \tag{4.29}$$

where the discriminant

$$\begin{aligned} \mathcal{D}_{n^2} = &\left[-2(1-P)\sum_{k=0}^{T^2-1} f_{kr+1}^1 + (1-2P)\rho^1 - \rho^2\right]^2 \\ &+ 4(1-P)\left[(1-P) f_{n^2}^2 \left(\rho^1 - \sum_{k=0}^{T^2-1} f_{kr+1}^1\right) + P f_{n^2-r}^1 \left(\rho^1 + \rho^2\right)\right] \end{aligned} \tag{4.30}$$

is positive provided $\forall\, P \in [0,1]$. If instead $P \geq \frac{1}{2}$, then the equilibrium value is again of the form (4.29) with the discriminant (4.30), but it is obtained by taking $f_j^{\mathsf{p}} = 0$, $\forall\ j < n^2$, $\forall\ \mathsf{p}$ and thus $f_{n^2}^2 = \rho^2$, see equation (4.28).

Let $j = n^2 + 1$, now $v_j \in \mathcal{V}^1$ but $v_j \notin \mathcal{V}^2$. The equilibrium equation for $\mathsf{p} = 1$ is computed by using (4.14b)-(4.16e). We obtain

$$-(1-P)\left(f_{n^2+1}^1\right)^2 + \left[-2(1-P)\sum_{l=0}^{T^2} f_{lr+1}^1 + (1-2P)\rho^1 - \rho^2\right] f_{n^2+1}^1 = 0 \tag{4.31}$$

and $f_{n^2+1}^1 = 0$ results the stable solution $\forall\ P \in [0,1]$. This consideration holds for each f_j^1, $n^2 + 1 < j \leq n^2 + r - 1$ because the equation resulting from $\frac{\mathrm{d}}{\mathrm{d}t} f_j^1 = 0$ is identical to (4.31). Thus, $(\mathbf{f}_r^\infty)_j^1 \equiv 0$, $n^2 + 1 \leq j \leq n^2 + r - 1$.

Now, let $j = n^2 + r$. If $V_{\max}^1 - V_{\max}^2 = m^{1,2}\Delta v$ with $m^{1,2} = 1$ then $n^2 + r = n^1$ and we can use mass conservation to find $(\mathbf{f}_r^\infty)_{n^2+r}^1$. Instead, if $m^{1,2} > 1$, we use the equations (4.14b)-(4.16e) in order to compute $\frac{\mathrm{d}}{\mathrm{d}t} f_{n^2+r}^1 = 0$. Since $f_j^1 \equiv 0$, if $j \neq kr + 1$, $k = 0, \dots, T^2$, we

find

$$-(1-P)\left(f^1_{n^2+r}\right)^2+\left[-2(1-P)\sum_{k=0}^{T^2}f^1_{kr+1}+(1-2P)\rho^1-\rho^2\right]f^1_{n^2+r}+Pf^1_{n^2}\left(\rho^1+\rho^2\right)=0. \tag{4.32}$$

If $P<\frac{1}{2}$ the stable solution of the above equation is

$$(\mathbf{f}_r^\infty)^1_{n^2+r}=\frac{-2(1-P)\sum_{k=0}^{T^2}f^1_{kr+1}+(1-2P)\rho^1-\rho^2+\sqrt{\mathcal{D}_{n^2+r}}}{2(1-P)} \tag{4.33}$$

where the discriminant

$$\mathcal{D}_{n^2+r}=\left[-2(1-P)\sum_{k=0}^{T^2}f^1_{kr+1}+(1-2P)\rho^1-\rho^2\right]^2+4(1-P)Pf^1_{n^2}\left(\rho^1+\rho^2\right) \tag{4.34}$$

is positive $\forall\, P\in[0,1]$. If instead $P\geq\frac{1}{2}$ then the stable root of (4.32) is again of the form (4.33) with the discriminant (4.34), but it is obtained by taking $f^1_j=0$, $\forall\, j\neq n^2$.

Equations (4.31) and (4.32) actually hold for each $n^2+1\leq j\leq n^1-1$. In particular, (4.31) is the equilibrium equation for the f^1_j's such that $j\neq n^2+kr$, $k=1,\dots,m^{1,2}-1$. Thus we find $(\mathbf{f}_r^\infty)^2_j=0$, $\forall\, P\in[0,1]$.

Conversely, (4.32) is the equilibrium equation for the f^1_j's such that $j=n^2+kr$, $k=1,\dots,m^{1,2}-1$. Therefore, the equilibrium value $(\mathbf{f}_r^\infty)^2_j=0$ is again of the form (4.33)-(4.34).

Finally, the last equilibrium value for the population $\mathsf{p}=1$ can be found by mass conservation, so that

$$(\mathbf{f}_r^\infty)^1_{n^1}=\rho^1-\sum_{k=1}^{n^1-1}f^1_k. \qquad \blacksquare$$

Theorem 4.12 ensures that the equilibrium values of the discretized model (4.17) can be found on the coarser grid, namely taking $r=1$. The result can be better appreciated by looking at the evolution towards equilibrium shown in Figure 4.4. In this figure, we consider two populations such that $V^1_{\max}=100$ km/h and $V^2_{\max}=V^1_{\max}-2\Delta v=50$ km/h. Then, $T^1=4$ and $T^2=2$. The different plots show the evolution towards equilibrium, starting from uniform initial distributions for $r=1$ (cyan) and $r=3$ (magenta), which correspond to $n^{\mathsf{p}}=5,13$ velocity grid points for the population $\mathsf{p}=1$ (top panels) and $n^{\mathsf{p}}=3,7$ velocity grid points for the population $\mathsf{p}=2$ (bottom panels). The left plots are obtained with the fraction of occupied space $s=0.2$, while the right plots with $s=0.6$. Note that different dynamics towards equilibrium are observed, for different values of the number n^{p}, $\mathsf{p}=1,2$, of grid points, but as equilibrium is approached, the values of the equilibria go to zero, except for the cells I^{p}_j, $\mathsf{p}=1,2$, corresponding to integer multiples of Δv. In fact, for $r=3$, the nonzero equilibrium values, marked with black squares, are

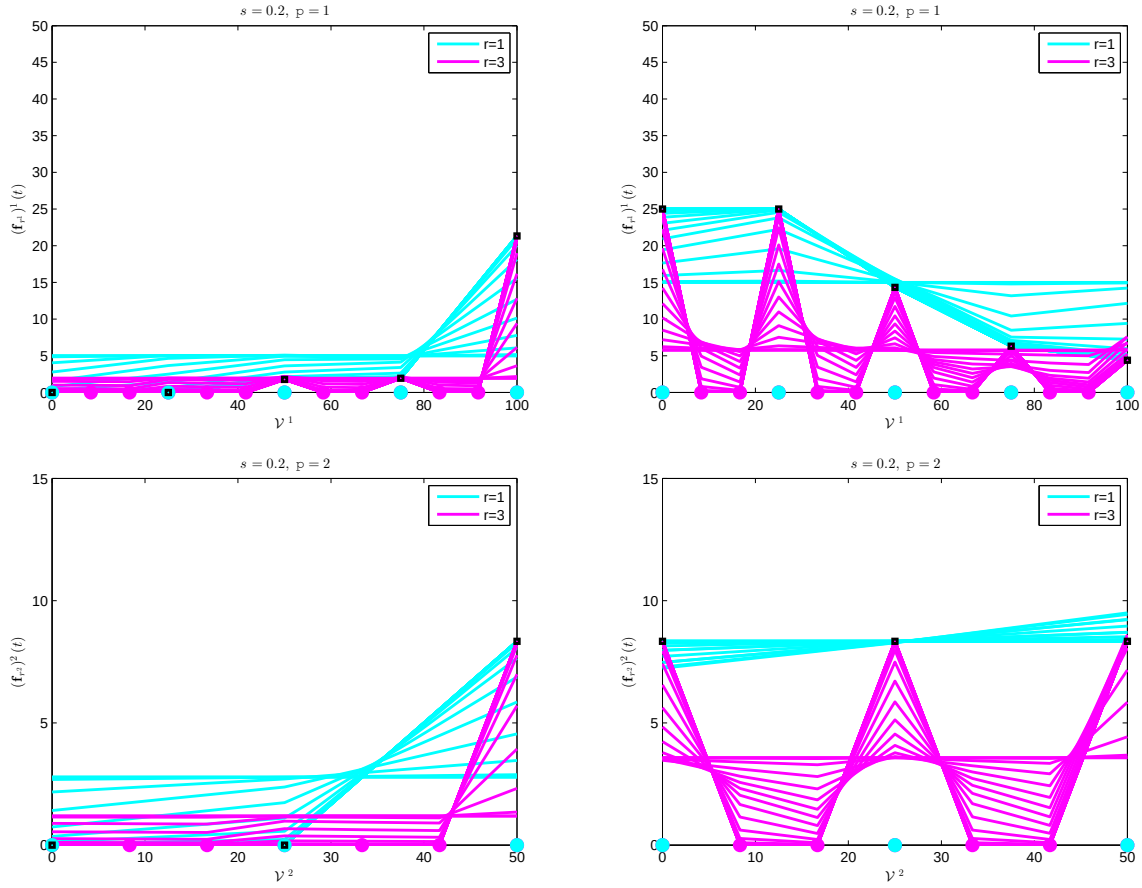

Figure 4.4: Evolution towards equilibrium of the ODE system (4.17) for the case of two populations, $\mathsf{p} = 1$ (top panels) and $\mathsf{p} = 2$ (bottom panels), with a fixed value of the velocity jump $\Delta v = 25$ km/h. The maximum velocities are $V^1_{\max} = 100$ km/h and $V^2_{\max} = 50$ km/h. The velocity grid is obtained with $r = 1$ (cyan) and $r = 3$ (magenta), which correspond to $n^1 = 5, 13$ and $n^2 = 3, 7$ grid points. Black squares indicate the equilibrium values.

related to the velocities of the grid with $r = 1$ and marked with cyan filled circles. While the additional velocities of the refined grid, marked with magenta filled circles, correspond to zero values of the equilibria.

We end the section with several remarks on the structure of the equilibrium solutions.

Remark 4.13 (Δv depending on p). In Section 4.3.1 we have assumed that the speed jump Δv is independent of p so that it is a fixed parameter for all classes of vehicles. Taking the velocity jump dependent on p would mean to consider another microscopic difference characterizing the types of vehicles. More precisely, we can use it in order to model the subjective behavior of drivers, since we can think of Δv as a parameter describing different types of drivers, more or less aggressive depending on the value of the jump in velocity.

Even with Δv dependent on p, equilibrium solutions preserve the property of being quantized that is non-zero on a reduced number of discrete velocities. Let us consider the same

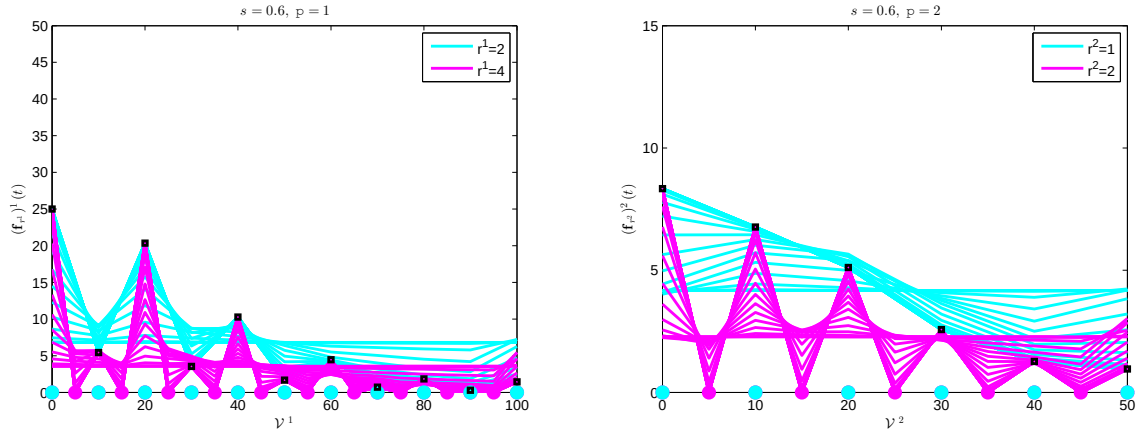

Figure 4.5: Evolution towards equilibrium of the ODE system (4.17) for the case of two populations, $\mathsf{p} = 1$ (left panels) and $\mathsf{p} = 2$ (right panels), with two different values of the velocity jump $\Delta v^1 = 20$ km/h and $\Delta v^2 = 10$ km/h. The maximum velocities are $V^1_{\max} = 100$ km/h and $V^2_{\max} = 50$ km/h. The velocity grid is obtained with $r^1 = 2$, $r^2 = 1$ (cyan) and $r^1 = 4$, $r^2 = 2$ (magenta). Black squares indicate the equilibrium values.

example shown in the right panels of Figure 4.4 with two populations, $\mathsf{p} = 1, 2$, having maximum velocities $V^1_{\max} = 100$ km/h and $V^2_{\max} = 50$ km/h. Now we take two different velocity jumps, $\Delta v^1 = 20$ km/h and $\Delta v^2 = 10$ km/h in order to model the case in which population $\mathsf{p} = 1$ is more aggressive than population $\mathsf{p} = 2$. We choose the discretization parameters r^1 and r^2 in such a way that the velocity grids of the two populations have the same spacing $\delta v = V^1_{\max}/r^1 = V^2_{\max}/r^2$. This means that we have to take $r^1 = 2r^2$. In Figure 4.5 we show the evolution towards equilibrium for both populations $\mathsf{p} = 1$ (left plot) and population $\mathsf{p} = 2$ (right plot). We start from uniform initial distributions and we consider two cases: first we choose $r^2 = 1$ (and therefore $r^1 = 2$) (cyan), then we choose $r^2 = 2$ (and therefore $r^1 = 4$) (magenta). These values correspond to $n^1 = 13, 25$ and $n^2 = 6, 11$ velocity grid points. Again we observe that equilibria are quantized. Precisely only the values related to the cells I^{p}_j, $\mathsf{p} = 1, 2$, corresponding to integer multiples of Δv^2, i.e. the minimum of the two jumps, give a non-zero contribution irrespective of grid refinements. In fact, the equilibrium values of population $\mathsf{p} = 1$ are quantized according to the velocity jump of population $\mathsf{p} = 2$.
Notice that in this case Δv^1 is an integer multiple of Δv^2 but the same phenomenon verifies in a more general situation.

Remark 4.14 (Unstable equilibria). Theorem 4.12 gives the uniqueness of the stable equilibria of the model. However, as already observed in Remark 3.12, unstable ones may occur if the initial condition is such that $f^{\mathsf{p}}_1(0) = 0$, $\forall\ \mathsf{p}$. In fact, the interaction rules in the case $v_* > v^*$ do not allow for a post-interaction velocity $v \in \mathcal{V}^{\mathsf{p}}$ which is lower than v^*. Thus if $f^{\mathsf{p}}_1(0) = 0$, i.e. there are no vehicles of the p-class with velocity v_1 at the initial time, interactions will not lead to an increase of f^{p}_1. In this sense, the equilibrium solution of the multi-population model does not only depend on the initial densities, but

also on the initial condition $f^{\mathsf{p}}(0,v)$ because "spurious" equilibria on sub-manifolds of the state space may appear. However, as showed in [75], these solutions are unstable: a small perturbation of $f_1^{\mathsf{p}}(0)$ is enough to trigger the evolution towards the stable equilibrium, which depends only on the initial densities.

Remark 4.15. In Theorem 4.12 the equilibria related to the sum of the distribution functions are identical to those computed in [75] and in Section 3.3.1 for the single-population δ model, see Theorem 3.9. This shows that the indifferentiability principle holds at equilibrium. However, Theorem 4.4, proved in Section 4.3, is more general because it states that the indifferentiability principle for the continuous multi-population model holds at all times.

Remark 4.16. In Section 2.4.3 we have computed the equilibrium solutions of the two-population lattice model (2.16) for the case $P \geq 1/2$. The aim was to investigate the impact of the choice of P on the transition from free to congested regime. In Theorem 4.12, instead, we have computed the equilibrium solutions of the multi-population model for each value of P. Again, the phase transition is mathematically explained by the bifurcation of the equilibria occurring when the critical value $P = 1/2$ is reached, see equation (4.25). In fact, as observed in Section 2.4.3, $P = 1/2$ marks the value in which also the equilibria related to the lower velocities, namely those speeds being lower than the $\min_{\mathsf{p}}\{V_{\max}^{\mathsf{p}}\}$, become filled up.
Finally, we notice that the equilibrium distribution (4.25) of vehicles with velocity in the lowest class I_1^{p} is the same computed in Section 2.4.3.

4.4 Fundamental diagrams of traffic

In this Section we present the fundamental diagrams obtained with the multi-population kinetic model described in this chapter. In particular, we wish to show that the scattering of data is again reproduced as a result of the heterogeneous composition of the flow. Since the model (4.17) is expressed for a generic number of populations, we focus on the case of a mixture composed of three types of vehicles. Such diagrams provide the relation between flux and density at the macroscopic level.

Macroscopic variables for the p-class of vehicles are recovered computing moments of the distribution functions f^{p}, see equations (4.1). However, fundamental diagrams are obtained by assuming that traffic is in equilibrium. Therefore, we compute the quantities (4.1) using the asymptotic distributions $(\mathbf{f}_r^{\infty})^{\mathsf{p}}$. Since for each population p the $(\mathbf{f}_r^{\infty})^{\mathsf{p}}$'s depend uniquely on the densities of all vehicle classes, at equilibrium we have that the flux is a function of the initial densities and it is computed as

$$\begin{aligned} q^{\mathsf{p}}(r) &= \int_{\mathcal{V}^{\mathsf{p}}} v\,(f^{\infty})^{\mathsf{p}}(v)\mathrm{d}v = \int_{\mathcal{V}^{\mathsf{p}}} v \sum_{j=1}^{n^{\mathsf{p}}} (\mathbf{f}_r^{\infty})_j^{\mathsf{p}}\, \frac{\chi_{I_j^{\mathsf{p}}}(v)}{\left|I_j^{\mathsf{p}}\right|}\mathrm{d}v \\ &= \left(\mathbf{f}_r^{1} infty\right)_1^{\mathsf{p}} v_1^{\mathsf{p}} + \sum_{j=2}^{n^{\mathsf{p}}-1} (\mathbf{f}_r^{\infty})_j^{\mathsf{p}}\, v_j^{\mathsf{p}} + (\mathbf{f}_r^{\infty})_{n^{\mathsf{p}}}^{\mathsf{p}}\, v_{n^{\mathsf{p}}}^{\mathsf{p}} \end{aligned} \tag{4.35}$$

where the velocities v_j^{p} are the mid points of the cells I_j^{p} resulting with the grid size $\delta v = \frac{\Delta v}{r}$ and the $(\mathbf{f}_r^{\infty})_j^{\mathsf{p}}$'s are the equilibrium solutions. We recall that the v_j^{p}'s for $j = 2, \dots, n^{\mathsf{p}}$ do not change when the grid is refined, i.e. when r increases, while the first and last velocity grid point approach zero and the maximum velocity of the p-class, respectively, when $r \to \infty$. Recall that Theorem 4.12 states that the equilibrium values of the discretized model do not depend on the discretization, i.e. on the grid size δv and on the discrete speeds v_j^{p}'s, but only on the velocity jump Δv. Therefore, the flux can be computed exactly using the values $(\mathbf{f}_1^{\infty})_j^{\mathsf{p}}$, $j = 1, \dots, T^{\mathsf{p}} + 1 = n^{\mathsf{p}}$. In other words, for the case of two populations we can exploit the explicit formulas for the equilibrium solutions given in Theorem 4.12. Instead, for more than two populations we numerically integrate the system (4.17) on the coarser velocity grid ($r = 1$) to recover the equilibrium values and using the results of Theorem 4.12 we obtain the exact flux as

$$q^{\mathsf{p}}(\infty) = \sum_{j=1}^{T^{\mathsf{p}}+1} (\mathbf{f}_1)_j^{\mathsf{p}} \, (j-1)\Delta v. \tag{4.36}$$

Notice that this result is due to the quantized structure of the equilibria, which is in turn a consequence of the quantized acceleration, i.e. the instantaneous jump of velocity from the actual one v_* to $\min\{v_* + \Delta v, V_{\max}^{\mathsf{p}}\}$, see equation (4.6). Finally, once the flux is given, the macroscopic speed of the p-class can be obtained as

$$u^{\mathsf{p}}(\infty) = \frac{q^{\mathsf{p}}(\infty)}{\rho^{\mathsf{p}}}. \tag{4.37}$$

Since in the space homogeneous case each density ρ^{p} is constant in time, the fraction of occupied space s remains also constant. Hence we study the total flux $Q = \sum_{\mathsf{p}} q^{\mathsf{p}}$ and the mean speed $U = \frac{\sum_{\mathsf{p}} q^{\mathsf{p}}}{\sum_{\mathsf{p}} \rho^{\mathsf{p}}}$ at equilibrium as functions of the total number of vehicles per unit length $N_{\mathsf{v}} = \sum_{\mathsf{p}} \rho^{\mathsf{p}}$ and of the fraction of occupied space s.

In the case of the single-population model [75] (see Section 3.5, the flux and the speed at equilibrium are single-valued functions of the initial density. However, this property does not reflect the structure of the fundamental diagrams provided by experimental data, because such diagrams are multivalued with a wide dispersion of the flux values in the congested phase of traffic, i.e. at high densities, see Section 2.2. Here, as done in Chapter 2 for the multi-population lattice model, the scattered behavior of the real data will be recovered because traffic is treated as a mixture of more than one population characterized by different physical features. In fact, note that the equilibria related to the p-population, and showed in Theorem 4.12, do not only depend on the initial density ρ^{p} but also on the values of the occupied space s. Thus, since the same value of s can be obtained with different compositions of the traffic mixture, for a given $s \in [0, 1]$ we may find different equilibria, hence different flux and speed values at equilibrium, depending on how the road is occupied.

In the following, we investigate the properties of the diagrams provided by the multi-population kinetic model. We show that they exhibits different regimes, or phases, of traffic

Table 4.1: Physical parameters of the four classes of vehicles chosen for the simulations.

	Fast Cars ($\mathsf{p} = C_\mathsf{f}$)	Slow Cars ($\mathsf{p} = C_\mathsf{s}$)	Vans ($\mathsf{p} = V$)	Trucks ($\mathsf{p} = T$)
Typical length l^p	4 m	4 m	6 m	12 m
Max. density $\rho^\mathsf{p}_{\max}$	250 veh./km	250 veh./km	166.6 veh./km	83.3 veh./km
Max. velocity $V^\mathsf{p}_{\max}$	120 km/h	80 km/h	120 km/h	80 km/h
Velocity jump Δv	40 km/h	40 km/h	40 km/h	40 km/h

and they reproduce the qualitative structure of experimental diagrams widely analyzed in [10, 26, 46, 76].

We introduce four typical classes of vehicles whose characterizing parameters are listed in Table 4.1 and all simulations are performed by choosing three of them. More precisely we consider *Fast Cars-Slow Cars-Trucks* (C_f-C_s-T) or *Fast Cars-Vans-Trucks* (C_f-V-T). The diagrams are computed by sampling three random values of the initial densities for any initial fraction of occupied space $s \in [0, 1]$. Moreover, recalling the computations already made in [75] to evaluate a physical velocity jump Δv, here we can consider $\Delta v = 40$ km/h. With this choice, the numbers of discrete velocities are $n^{C_\mathsf{f}} = n^V = 4$ and $n^{C_\mathsf{s}} = n^T = 3$.

Free phase of traffic This traffic regime occurs at low densities, when there is a large distance between vehicles and the interactions are rare. Thus, we expect that the velocity of vehicles is ruled by the maximum allowed speed, which in this framework depends on the mechanical characteristics of the vehicles (e.g. when we assume $V^{C_\mathsf{f}}_{\max} > V^T_{\max}$) or on the type of drivers (e.g., when we assume that there are two types of cars such that $V^{C_\mathsf{f}}_{\max} > V^{C_\mathsf{s}}_{\max}$). Therefore, in the free phase of traffic the flux increases nearly linearly with respect to the total density, the data are not widely scattered and are contained in a cone whose upper and lower branch have a slope proportional to $\max_\mathsf{p}\{V^\mathsf{p}_{\max}\}$ and $\min_\mathsf{p}\{V^\mathsf{p}_{\max}\}$ respectively, $\forall\ \mathsf{p} \in \{C_\mathsf{f}, C_\mathsf{s}, V, T\}$. For instance, in Figure 4.6 we show the free phase of the diagrams provided by the multi-population model with three classes of vehicles. This regime is obtained by taking only the values of the fraction of road occupancy for which $P \geq \frac{1}{2}$. In fact, as proved in Theorem 4.12 and as shown in the left panels of Figure 4.4, this choice produces equilibria of the form

$$\mathbf{f}^{C_\mathsf{f}} = \underbrace{[0, 0, *, *]}_{n^{C_\mathsf{f}}=4}, \quad \mathbf{f}^{C_\mathsf{s}} = \underbrace{[0, 0, \rho^{C_\mathsf{s}}]}_{n^{C_\mathsf{s}}=3}, \quad \mathbf{f}^V = \underbrace{[0, 0, *, *]}_{n^V=4}, \quad \mathbf{f}^T = \underbrace{[0, 0, \rho^T]}_{n^T=3}.$$

Thus, all classes of vehicles travel at high velocities and in particular the flux of slow cars and trucks is always proportional to the their maximum velocity $V^{C_\mathsf{s}}_{\max}$ and $V^T_{\max}$ respectively. Instead, the flux values of fast cars and vans depend also on the maximum velocity of slow cars and trucks. In the left panel of Figure 4.6 we consider the test case C_f-C_s-T and we observe that the flux values obtained are scattered in the whole cone, in contrast with the case C_f-V-T shown in the right panels in which

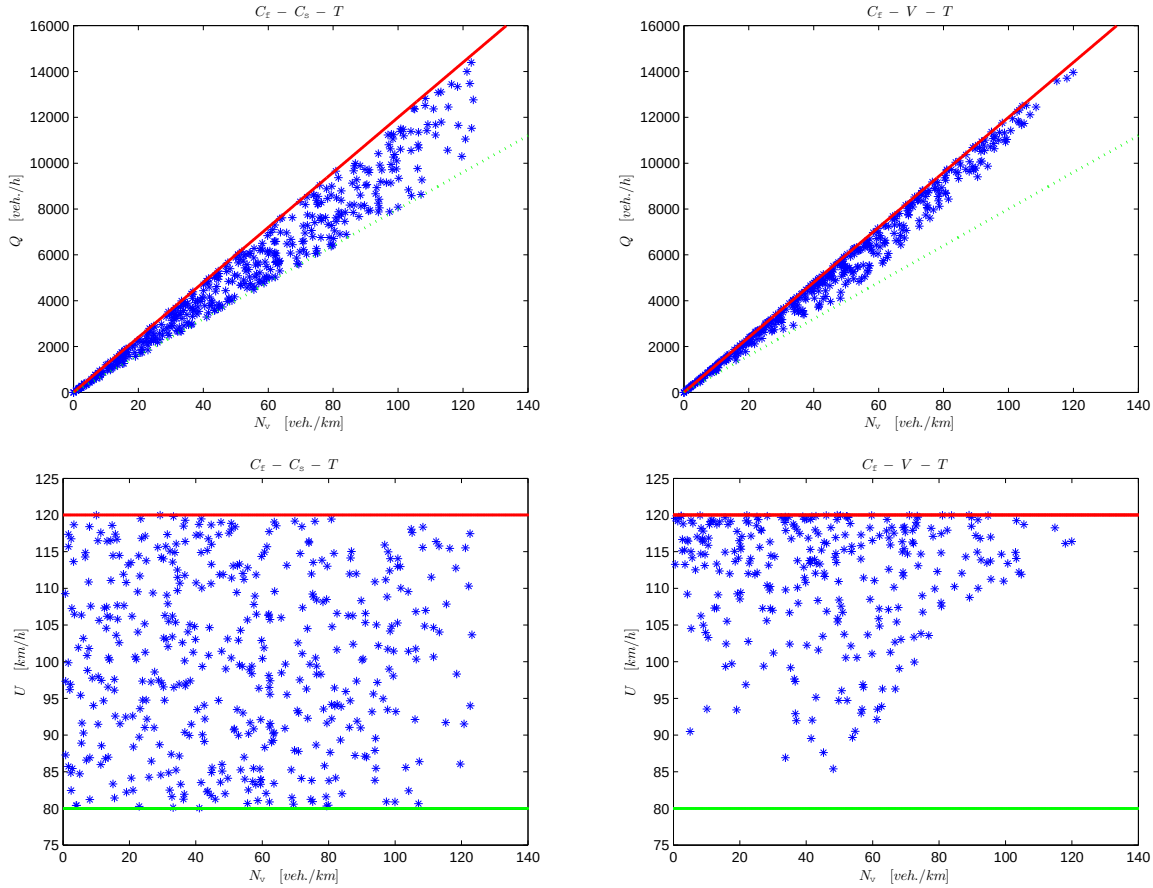

FIGURE 4.6: Top: free phase of the flux-density diagrams. Bottom: free phase of the speed-density diagrams. On the left we consider the three populations C_f-C_s-T, on the right C_f-V-T. The data are obtained for values of the fraction of road occupancy such that $P \geq \frac{1}{2}$. In the top panels the solid red line and the dotted green line have slope respectively as the maximum velocity and the minimum velocity of the three populations. The probability P is taken as in (2.9) with $\alpha = \gamma = 1$.

both fast cars and vans travel at speed 120 km/h and therefore the flux values are mainly distributed on the upper branch. This consideration can be reinforced by looking at the macroscopic speed diagrams, bottom panels of Figure 4.6.

Phase transition It represents the transition between the free and the congested phase of traffic. The flux is maximum when the critical value of the fraction of occupied space s, at which $P = 1/2$ and the phase transition occurs, is reached. If s increases then we observe a decrease of the flux and of the mean speed in the diagrams of traffic. From a mathematical point of view, the phase transition occurs when there is the bifurcation of the equilibrium values, that is when P becomes smaller than $\frac{1}{2}$. In fact, when $P \geq \frac{1}{2}$ all vehicles are moving and only when $P < \frac{1}{2}$ the lower speed classes begin to fill up, see equation (4.25) in Theorem 4.12. Since P is a function of

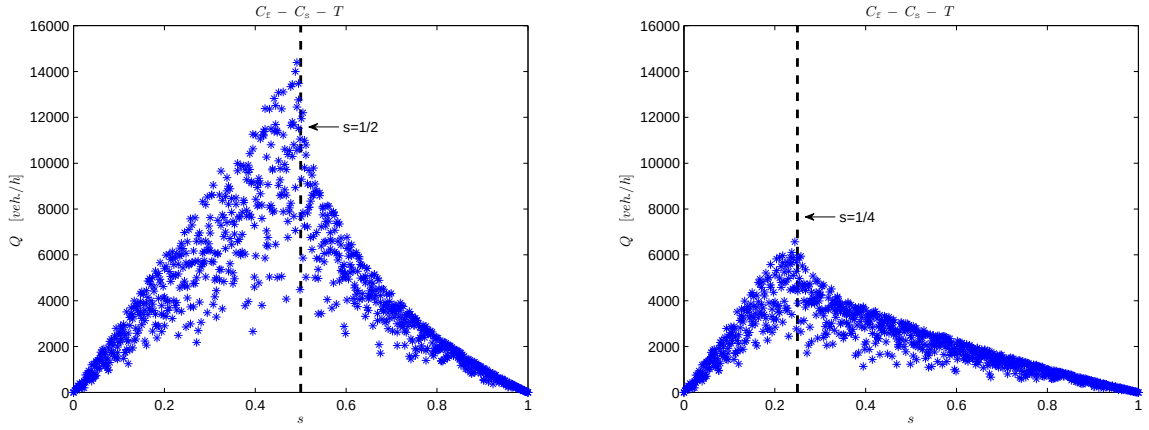

Figure 4.7: Diagrams of the flux vs. the fraction of occupied space for the test case C_f-C_s-T. The probability P is taken as in (2.9) with $\alpha = 1$ and $\gamma = 1$ (left), $\gamma = \frac{1}{2}$ (right).

s, the choice of the probability P influences the critical value. In order to investigate this phenomenon, in Figure 4.7 we consider the total diagram of the flux with respect to the fraction of occupied space s. In both panels we consider the law given in (2.9) with $\alpha = 1$, but we choose two different values of $\gamma \in (0, 1]$: more precisely, $\gamma = 1$ and $\gamma = \frac{1}{2}$ in the left and right plot, respectively. Note that the critical value of the fraction of occupied space decreases from $s = \frac{1}{2}$ to $s = \frac{1}{4}$. In fact, with (2.9)

$$P < \frac{1}{2} \quad \Longleftrightarrow \quad s > \left(\frac{1}{2}\right)^{\frac{1}{\gamma}}$$

and this means that high values of γ increase the value of s at which the transition between the two regimes of traffic occurs. Thus, $\gamma > 1$ is not a good choice because it does not reflect the structure of the phase transition usually observed in the experimental diagrams.

Congested phase of traffic This traffic regime occurs at high densities, that is when the fraction of occupied space s exceeds the critical value. The congested phase is characterized by frequent interactions among vehicles which are forced to slow down, i.e. they cannot travel at the same high speeds as in free road conditions, because traffic becomes more and more jammed. As a consequence, the flux decreases as the fraction of occupied space increases and the experimental diagrams exhibit a large scattering of the flux values. In the congested phase, therefore, the flux can hardly be approximated by a single-valued function of the density. The scattered behavior is automatically reproduced by our multi-population kinetic model, see the left panels of Figure 4.8 in which we plot the total flux- and speed-density diagrams for the test case C_f-V-T with the probability law (2.9). Recalling that the diagrams of traffic are obtained by means of the equilibrium distributions, the multi-population model naturally accounts for the dispersion of the flux values in the congested phase

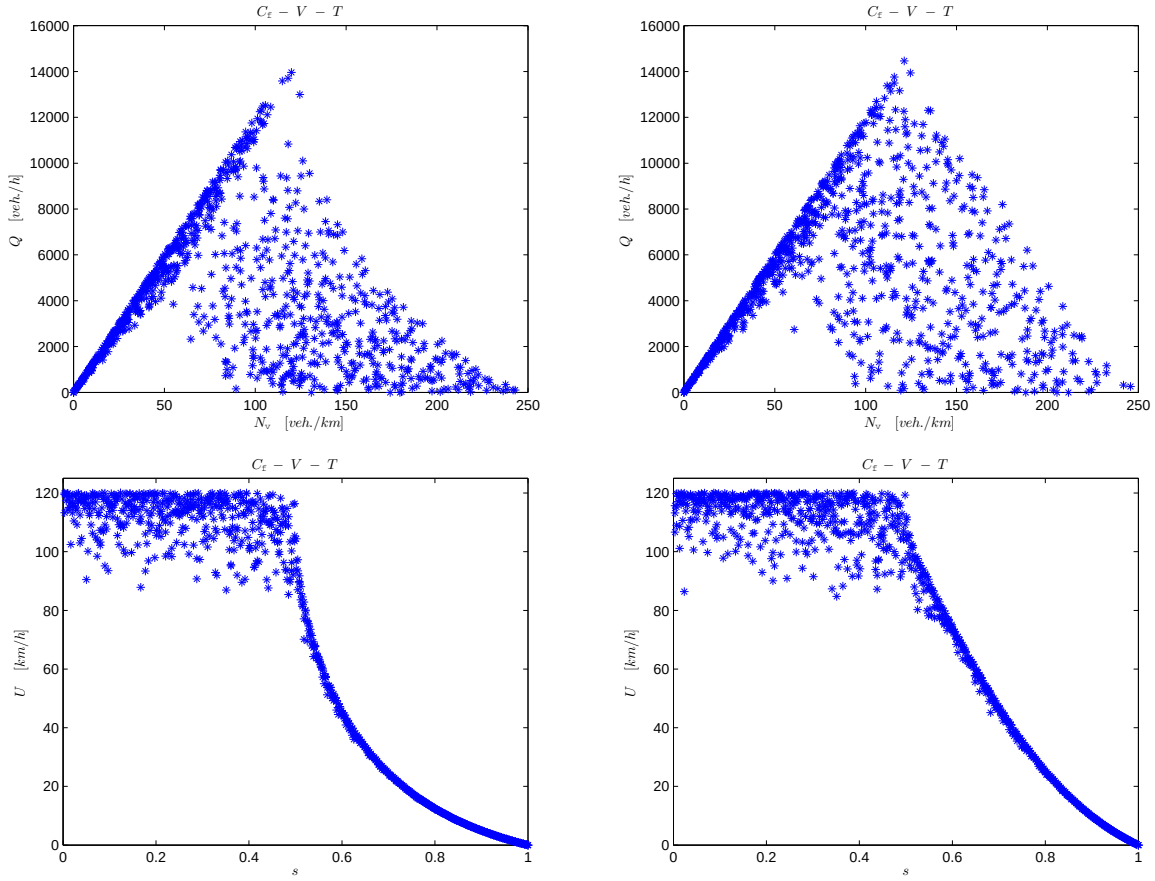

Figure 4.8: Top: flux-density diagrams. Bottom: diagrams of the speed vs. the fraction of occupied space. We have considered the three populations C_f-V-T. In the left panels the probability of changing velocity P is taken as in (2.9) with $\alpha = \gamma = 1$, while in the right panels the probability P is as in (4.38) with $s_c = \frac{1}{2}$ and $\mu = -\frac{1}{8}$.

because the equilibrium solutions do not only depend on the fraction of occupied space s but also on the single densities of the vehicles. Therefore, the explanation for the multivalued behavior is based on the consideration that the flow along a road is strongly influenced by the composition of the traffic mixture. In particular, this aspect is evident at high densities because the different mechanical characteristics (the typical length) of the vehicles on the road become a key factor to adjust the speed in congested conditions. Conversely, if we focus on the diagrams of the speed vs. the fraction of occupied space at the bottom of Figure 4.8, we deduce that in free flow conditions the macroscopic speed is influenced by the fact that fast vehicles slow down as a consequence of their interactions with slower vehicles. In contrast, at high values of s, all types of vehicles are forced to slow down, reaching the same macroscopic speed. These remarks reflect the daily experience of driving on highways, in particular the fact that in congested flow all vehicles tend to travel at the same speed, which steadily decreases as the traffic congestion increases.

Capacity drop The flux-density diagram in the top-left panel of Figure 4.8 is very similar to the experimental ones, whose main characteristics are well reproduced. However, as observed also in the single-population model [75], see Section 3.5, the diagrams seem to be strictly dependent on T^{p}, which defines uniquely the number of discrete velocities once $V^{\mathsf{p}}_{\max}$ and Δv are given. In fact, the capacity drop, that is the jump between the maximum flux values in free and congested phases, see e.g. [88], becomes sharper and sharper when T^{p} increases. For instance, with the choice of the physical parameters listed in Table 4.1, the number of velocities of fast cars is $n^{C_{\mathsf{f}}} = 4$ and this provides a sharp decrease of the flux of the C_{f}-class beyond the critical fraction of occupied space. Clearly, this phenomenon influences also the capacity drop of the total diagram obtained with the multi-population model. We try to overcome this drawback acting on the law which defines the dependence of P on s. To this end, we introduce a new law relating P to s in order to better fit experimental data. As a matter of fact, the sharp transition is due to over-crowding of the low-speed equilibrium distributions, also for values of s just greater than the critical value. Thus, if $P_\gamma(s)$ is the γ-*law* given in equation (2.9), the purpose is now to introduce a new and less simplistic function $P(s)$ such that $P_\gamma(s) < P(s) < \frac{1}{2}$, $\forall\, s > s_c$, where s_c is the critical value of s obtained with the γ-law, i.e. $s_c = \left(\frac{1}{2}\right)^{\frac{1}{\gamma}}$. Thus, when s just exceeds s_c, the new probability $P(s)$ provides an under-crowding of the first equilibrium distributions (4.25). As a consequence, the maximum flux value of the congested phase increases and the capacity drop abates. Recalling that P is the probability of achieving the maximum speed prescribed by the interaction rules, the desired function $P(s) \in [0, 1]$ should satisfy the following properties:

1. $P(0) = 1$: when the road is empty, the probability of accelerating is maximum;
2. $P(1) = 0$: in contrast to the previous request, the probability is zero in jammed traffic situations;
3. $P(s_c) = \frac{1}{2}$: we impose that the transition from free to congested phase corresponds to the bifurcation of the equilibrium solutions and it occurs at $s = s_c$. The value of the critical space can be chosen by means of experimental data;
4. $\frac{\mathrm{d}}{\mathrm{d}s} P_\gamma|_{s=s_c^+} < \frac{\mathrm{d}}{\mathrm{d}s} P|_{s=s_c^+} := \mu < 0$: since any reasonable P should be a decreasing function of s, this is a sufficient condition to verify $P_\gamma(s) < P(s) < \frac{1}{2}$, $\forall\, s > s_c$. Thus, since γ is uniquely determined once the value of the critical space is fixed, we require that $\mu > \frac{\mathrm{d}}{\mathrm{d}s} P_\gamma|_{s=s_c^+} = -\gamma s_c^{\gamma-1} = -\gamma \left(\frac{1}{2}\right)^{1-\frac{1}{\gamma}}$.

In order to satisfy the four properties above and since the equilibrium solutions do not depend on the analytical expression of $P(s)$ (for $s \in [0, s_c]$) we consider P as a piecewise function of s, so that

$$P(s) = P_1(s)\chi_{[0,s_c]}(s) + P_2(s)\chi_{(s_c,1]}(s) \tag{4.38}$$

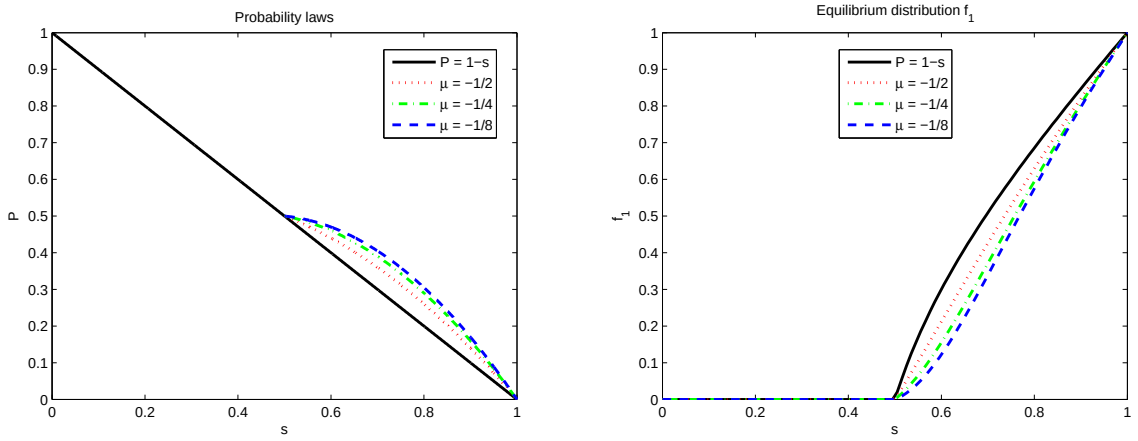

FIGURE 4.9: Left: the probability law (2.9) (black solid line) with $s_c = \frac{1}{2}$, $\alpha = \gamma = 1$, and the probability law (4.38), which differs from the γ-law only for $s > s_c = \frac{1}{2}$, obtained with three different values of the slope μ for $s = s_c$. Right: the asymptotic distribution f_1 (lower speed) obtained with the probability laws considered in the left panel.

where $P_1(s)$ is a linear polynomial satisfying the first and the third property, while $P_2(s)$ is a quadratic polynomial satisfying the second, the third and the fourth property. Therefore

$$P_1(s) = 1 - \frac{s}{2s_c}, \quad P_2(s) = as^2 + bs + c$$

the coefficients of P_2 being

$$a = \frac{2\mu(s_c - 1) - 1}{2(s_c - 1)^2}, \quad b = -\frac{\mu(s_c^2 - 1) - s_c}{(s_c - 1)^2}, \quad c = \frac{2s_c\left[\mu(s_c - 1) - 1\right] + 1}{2(s_c - 1)^2}.$$

For simplicity, in the left panel of Figure 4.9 we consider the probability laws with $s_c = \frac{1}{2}$. Thus, $\gamma = 1$ and the γ-law (2.9) writes as $P = 1 - s$, while the piecewise probability law (4.38) is plotted for different values of the slope μ computed in $s = s_c = \frac{1}{2}$ such that $\mu > -1 = \frac{\mathrm{d}}{\mathrm{d}s} P_\gamma|_{s=s_c=\frac{1}{2}}$. Notice that the probability values resulting from the piecewise law increase for $\forall\ s > s_c$ when μ is increased and this provides a little decrease of the first equilibrium distribution. This can be seen it in the right panel of Figure 4.9, in which we plot the asymptotic distribution f_1 as a function of s for the case of a single-population. Thus, the piecewise law allows one to reduce the sharp capacity drop. For instance, this can be appreciated by comparing the diagrams in the left panels of Figure 4.8 obtained with the γ-law and the diagrams in the right panels of Figure 4.8 obtained with the piecewise probability law.

Chapter 5

Multivalued fundamental diagrams of traffic flow in the kinetic Fokker-Planck limit

5.1 Motivation

In the previous chapters we have introduced a kinetic model for traffic flow which provides a good agreement between the theoretical and the experimental diagrams. In particular, the extension to a multi-population framework allowed us to explain the scattering of data as a result of the intrinsic heterogeneity characterizing the flow of traffic.

In [85] and in this chapter, we wish to study in detail the impact of the microscopic rules (and thus of the modeling choices) describing the behavior of drivers on the macroscopic traffic dynamics. Therefore, throughout the chapter we follow an approach being intrinsically multiscale because we continually compare the microscopic and the macroscopic scale.

To this end, we recall that our aim requires the ability to compute the asymptotic kinetic distribution from which to recover the macroscopic traffic variables at equilibrium. Although in the previous chapters the analytical expression of the stationary solution is found using a suitable choice of the microscopic interactions (which leads to a quantized asymptotic state), in general the interaction integrals appearing in kinetic Boltzmann-type models for traffic flow typically do not provide explicitly the equilibrium distribution and they are very demanding from a computational point of view, see e.g. [48].

For this reason, in [85] and in this chapter, starting from a Boltzmann-type model we derive a Fokker-Planck approximation by means of a suitable time scaling (the *grazing collision limit*, see e.g. [21, 22, 65, 67, 84]). In this way, the interaction integrals of the collision operator are replaced by differential operators, allowing us to retain the principal part of the microscopic interactions while making the Boltzmann-type model more amenable to analytical investigations. In particular we follow the technique introduced in [41] for traffic flow, or in [81] in the context of opinion formation models and in [65] for gas-dynamics.

However, although the present chapter can be considered as a natural sequel of [41], in contrast here we simplify the grazing collision limit, which now does not depend on free parameters.

Thi microscopic behavioral rules are affected by the microscopic average conditions of traffic, thereby establishing a feedback between the small and the large scales of the phenomenon. In fact, in contrast to the binary rules introduced in the previous chapters, here we take into account mean field interactions assuming thus that drivers decide to adjust their velocity using as reference the mean speed. In particular, we analyze three possible modeling of the microscopic rules showing that they influence the qualitative structure of fundamental diagrams. Moreover, in all the cases we can recover multivalued diagrams as a result of the existence of a one-parameter family of stationary solutions. We prove that this degree of freedom synthesizes the different properties of the flow which can induce different macroscopic dynamics. We also improve the multivalued diagrams obtained in [44], in which the authors introduce a Fokker-Planck-type multilane model and recover scattered data as a consequence of the introduction of a probability of lane changing. As a matter of fact, the diagrams show only a small range of density in which the flux of vehicles is multivalued. In addition to that, they reproduce a capacity drop which is too sharp.

The chapter is organized as follows. In Section 5.2 we introduce the microscopic interaction rules and we discuss the similarities with other models. In particular, we show that the rules can be obtained by averaging the post-interaction speeds prescribed in [75] with the addition of a stochastic perturbation due to the inability of the drivers to adjust precisely their speed. In contrast to [41], another stochastic term is introduced, which models the influence of the road congestion on the drivers' behavior. In Section 5.3 we derive the Fokker-Planck model as the grazing collision limit of the Boltzmann-type equation. In Section 5.4 we recover the time-asymptotic kinetic distributions in general form. Then, we specify the interaction rules by choosing the desired speeds of the drivers in braking and acceleration scenarios and we study the fundamental diagrams resulting from two cases. We show that a particular choice of the desired speeds allows one to reproduce the closures law for macroscopic models, as for instance the Greenshields' closure [32]. Conversely the diagrams obtained from the second set of desired speeds reproduce very well the qualitative structure of experimental data, in particular their scattering in the congested flow regime.

5.2 Boltzmann model

Recalling that the core of a kinetic model for traffic flow is the modeling of the microscopic interactions among the vehicles, we first discuss the choice of a set of interaction rules and then we recover a Boltzmann-type equation. As usual, the model is characterized by a collision term which describes the relaxation of the kinetic distribution towards equilibrium.

Here, we assume that drivers react to the mean speed of the surrounding vehicles. Thus, they adjust their velocity by comparing their actual speed with the macroscopic

velocity u. We recall that, in kinetic theory, the macroscopic variables are recovered as moments of the kinetic distribution function $f = f(t, v) : \mathbb{R}^+ \times \mathcal{V} \to \mathbb{R}^+$. Here we assume that $\mathcal{V} = [0, V_{\max}]$ is the space of the microscopic velocities, $V_{\max} > 0$ being the maximum speed, which usually depends on the mechanical characteristics of the vehicles, on imposed speed limits or on the type of drivers. Then

$$\rho(t) = \int_0^{V_{\max}} f(t, v)\mathrm{d}v, \quad q(t) = \int_0^{V_{\max}} v f(t, v)\mathrm{d}v, \quad u(t) = \frac{1}{\rho(t)} \int_0^{V_{\max}} v f(t, v)\mathrm{d}v,$$

where as usual ρ is the vehicle density, u is the mean speed and $q = \rho u$ is the flux.

Remark 5.1. As done in the previous chapters, throughout the chapter we consider the "spatially homogeneous case", i.e. we assume that vehicles are uniformly distributed along the road so that the kinetic distribution function f depends only on their microscopic speed $v \in \mathcal{V}$ but not on their position x. This assumption allows for a direct focus on the interaction dynamics among the vehicles, neglecting possible space inhomogeneities.

5.2.1 Microscopic model

Let v_* be the pre-interaction velocity of a vehicle and let u be the mean speed of the flow. We distinguish two cases:

Acceleration Vehicles tend to increase their speed when they are slower than the speed of the flow, namely if $v_* < u$;

Braking Vehicles tend to decrease their speed when they are faster than the speed of the flow, namely if $v_* > u$.

Remark 5.2. Notice that we do not model the scenario in which $v_* = u$, when it is realistic to assume that vehicles do not change their speed. We will see that this case does not give contribution in the Fokker-Planck approximation, see Section 5.3.

We point out that the interaction rules in traffic flow are different from the gas dynamics case. In particular, the post-interaction speeds resulting from the two scenarios described above are not necessarily symmetric. Therefore, from a microscopic point of view, we can prescribe the following form of the output velocity v resulting from acceleration and braking:

$$v = v_* + \epsilon\, P(\rho)\, \Delta v_A(v_*, \rho) + \sqrt{\epsilon\, Q_A(\rho)}\, \Delta v_A(v_*, \rho)\, \xi, \quad \text{if} \quad v_* < u \tag{5.1a}$$

$$v = v_* - \epsilon\, (1 - P(\rho))\, \Delta v_B(v_*, u, \rho) + \sqrt{\epsilon\, Q_B(\rho)}\, \Delta v_B(v_*, u, \rho)\, \xi, \quad \text{if} \quad v_* > u \tag{5.1b}$$

where

- $\Delta v_A(v_*, \rho)$ is the jump of velocity in the acceleration interaction. We assume that

$$\Delta v_A(v_*, \rho) := V_A(v_*, \rho) - v_*.$$

The quantity $V_A(v_*, \rho) \in (v_*, V_{\max}]$ is the desired speed of a vehicle that increases its velocity v_*. In a realistic framework, $V_A(v_*, \rho)$ cannot be taken as a fixed parameter. Therefore, in contrast to [41], we take $V_A(v_*, \rho)$ dependent on the actual speed v_*, in order to preserve the bounds of the acceleration, see [53]. Potentially, one can consider the case in which the desired speed $V_A(v_*, \rho)$ depends also on the density of vehicles ρ, see Section 5.4.1;

- Δv_B, instead, is the jump of velocity in the braking interaction. As discussed for $\Delta v_A(v_*, \rho)$, we consider

$$\Delta v_B(v_*, u, \rho) := v_* - V_B(u, \rho).$$

The quantity $V_B(u, \rho) \in [0, v_*)$ is the desired speed of a vehicle which is decreasing its velocity v_*. Notice that, in contrast to the desired speed in acceleration, $V_B(u, \rho)$ is not a function of v_* but it depends on the macroscopic flux, in particular on the local density ρ and on the mean speed u. In fact, in the braking scenario, the desired speed is mainly influenced by the conditions of the traffic flow. For instance, let us consider the case in which a driver bumps into a jam. Initially the driver travels with a velocity larger than the the speed of the flow in front of him, i.e. $v_* \gg u$. Then, the driver must brake and adjust his speed to the traffic condition ahead independently of the value of his actual velocity v_*. Therefore we expect that the jump of velocity $\Delta v_B(v_*, u, \rho)$ is greater when the difference between the actual speed and the mean speed is larger, as for instance in [41];

- ξ is a random variable with given distribution $\eta(\xi)$, having zero mean and variance σ^2. The presence of ξ allows one to include a noise term proportional to the velocity jump. From the modeling point of view, the noise term is introduced in order to consider the fact that drivers are not able to estimate and to reach precisely the desired speed after acceleration and braking, as prescribed in (5.1);

- $\epsilon \in (0, 1)$ is a deterministic and dimensionless parameter which models the time scaling. We notice that for $\epsilon \to 0$ we have $v \to v_*$ for both $v_* < u$ and $v_* > u$. This means that ϵ controls also the strength of the microscopic interactions;

- $P(\rho)$ is the probability of accelerating taken as a decreasing function of the local density ρ, as discussed in Section 2.3.2. It allows one to define the post-interaction speeds as functions of the density. Thus, the post-interaction speed v defined by the rules (5.1) is not deterministically fixed. Although several laws of the probability function $P(\rho)$ can be taken into account in order to better fix experimental data, see e.g. [74] or Section 4.4, we will consider the simplest choice

$$P(\rho) = 1 - \frac{\rho}{\rho_{\max}}, \tag{5.2}$$

which corresponds to (2.9) with $\alpha = \gamma = 1$ and where $\rho_{\max}$ is the maximum density taken as the maximum number of vehicles per unit length in bumper-to-bumper conditions;

- $Q_A(\rho)$ and $Q_B(\rho)$ are functions of the density ρ which modulate the variation of the velocity due to the noise term. In particular, we assume that the uncertainty in accelerating and braking vanishes in free road and jammed conditions, namely when vehicles tend to travel at the maximum speed or to stop, respectively. From now on, we will always take
$$Q_A(\rho) = P, \quad Q_B(\rho) = 1 - P. \tag{5.3}$$
These simple choices allow one to simplify the microscopic model (5.1) and at the same time they reproduce realistic macroscopic behaviors of traffic flow, see Section 5.4.

Let us illustrate the model considering a few typical cases. Let $\rho \approx \rho_{\max}$, namely let us suppose that the road is almost congested. Then $P(\rho) \approx 0$ and the second term in (5.1a) vanishes. Since $Q_A(\rho) \approx 0$ when $\rho \approx \rho_{\max}$, it results $v \to v_*$ if $v_* < u$. Thus vehicles tend to keep their velocities even if they are slower than the speed of traffic as the road becomes congested. In contrast, if $v_* > u$, the post-interaction speed v is less than the pre-interaction speed v_*, see (5.1b), thus fast vehicles reduce the velocity in order to reach the desired speed $V_B(u, \rho)$. On the contrary, if $\rho \approx 0$ then $P(\rho) \approx 1$, i.e. the probability of accelerating becomes larger as the road becomes free. Therefore, using the rules (5.1), the post-interaction speed v is greater than v_* if $v_* < u$, namely slow vehicles increase their velocity in order to reach the desired speed $V_A(v_*, \rho)$. Conversely, $v \to v_*$ in the opposite case $v_* > u$, i.e. fast vehicles tend to keep their high speed.

Using definitions (5.3), the microscopic interaction rules (5.1) can be written as

$$v = v_* + \sqrt{\epsilon\, P(\rho)}\, \Delta v_A(v_*, \rho) \left(\sqrt{\epsilon\, P(\rho)} + \xi \right), \quad \text{if} \quad v_* < u \tag{5.4a}$$

$$v = v_* - \sqrt{\epsilon\, (1 - P(\rho))}\, \Delta v_B(v_*, u, \rho) \left(\sqrt{\epsilon\, (1 - P(\rho))} + \xi \right), \quad \text{if} \quad v_* > u \tag{5.4b}$$

It is clear that the above expressions are defined by including two levels of stochasticity. The first one is modeled by the terms at the right-hand side of equations (5.4) that do not involve the random variable ξ. These terms concern the non-deterministic outcome of the vehicle interactions and which give rise to an average post-interaction speed depending on the probability of accelerating. The second level of stochasticity is instead modeled by the terms in (5.4) that involve the random variable ξ. These terms perturb the average post-interaction speed as a result of the unpredictability of the individual behavior of the drivers.

Remark 5.3 (Bounded speeds). We expect that the post-interaction speed v is such that $v \in [v_*, V_A]$ when accelerating (i.e. $v_* < u$) and $v \in [V_B, v_*]$ when braking (i.e.

$v_* > u$). We can show that this is indeed guaranteed by making suitable assumptions on the random variable ξ. For the equation (5.4a) we can write

$$v = v_*(1 - \epsilon P - \sqrt{\epsilon P}\xi) + V_A(\epsilon P + \sqrt{\epsilon P}\xi).$$

Thus v is a convex combination of the pre-interaction velocity v_* and of the desired speed V_A if and only if

$$-\frac{\epsilon P}{\sqrt{\epsilon P}} \leq \xi \leq \frac{1 - \epsilon P}{\sqrt{\epsilon P}}.$$

Instead, in the case (5.4b) we can write

$$v \leq v_*(1 - \epsilon(1-P) + \sqrt{\epsilon(1-P)}\xi) + V_B(\epsilon(1-P) - \sqrt{\epsilon(1-P)}\xi).$$

Thus v results again in a convex combination of the pre-interaction velocity v_* and of the desired speed V_B if and only if

$$\frac{\epsilon(1-P) - 1}{\sqrt{\epsilon(1-P)}} \leq \xi \leq \frac{\epsilon(1-P)}{\sqrt{\epsilon(1-P)}}.$$

Finally, the two bounds are simultaneously preserved if

$$\max\left\{-\frac{\epsilon P}{\sqrt{\epsilon P}}, \frac{\epsilon(1-P) - 1}{\sqrt{\epsilon(1-P)}}\right\} \leq \xi \leq \min\left\{\frac{1 - \epsilon P}{\sqrt{\epsilon P}}, \frac{\epsilon(1-P)}{\sqrt{\epsilon(1-P)}}\right\}.$$

Since in the sequel we will be interested in the behavior of the model for small values of ϵ, then in the limit we can allow $|\xi| \in [0, +\infty)$. However, observe that the post-interaction speeds are again bounded because $v \to v_*$ for $\epsilon \to 0$.
The above bounds do not preserve in principle that ξ has zero mean. Nevertheless, bounds satisfying this request can be easily obtained. For instance, in the simple case $\epsilon = 1$, straightforward computations lead to the following bounds:

$$|\xi| \leq \frac{1-P}{\sqrt{P}}, \quad \text{if } P \geq 1/2 \quad \text{or} \quad |\xi| \leq \frac{P}{\sqrt{1-P}}, \quad \text{if } P < 1/2$$

which ensure that ξ has zero mean.

5.2.2 Comparison with other models

The interaction rules prescribed in (5.4) can be obtained as a generalization of the stochastic interaction rules given in [75] or in Section 3.2.1, see the case of the quantized acceleration. There the post-interaction speed is given by

$$v = \begin{cases} V_A \text{ with probability } P,\ v_* \text{ with probability } 1-P, & \text{if } \ v_* < v^* \quad (5.5a) \\ v_* \text{ with probability } P,\ V_B \text{ with probability } 1-P, & \text{if } \ v_* > v^* \quad (5.5b) \end{cases}$$

where v^* is the microscopic velocity of the leading vehicle. In fact, in the previous chapters, we have considered binary interactions in which a vehicle first compares its velocity v_* with the velocity v^* of the vehicle ahead, and then decides in probability how to change its speed. Since in the present framework we are interested in mean field interactions, v^* is replaced by the macroscopic speed u and, apart from the additional noise term ξ and the scaling factor ϵ, the rules (5.4) can be indeed recovered as mean speed of the rules (5.5a)-(5.5b).

Notice that (5.5a)-(5.5b) correspond to the so-called δ model in [75] and in Chapter 3, which describes the situation of instantaneous change of velocity produced by jumps in velocity, from v_* to V_A (acceleration) or to V_B (braking). Clearly, more refined models are present in the literature, see e.g. [48]. Also in [75] and in Chapter 3 a less simplistic model is considered, in which the output speed is uniformly distributed over a bounded range of velocities, the so-called χ model in Section 3.2.1. However, looking at the fundamental diagrams of traffic, it is proved that the essential information at equilibrium is already caught by the δ model.

This fact can be also mathematically investigated by computing the evolution equation for the macroscopic speed. In fact, assuming mean field interactions (in the sense specified above), the model introduced in [75] and in Chapter 3 specializes as

$$\partial_t f(t,v) = \rho \int_0^{V_{\max}} A(v_* \to v|u;\rho) f(t,v_*) \mathrm{d}v_* - \rho f(t,v). \tag{5.6}$$

In fact, noticing that $A(v_* \to v|u;\rho)$ does not depend on v^*, the above equation can be obtained starting from (3.2) (with $\eta = 1$) by explicating $\int_{\mathcal{V}} f(t,v^*)\mathrm{d}v^* = \rho$. The transition probability $A(v_* \to v|u;\rho)$ models the stochastic microscopic interaction rules. It writes as

$$A(v_* \to v|u;\rho) = \begin{cases} P\,\mathsf{Acc}(v) + (1-P)\delta_{v_*}(v), & \text{if} \quad v_* < u \\ P\delta_{v_*}(v) + (1-P)\,\mathsf{Brak}(v), & \text{if} \quad v_* > u \end{cases}$$

where Acc and Brak are probability densities prescribing the speed after acceleration and braking, respectively. In the δ model (see (3.3)) it results

$$\mathsf{Acc}(v) = \delta_{V_A}(v), \quad \mathsf{Brak}(v) = \delta_{V_B}(v) \tag{5.7}$$

while for the χ model (see (3.4)) one has

$$\mathsf{Acc}(v) = \frac{\chi_{[v_*,V_A]}(v)}{V_A - v_*}, \quad \mathsf{Brak}(v) = \frac{\chi_{[V_B,v_*]}(v)}{v_* - V_B}. \tag{5.8}$$

Substituting the explicit expression of $A(v_* \to v|u;\rho)$ in (5.6), multiplying for v and integrating over the velocity space $\mathcal{V}$, we find the evolution equation for the macroscopic speed. In particular, for the choice (5.7) we get

$$\frac{\mathrm{d}}{\mathrm{d}t}u(t) = P\int_0^u (V_A - v_*) f(t,v_*)\mathrm{d}v_* + (1-P)\int_0^u (v_* - V_B) f(t,v_*)\mathrm{d}v_*$$

while for the choice (5.8) we obtain

$$\frac{\mathrm{d}}{\mathrm{d}t}u(t) = \frac{1}{2}\left\{P\int_0^u (V_A - v_*)f(t,v_*)\mathrm{d}v_* + (1-P)\int_0^u (v_* - V_B)f(t,v_*)\mathrm{d}v_*\right\}.$$

We notice that the two differential equations for u differ only in a multiplicative constant. This means that the steady state of the macroscopic speed does not depend on the specific choice, either (5.7) or (5.8), of the probability densities Acc and Brak. In fact only the relaxation rate towards the equilibrium is influenced by the presence of the multiplicative factor.

The previous considerations justify the choice of the simpler δ model as a starting point for the derivation of the interaction rules (5.4). However, notice that in the present framework we include also the noise term, accounting for output speeds which are not precisely determined.

Remark 5.4. We notice that the assumption of mean field interactions leads to a linear collision operator with respect to the kinetic distribution f, see equation (5.6). In contrast, the quadratic collision operator, characterizing the model introduced in Chapter 3, is due to the choice of binary interactions which justify the presence of the product between the kinetic distributions of the candidate and the field vehicles, see equation (3.2).

The microscopic interaction rules given in (5.4) are very similar to those chosen in [41]. There the post-interaction speed are given by

$$v = v_* + A\,(V_A - v_*) + \nu(v_*)\,(V_A - v_*)^\kappa\,\xi, \quad \text{if} \quad v_* < u \tag{5.9a}$$

$$v = v_* - B\,(v_* - V_B) + \nu(v_*)\,(v_* - V_B)^\kappa\,\xi, \quad \text{if} \quad v_* > u. \tag{5.9b}$$

where $\kappa \geq 1$ is an exponent that calibrates the dependence of the noise on the braking/acceleration dynamics and $0 \leq \nu(v_*) \leq 1$ is a function that vanishes at the extreme values of the velocity.

However, some important differences are introduced in the present work. In fact, in (5.9) the jumps of velocity modeled by the second terms of the right-hand side are fixed since they do not depend on the level of congestion of the traffic. Moreover, these jumps are modulated by two non-negative constants $A, B \in [0,1]$ controlling the strength of the interactions, which, however, do not play the role of the time-scaling parameters. Therefore, when a time scaling is applied, the authors need to make assumptions on the way in which the ratio of these parameters behaves in the grazing collision limit. In this way, they produce some arbitrary constants which are not actually model parameters and they use them in order to recover some Fokker-Planck model already studied in the literature.

5.2.3 Derivation of the Boltzmann equation with the microscopic interaction rules (5.4)

As mentioned in Section 5.1, here we recover the Fokker-Planck equation as a limit of a Boltzmann model for traffic flow with the aim of making the study of stationary solutions

and of fundamental diagrams amenable to analysis. To this end, it is useful to derive preliminarily a weak form of the Boltzmann equation.

The derivation of a general Boltzmann-type equation for the case of binary interactions whose post-interaction states are influenced by random variables is given e.g in [66, Chap. 1, Sect. 1.4] and in [40] for traffic flow models. However, since in the present framework we deal with mean field interactions, we follow a different approach based on a formulation similar to (5.6).

For the post-interaction rules (5.4) the transition probability is simply

$$A(v_* \to w|u;\rho) = \delta_v(w),$$

where v is given case-wise by either (5.4a) or (5.4b) and includes also the random variable ξ.

Recalling that we are considering mean field microscopic interactions, the evolution equation for the kinetic distribution f becomes then

$$\partial_t f(t,w) = \tilde{\eta}\int_{-\infty}^{+\infty}\int_0^{V_{\max}} A(v_* \to w|u;\rho) f(t,v_*)\mathrm{d}v_*\eta(\xi)\mathrm{d}\xi - \tilde{\eta} f(t,w), \tag{5.10}$$

where $\tilde{\eta}^{-1}$ has dimension of time and, henceforth, since we consider the spatially homogeneous model, without loss of generality we will take $\tilde{\eta} = 1$.

To pass to the weak form we multiply equation (5.10) by a test function $\phi \in C(\mathcal{V})$ and integrate over $\mathcal{V}$:

$$\frac{\mathrm{d}}{\mathrm{d}t}\int_0^{V_{\max}} \phi(w) f(t,w)\mathrm{d}w = \left\langle \int_0^{V_{\max}} (\phi(v) - \phi(v_*)) f(t,v_*)\mathrm{d}v_* \right\rangle \tag{5.11}$$

where the operator $\langle\cdot\rangle$ denotes the mean with respect to the distribution η, namely

$$\langle g\rangle = \int_{-\infty}^{+\infty} g(\xi)\eta(\xi)\mathrm{d}\xi.$$

From (5.11) it is clear that $\phi(w) = 1$ is a collision invariant which guarantees the conservation of the total number of vehicles. Moreover, it represents the only conservation property satisfied by the kinetic equation, as usual in a traffic flow model.

Synchronized flow

If we consider $\phi(w) = w$ in (5.11) and we divide by the density ρ we can recover the evolution equation for the macroscopic speed:

$$\frac{\mathrm{d}}{\mathrm{d}t}u(t) = \frac{1}{\rho}\left\langle \int_0^{V_{\max}} (v - v_*) f(t,v_*)\mathrm{d}v_* \right\rangle.$$

Using the microscopic rules (5.4) to express the post-interaction speed v, we get

$$\frac{\mathrm{d}}{\mathrm{d}t}u(t) = \frac{1}{\rho}\int_0^u \epsilon P\Delta v_A f(t,v_*)\mathrm{d}v_* - \frac{1}{\rho}\int_u^{V_{\max}} \epsilon(1-P)\Delta v_B f(t,v_*)\mathrm{d}v_*, \tag{5.12}$$

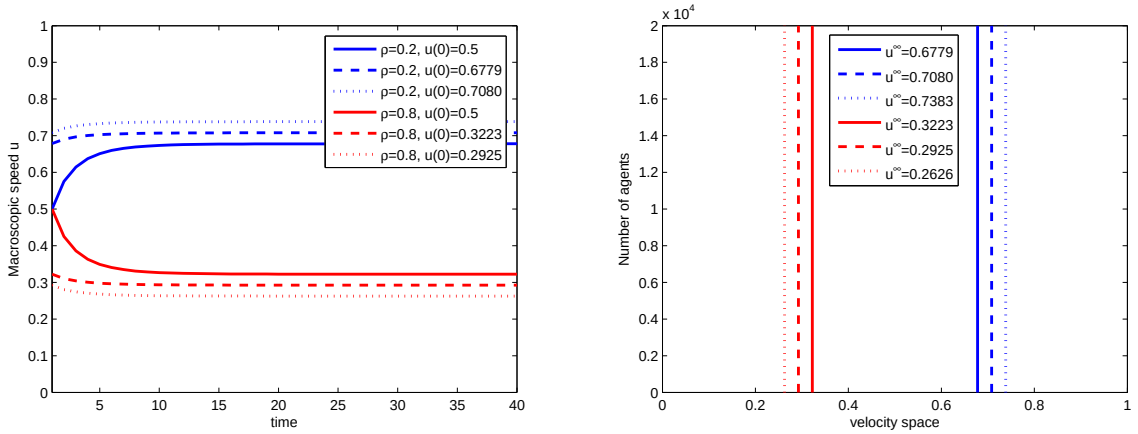

Figure 5.1: Left: evolution towards equilibrium of the macroscopic speed u starting from different initial conditions. Right: distribution of the microscopic velocities at equilibrium.

where we have used the fact that the random variable ξ has zero mean. Suppose that the desired speeds V_A and V_B do not depend on the pre-interaction velocity v_* and take, as assumed for instance in [41], $V_A = V_B = u$. In this case $\Delta v_A = -\Delta v_B$ and using equation (5.12) a straightforward computation provides

$$\frac{\mathrm{d}}{\mathrm{d}t}u(t) = -\frac{\epsilon}{2\rho}(1-2P)\int_0^{V_{\max}} |u - v_*|\, f(t, v_*)\mathrm{d}v_*. \tag{5.13}$$

Observe that $\frac{\mathrm{d}}{\mathrm{d}t}u(t) = 0$ if and only if $f(v) = \rho\delta_u(v)$ which gives thus a steady solution corresponding to the phenomenon of synchronized traffic flow, in which all vehicles travel at the same speed u.

Moreover, notice that $\frac{\mathrm{d}}{\mathrm{d}t}u(t) > 0$ if $P > 1/2$, which means that u is increasing, i.e. $u \to V_{\max}$, until $f(v) = \rho\delta_u(v)$. While, if $P < 1/2$, $\frac{\mathrm{d}}{\mathrm{d}t}u(t) < 0$, which means that u is decreasing, i.e. $u \to 0$, until $f(v) = \rho\delta_u(v)$. Therefore the sign of $\frac{\mathrm{d}}{\mathrm{d}t}u(t)$ is defined by the density ρ at initial time while the equilibrium value of the speed depends also on the initial condition $u(0)$. We stress that this analysis provides information only on the structure of the steady state of the kinetic distribution f but the macroscopic equation (5.13) for the average speed u is not sufficient by itself to compute the equilibrium value of u.

This aspect is also numerically investigated in Figure 5.1 in which we propose a DSMC (Direct Simulation Monte Carlo) simulation for the kinetic equation (5.10) with the microscopic rules (5.4) taking $V_A = V_B = u$. In particular, as in several kinetic models, we use the Nanbu-like asymptotic method [8] which we reformulate in Algorithm 1 for the model (5.10)-(5.4). This approach consists in using a probabilistic interpretation of the Boltzmann-type kinetic model. In fact, let

$$G[f](t,w) = \int_{-\infty}^{+\infty}\int_0^{V_{\max}} A(v_* \to w|u;\rho) f(t,v_*)\mathrm{d}v_*\eta(\xi)\mathrm{d}\xi,$$

then we can write the model (5.10) as

$$\partial_t f(t,w) = \tilde{\eta}G[f](t,w) - \tilde{\eta}f(t,w)$$

where, without loss of generality, we assume that all the quantities, as the maximum speed and the density, are normalized and f is such that $\int_{\mathcal{V}} f(t,w)dw = 1$. Therefore, f is nothing but the kinetic distribution scaled with ρ and the fraction of vehicles is recovered by computing $\rho f(t,w)$. Now consider a time interval $[0, T_{\max}]$ discretized in M intervals of size Δt and let f^n be the approximation of $f(t^n = n\Delta t, w)$. Then, for a small time step Δt we get

$$\frac{f^{n+1} - f^n}{\Delta t} = \tilde{\eta} G[f^n](t,w) - \tilde{\eta} f^n$$

from which we obtain the update of the kinetic functions as in the forward Euler scheme:

$$f^{n+1} = (1 - \tilde{\eta}\Delta t) f^n + \tilde{\eta}\Delta t G[f^n](t,w) \tag{5.14}$$

where, since f^n is a probability density and thanks to mass conservation, also $G[f^n](t,w)$ is a probability density. Taking $\tilde{\eta}\Delta t \leq 1$ then also the update f^{n+1} is a probability density, since it is a convex combination of probability densities. From a probabilistic interpretation, vehicles will not collide with probability $1 - \tilde{\eta}\Delta t$ and it will interact with probability $\tilde{\eta}\Delta t$, according to the collision law described by $A(v_* \to v | u(t); \rho)$. Recall that $\tilde{\eta}^{-1}$ has the dimension of time, thus $1 - \tilde{\eta}\Delta t$ has sense. Since our aim is the study of the asymptotic state arising from the microscopic interactions, the natural choice is to take $\Delta t = \frac{1}{\tilde{\eta}}$.

For further details on binary interaction methods for kinetic equations see e.g. the paper [2] on microscopic models of flocking and swarming or the paper [40] on traffic flow models or the book [66].

In Figure 5.1, Algorithm 1 is applied with $N = 20000$ samples and $M = 40$ time steps. In the left panel we show the evolution towards equilibrium of the macroscopic speed u for two values of the density of vehicles. Precisely, the blue lines are referred to $\rho = 0.2$, and thus $P = 0.8$ using the definition (5.2), while the red lines are referred to $\rho = 0.8$, and thus $P = 0.2$. We use different hatchings for the lines in order to mark the evolution obtained with different starting values of the mean speed. We notice that we find different equilibrium speeds depending on the initial condition $u(0)$ while the trend is influenced by the value of P. In fact, in each case, if $P > 1/2$ (resp. $P < 1/2$), the mean speed increases (resp. decreases), see equation (5.13), until it reaches the equilibrium value u^∞ which is function of $u(0)$. Thus, as usual, the stationary mean speed can be computed by using the solution of the kinetic model while the macroscopic equation (5.13) is not sufficient to determine u^∞.

For instance, focus on the case $P = 0.8$. The evolution marked with the solid line is obtained by sampling the particles from a uniform distribution on $[0, 1]$ at initial time. Thus the initial value of the mean speed u is $u(0) \approx 0.5$. Since $P > 1/2$, the speed u increases during time evolution until the equilibrium value $u^\infty \approx 0.6779$. This value is used as initial condition of the evolution marked with the dashed line. The trend is again increasing, since $P > 1/2$, and we obtain a different equilibrium value $u^\infty \approx 0.7080$. The same procedure is applied in order to compute the evolution marked with the dotted line and similar considerations hold for the case $P = 0.2$.

Algorithm 1 Nanbu algorithm for the model (5.10)-(5.4) with $V_A = V_B = u$ and $\epsilon = 1$.

Take N samples of the microscopic velocities v_j^0, $j = 1, \dots, N$ from the initial density $f^0(v)$;
fix ρ_0 being the initial density of vehicles and thus the probability of changing velocity P;
for $n = 0$ **to** M **do**
  compute the macroscopic speed $u^n = \frac{1}{N} \sum_{j=1}^{N} v_j^i$;
  for $j = 1$ **to** N **do**
    if $P \geq 1/2$ **then**
      sample ξ from a zero mean distribution η living on $\left[-\frac{1-P}{\sqrt{P}}, \frac{1-P}{\sqrt{P}}\right]$;
    else
      sample ξ from a zero mean distribution η living on $\left[-\frac{P}{\sqrt{1-P}}, \frac{P}{\sqrt{1-P}}\right]$;
    end if
    if $v_j^n \leq u^n$ **then**
      compute $v_j^{n+1} = v_j^n + \sqrt{P}(u - v_j^n)\left(\sqrt{P} + \xi\right)$;
    else
      compute $v_j^{n+1} = v_j^n - \sqrt{1-P}(v_j^n - u)\left(\sqrt{1-P} + \xi\right)$.
    end if
  end for
end for

Finally, in the right panel of Figure 5.1 we show that all the equilibrium values of the mean speed are indeed reached when all vehicles travel at the same velocity, i.e. $f(v) = \rho\delta_{u^\infty}(v)$ being u^∞ function of $u(0)$.

Although we can say nothing on the uniqueness of the synchronized steady solutions, we emphasize that this situation can occur at each density, while in experimental studies it occurs only for certain values of ρ, see e.g. [46]. For this reason, we will not analyze deeply this aspect in the following but we will show that this solution is preserved by the Fokker-Planck approximation.

5.3 Fokker-Planck approximation

The main drawback of a Boltzmann model is the complexity of the integral collision operator which makes the investigation of steady states difficult. Observe that the explicit knowledge of the asymptotic distribution is crucial both for computing the diagrams of traffic without expensive numerical simulations and for developing closure laws for macroscopic model. In fact, a kinetic model provides quite naturally speed-density relations arising from the microscopic interaction rules among the vehicles rather than from intuitive considerations.

In order to obtain simpler kinetic models, the goal is to replace the integral operator with differential operators. To this end, starting from the Boltzmann model (5.11) we

derive a Fokker-Planck model using a technique similar to the one introduced for instance in [21, 22, 67, 84] and already used in [41] for non-symmetric interaction rules, or in [65] for gas-dynamics and in [81] for opinion formation. However, as discussed at the end of Section 5.2.2, here, in contrast with [41], the interaction rules (5.4) allow us to simplify the procedure of the grazing collision limit avoiding the definition of several free parameters and additional assumptions on the test function.

From now on, let us to consider $\phi \in C_c^\infty(\mathcal{V})$. Starting from (5.11), we first scale the time using the same parameter ϵ appearing in (5.4), setting

$$\tau = \epsilon t, \quad f(t,v) = \tilde{f}(\tau, v).$$

For brevity, in the following we omit the use of the tilde and we indicate by f the scaled distribution function. Then, braking up the integrals, equation (5.11) writes as

$$\partial_\tau \int_0^{V_{\max}} \phi(w) f(\tau, w) \mathrm{d}w = \mathcal{A} + \mathcal{B}.$$

where

$$\mathcal{A} = \frac{1}{\epsilon}\left\langle \int_0^u (\phi(v) - \phi(v_*)) f(\tau, v_*)\mathrm{d}v_* \right\rangle, \quad \mathcal{B} = \frac{1}{\epsilon}\left\langle \int_u^{V_{\max}} (\phi(v) - \phi(v_*)) f(\tau, v_*)\mathrm{d}v_* \right\rangle.$$

are the acceleration and braking collision kernels respectively. We study explicitly only the case $v_* < u$. Similar computations can be easily repeated for $v_* > u$. Since for small values of ϵ we have $v \approx v_*$, we can compute the Taylor expansion up to second order of $\phi(v) - \phi(v_*)$ around v_*:

$$\phi(v) - \phi(v_*) = \phi'(v_*)(v - v_*) + \frac{1}{2}\phi''(\overline{v_*})(v - v_*)^2, \quad \overline{v_*} \in (v_*, v)$$

with v defined in this case by (5.4a). Substituting $v - v_*$ in the above expansion, the acceleration part of the collision kernel becomes

$$\begin{aligned}\mathcal{A} =& \frac{1}{\epsilon}\left\langle \int_0^u (\epsilon P \Delta v_A + \sqrt{\epsilon P}\Delta v_A \xi)\phi'(v_*) f(\tau, v_*)\mathrm{d}v_* \right\rangle \\ &+ \frac{1}{2\epsilon}\left\langle \int_0^u (\epsilon P \Delta v_A + \sqrt{\epsilon P}\Delta v_A \xi)^2 \phi''(v_*) f(\tau, v_*)\mathrm{d}v_* \right\rangle \\ &+ \frac{1}{\epsilon}\langle R_{\mathcal{A}}(f, \eta, \phi)\rangle,\end{aligned}$$

where

$$R_{\mathcal{A}}(f,\eta,\phi) = \frac{1}{2}\int_0^u (\epsilon P \Delta v_A + \sqrt{\epsilon P}\Delta v_A \xi)^2 (\phi''(\overline{v_*}) - \phi''(v_*)) f(\tau, v_*)\mathrm{d}v_*$$

is the remaining term that vanishes as $\epsilon \to 0$. In fact, since ϕ is a smooth function, the second derivative ϕ'' is Lipschitz continuous, thus

$$\exists\, \mathrm{L} \geq 0 \text{ s.t. } \left|\phi''(\overline{v_*}) - \phi''(v_*)\right| \leq \mathrm{L}\left|\overline{v_*} - v_*\right|.$$

Recalling that $\overline{v_*} \in (v_*, v)$, we have $|\overline{v_*} - v_*| = \theta\,|v - v_*|$ for some $\theta \in (0,1)$. Therefore

$$\mathrm{L}\,|\overline{v_*} - v_*| \leq \mathrm{L}\,|v - v_*| \leq \mathrm{LC}\sqrt{\epsilon}$$

where $\mathrm{C} = \mathrm{C}(\max\{\Delta v_A\}, \xi_{\max})$ and

$$\begin{aligned}\frac{1}{\epsilon}\,|\langle R_{\mathcal{A}}(f,\eta,\phi)\rangle| &\leq \frac{1}{2\epsilon}\int_{-\infty}^{+\infty}\int_0^u (v-v_*)^2\,|\phi''(\overline{v_*}) - \phi''(v_*)|\,f(\tau,v_*)\mathrm{d}v_*\eta(\xi)\mathrm{d}\xi \\ &\leq \frac{\mathrm{LC}\epsilon^{\frac{3}{2}}}{2\epsilon}\int_{-\infty}^{+\infty}\int_0^u f(\tau,v_*)\mathrm{d}v_*\eta(\xi)\mathrm{d}\xi \xrightarrow{\epsilon\to 0^+} 0.\end{aligned}$$

Thus, computing the limit for $\epsilon \to 0$, corresponding to a situation in which the interactions are frequent but they produce only small variations in the output velocities, and using the identities

$$\int_{-\infty}^{+\infty}\eta(\xi)\mathrm{d}\xi = 1, \quad \int_{-\infty}^{+\infty}\xi\eta(\xi)\mathrm{d}\xi = 0, \quad \int_{-\infty}^{+\infty}\xi^2\eta(\xi)\mathrm{d}\xi = \sigma^2,$$

we obtain

$$\lim_{\epsilon\to 0}\mathcal{A} = P\int_0^u \Delta v_A\phi'(v_*)f(\tau,v_*)\mathrm{d}v_* + \frac{\sigma^2 P}{2}\int_0^u (\Delta v_A)^2\,\phi''(v_*)f(\tau,v_*)\mathrm{d}v_*.$$

The same considerations apply also to the braking part of the collision kernel. In particular, one verifies that $R_{\mathcal{B}}(f,\eta,\phi) \to 0$ as $\epsilon \to 0$ and

$$\lim_{\epsilon\to 0}\mathcal{B} = -(1-P)\int_u^{V_{\max}} \Delta v_B\phi'(v_*)f(\tau,v_*)\mathrm{d}v_* + \frac{\sigma^2(1-P)}{2}\int_u^{V_{\max}} (\Delta v_B)^2\,\phi''(v_*)f(\tau,v_*)\mathrm{d}v_*.$$

Finally, in order to derive the strong formulation of the Fokker-Planck equation, we write the weak form resulting from the grazing collision limit as

$$\begin{aligned}\partial_\tau\int_0^{V_{\max}}\phi(v)f(\tau,v)\mathrm{d}v =& P\int_0^{V_{\max}}\chi_{[0,u]}(v_*)\phi'(v_*)\Delta v_A f(\tau,v_*)\mathrm{d}v_* \\ &- (1-P)\int_0^{V_{\max}}\chi_{[u,V_{\max}]}(v_*)\phi'(v_*)\Delta v_B f(\tau,v_*)\mathrm{d}v_* \\ &+ \frac{\sigma^2 P}{2}\int_0^{V_{\max}}\chi_{[0,u]}(v_*)\phi''(v_*)\,(\Delta v_A)^2\,f(\tau,v_*)\mathrm{d}v_* \\ &+ \frac{\sigma^2(1-P)}{2}\int_0^{V_{\max}}\chi_{[u,V_{\max}]}(v_*)\phi''(v_*)\,(\Delta v_B)^2\,f(\tau,v_*)\mathrm{d}v_*.\end{aligned} \tag{5.15}$$

Integrating by parts each term of the right-hand side of (5.15) and using the fact that $\phi(0) = \phi(V_{\max}) = \phi'(0) = \phi'(V_{\max}) = 0$, we recover the following strong form of the Fokker-Planck equation:

$$\begin{aligned}\partial_\tau f(\tau,v) =& -\partial_v\left[f(\tau,v)\left(P\chi_{[0,u]}(v)\Delta v_A - (1-P)\chi_{[u,V_{\max}]}(v)\Delta v_B\right)\right] \\ &+ \frac{\sigma^2}{2}\partial_{vv}\left[f(\tau,v)\left(P\chi_{[0,u]}(v)\,(\Delta v_A)^2 + (1-P)\chi_{[u,V_{\max}]}(v)\,(\Delta v_B)^2\right)\right]\end{aligned} \tag{5.16}$$

as limit of the Boltzmann model (5.11) based on the microscopic rules (5.4). Observe that (5.16) can be rewritten in the usual formulation of a Fokker-Planck-type model for traffic flow:

$$\partial_\tau f(\tau, v) + \partial_v \left[f(\tau, v) B(v, u, \rho) - D(v, u, \rho) \partial_v f(\tau, v) \right] = 0, \tag{5.17}$$

see for instance the prototype example introduced in [44]. In the present framework, the acceleration/braking operator $B(v, u, \rho)$ is

$$\begin{aligned} B(v, u, \rho) =& P\chi_{[0,u]}(v)\Delta v_A - (1-P)\chi_{[u,V_{\max}]}(v)\Delta v_B \\ & - \frac{\sigma^2}{2}\partial_v \left(P\chi_{[0,u]}(v) \left(\Delta v_A\right)^2 + (1-P)\chi_{[u,V_{\max}]}(v) \left(\Delta v_B\right)^2 \right) \end{aligned} \tag{5.18}$$

while the diffusive operator $D(v, u, \rho)$ is

$$D(v, u, \rho) = \frac{\sigma^2}{2} \left(P\chi_{[0,u]}(v) \left(\Delta v_A\right)^2 + (1-P)\chi_{[u,V_{\max}]}(v) \left(\Delta v_B\right)^2 \right). \tag{5.19}$$

As we will see in Section 5.4, the stationary solution of (5.17) can be obtained avoiding the explicit computation of derivatives of characteristic functions that may result in Dirac functions.

Remark 5.5 (Boundary conditions). In contrast to the Boltzmann model, in which ρ is automatically conserved, in the Fokker-Planck model the density remains constant in time and thus it is an invariant of the model (5.17) if, for any choices of V_A and V_B, the following boundary condition holds

$$f(\tau, v) B(v, u, \rho) - D(v, u, \rho) \partial_v f(\tau, v) \Big|_{v=0}^{v=V_{\max}} = 0 \tag{5.20}$$

at each time τ.

5.4 Fundamental diagrams

In this section, we investigate the fundamental diagrams of traffic flow resulting from the Fokker-Planck model (5.17). Since we are interested in reproducing the features of experimental diagrams, as the phase transition and the multivalued behavior, we show that a particular choice of the desired speeds allows us to obtain diagrams which exhibit the qualitative properties of data. Therefore, we will analyze the influence of microscopic interactions on macroscopic dynamics.

As usual, macroscopic diagrams are recovered by computing the macroscopic quantities as moments of the time-asymptotic kinetic distribution $f^\infty(v)$. Notice that, using the Fokker-Planck model, $f^\infty(v)$ can be computed easily by solving an ordinary differential equation. In fact, at the steady state, the time derivative of the distribution function in (5.17) must be zero and thus we are led to the following homogeneous ODE:

$$f'(v) = \frac{B(v, u, \rho)}{D(v, u, \rho)} f(v), \quad v \in [0, V_{\max}] \tag{5.21}$$

whose solution can be written in form of exponentials once the cases $v < u$ and $v > u$ are distinguished.

Using the separation of variables method, the time-asymptotic solution for general jumps of velocity Δv_A and Δv_B can be computed explicitly substituting (5.18) and (5.19) in (5.21) and it is given by

$$f^\infty(v) = f^\infty(u^-)\left(\frac{\Delta v_A(v,\rho)|_{v=u}}{\Delta v_A(v,\rho)}\right)^2 \exp\left(-\frac{2}{\sigma^2}\int_v^u \frac{1}{\Delta v_A(s,\rho)}\mathrm{d}s\right), \quad \text{if} \quad v < u \tag{5.22a}$$

$$f^\infty(v) = f^\infty(u^+)\left(\frac{\Delta v_B(v,u,\rho)|_{v=u}}{\Delta v_B(v,u,\rho)}\right)^2 \exp\left(-\frac{2}{\sigma^2}\int_u^v \frac{1}{\Delta v_B(s,u,\rho)}\mathrm{d}s\right), \quad \text{if} \quad v > u \tag{5.22b}$$

which indeed depends on three unknown parameters, the mean speed u, $f^\infty(u^-)$ and $f^\infty(u^+)$. The latter two are the left and right limits, respectively, of f^∞ at $v = u$, that here we take as two integration constants.

Equivalently we can think of (5.22a) as parametrized by $rf^\infty(u^+)$, with

$$r = \frac{f^\infty(u^-)}{f^\infty(u^+)}. \tag{5.23}$$

Notice that imposing the constraint on the zeroth moment (i.e. mass conservation) of the distribution function

$$\rho = \int_0^{V_{\max}} f^\infty(v)\mathrm{d}v \tag{5.24}$$

is not sufficient to define uniquely both r and $f^\infty(u^+)$. In fact, the constraint (5.24) leads to a single equation

$$f^\infty(u^+)\left(r\rho^- + \rho^+\right) = \rho$$

with two unknowns, where

$$\rho^- = \int_0^u f^\infty(v)\mathrm{d}v, \quad \rho^+ = \int_u^{V_{\max}} f^\infty(v)\mathrm{d}v$$

are the partial densities of slow and fast vehicles (with respect to the mean speed). Thus, we obtain a family of steady solutions and without loss of generality we assume that f^∞ will be parametrized by the ratio r, so that

$$f^\infty(u^-) = \frac{r\rho}{r\rho^- + \rho^+}, \quad f^\infty(u^+) = \frac{\rho}{r\rho^- + \rho^+}. \tag{5.25}$$

For $r = 1$ we obtain continuous asymptotic distributions at $v = u$, while for $r \neq 1$ we allow for discontinuous distributions at $v = u$. This is the mathematical key which allows us to recover multivalued diagrams of traffic as a result of the existence of a one-parameter family of solutions. In fact, for each value of the ratio r we obtain a corresponding time-asymptotic solution. Thus different values of r give different equilibrium speeds, for a fixed density ρ. Usually, in the literature only continuous solutions were considered, see e.g. [44]

in which a "small" multivalued behavior is obtained by means of the probability of lane changing.

The equilibrium value of the macroscopic speed u is obtained by solving a non-linear equation coming from the constraint on the first moment of the distribution function and from (5.24)

$$\int_0^{V_{\max}} v f^\infty(v)\mathrm{d}v = \rho u = u\int_0^{V_{\max}} f^\infty(v)\mathrm{d}v. \tag{5.26}$$

The identity (5.26) provides the nonlinear equation $R(u) = 0$, with

$$R(u) := \int_0^{V_{\max}} (u - v) f^\infty(v)\mathrm{d}v. \tag{5.27}$$

Solving it for each value of the density in $[0, \rho_{\max}]$ we find the speed at equilibrium which defines therefore a relation between the density ρ and the mean speed u of the flow. Since $R(u) = 0$ defines a nonlinear equation, in principle it might have zero or more than one solution.

Finally, observe that without diffusion, namely if $\sigma^2 \to 0$, then the two exponentials in (5.22) tend to 1. This means that the general steady state (5.22), and thus the equilibrium speed, is influenced only by the choice of the desired speed V_A and V_B. In fact, in this case the microscopic rules (5.4) become purely deterministic, provided $P(\rho)$.

Remark 5.6 (Synchronized flow). In Paragraph "Synchronized flow" in Section 5.2.3 we have proved that the distribution function $f(v) = \rho\delta_u(v)$ is a stationary solution of the Boltzmann model (5.11) based on the interactions (5.4), when $V_A = V_B = u$. This solution is preserved in the Fokker-Planck approximation. We use the weak form of the model (5.17) in order to prove that $f(v) = \rho\delta_u(v)$ is, in distributional sense, the trivial steady state of the Fokker-Planck-type equation. In fact, assuming ϕ as a test function with compact support in $\mathcal{V}$, $f(v)$ is a weak stationary solution if

$$\int_0^{V_{\max}} \phi(v)\partial_v \left(f(v)B(v,u,\rho) - D(v,u,\rho)\partial_v f(v)\right)\mathrm{d}v = 0.$$

Integrating by parts the left-hand side of the above equation we get

$$-\int_0^{V_{\max}} \phi'(v)B(v,u,\rho)f(v)\mathrm{d}v - \int_0^{V_{\max}} \partial_v(\phi'(v)D(v,u,\rho))f(v)\mathrm{d}v.$$

Taking $f(v) = \rho\delta_u(v)$ we obtain

$$\int_0^{V_{\max}} \phi'(v)B(v,u,\rho)f(v)\mathrm{d}v = \rho B(u,u,\rho) = 0$$

$$\int_0^{V_{\max}} \partial_v(\phi'(v)D(v,u,\rho))f(v)\mathrm{d}v = \rho\phi''(v)D(u,u,\rho) + \rho\phi'(v)\partial_v D(v,u,\rho)|_{v=u} = 0.$$

In fact, the choice $V_A = V_B = u$ leads to a degeneracy at $v = u$ in the acceleration/braking operator B, in the diffusion operator D and in its derivative, since

$$\begin{aligned} B(v,u,\rho) =& P(u-v)\chi_{[0,u]}(v) - (1-P)(v-u)\chi_{[u,V_{\max}]}(v) - \partial_v D(v,u,\rho) \\ \partial_v D(v,u,\rho) =& \frac{\sigma^2}{2}\Big[-P(u-v)^2\delta_u(v) - 2P(u-v)\chi_{[0,u]}(v) \\ & +(1-P)(v-u)^2\delta_u(v) + 2(1-P)(v-u)\chi_{[u,V_{\max}]}(v)\Big]. \end{aligned}$$

Now, let us study two particular models obtained with different choices of the desired speeds. In both cases, we formulate the explicit steady state and the expression of the function $R(u)$ which defines the equilibrium speed. We show that the two choices provide meaningful diagrams of traffic (flux-density and speed-density relationships).

5.4.1 Case 1

Here we assume

$$V_A = v + P(V_{\max} - v), \quad V_B = Pu. \tag{5.28}$$

This means that, in acceleration, the desired speed is a certain velocity in $[v, V_{\max}]$ depending on the value of the probability of accelerating P and thus on the density of vehicles. Instead, when braking, the desired speed is a velocity in $[0, u]$ and depends only on macroscopic quantities, as discussed in Section 5.2. With this choice and evaluating explicitly the integrals appearing in (5.22), the asymptotic distribution f^∞ becomes

$$f^\infty(v) = f^\infty(u^-)\left(\frac{V_{\max}-u}{V_{\max}-v}\right)^{c^A}, \quad \text{if} \quad v < u \tag{5.29a}$$

$$f^\infty(v) = f^\infty(u^+)\left(\frac{u-Pu}{v-Pu}\right)^{c^B}, \quad \text{if} \quad v > u \tag{5.29b}$$

where $c^A = \frac{2}{\sigma^2 P} + 2$ and $c^B = \frac{2}{\sigma^2} + 2$. In the sequel we consider $P = 1 - \rho$. Recall that the equilibrium speed is found by solving the constraint (5.26), which leads to the non-linear equation $R(u) = 0$. For the steady solution (5.29) we have

$$R(u) = f^\infty(u^-)\underbrace{\int_0^u (u-v)\left(\frac{V_{\max}-u}{V_{\max}-v}\right)^{c^A} \mathrm{d}v}_{R_A(u)} - f^\infty(u^+)\underbrace{\int_u^{V_{\max}} (v-u)\left(\frac{u-Pu}{v-Pu}\right)^{c^B} \mathrm{d}v}_{R_B(u)}.$$

Computing explicitly both integrals we obtain

$$R_A(u) = \frac{(V_{\max}-u)^2}{(c^A-2)(c^A-1)} - \frac{V_{\max}^{2-c^A}(V_{\max}-u)^{c^A}}{(c^A-2)(c^A-1)} - \frac{uV_{\max}^{1-c^A}(V_{\max}-u)^{c^A}}{c^A-1} \tag{5.30a}$$

$$\begin{aligned} R_B(u) =& \frac{(u-Pu)^2}{(c^B-2)(c^B-1)} - \frac{(u-Pu)^{c^B}(V_{\max}-Pu)^{2-c^B}}{(c^B-2)(c^B-1)} \\ & - \frac{(u-Pu)^{c^B}(V_{\max}-u)(V_{\max}-Pu)^{1-c^B}}{(c^B-1)} \end{aligned} \tag{5.30b}$$

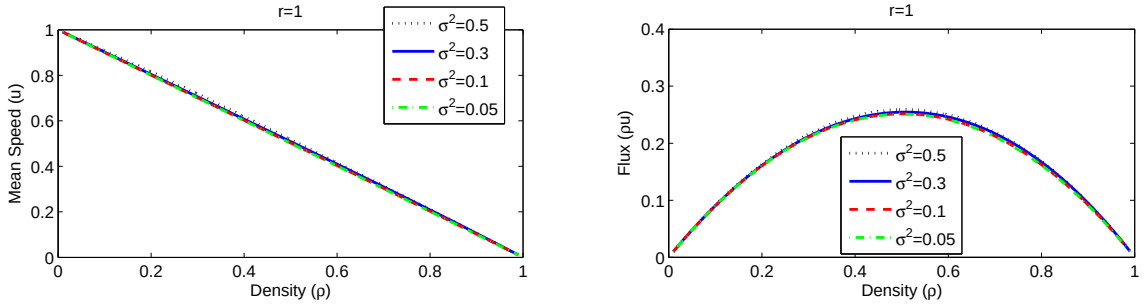

Figure 5.2: Diagrams of traffic using the desired speeds (5.28). We take $r = 1$ and we show the dependence on the variance σ^2.

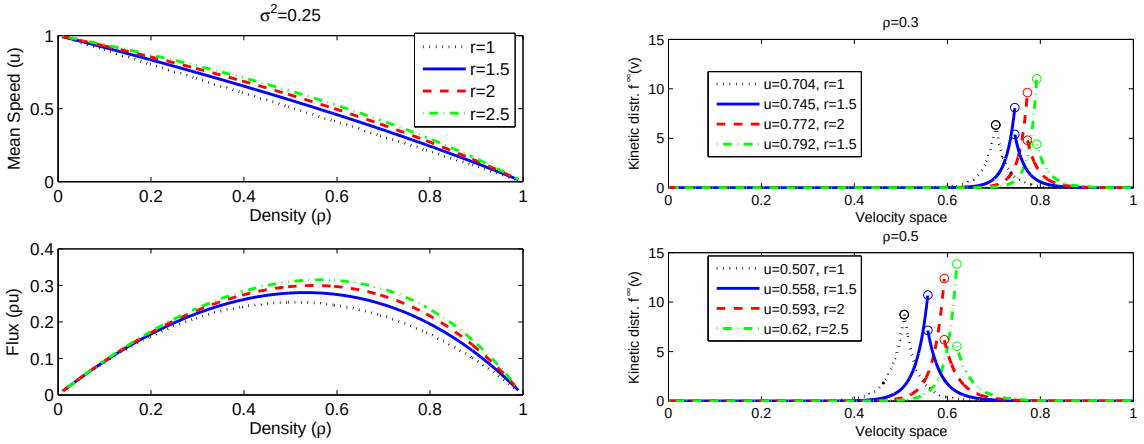

Figure 5.3: Left panels: diagrams of traffic using the desired speeds (5.28). We take $\sigma^2 = 0.25$ and we study the dependence on the parameter r which permits to find a region of scattered values. Right panels: we plot the related equilibrium distributions for $\rho = 0.3$ (top) and $\rho = 0.5$ (bottom). The circles define the values $f(v)$ for $v \to u^-$ and $v \to u^+$.

Unfortunately, since $R(0) = R(1) = 0$ we cannot ensure that $\exists u \in [0, V_{\max}]$ such that $R(u) = 0$. However, numerically we observe that the nonlinear equation $R(u) = 0$ does not provide more than one solution $u \in (0, 1)$.

In Figure 5.2 and 5.3 we show the diagrams of traffic by varying the parameters of the model. In particular, in Figure 5.2 we study the influence of σ^2 on the speed and on the flux. The diagrams are reproduced by considering only continuous steady state, namely we fix $r = 1$ and then we compute $f^\infty(u^+)$ and $f^\infty(u^-)$ from equation (5.24) and (5.23). The equilibrium values are obtained by solving numerically $R(u) = 0$ and the top plots show the speed-density diagrams, while the bottom ones show the flux-density diagrams. In all simulations we set $\rho_{\max} = V_{\max} = 1$. The probability of accelerating P is taken as prescribed in (5.2). The variance σ^2 seems to produce only small variations in the equilibrium values of the speed. More precisely, it does not influence deeply the free and the congested phase of traffic but only the values near the phase transition. Therefore, acting on σ^2 we are not able to reproduce a meaningful scattering of the flux values.

In the left panels of Figure 5.3 we consider the diagrams obtained with $\sigma^2 = 0.25$, but modifying the parameter r, see equation (5.23). This allows us to take into account different steady state according to the jump at $v = u$. The corresponding stationary solutions appear in the right panels for two values of $\rho = 0.3, 0.5$. We point out that now we obtain a more significant and accentuated dispersion of the values of macroscopic quantities in a large range of density. Note that the dispersion is very small for low and high densities, which is in accord with experimental surveys. The circles in the right plots are in order to show the values of the steady states $f^\infty(v, r)$ for $v \to u^-$ and $v \to u^+$, which coincide only for the black dotted distribution corresponding to the continuous case, with $r = 1$. The role and the meaning of the parameter r will be further clarified in Section 5.4.3.

Now, we focus on an important result which establishes connections between the macroscopic closures and the generic probability of accelerating P used at the microscopic level in the present kinetic framework.

Theorem 5.7. – *Let $r = 1$, that is consider only continuous asymptotic kinetic distributions* (5.22)*. In the limit $\sigma^2 \to 0$, the kinetic model* (5.17) *with desired speeds* (5.28) *provides the macroscopic closure*

$$u(\rho) = V_{\max} P(\rho), \quad 0 \le \rho \le \rho_{\max},$$

where $P : [0, \rho_{\max}] \to [0, 1]$ is a probability function.

Proof. In order to prove the statement we have to verify that $u = V_{\max} P(\rho)$ is solution of the non-linear equation $R(u) = f^\infty(u^-) R_A(u) - f^\infty(u^+) R_B(u)$ for $\sigma^2 \to 0$, with $R_A(u)$ and $R_B(u)$ defined in (5.30). Substituting $u = V_{\max} P(\rho)$ in the expression of $R_A(u)$ we find

$$R_A(V_{\max} P(\rho)) = \frac{V_{\max}^2 (1 - P(\rho))^2}{(c^A - 2)(c^A - 1)} - \frac{V_{\max}^2 (1 - P(\rho))^{c^A}}{(c^A - 2)(c^A - 1)} - \frac{V_{\max}^2 P(\rho)(1 - P(\rho))^{c^A}}{c^A - 1}.$$

Since $c^A = \frac{2}{\sigma^2 P(\rho)} + 2 \to \infty$ for each fixed ρ when $\sigma^2 \to 0$, we have that

$$\frac{V_{\max}^2 (1 - P(\rho))^2}{(c^A - 2)(c^A - 1)} \xrightarrow{\sigma^2 \to 0} 0,$$

while

$$\frac{V_{\max}^2 (1 - P(\rho))^{c^A}}{(c^A - 2)(c^A - 1)} \xrightarrow{\sigma^2 \to 0} 0, \quad \frac{V_{\max}^2 P(\rho)(1 - P(\rho))^{c^A}}{c^A - 1} \xrightarrow{\sigma^2 \to 0} 0$$

because $0 \le 1 - P(\rho) \le 1$. Therefore, $R_A(V_{\max} P(\rho)) \to 0$ in the limit $\sigma^2 \to 0$. The same considerations can be applied for the braking part. In fact, substituting $u = V_{\max} P(\rho)$ in $R_B(u)$ we find

$$\begin{aligned} R_B(V_{\max} P(\rho)) = & \frac{V_{\max}^2 P(\rho)^2 (1 - P(\rho))^2}{(c^B - 1)(c^B - 2)} - \frac{V_{\max}^2 P(\rho)^{c^B} (1 - P(\rho))^2 (1 + P(\rho))^{2 - c^B}}{(c^B - 1)(c^B - 2)} \\ & - \frac{V_{\max}^2 P(\rho)^{c^B} (1 - P(\rho))^2 (1 + P(\rho))^{1 - c^B}}{c^B - 1}. \end{aligned}$$

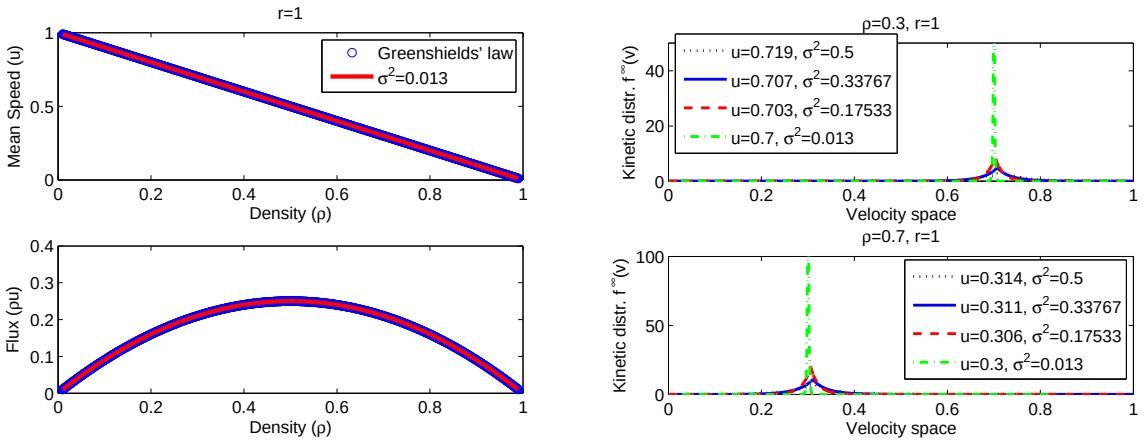

Figure 5.4: Left panels: diagrams of traffic obtained with the Greenshields' closure law (blue data) and the kinetic model with desired speeds $V_A = v + P(V_{\max} - v)$ and $V_B = Pu$, fixing $r = 1$ and $\sigma^2 = 0.013$. Right panels: the equilibrium distributions for decreasing values of the variance σ^2 and $\rho = 0.3$ (top), $\rho = 0.7$ (bottom).

Recall that $c^B = \frac{2}{\sigma^2} + 2$ and thus $c^B \to \infty$ when $\sigma^2 \to 0$. While, since $1 \leq 1 + P(\rho) \leq 2$ and $1 - c^B < 0$, one verifies that $1 + P(\rho)^{2-c^B} \to 0$ and $1 + P(\rho)^{1-c^B} \to 0$. These facts guarantee that $R_B(V_{\max} P(\rho)) \to 0$, in the limit $\sigma^2 \to 0$ and the thesis is proved. ■

The previous proposition ensures that an empirical closure law $u(\rho)$ between the mean speed and the density (see e.g. [78, Chap. 10.1]) can be derived from a kinetic approach based on a microscopic model in which the rules are given by (5.4), with suitable choices of the probability of accelerating P. In other words, in this framework the probability P, which influences the microscopic behavior of drivers, can explain also the macroscopic trend of the flow when $\sigma^2 \to 0$.

This relation is investigated numerically in Figure 5.4 for the Greenshields' closure frequently used in macroscopic traffic models, see [32]. Let $\rho_{\max} = V_{\max} = 1$. In the left panels, we show the diagrams of traffic provided by the Greenshields' law $u(\rho) = 1 - \rho$ (blu data) and by the Fokker-Planck model discussed in this paragraph (red data) with $\sigma^2 = 0.013$. The convergence rate of the equilibrium speeds to the relation $u(\rho) = 1 - \rho$ when $\sigma^2 \to 0$ is given in Table 5.1 in which the distance is computed as $\|(1 - \boldsymbol{\rho}) - \mathbf{u}^\infty\|_2$, where $\boldsymbol{\rho}$ is a vector of densities and $\mathbf{u}^\infty$ is a vector of the equilibrium values found by solving $R(u) = 0$ for each density in $\boldsymbol{\rho}$. One can observe that the error goes to zero as $\sigma^2 \to 0$ with sub-linear rate. In the right panels of Figure 5.4 we plot the continuous stationary kinetic distributions (5.29) for $\rho = 0.3$ (top plot), $\rho = 0.7$ (bottom plot) and several decreasing values of the variance σ^2. As $\sigma^2 \to 0$, the equilibrium distributions approach a Dirac delta centered in $u(\rho) = 1 - \rho$, namely all vehicles travel with same speed at equilibrium. This fact is not surprising because when $\sigma^2 \to 0$ the microscopic rules (5.4) become purely deterministic and the diffusion operator in the Fokker-Planck equation (5.17) vanishes.

Table 5.1: Table of the distance $\|(1-\boldsymbol{\rho}) - \mathbf{u}^\infty\|_2$ between the Greenshields' equilibrium speeds $1-\boldsymbol{\rho}$ and th equilibrium ones $\mathbf{u}^\infty$ of the kinetic model with desired speeds (5.28).

σ^2	Distance (2-norm)	Rate
0.5	$4.4872E-01$	-
0.25	$1.8192E-01$	1.0672
0.125	$9.2778E-02$	0.7131
0.0625	$4.7283E-02$	0.7279
0.03125	$2.3873E-02$	0.7491
0.015625	$1.1995E-02$	0.7602

5.4.2 Case 2

Here we assume

$$V_A = \min\{v+\Delta v, V_{\max}\}, \quad V_B = Pu. \tag{5.31}$$

Thus we do not modify the desired speed in braking with respect the previous case. Instead, in acceleration, we assume that the desired speed is not influenced by the congestion level of the flow. More precisely, we model the situation in which, once a driver decides to accelerate, the desired speed is reached with a fixed jump of velocity, so that V_A is $v+\Delta v$ if the resulting speed is smaller than $V_{\max}$, while $V_A = V_{\max}$ when $V_{\max} - v < \Delta v$. In this case the amplitude of the jump is less than Δv. Observe that this choice was introduced in [75] and in Section 3.2.1, see the case of the quantized acceleration that is the δ model (3.3). The parameter Δv would be a finite parameter which models the physical velocity jump performed in acceleration. Clearly, it may depend on the mechanical microscopic characteristics of vehicles, as in the multi-population framework (see [74] or Chapter 4), but here we will assume that it is constant. With this choice and evaluating explicitly the integrals in (5.22), the asymptotic distribution f^∞ writes as

$$f^\infty(v) = f^\infty(u^-) \begin{cases} \exp\left(\frac{c-2}{\Delta v}(v-u)\right), & v < u < V_{\max} - \Delta v \\ \left(\frac{V_{\max}-u}{\Delta v}\right)^c \exp\left(\frac{c-2}{\Delta v}(v+\Delta v - V_{\max})\right), & v < V_{\max} - \Delta v < u\,, \\ \left(\frac{V_{\max}-u}{V_{\max}-v}\right)^c, & V_{\max} - \Delta v < v < u \end{cases} \quad \text{if} \quad v < u \tag{5.32a}$$

$$f^\infty(v) = f^\infty(u^+) \left(\frac{u-Pu}{v-Pu}\right)^c, \quad \text{if} \quad v > u \tag{5.32b}$$

where now $c := c^A = c^B = \frac{2}{\sigma^2} + 2$. The kinetic distribution f^∞ given in (5.32a) for $v < u$ can be computed by studying separately the cases $\min\{v+\Delta v, V_{\max}\} = v+\Delta v$ and $\min\{v+\Delta v, V_{\max}\} = V_{\max}$.

Recall that the non-linear equation $R(u) = 0$ is determined by the constraint (5.26). Since the steady distributions (5.29) and (5.32) differ only for $v < u$, $R_B(u)$ is already

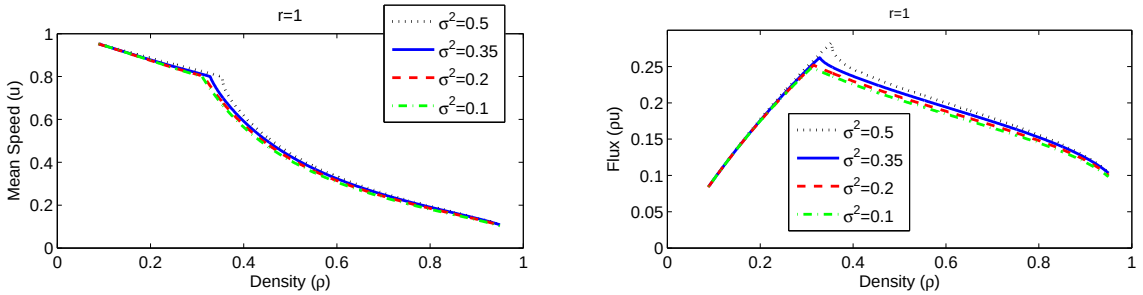

Figure 5.5: Macroscopic diagrams of traffic using the desired speeds (5.31). We take $r = 1$, $\Delta v = 0.2$, for several values of the variance σ^2.

defined by (5.30b) and we need to recompute only $R_A(u)$. For the steady solution (5.32a), R_A is defined as

$$R_A(u) = f^\infty(u^-) \begin{cases} \int_0^u (u-v) \exp\left(\frac{c-2}{\Delta v}(v-u)\right) \mathrm{d}v, & \text{if } u < V_{\max} - \Delta v \\ \int_0^{V_{\max}-\Delta v} (u-v) \left(\frac{V_{\max}-u}{\Delta v}\right)^c \exp\left(\frac{c-2}{\Delta v}(v+\Delta v - V_{\max})\right) \mathrm{d}v & \\ + \int_{V_{\max}-\Delta v}^u (u-v) \left(\frac{V_{\max}-u}{V_{\max}-v}\right)^c \mathrm{d}v, & \text{if } u > V_{\max} - \Delta v \end{cases}.$$

Computing explicitly the integrals, we find

$$R_A(u) = \begin{cases} \left(\frac{\Delta v}{c-2}\right)^2 \left(1 - \exp(-\frac{(c-2)}{\Delta v}u)\right) - \frac{\Delta v}{c-2} u \exp(-\frac{(c-2)}{\Delta v}u), & \text{if } u < V_{\max} - \Delta v \\ \frac{\Delta v}{c-2} \left(\frac{V_{\max}-u}{\Delta v}\right)^c \left[u + \Delta v - V_{\max} - u \exp(-\frac{c-2}{\Delta v}(V_{\max} - \Delta v))\right] & \\ + \left(\frac{\Delta v}{c-2}\right)^2 \left(\frac{V_{\max}-u}{\Delta v}\right)^c \left[1 - \exp(-\frac{c-2}{\Delta v}(V_{\max} - \Delta v))\right] & \text{if } u > V_{\max} - \Delta v \\ + \frac{(V_{\max}-u)^c}{c-1} \left[(V_{\max} - u - \Delta v)\Delta v^{1-c} + \frac{(V_{\max}-u)^{2-c}}{c-2} - \frac{\Delta v^{2-c}}{c-2}\right]. & \end{cases} \tag{5.33}$$

In Figure 5.5 we study the influence of σ^2 on the mean speed and on the flux for $r = 1$, that is allowing only continuous steady states. As already discussed, the equilibrium values are obtained by solving numerically $R(u) = 0$. The top plots show the speed-density diagrams, while at the bottom we have the flux-density diagrams. In all simulations we set $\rho_{\max} = V_{\max} = 1$. The probability of accelerating P is taken as prescribed in (5.2). The parameter Δv is chosen as 0.2. As in Case 1, the variance σ^2 seems to produce only small variations in the equilibrium values of the macroscopic speed and of the flux. Only the values near to the phase transition are affected, in particular they become sharper when σ^2 increases. Again, a multivalued behavior cannot be obtained by acting on σ^2.

Next we consider the diagrams obtained with $\sigma^2 = 0.5$ but depending on the parameter r which allows one to take into account different steady states according to their regularity at $v = u$, see equation (5.23). The right panels of Figure 5.6 show the stationary distributions for $\rho = 0.3, 0.5$. In the left panels of Figure 5.6, instead, we show that now we obtain a more significant and accentuated dispersion of the equilibrium values in a larger range

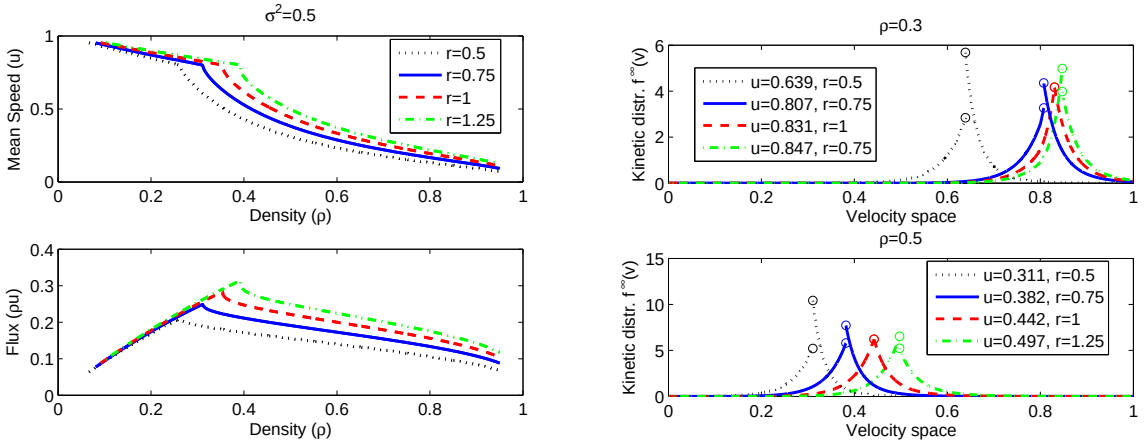

Figure 5.6: Left panels: macroscopic diagrams of traffic using the desired speeds (5.31). We take $\sigma^2 = 0.5$, $\Delta v = 0.2$ and we study the dependence on the parameter r. Right panels: equilibrium distributions for $\rho = 0.3$ (top) and $\rho = 0.5$ (bottom). The circles define the values $f(v)$ for $v \to u^-$ and $v \to u^+$.

of densities. The dispersion of data becomes small at low and high densities and this is in accordance with experimental data.

We stress the fact that the kinetic theory allows us to explain both the theoretical and the experimental fundamental diagrams in terms of microscopic rules. In fact, on the one hand, with the the desired speeds (5.28) we reproduce the heuristic closure laws used in the macroscopic modeling, as for instance the Greenshields' law, see Proposition 5.7. On the other hand, the desired speeds (5.31) allow us to reproduce well experimental data.

Let us focus first on the free-flow phase. This regime occurs at low densities, i.e when the road is not congested, thus there is a large distance among the vehicles, the interactions are rare and the velocity of the flow can be high. In Figure 5.6 we observe that the flux increases nearly linearly with respect to the density of vehicles and the dispersion of the data is small. Nevertheless, the average velocity of the vehicles does not coincide with the maximum allowed speed. In fact, looking at the speed-density diagrams, we note that the macroscopic speed decreases as the density increases. This means that the model does not provide stationary solutions being Dirac delta centered in the maximum speed $V_{\max}$ when the density is less than a fixed value, see e.g. the quantized steady state distributions analytically computed in [75] and in Section 3.3 for the δ model, see Theorem 3.4 and Theorem 3.9. This result seems to be coherent with the experience because one tends to travel at the maximum speed only in really free road conditions while the velocity is reduced as the number of vehicles on the road increases. However, observe that, as we expect, the decrease of the mean speed is not so fast to cause a decrease of the average flux.

Now, let us focus on the congested phase of traffic. In this regime the road becomes progressively jammed, thus the interactions among the vehicles are more frequent and drivers tend to control their velocity with respect the speed of the flow which is forced to

decrease due to the large number of vehicles. As a consequence, in Figure 5.6 we observe that the flux decreases as the density of the vehicles increases because of a drastic reduction of the mean speed. Moreover, there is a range of densities in which it is evident that we can obtain scattered values in the flux-density plane. However, as the road becomes jammed, the possible scattering reduces because the distance between the equilibrium curves reduces, see for instance the speed-density diagram in Figure 5.6. This is consistent with the daily experience of driving on highways, because in congested flow all vehicles tend to travel at the same speed.

Finally, notice that, for increasing values of r, the diagrams provided by the present kinetic model reproduce naturally the phenomenon of the capacity drop, that is the sharp decrease of the flux across a density value. In fact, it is possible to identify the so-called critical density in which there is a phase transition between the free and the congested regimes.

The above descriptions are totally in agreement with the analysis of the experimental diagrams provided in Section 2.2 or e.g. in [46, 76].

5.4.3 The role of r and comparisons with data

Since the aim of this chapter is to investigate the dependence between the structure of fundamental diagrams and the microscopic dynamics, in this section we propose comparisons with experimental data. To this end, we also analyze the role of the free parameter r, which parametrizes the family of equilibrium distributions f^∞, and we show that it is the key to reproduce multivalued diagrams.

We recall from equation (5.23) that r is not easily recognized as a physical parameter, because it gives information on the regularity of f^∞ at $v = u$. In fact, r is the ratio between the two integration constants arising from the solution of the ODE (5.21). Therefore, we need to give a recipe in order to choose the parameter and to understand whether we can associate different values of r to the same flow.

To this end, in the following, although it seems that the scattering of data is due only to a mathematical fact, we prove that r can actually be linked to observable/measurable macroscopic quantities of the flow. Start from the quantity $R(u)$ given in (5.27). We observe that it is a function also of the density ρ and of the parameter r when they are not fixed a priori. In fact, as discussed at the beginning of Section 5.4, applying the constraint (5.24) and assuming that f^∞ is parametrized by the ratio (5.23), we find the expressions (5.25) of the two integration constants. Then, the quantity R given in (5.27) can be written as

$$R(u, \rho, r) = \frac{r\rho}{r\rho^- + \rho^+} R_A(u, \rho) - \frac{\rho}{r\rho^- + \rho^+} R_B(u, \rho)$$

where R_A and R_B are defined by (5.30a)-(5.30b) and (5.33)-(5.30b) when the desired speeds are chosen as (5.28) and (5.31), respectively. By Implicit Function Theorem we have that

$R(u, \rho, r) = 0$ defines implicitly a function

$$r = r(u, \rho) = \frac{R_B(u, \rho)}{R_A(u, \rho)} \tag{5.34}$$

in each neighborhood of (u_0, ρ_0, r_0) such that $R(u_0, \rho_0, r_0) = 0$ provided that $u_0 \neq 0$, $u_0 \neq V_{\max}$, $\rho_0 \neq 0$ because in this case one has $\partial_r R(u, \rho, r) \neq 0$. The function (5.34) thus establishes a link between the free parameter r and the macroscopic quantities of traffic.

Experimental data show several values of the mean speed u at equilibrium for the same value of the density ρ, correspondingly the relation (5.34) states that, for any fixed ρ, there exist more values of r related to the same flow. Therefore, the analytical origin of the multivalued region is explained here by the presence of a family of equilibrium solutions parametrized by r. The parameter r is the degree of freedom (in addition to ρ) being necessary to equilibrium in order to describe the dispersion of data. In other words, we can think that r synthesizes the different properties of the flow (as the composition of the traffic flow or the structural characteristics of the road) which induce different macroscopic dynamics for a given value of the density ρ. For instance, comparing this result with our multi-population models [74, 76] (see Chapter 2 and Chapter 4), we can suppose that r takes into account the heterogeneous composition of the vehicles on the road.

In Figure 5.7 we compare the diagrams obtained using the desired speeds (5.31) and the experimental measurements provided on a USA highway by the Minnesota Department of Transportation in 2003 (left panel), kindly granted by Seibold et al. [79], and in Viale del Muro Torto in Rome (Italy) (right panel), see the review [70]. We focus only on the modeling (5.31) of the desired speeds because the structure of the diagrams resulting from this choice is totally in agreement with experimental data. In order to choose r using the data we first individuate a density ρ and we select from the experimental diagram all values of the flux q at equilibrium corresponding to the fixed ρ. Then we compute the mean speed $u = q/\rho$, so that we can evaluate the relation (5.34) for each pair (u, ρ) in order to determine r. Finally, we plot the corresponding "theoretical" diagrams.

More precisely, in both panels of Figure 5.7 we fix two values of the normalized density $\rho = 0.2, 0.8$, taking as maximum density in the right panel $\rho_{\max} = 250$ vehicles per kilometer. For each of the two densities we consider three flux values, the maximum $q_1 = \max(q(\rho))$, the minimum $q_2 = \min(q(\rho))$ and finally the mean value $q_3 = (q_1 + q_2)/2$. The intersections of the green dashed lines individuate the pairs of data $(\rho = 0.2, q_i)$, $i = 1, 2, 3$, while the intersections of the blue dashed lines individuate the pairs of data $(\rho = 0.8, q_i)$, $i = 1, 2, 3$. For each pair of data the normalized mean speed is computed as $u = q/(\rho u_{\max})$ where $u_{\max}$ is the maximum speed and is approximated with the linear interpolation of the free flow regime. Finally, the pairs (u, ρ) define three values of the parameter r for each fixed density by means of equation (5.34). The green diagrams are related to $\rho = 0.2$, while the blue diagrams are related to $\rho = 0.8$. We observe that there is a remarkable correspondence between the "theoretical" and the experimental diagrams. In fact, the equilibrium curves provided by the present kinetic model reproduce on the whole the structure of the experimental data, included the scattering, both in the free and the congested regime. This means that, in addition to explaining the dispersion with the

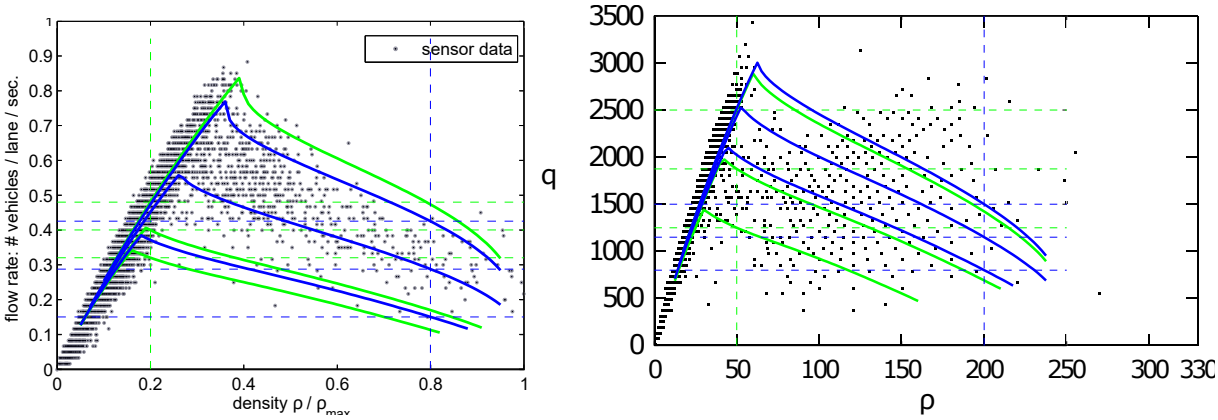

Figure 5.7: Comparison between the diagrams provided by the present kinetic model with desired speeds (5.31) and the experimental diagrams provided by kind permission of Seibold et al. [79] (left panel) and experimental data collected in one week in Viale del Muro Torto, Rome (Italy), from [70] (right panel). The parameters of the model are set as $\sigma^2 = 0.5$ and $\Delta v = 0.2$. The green curves are related to the density $\rho = 0.2$, while the blue curves are related to the density $\rho = 0.8$. The free parameter r is computed using the relation (5.34).

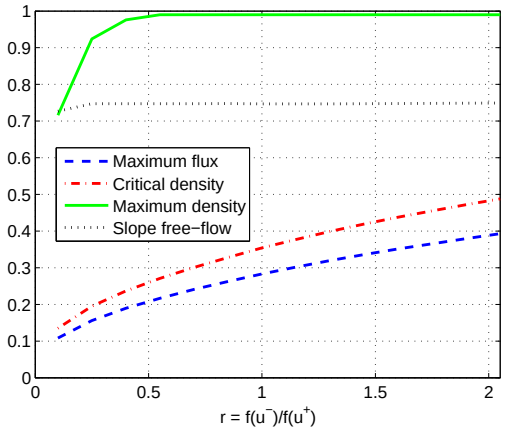

Figure 5.8: Monotone relation between the ratio $r = \frac{f^\infty(u^-)}{f^\infty(u^+)}$ and the maximum flux (blue dashed line), the critical density (red dot-dashed line), the maximum density (green solid line), the slope in the free-flow regime (black dotted line).

variability of r, the microscopic model is already endowed with the other physical characteristics of traffic, included the phase transition. We stress that we do not interpolate the data. We have only one degree of freedom and the remaining features are explained by the model itself.

Finally, in Figure 5.8 we show the relation holding between the parameter r and some macroscopic quantities: precisely, the maximum value of the flux (blue dashed line), the value of the critical density (red dash-dotted line), the maximum value of the density (green solid line) and the slope of the free flow branch (black dotted line). We observe an increasing monotone dependence which allows us to state that only a limited range of

values for r can be admissible. In fact, for example, for larger r the critical density becomes too high when compared to that provided by experimental data.

Chapter 6

Conclusions, applications and perspectives

6.1 Summary

This thesis was devoted to introducing mathematical models for traffic flow based on kinetic theory. The starting aim was to propose a model which, on one hand, improves some characteristics of already existing models and, on the other hand, is suitable for mathematical investigations.

In details, the most important achievements can be summarized as follows (with reference to the scheme in Figure 1):

- **Introduction of a multi-population kinetic model for traffic flow based on the single-population model of Fermo and Tosin [26]:** in Chapter 2, we describe a kinetic model for vehicular traffic with a new structure which accounts for the heterogeneous composition of traffic flow. Our approach differs from standard kinetic models in that we consider two distribution functions describing two classes of vehicles with different physical features, in this case the typical length of a vehicle and its maximum speed.

  As in [26], which inspired the present model, we have assumed a discrete space of microscopic speeds and we have expressed vehicle interactions in terms of transition probabilities among the admissible speed classes. We have then used our two-population kinetic model to derive the fundamental diagrams predicted by the simulated dynamics. Even with a small number of microscopic speeds, such diagrams feature a structure closely resembling experimental data. In particular, they are characterized by a marked phase transition: at low vehicle densities (free flow) the flux increases almost linearly with small standard deviation, while beyond a critical density the flow decreases taking widely scattered values (congested flow). We also wish to note that the model is very simple: the complexity of a real flow is clustered in the characteristics of only two distinct populations, with a very small number of microscopic velocities.

Several authors have dealt with this problem, cf. e.g., [26, 79]. In particular, in [26] this phenomenon is explained by invoking the uncertainty of the drivers' behavior in terms of standard deviation of the statistical distribution of speeds at equilibrium. However, such an approach predicts a zero standard deviation in the free phase of traffic and furthermore interprets the scattered distribution of the data in the congested phase as a consequence of the variability of the microscopic speeds at equilibrium. In our case, instead, we have not only recovered the sharp phase transition, which seems to result naturally from our kinetic approach, but we have also obtained the scattered behavior at a genuinely macroscopic level as a consequence of the fact that a given road occupancy can be obtained with different compositions of the mixture. In other words, if the flux is given as a function of the number of vehicles crossing a section of road in a unit time, then our model indicates that the scattering may be due to the simultaneous presence of different types of vehicles. On the other hand, in the congested phase the mean speed of the vehicles seems to depend only on the degree of congestion of the road.

From a mathematical point of view, we have shown that our two-population model satisfies an indifferentiability principle, which makes it consistent with the original single-population model [26] when the particles composing the mixture share the same physical characteristics (in our case the vehicle length and maximum speed). This property, enforced in [3], is not trivial, and several kinetic models for gas mixtures possess it only at equilibrium [33, 34]. Moreover, by means of an analysis of the equilibria of the system we have also computed the critical density at which the transition occurs showing that it depends on the probability of acceleration.

These results were published in [76].

- **Introduction of a kinetic model based on a continuous-velocity space having an explicit expression of the stationary distribution:** since the hypothesis of a lattice of speeds is artificial, and moreover the model [26] does not converge as the lattice approaches a continuous distribution, in Chapter 3 we have studied two kinetic models for vehicular traffic based on a continuous space of microscopic speeds. We have assumed a Boltzmann-like framework describing binary interactions and we have analyzed the space homogeneous case to study the asymptotic behavior of the distribution function together with the resulting flux-density diagrams.

  In contrast to the lattice-velocity approach of [26], these models are characterized by a parameter Δv, that has physical relevance and is related to the maximum speed variation of a vehicle in a unit of time. The two models are defined by the transition probability of gaining a certain velocity and they differ only in the modeling of the acceleration interaction.

  First of all we have studied the case in which the resulting speed after an acceleration is obtained by a velocity jump from v_* to $v_*+\Delta v$, where v_* is the pre-interaction speed. We have referred to this model as δ model and we have found a class of asymptotic distributions which is atomic with respect to the velocity variable. In other words

it is a linear combination of Dirac delta functions centered in a finite number of velocities. The number T of delta functions contributing to the stable equilibrium distribution is controlled by the acceleration parameter through the relation $T = V_{\max}/\Delta v$. In other words, the velocities which really are important at equilibrium are those spaced by Δv. This result means that the number of discrete velocities necessary to completely describe the equilibrium distribution function is implicitly determined by the acceleration parameter Δv. The main consequence of this result is that there is a connection, at equilibrium, between the continuous-velocity δ model and a discrete-velocity one which however, in contrast to the model [26], is more robust because the distance of two adjacent velocities in the discrete lattice now has a physical meaning. Observe that, in turn, this means that we are able to compute the asymptotic distribution numerically with only *few* velocities in the grid, i.e. without the need of integrating the kinetic equation in the limit. This fact makes the model efficient from a numerical point of view.

Our numerical investigations have suggested also that the class of quantized equilibria is unique. In fact, since we have discretized the kinetic equation using a piecewise constant reconstruction, our scheme would be capable to compute absolutely continuous steady states, but as a matter of fact only quantized ones were found.

Instead, in the second model (χ model) we have prescribed the acceleration interaction in a way that is closer to the modeling given in [48], but again respecting the physical relevance of Δv. In fact, we have assumed that the output speed after acceleration is uniformly distributed over the range $[v_*,\, v_* + \Delta v]$. We have shown that the χ model with acceleration parameter Δv gives a macroscopic behavior similar to the one provided by the simpler δ model with acceleration parameter $\Delta v/2$, as it can be seen by studying the macroscopic properties of the two models and comparing their fundamental diagrams, notwithstanding the fact that the respective asymptotic distribution functions do not approach each other. Thus the χ model, despite the more sophisticated description of interactions, gives the same macroscopic information of the simpler and computationally much cheaper δ model, at least at equilibrium. We have proved that both models provide a bounded macroscopic acceleration, studying the evolution in time of the macroscopic velocity, and its relation with the parameter Δv.

The results obtained suggest that the quantized acceleration is sufficient for the kinetic modeling of traffic. This is crucial to make kinetic modeling of complex traffic flows amenable to computations. Note also that here the acceleration remains controlled by Δv. . Moreover the complete knowledge of the equilibrium distribution is crucial to derive macroscopic models with a rich enough closure law resulting naturally as consequence of the microscopic interactions. Thus, without the need of prescribing heuristic speed-density relations, we obtain fundamental diagrams with a phase transition and a capacity drop as those occurring in experimental data.

These results were proposed in the submitted paper [75].

- **Generalization of the δ model to a multi-population framework:** the particular structure of the equilibrium distribution provided by the δ model in Chapter 3 allows one to generalize this framework to richer models which describe the complex nature of traffic flow. For instance, in Chapter 4, we have considered the case of a multi-population model, since we have observed in Chapter 2 that the description of traffic flow as a mixture of more classes of vehicles allows us to reproduce multivalued fundamental diagrams.

  In fact, the aim was to refine the construction of the multi-population kinetic model introduced in Chapter 2 based on a discrete space of microscopic speeds in order to make it more amenable to a sound physical interpretation and to mathematical analysis. We have generalized the single-population δ model, introduced in Chapter 3, to the case of more than one class of vehicles. In particular, we have considered continuous and bounded velocity spaces and we have introduced a fixed parameter Δv^{p} to account for the physical velocity jump undergone by a vehicle belonging to the class p that increases its speed. The types of vehicles are characterized by few microscopic features, again the typical length of a vehicle and the maximum speed. After modeling the collision terms describing the acceleration and the slowing down interactions, we have proved that the model satisfies the indifferentiability principle at all times, which makes it consistent with the original δ model when all vehicles have the same physical characteristics.

  Next, taking advantage of the results provided in Chapter 3, we have discretized the model in order to investigate numerically the asymptotic kinetic distributions. Again, the structure of the equilibrium solutions of the δ models is formed: the equilibrium distributions approach a series of delta functions centered on a finite number of velocities. More precisely, these velocities are integer multiples of the minimum $\min_{\mathsf{p}} \Delta v^{\mathsf{p}}$. It is worth stressing that the knowledge of the equilibrium distributions is crucial for both the study of average characteristics of traffic, such as the flux- and the speed-density relations, and for the derivation of macroscopic equations from the kinetic approach, because the richer closure law provided by the kinetic approach can be used. For instance, one can consider a system of first order macroscopic equations describing the evolution of the density of each population, as in [7] but using the closure provided by the kinetic model.

  We have also studied the analytical properties of the system of ordinary differential equations resulting from the discretization of the continuous-velocity model. We have proved the well-posedness of the Cauchy problem, in the sense that the solution exists, is unique, depends continuously on the initial data, and moreover remains non-negative and bounded by the initial mass. In addition to that, we have provided the explicit formulas for the equilibrium distribution functions which define the fundamental diagrams. Equilibria are uniquely determined by the total initial mass and the proportion of the vehicles of each class.

  We notice that these results are very close to those of [74], but here we modified the

interaction rules in order to make the model consistent with the δ model discussed in Chapter 3 when populations have the same microscopic characteristics.

- **Investigation of the multiscale dynamics in traffic flow:** in Chapter 5, starting from interaction rules derived from those introduced in [41] and in Chapter 3, we have computed a Fokker-Planck model for traffic flow as the grazing collision limit of a Boltzmann-type model. This approximation allows to retain the principal part of the microscopic interactions while making the Boltzmann-type equation more amenable to analytical investigations. In particular, we have aimed at analyzing the influence of the microscopic interactions on the collective dynamics of the flow. To this end, we have proposed microscopic behavioral rules affected by the macroscopic average conditions of traffic, thereby establishing a feedback between the small and the large scales of the phenomenon. The Fokker-Planck approximation allows to compute easily the asymptotic time-distribution of the model for a general set of rules which are completely defined once the desired speeds are chosen. In particular, we have considered three different modeling of the desired speeds: the first one preserves the synchronized traffic states (studied here also by means of a Monte-Carlo simulation), the second one links the microscopic probability of accelerating to the macroscopic relations (for example the Greenshields' closure law [32]) and finally the third one leads to fundamental diagrams which have the same qualitative properties of experimental data.

  The model permits also to reproduce the multivalued structure of experimental diagrams. The mathematical key allowing for the scattering of the flux values is the existence of a one-parameter family of stationary distributions. We have shown that the positive parameter which singles out one of the possible distributions has a strong link with the macroscopic properties of the flow, in particular the density and the mean speed of vehicles.

  These results were proposed in the submitted paper [85].

6.2 Macroscopic model with kinetic closure

As already anticipated in the Introduction (see the scheme in Figure 1), the results of this thesis permit to derive closure laws for macroscopic equations of vehicular traffic which are not based on heuristic or empirical considerations. In fact, the equilibria of the models proposed in this thesis can be written explicitly, and therefore we have a sort of Maxwellian equilibrium distribution, which can be exploited to find a closure law at the macroscopic level, moreover without the need of computing the evolution to equilibrium of the kinetic model. Since the kinetic closure laws provide fundamental diagrams which have remarkable correspondence with experimental data, we can use the results of this thesis to propose a new macroscopic model, based on the "Maxwellian" distribution we have found and we expect to obtain simulations which reproduce accurately the dynamics of traffic.

Consider the case of a single population of vehicles and the following first order equation

$$\partial_t \rho(t,x) + \partial_x(\rho u)(t,x) = 0, \tag{6.1}$$

where, as usual, ρ, u and (ρu) are the density, the mean speed and the flux, respectively. From Section 1.2 we know that equations of type (6.1) require to be closed with a relation which prescribes the mean speed u as a function of the density ρ.

The knowledge of the analytical expression of the asymptotic distribution provided by our kinetic models permits to assign the fundamental relations without using the heuristic laws discussed in Section 1.2. In fact, in the kinetic theory, macroscopic diagrams arise naturally from a statistical approach based on a detailed characterization of the microscopic behaviors. Thus the closure can be directly derived by means of the time-asymptotic distribution f^∞ of the δ kinetic model introduced in Chapter 3 defining the following map:

$$\rho \mapsto u(\rho) = \frac{1}{\rho}\int_{\mathcal{V}} v f^\infty(x,v)\mathrm{d}v. \tag{6.2}$$

We notice that the fundamental relations provided by our kinetic model have two main properties:

1. they are continuous: in fact, from Theorem 3.9 it is clear that

$$\lim_{P\to\frac{1}{2}^+}\int_{\mathcal{V}} v f^\infty(x,v)\mathrm{d}v = \lim_{P\to\frac{1}{2}^-}\int_{\mathcal{V}} v f^\infty(x,v)\mathrm{d}v = \rho_c V_{\max},$$

   where ρ_c is the density value such that $P(\rho_c) = 1/2$. Thus, there is no need to treat the macroscopic model (6.1)-(6.2) with suitable techniques for conservation laws with discontinuous fluxes;

2. the flux-density diagram is not convex: in fact, it is linear in the free flow regime (i.e when $\rho \le \rho_c$) and it is convex in the congested regime (i.e when $\rho > \rho_c$), see the two-phase fundamental diagrams provided in Section 3.5.

The non-convexity of the flux-density diagram represents the most interesting property because it permits to obtain solutions different from those based on the classical closure laws. In fact, when the flux is convex, the solution to a Riemann problem is always either a shock or a rarefaction wave. In contrast, when the flux is not convex, the entropy solution might involve both. In a general situation, if the flux has more inflection points, then the solution might involve several shocks and rarefactions. In order to solve a Riemann problem, we use the same considerations performed by Leveque [56]. However, see also Bressan [12] for a more rigorous and detailed treatment. In fact, as investigated in [12, 56], the solution of a Riemann problem can be easily determined from the graph of the flux function by constructing the convex hull of the set

$$\mathcal{S}_{RL} = \left\{(\rho, y) \in \mathbb{R}^2 :\ \rho_R < \rho < \rho_L,\ y < \rho u(\rho)\right\}, \tag{6.3}$$

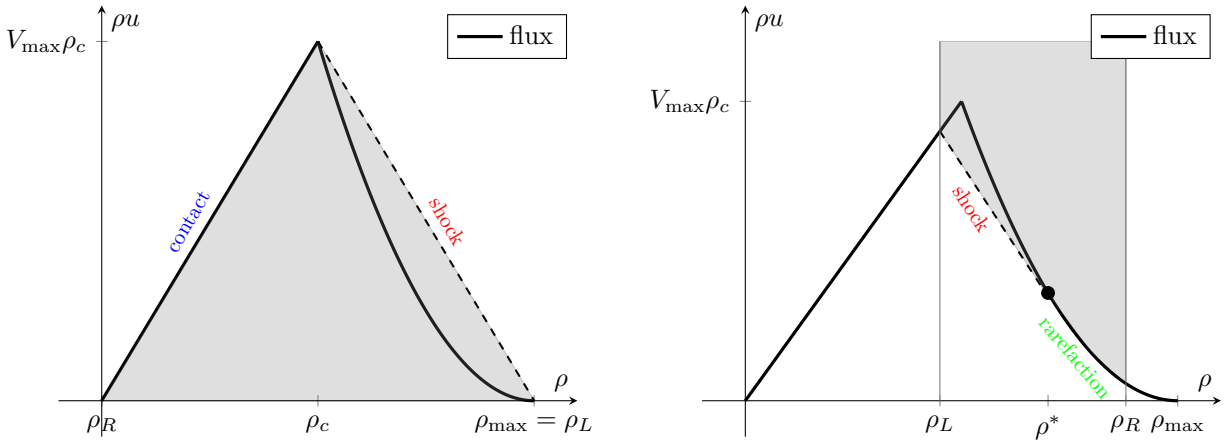

Figure 6.1: Solution of Riemann problems in the cases $\rho_R < \rho_L$ (left) and $\rho_L < \rho_R$ (right). The shaded area represent the convex hulls of the sets $\mathcal{S}_{RL}$ and $\mathcal{S}_{LR}$, respectively

when the initial states are such that $\rho_R < \rho_L$. Otherwise, when $\rho_L < \rho_R$ the convex hull of the set

$$\mathcal{S}_{LR} = \left\{(\rho, y) \in \mathbb{R}^2 : \ \rho_L < \rho < \rho_R, \ y > \rho u(\rho)\right\} \tag{6.4}$$

has to be considered. Then, shock waves correspond to the straight line portions of the boundary of the convex hulls which may not coincide with the flux function; while rarefaction waves and contact discontinuities correspond to the portions of the boundary of the convex hulls which coincide with the flux function.

To illustrate the phenomenon of the non-convexity of the flux function, in the following we focus on two Riemann problems involving two physical situations in traffic flow.

Starting from a traffic light. In the left panel of Figure 6.1 we consider the Riemann problem with initial states $\rho_L = \rho_{\max}$ and $\rho_R = 0$ that represents the density of vehicles on a road when a traffic light becomes green and vehicles in the queue can accelerate into an empty road. Since $\rho_R < \rho_L$, the solution to the Riemann problem can be determined by considering the convex hull of the set (6.3), that is the smallest convex set containing the set defined by the flux function. The upper boundary of $\mathcal{S}_{RL}$ follows the linear part of the flux function up to $(\rho_c, \rho_c u(\rho_c))$, i.e. in the free-flow regime, and then is composed of a straight line segment linking the point $(\rho_c, \rho_c u(\rho_c))$ to $(\rho_{\max}, 0)$. Since the flux function is linear for $\rho \leq \rho_c$, the segment where the boundary of $\mathcal{S}_{RL}$ follows the diagrams produces a contact discontinuity propagating at the maximum speed of vehicles $V_{\max}$. In fact, from the equilibrium distribution of the kinetic model it follows that the linear branch of the flux function increases as $\rho V_{\max}$. Instead, the straight line of the boundary of $\mathcal{S}_{RL}$ represents a shock with negative speed. Thus, the solution is composed by two waves: a backward propagating shock wave jumping from ρ_L to ρ_c and a contact discontinuity connecting ρ_c to ρ_R. Thus the critical density ρ_c plays the role of the post-shock intermediate state.

In the top panels of Figure 6.2 we show the solution obtained solving numerically the first order macroscopic equation with the Greenshields closure (left) and the Aw-Rascle

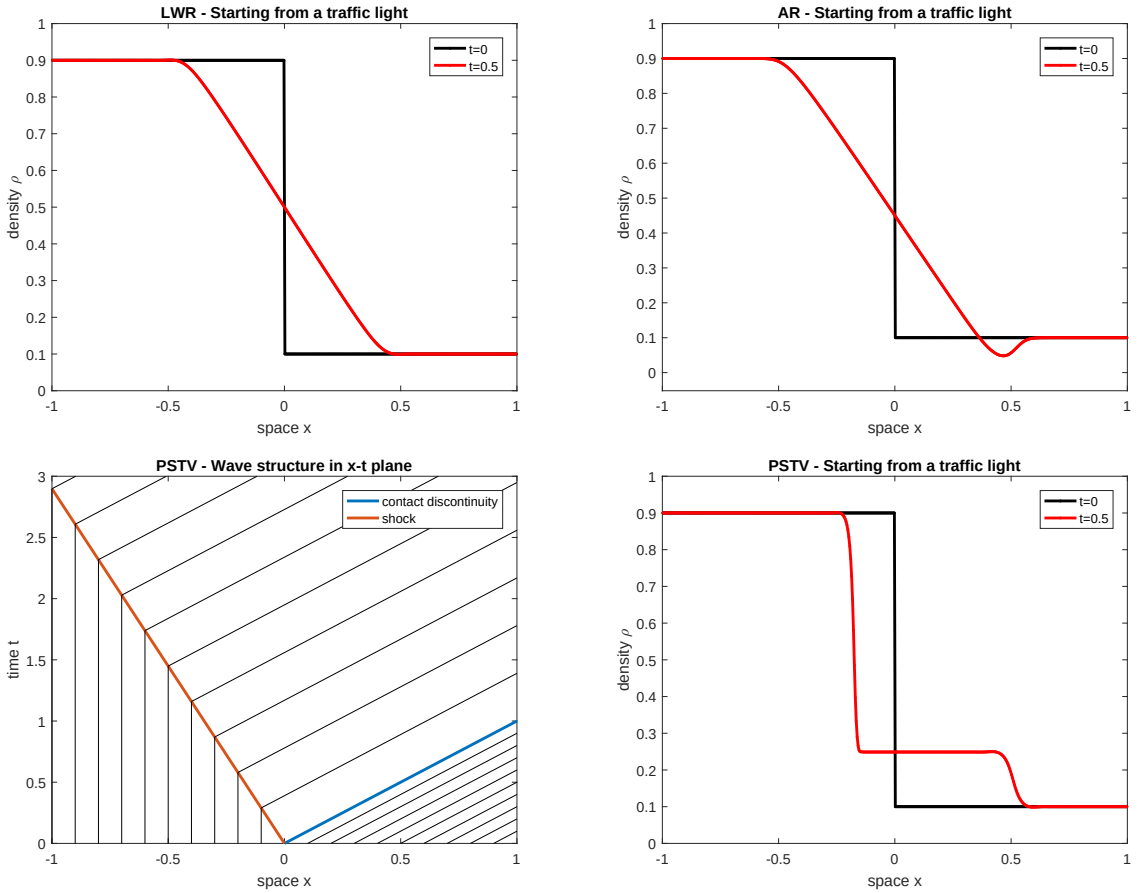

Figure 6.2: Starting from a traffic light solution obtained with the LWR first order model [59, 77] (top left), with the Aw and Rascle second order model [5] (top right) and with the macroscopic first order model (6.1) using the kinetic closure (6.2) derived in this thesis (bottom right). The bottom left panel shows the wave structure.

second order model (right), using a firs order finite volume scheme. While in the bottom panels we show the characteristics (left) and the solution (right) provided by the model (6.1) using the kinetic closure. We choose the initial states $\rho_L = 0.9$ and $\rho_R = 0.1$. The solution is characterized by a shock wave followed by a contact discontinuity. In particular, the shock wave would represent a sudden acceleration of vehicles when the traffic light becomes green. We notice that the structure of this solution can be reproduced by Daganzo's closure [18], see Figure 1.1d. However, the lack of experimental data does not make possible the validation of this type of solution.

Formation of a queue. We consider the Riemann problem with initial states $0 < \rho_L < \rho_c < \rho_R < \rho_{\max}$. The same idea of the previous case works but now we look instead at the convex hull of the set of points above the flux function, see equation (6.4). According to the values of ρ_L and ρ_R the convex hull construction can give three different solutions: a single shock with positive speed, a single shock with negative speed, or a shock with

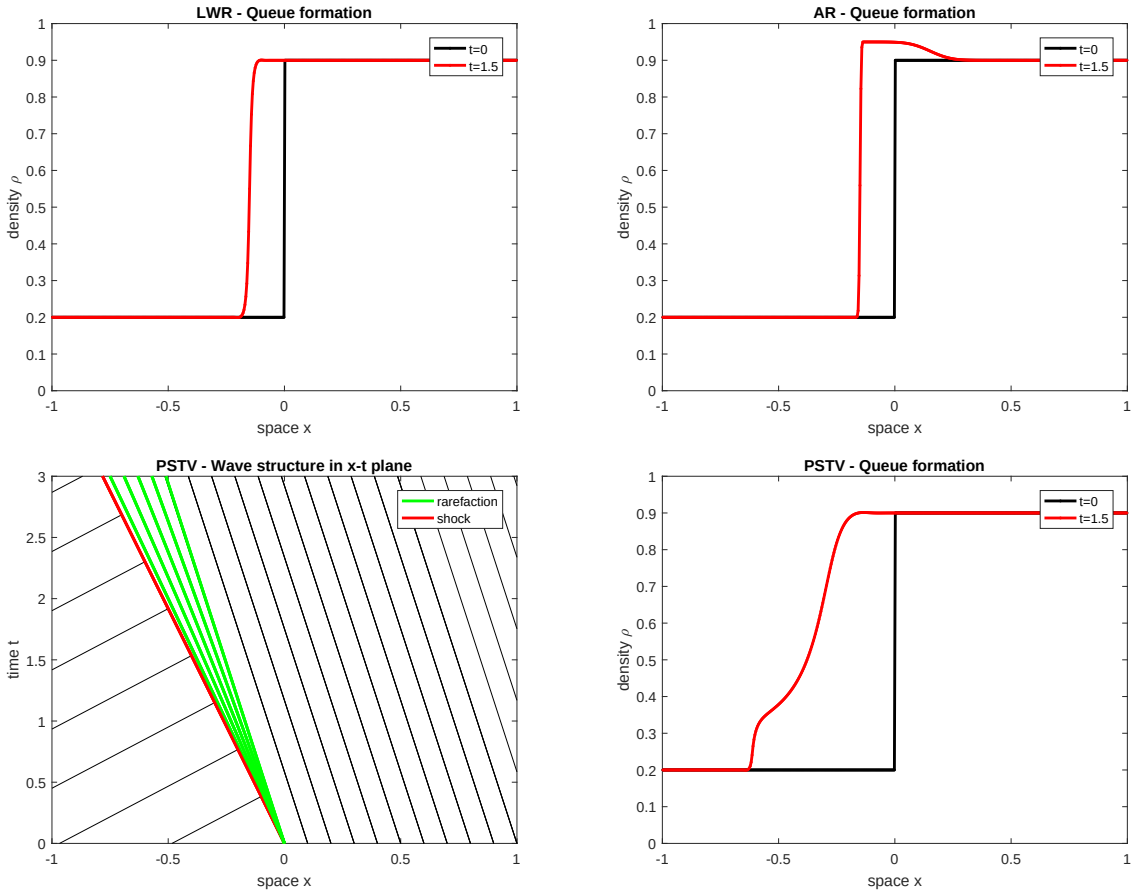

Figure 6.3: Formation of a queue solution obtained with the LWR first order model [59, 77] (top left), with the Aw and Rascle second order model [5] (top right) and with the macroscopic first order model (6.1) using the kinetic closure (6.2) derived in this thesis (bottom right). The bottom left panel shows the wave structure.

negative speed followed by a rarefaction wave. In the right panel of Figure 6.1 we show the latter case in which the dashed line segment represents the shock linking ρ_L to the intermediate state ρ^*, which is located at the point where the convex hull is tangent to the flux function. In the region between ρ^* and ρ_R, the solution is a rarefaction wave following the flux function itself.

In the bottom panels of Figure 6.3 we show the characteristics (left) and the solution (right) provided by the model (6.1) using the kinetic closure with initial data $\rho_L = 0.2$ and $\rho_R = 0.9$. The shock represents a sudden braking (when drivers perceive ahead the congestion of the road), which then becomes weaker inducing the rarefaction wave. Again, in the top panels we show the solution for the classical first and second order macroscopic models, obtained with a first order finite volume scheme.

The above analysis can be easily applied in order to solve all possible Riemann problems arising from equation (6.1) with the non-convex flux function derived from the map (6.2). In Figure 6.4 we summarize all the possible cases.

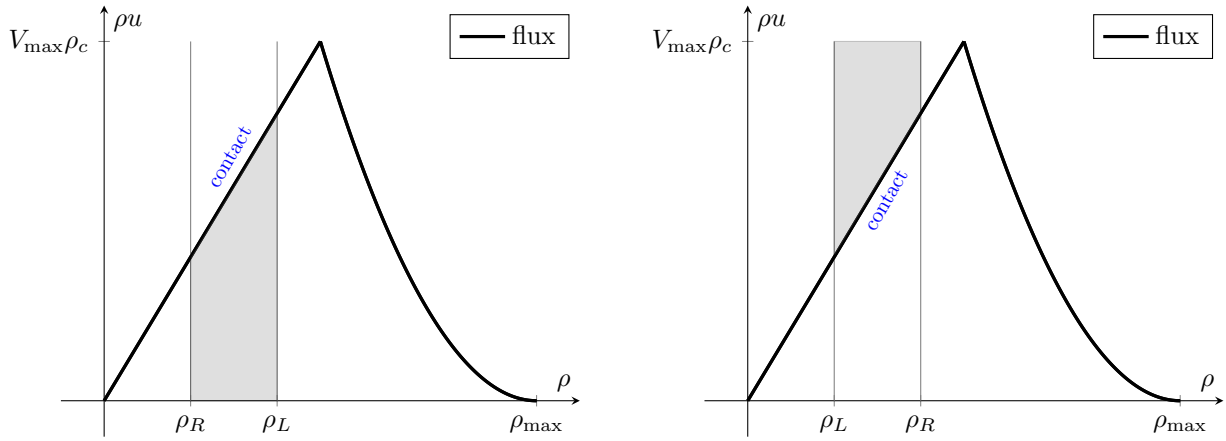

(A) $\rho_R < \rho_L < \rho_c$ (left) and $\rho_L < \rho_R < \rho_c$ (right).

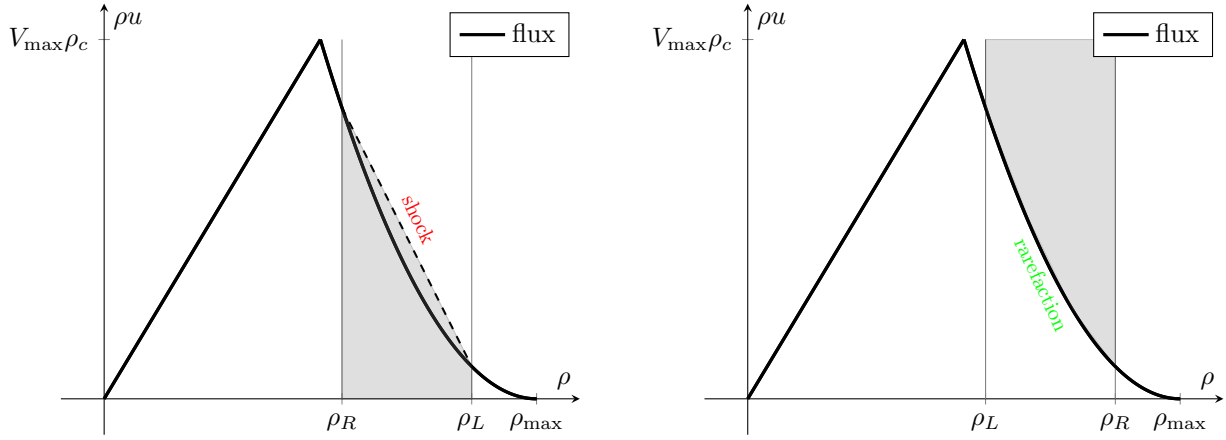

(B) $\rho_c < \rho_R < \rho_L$ (left) and $\rho_c < \rho_L < \rho_R$ (right).

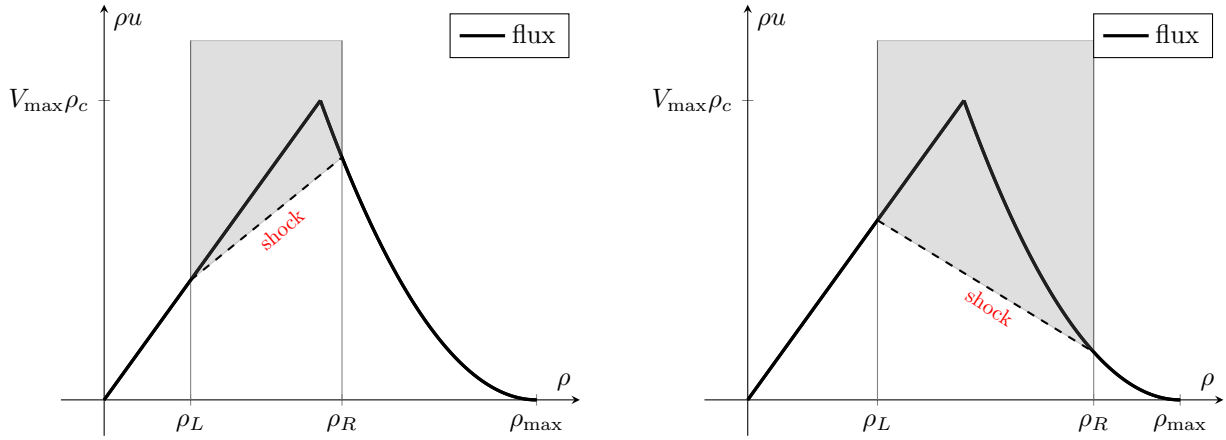

(C) $\rho_L < \rho_c < \rho_R$ with $(\rho u)_L < (\rho u)_R$ (left) and $\rho_L < \rho_c < \rho_R$ with $(\rho u)_R < (\rho u)_L$ (right).

Figure 6.4: Solutions of Riemann problems. The shaded area represent the convex hulls.

The numerical solutions of the macroscopic model with the kinetic closure (see the bottom-right panels of Figure 6.2 and Figure 6.3) are computed with the one-dimensional third order CWENO scheme [58]. In contrast to the WENO schemes [45, 80], the CWENO methods are characterized by the uniform accuracy in the whole computational cell, which makes them particularly suited for integrating balance laws. In this context, the CWENO third order scheme is performed in order to reproduce well the wave structure of the solutions, as for instance the contact discontinuity in the bottom-right panel in Figure 6.2.

We wish to stress that, in addition to traffic flow models, we have introduced CWENO schemes of arbitrary order in [17], in which the analysis of very high order CWENO reconstructions is proposed.

6.3 Future perspectives

In our opinion, this thesis and the previous section open up several research perspectives.

Multi-population macroscopic model with kinetic closure. First of all, we notice that the macroscopic equation (6.1), expressed for a single-population of vehicles, can be generalized to the case of multiple populations, thus considering a system of first order equations of the type

$$\partial_t \rho^{\mathsf{p}}(t,x) + \partial_x (\rho u)^{\mathsf{p}}(t,x) = 0, \tag{6.5}$$

where the index p labels the different class of vehicles. In this case, one can consider the closure derived from the multi-population kinetic model introduced in this thesis. We recall that, as in the single-population case, we are able to compute also the analytical expression of the equilibrium distributions in the case of multiple populations. Thus, the closure law can be expressed explicitly and used for solving the macroscopic equation (6.5) without the need of computing the steady-state of the kinetic model at each time. In this context, comparisons with the multi-population macroscopic model of Benzoni-Gavage and Colombo [7] can be performed.

Inhomogeneous kinetic models. The natural sequel of this work would be the extension of the single- and multi-population kinetic models proposed in this thesis to the spatially inhomogeneous case. Compared to the spatially homogeneous case studied in this thesis, this extension would allow to analyze non-equilibrium effects in the dynamics of traffic, which for instance might shed light on the structure of shocks and contact discontinuities exhibited by the solutions of the macroscopic Riemann problems studied above, and the phenomenon of the stop&go waves. To this end, both numerical and modeling difficulties have to be tackled.

We think that the study of inhomogeneous kinetic models is necessary because they are able to simulate traffic dynamics out of equilibrium. We stress the fact that, in contrast, macroscopic models reproduce traffic situations assuming that the flow is at equilibrium.

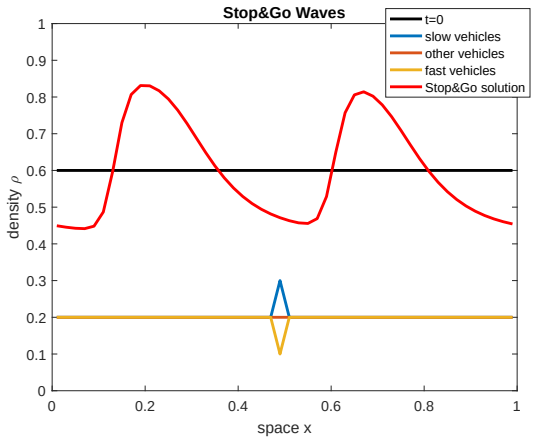

Figure 6.5: Stop&go wave solution provided by our spatially inhomogeneous kinetic model.

This assumption may provide non-realistic phenomena, as for instance in the starting from a traffic light considered in Section 6.2. In fact, everyday life experience suggests that the contact discontinuity traveling with the maximum speed of cars should be replaced with a rarefaction wave representing the weaker acceleration following the harder one close to the traffic light. Moreover, we cannot expect that a first order equation is able to reproduce the stop&go wave solution since the maximum principle holds. For these reasons, it would be interesting to derive a spatially inhomogeneous kinetic model based on our modeling of the collision term. This research perspective requires an efficient numerical method to treat the possible stiffness. The backward wave propagation can be obtained rewriting the collision term using non-local interactions, as in Klar and Wegener [49], or using flux limiters in the convective term, as proposed by Fermo and Tosin [25].

We are currently working on the spatially inhomogeneous version of our single-population kinetic model. In particular, the model is based on the splitting of the collision operator in two terms. One describes the local interactions, taking place among vehicles located at the same space position. Instead, the other one describes the non-local interaction and is therefore characterized by the introduction of a parameter describing the physical visibility distance. This parameter allows to model the realistic situation in which drivers react also to the traffic condition ahead. Although this work is in progress, a preliminary analysis seems to show that the model is able to reproduce the stop&go waves. For instance, see Figure 6.5 in which we compute the numerical solution provided by our spatially inhomogeneous single-population kinetic model. At initial time the density is constant in space, $\rho(t = 0, x) = 0.6$, but the center computational cell is characterized by the presence of more slow vehicles, compared to the other cells. This situation produces a perturbation in the flow of vehicles which, in turn, causes the generation of a classical stop&go wave solution.

Multi-lane roads and road networks. Another possible and natural extension of the kinetic models proposed in this thesis is the derivation of new models being able to

describe traffic in multiple lane-roads or a network of roads, thus including also ramps and intersections. These generalizations are crucial for forecasts of traffic flow. The modeling challenge lies in keeping the computational cost of the kinetic model low. In the literature, multilane models were built by considering several kinetic distributions, one for each lane, see for instance [9, 50, 51, 60]. This choice increases the model complexity. We think that the multi-population framework can be successfully used to consider multilane models with a reduced computational cost. The modeling of lane changing might be neglected and the presence of multiple lanes could be taken into account by using the notion of the fraction of occupied space. In fact, one can assume that different classes of vehicles react to different road occupancy depending on the number of lanes that they can occupy, taking into account that some lanes are usually prohibited to certain populations of vehicles.

Multi-population Fokker-Planck models. Finally, concerning the Fokker-Planck model, we think that the less demanding structure when compared to the full Boltzmann-type model provides as a natural sequel the study of a multi-population model based on the mean-field interaction rules prescribed in Chapter 5. In fact, in the approximation that vehicles are affected only by the average properties of the flow, the binary interaction terms of the Boltzmann equations are replaced by simpler mean-field terms for all populations of vehicles. Thus, each equation contains only one collision operator and furthermore equations are coupled only through the macroscopic density ρ and the mean speed u, a fact which permits to keep under control the complexity of the model. On the other hand, we expect to obtain multivalued diagrams as a result of the heterogeneous composition of the flow, as in Chapter 2 and in in Chapter 4, without allowing for discontinuous stationary distributions.

Bibliography

[1] *75 Years of the Fundamental Diagram for Traffic Flow Theory: Greenshields Symposium*, 2011. Transportation Research Board, Circular E-C149.

[2] G. Albi and L. Pareschi, *Binary interaction algorithms for the simulation of flocking and swarming dynamics*, Multiscale Model. Simul., 11 (2013), pp. 1–29.

[3] P. Andries, K. Aoki, and B. Perthame, *A consistent BGK-type model for gas mixtures*, tech. report, Institut National De Recherche En Informatique Et En Automatique, 2001. Rapport de recherche n.4230.

[4] A. Aw, A. Klar, T. Materne, and M. Rascle, *Derivation of continuum traffic flow models from microscopic follow-the-leader models*, SIAM J. Appl. Math., 63 (2002), pp. 259–278.

[5] A. Aw and M. Rascle, *Resurrection of "second order" models of traffic flow*, SIAM J. Appl. Math., 60 (2000), pp. 916–938 (electronic).

[6] M. Bando, K. Hasebe, A. Nakayama, A. Shibata, and Y. Sugiyama, *Dynamical model of traffic congestion and numerical simulation*, Phys. Rev. E, 51 (1995), pp. 1035–1042.

[7] S. Benzoni-Gavage and R. M. Colombo, *An n-populations model for traffic flow*, Eur. J. Appl. Math., 14 (2003), pp. 587–612.

[8] A. V. Bobylev and K. Nanbu, *Theory of collision algorithms for gases and plasmas based on the Boltzmann equation and the Landau-Fokker-Planck equation*, Phys. Rev. E, 61 (2000), pp. 4576–86.

[9] I. Bonzani and L. M. G. Cumin, *Modelling and simulations of multilane traffic flow by kinetic theory methods.*, Comput. Math. Appl., 56 (2008), pp. 2418–2428.

[10] R. Borsche, M. Kimathi, and A. Klar, *A class of multi-phase traffic theories for microscopic, kinetic and continuum traffic models*, Comput. Math. Appl., 64 (2012), pp. 2939–2953.

[11] M. Brackstone and M. McDonald, *Car-following: a historical review*, Transport. Res. F-Traf., 2 (1999), pp. 181–196.

[12] A. Bressan, *Hyperbolic systems of conservation laws. The one-dimensional Cauchy problem*, Oxford University Press, 2000.

[13] S. Brull, V. Pavan, and J. Schneider, *Derivation of a BGK model for mixtures*, Eur. J. Mech. B-Fluid, 33 (2012), pp. 74–86.

[14] C. Cercignani and M. Lampis, *On the kinetic theory of a dense gas of rough spheres*, J. Statist. Phys., 53 (1988), pp. 655–672.

[15] R. M. Colombo, *Hyperbolic phase transition in traffic flow*, SIAM J. Appl. Math., 63 (2002), pp. 708–721.

[16] V. Coscia, M. Delitala, and P. Frasca, *On the mathematical theory of vehicular traffic flow. II. Discrete velocity kinetic models*, Internat. J. Non-Linear Mech., 42 (2007), pp. 411–421.

[17] I. Cravero, G. Puppo, M. Semplice, and G. Visconti, *CWENO: uniformly accurate reconstructions for balance laws.* Submitted. arXiv:1607.07319.

[18] C. F. Daganzo, *The cell transmission model: a dynamic representation of highway traffic consistent with the hydrodynamic theory*, Transport. Res. B-Meth., 28 (1994), pp. 269–287.

[19] ——, *Requiem for second-order fluid approximation to traffic flow*, Transport. Res. B-Meth., 29 (1995), pp. 277–286.

[20] M. Delitala and A. Tosin, *Mathematical modeling of vehicular traffic: a discrete kinetic theory approach*, Math. Models Methods Appl. Sci., 17 (2007), pp. 901–932.

[21] L. Desvillettes, *On asymptotics of the Boltzmann equation when the collisions become grazing*, Transport. Theor. Stat., 21 (1992), pp. 259–276.

[22] R. J. DiPerna and P. L. Lions, *On the Fokker-Planck-Boltzmann equation*, Commun. Math. Phys., 120 (1988), pp. 1–23.

[23] S. Fan, *Data-fitted generic second order macroscopic traffic flow models*, PhD thesis, Temple University, 2013.

[24] S. Fan, M. Herty, and B. Seibold, *Comparative model accuracy of a data-fitted generalized Aw-Rascle-Zhang model*, Netw. Heterog. Media., 9 (2014), pp. 239–268.

[25] L. Fermo and A. Tosin, *A fully-discrete-state kinetic theory approach to modeling vehicular traffic*, SIAM J. Appl. Math., 73 (2013), pp. 1533–1556.

[26] ——, *Fundamental diagrams for kinetic equations of traffic flow*, Discrete Contin. Dyn. Syst. Ser. S, 7 (2014), pp. 449–462.

[27] ——, *A fully-discrete-state kinetic theory approach to traffic flow on road networks*, Math. Models Methods Appl. Sci., 3 (2015), pp. 423–461.

[28] P. Freguglia and A. Tosin, *Proposal of a risk model for vehicular traffic: A boltzmann-type kinetic approach*, Commun. Math. Sci., (2016). Preprint: arXiv:1506.05422.

[29] M. Garavello and B. Piccoli, *Traffic Flow on Networks – Conservation Laws Models*, AIMS Series on Applied Mathematics, American Institute of Mathematical Sciences (AIMS), Springfield, MO, 2006.

[30] D. C. Gazis, R. Herman, and R. W. Rothery, *Nonlinear follow-the-leader models of traffic flow*, Operations Res., 4 (1961), pp. 545–567.

[31] H. Greenberg, *An analysis of traffic flow*, Operations Research, 7 (1959), pp. 79–85.

[32] B. D. Grienshields, *A study of traffic capacity*, Proceedings of the Highway Research Record, 14 (1935), pp. 448–477.

[33] M. Groppi and G. Spiga, *A BGK-type approach for chemically reacting gas mixtures*, Phys. Fluids, 16 (2004), pp. 4273–4284.

[34] B. B. Hamel, *Kinetic model for binary gas mixtures*, Phys. Fluids, 8 (1965), pp. 418–425.

[35] D. Helbing and A. Greiner, *Modeling and simulation of multilane traffic flow*, Phys. Rev. E 55, (1997), pp. 5498–5508.

[36] M. Herty and R. Illner, *On stop-and-go waves in dense traffic*, Kinet. Relat. Models, 1 (2008), pp. 437–452.

[37] ——, *Analytical and numerical investigations of refined macroscopic traffic flow models*, Kinet. Relat. Models, 3 (2010), pp. 311–333.

[38] ——, *Coupling of non-local driving behaviour with fundamental diagrams*, Kinet. Relat. Models, 5 (2012).

[39] M. Herty, C. Kirchner, and A. Klar, *Instantaneous control for traffic flow*, Math. Methods Appl. Sci., 30 (2007), pp. 153–169.

[40] M. Herty, A. Klar, and L. Pareschi, *General kinetic models for vehicular traffic flows and Monte-Carlo methods*, Comput. Methods Appl. Math., 5 (2005), pp. 155–169.

[41] M. Herty and L. Pareschi, *Fokker-Planck Asymptotics for Traffic Flow Models*, Kinet. Relat. Models, 1 (2010), pp. 165–179.

[42] M. Herty, L. Pareschi, and M. Seaid, *Enskog-like discrete velocity models for vehicular traffic flow*, Netw. Heterog. Media, 2 (2007), pp. 481–496.

[43] M. L. L. Iannini and R. Dickman, *Kinetic theory of vehicular traffic*, Am. J. Phys., 84 (2016), pp. 135–145.

[44] R. Illner, A. Klar, and T. Materne, *Vlasov-Fokker-Planck models for multilane traffic flow*, Commun. Math. Sci., 1 (2003), pp. 1–12.

[45] G. S. Jiang and C. W. Shu, *Efficient Implementation of Weighted ENO Schemes*, J. Comput. Phys., 126 (1996), pp. 202–228.

[46] B. S. Kerner, *The Physics of Traffic*, Understanding Complex Systems, Springer, Berlin, 2004.

[47] B. S. Kerner and S. L. Klenov, *A microscopic model for phase transitions in traffic flow*, J. Phys. A, 35 (2002), pp. L31–L43.

[48] A. Klar and R. Wegener, *A kinetic model for vehicular traffic derived from a stochastic microscopic model*, Transport. Theor. Stat., 25 (1996), pp. 785–798.

[49] ——, *Enskog-like kinetic models for vehicular traffic*, J. Stat. Phys., 87 (1997), p. 91.

[50] ——, *A hierarchy of models for multilane vehicular traffic. I. Modeling*, SIAM J. Appl. Math., 59 (1999), pp. 983–1001 (electronic).

[51] ——, *A hierarchy of models for multilane vehicular traffic. II. Numerical investigations*, SIAM J. Appl. Math., 59 (1999), pp. 1002–1011 (electronic).

[52] ——, *Traffic flow: models and numerics*, in Modeling and computational methods for kinetic equations, Model. Simul. Sci. Eng. Technol., Birkhäuser Boston, Boston, MA, 2004, pp. 219–258.

[53] J. P. Lebacque, *Two-phase bounded-acceleration traffic flow model: analytical solutions and applications*, Transport. Res. Record, 1852 (2003), pp. 220–230.

[54] J. P. Lebacque and M. M. Khoshyaran, *A variational formulation for higher order macroscopic traffic flow models of the GSOM family*, Procedia - Social and Behavioral Sciences, 80 (2013), pp. 370–394.

[55] W. Leutzbach, *Introduction to the Theory of Traffic Flow*, Springer, New York, 1988.

[56] R. J. LeVeque, *Numerical methods for conservation laws*, Lectures in Mathematics: ETH Zürich, Birkhäuser, Basel, 1992.

[57] R. J. Leveque, *Balancing source terms and flux gradients in high-resolution Godunov methods: the quasi-steady wave-propagation algorithm*, J. Comput. Phys., 146 (1998), pp. 346–365.

[58] D. Levy, G. Puppo, and G. Russo, *Central WENO schemes for hyperbolic systems of conservation laws*, M2AN Math. Model. Numer. Anal., 33 (1999), pp. 547–571.

[59] M. J. Lighthill and G. B. Whitham, *On kinematic waves. II. A theory of traffic flow on long crowded roads*, Proc. Roy. Soc. London. Ser. A., 229 (1955), pp. 317–345.

[60] M. Lo Schiavo, *A personalized kinetic model of traffic flow*, Math. Comput. Modelling, 35 (2002), pp. 607–622.

[61] A. R. Méndez and R. M. Velasco, *Kerner's free-synchronized phase transition in a macroscopic traffic flow model with two classes of drivers*, J. Phys. A: Math. Theor., 46 (2013).

[62] P. Nelson, *A kinetic model of vehicular traffic and its associated bimodal equilibrium solutions*, Transport. Theor. Stat., 24 (1995), pp. 383–409.

[63] S. Noelle, N. Pankratz, G. Puppo, and J. Natvig, *Well balanced finite volume schemes of arbitrary order of accuracy for shallow water flows*, J. Comput. Phys., 213 (2006), pp. 474–499.

[64] S. Noelle, Y. Xing, and C. Shu, *High order well-balanced finite volume WENO schemes for shallow water equation with moving water*, J. Comput. Phys., 226 (2007), pp. 29–58.

[65] L. Pareschi and G. Toscani, *Self-Similarity and Power-Like Tails in Nonconservative Kinetic Models*, J. Stat. Phys., 124 (2006), pp. 747–779.

[66] ——, *Interacting Multiagent Systems. Kinetic equations and Monte Carlo methods*, Oxford University Press, 2013.

[67] L. Pareschi, G. Toscani, and C. Villani, *Spectral methods for the non cut-off Boltzmann equation and numerical grazing collision limit*, Numer. Math., 93 (2003), pp. 527–548.

[68] S. L. Paveri-Fontana, *On Boltzmann-like treatments for traffic flow: a critical review of the basic model and an alternative proposal for dilute traffic analysis*, Transport. Res., 9 (1975), pp. 225–235.

[69] H. J. Payne, *Models of freeway traffic and control*, in Math. Models Publ. Sys., vol. 1, Simul. Council Proc. 28, 1971, pp. 51–61.

[70] B. Piccoli and A. Tosin, *Vehicular traffic: A review of continuum mathematical models*, in Encyclopedia of Complexity and Systems Science, R. A. Meyers, ed., vol. 22, Springer, New York, 2009, pp. 9727–9749.

[71] L. A. Pipes, *An operational analysis of traffic dynamics*, J. Appl. Phys., 24 (1953), pp. 274–281.

[72] I. Prigogine, *A Boltzmann-like approach to the statistical theory of traffic flow*, in Theory of traffic flow, R. Herman, ed., Amsterdam, 1961, Elsevier, pp. 158–164.

[73] I. Prigogine and R. Herman, *Kinetic theory of vehicular traffic*, American Elsevier Publishing Co., New York, 1971.

[74] G. Puppo, M. Semplice, A. Tosin, and G. Visconti, *Analysis of a multi-population kinetic model for traffic flow*, Commun. Math. Sci. Accepted. arXiv:1511.06395.

[75] ——, *Kinetic models for traffic flow resulting in a reduced space of microscopic velocities*. Submitted. arXiv:1507.08961.

[76] ——, *Fundamental diagrams in traffic flow: the case of heterogeneous kinetic models*, Commun. Math. Sci., 14 (2016), pp. 643–669.

[77] P. I. Richards, *Shock waves on the highway*, Operations Res., 4 (1956), pp. 42–51.

[78] M. Rosini, *Macroscopic models for vehicular flows and crowd dynamics: theory and applications*, Springer, Basel, Switzerland, 2013.

[79] B. Seibold, M. R. Flynn, A. R. Kasimov, and R. R. Rosales, *Constructing set-valued fundamental diagrams from jamiton solutions in second order traffic models*, Netw. Heterog. Media, 8 (2013), pp. 745–772.

[80] C. W. Shu, *Essentially Non-Oscillatory and Weighted Essentially Non-Oscillatory Schemes for Hyperbolic Conservation Laws*, 1997. NASA ICASE report 97-65.

[81] G. Toscani, *Kinetic models of opinion formation*, Commun. Math. Sci., 3 (2006), pp. 481–496.

[82] A. Tosin, *Discrete kinetic and stochastic game theory for vehicular traffic: Modeling and mathematical problems*, PhD thesis, Politecnico di Torino, 2008.

[83] R. T. Underwood, *Speed, volume, and density relationships: Quality and theory of traffic flow*, Yale Bureau of Highway Traffic, (1961), pp. 141–188.

[84] C. Villani, *Conservative forms of Boltzmann's collision operator: Landau revisited*, ESAIM Math. Model. Numer. Anal., 33 (1999), pp. 209–227.

[85] G. Visconti, M. Herty, G. Puppo, and A. Tosin, *Multivalued fundamental diagrams of traffic flow in the kinetic Fokker-Planck limit*. Submitted. arXiv:1607.08530.

[86] G. B. Whitham, *Linear and Nonlinear Waves*, Wiley-Interscience, New York, 1974.

[87] H. M. Zhang, *A non-equilibrium traffic model devoid of gas-like behavior*, Transport. Res. B-Meth., (2002), pp. 275–290.

[88] H. M. Zhang and T. Kim, *A car-following theory for multiphase vehicular traffic flow*, Transport. Res. B-Meth., 39 (2005), pp. 385–399.